Greenhouse gas cycling in the marine environment

- from coast to open ocean

Dissertation

zur Erlangung des Grades eines Doktors der Naturwissenschaften

- Dr. rer. nat. -

im Fachbereich Geowissenschaften der

Universität Bremen

Jan Niccolo von Arx

Bremen, Juli 2023

Die Arbeit wurde im Zeitrahmen April 2019 bis Juli 2023 innerhalb des Programms „The International Max Planck Research School of Marine Microbiology (MarMic)" angefertigt. Die Resultate der Arbeit wurden am Max-Planck-Institut für Marine Mikrobiologie in der Abteilung Biogeochemie, Forschungsgruppe Treibhausgase erarbeitet.

Datum des Promotionskolloqiums: 21. September. 2023

Autor: **Jan Niccolo von Arx**

Universität Bremen

Max-Planck-Institut für Marine Mikrobiologie

Gutachter: **Prof. Dr. Marcel M. M. Kuypers**

Universität Bremen

Max-Planck-Institut für Marine Mikrobiologie

Zweitgutachter: **Dr. Claudia Frey**

Universität Basel

Table of Contents

Acknowledgments ..... **v**

Summary **1**

Zusammenfassung **4**

Chapter I **7**

1) Greenhouse gas effect
2) Methane
3) Nitrous oxide
4) Study sites
5) Aims and Outline

Chapter II **52**

Methylphosphonate-driven methane formation and its link to primary production in the oligotrophic North Atlantic

Chapter III **105**

Nitrous oxide cycling in the suboxic zone of the Black Sea

Chapter IV **146**

Nitrous oxide cycling in the coastal Peruvian oxygen minimum zone

Chapter V **195**

Discussion and Outlook

Appendix **214**

Author Contributions

Versicherung an Eides Statt

Acknowledgments

I would like to express my gratitude and heartfelt thanks to all the lovely people who have accompanied me on this PhD journey in both a professional and personal setting. Each one of you has made the labours of the last years more enjoyable.

… Marcel Kuypers - Thank you so much for giving me the opportunity to do my PhD in your department and welcoming me with open arms. I thoroughly enjoyed the chance of working with you and especially valued our stimulating scientific discussions. I really appreciate your advice and guidance and who could forget help with carrying the winch of the pump CTD in Peru!

… Jana Milucka - Thank you so much for giving me the opportunity to do amazing research all over the world. I am always going to be grateful for all the guidance, help, teaching and kindness you have shown me. Thank you for all the hours spent looking at data, discussing science and life and especially writing together, I thoroughly enjoyed it. I am also immensely grateful for the reassurances you always give me and for indulging me when I arrive with my list.

… Claudia Frey - Thank you very much for agreeing to be the reviewer for my thesis. I thoroughly enjoyed getting to know you, albeit briefly, over the course of the last years and I really appreciate all the scientific discussions we have had.

… Daan - Thank you so much for trying to help me understand some bioinformatics and for your inputs during my committee meeting. Thank you for all the laughs and the great time at the ISME conference.

… Gaute - Thank you so much for everything you have taught me painstakingly over the years, from field work to the magic of stable isotope experiments, you have always been there and I could not have done any of this without your incredible patience. Thank you for spending tens of hours (if not more) looking at spreadsheets together and making sense of all the complexity. Last but not least, thanks for sharing a drink and a laugh after many hard working days.

… Hannah - Dear Dr Marchant I can never thank you enough for welcoming me with open arms all those years ago when I started my master thesis. Thank you for all your help, guidance and scientific discussions throughout the years. Especially these last weeks would have been impossible without all the time, energy and passion you have invested in helping me. Finally thanks for all the laughs and sharing my terrible taste in early 2000s Britpop.

… Kathi - Thank you so much for everything, least of all welcoming me into the department all those years ago as a master student that set the foundation of this PhD work. Thank you for all the great field trips and endless enthusiasm for new and exciting projects. Thank you for all your input during my committee meetings and for assuring me that one does not need to wear formal wear to a scientific conference.

… Wiebke - Thank you so much for all of your teaching and help with primary productivity experiments. Thanks for all of your insights during my committee meetings and the organisation and aid you gave during our long Barbados field trip. I also really appreciate that your office door was always open for all of my endless questions.

… Arzhang, Benni, Boran, Bram, Guodong, Jon, Miriam, Shengjie, Sina, Soeren, Sten and Tim - thank you all so much for your teaching, help and numerous scientific discussions over the years.

… Daniela, Gabi, Kirsten, Mandy, Nadine, Nina, Sandra, Swantje and Vera - Thank you all so much for all your constant help, support, kindness and measurements, without none of the data generated for this thesis would have been possible. Thank you for your patience when showing me new methods and for being great colleagues. I would like to express special gratitude to Gabi for literally running thousands of samples for me on the mass spectrometer, including many test runs. Nadine thank you so much for always responding promptly and putting my fears to rest when the Picarro decided to do something strange, obviously always on a Friday evening.

… Ulrike - Thank you so much for all of your help with organising conferences, field trips and committee meetings.

… all former and current Biogeo PhD students - Abiel, Alexander, Clarissa, Caroline, Fabian, Jördis, Judith, Julia, Juliane, Linus, Louison, Margarita, Mertcan, Niek, Nadine, Paloma, Siqi, Qiong and Valeria thank you all for being amazing people that have made the years much lovelier. Thank you all for your help, feedback, fruitful discussions, field trips and conferences.

… Farooq - Thank you so much for everything, all the laughs in the office, all the ups and downs associated with a PhD, all the endless editing on my figures, all the plans about farming. You are a truly wonderful person and an inspiration. I cannot imagine getting to this point without you.

… Angèle and Grace thank you both for being such wonderful and exceptional students and for bearing with me teaching molecular work.

… MarMic class of 2022 - Andrey, Caro, Darjan, Hagen, Jan, Johanna, Matija, Mara, Marion, Nevena, Olivia, Paloma, Patric, Taylor and Ulrike, thank you all for the great start of this endeavour.

… Everyone else who was involved in field trips, experiments and everyday life at the Institute - Thank you all so much for everything.

… Caro and Johanna - Thank you both so much for being the great friends that you are. Thank you for sharing the ups and downs, always with good food and copious amounts of alcohol. Thank you for your endless attempts to get me to socialise and for not getting endlessly frustrated with me.

… Mum, Dad, Amy, Robin, Groma, Gropa, Mama, Aeti thank you all so much for being my comforting rock, for your endless support and love and for believing in me. I could not have done this without all of you.

… Bruno, Leo, Max, Robin - thank you all for being great friends and keeping me sane during the pandemic. Thank you for all the nights playing DnD, Magic, Total war and many other numerous activities.

… Amber - without you above all, none of this would have been possible. Thank you for always being there for me, my constant companion and comfort. Thank you for bearing with me for now over six years of being apart in separate countries and somehow not getting fed up with me. Thank you for going through all of this with me, my ups and downs but always assuring and being steadfast. Thank you so much for making my English better and being my constant editor. I love you so much.

Summary

The consequences of global warming are omnipresent, especially with current record heat waves in Europe, North America and Asia. The natural greenhouse gas effect is essential for human life on Earth but anthropogenic activity increases greenhouse gas emissions and amplifies this warming effect. Global warming also has a significant impact on marine environments, making them more thermally stratified, acidic and oxygen-depleted, thereby disrupting the natural cycle of greenhouse gases.

Methane and nitrous oxide (N_2O) are important greenhouse gases with key functions in marine biogeochemistry and can be both formed and consumed by microbial activity. However, emerging discoveries regarding both methane and N_2O highlight the need for further investigations of the underlying microbial transformations, as our understanding remains incomplete. For example, methane formation was thought to be a strictly anaerobic process until it has been shown to also occur in fully oxygenated environments, possibly by a plethora of microbial pathways. N_2O formation and consumption is well documented, particularly in oxygen-limited environments but both coastal environments and oxygen-limited environments without significant N_2O accumulation remain understudied. Thus understanding the physico-chemical driving factors of these greenhouse gas cycles and the underlying microbial activities and communities is vital for predicting the effects of continuous climate disruptions and the resulting consequences for the fluxes of these greenhouse gases to the atmosphere.

To address some of these knowledge gaps, this thesis explored microbial methane and N_2O cycling in different oceanic regions by combining extensive field measurements using stable isotope incubation experiments and molecular analyses to determine the underlying microbial pathways and controlling factors.

Current research suggests that methylphosphonate (MPn) utilisation can lead to methane formation in oxygenated waters, especially in phosphate-limited environments, where the microbial community can use it as an alternative phosphorus source. In **chapter II**, we explored the extent of MPn-driven methane formation, using ^{13}C-MPn, in the upper 200 metres of the western Tropical North Atlantic off Barbados and the microbial community and controlling factors behind their activity. We show that MPn was a major methane precursor, with the highest methane formation

found in the surface waters above the deep chlorophyll maximum. Interestingly, methane formation was detected even in the presence of phosphate, a more energetic phosphorus source, suggesting that MPn-driven methane formation may extend into more phosphate replete environments. Phylogenetic analysis of the *phnJ*, the marker gene for MPn-driven methane formation, identified a diverse microbial community. *Alphaproteobacteria* generally dominated the microbial community possessing the *phnJ* gene, whereas the cyanobacterium *Trichodesmium* was most abundant in the surface waters. Our results suggest there is a link between primary productivity and methane formation and we conclude that phosphonates, including MPn, could account for 11% of the phosphorus requirement of primary producers in the surface waters.

In **chapter III** we investigated N_2O cycling in the suboxic zone of the Black Sea. Despite harbouring a massive oxygen-limited water column, the Black Sea is only considered to be a minor source of N_2O to the atmosphere. It has been suggested previously that there is an active N_2O cycle in the suboxic zone but the pathways and microbial community responsible remain poorly constrained. We used ^{15}N-based stable isotope incubation experiments to identify the main pathways of N_2O formation (aerobic ammonia oxidation and denitrification) and consumption. We were able to demonstrate that aerobic ammonia oxidation led to small but persistent rates in contrast to nitrite reduction which led to sporadic but explosive rates of N_2O formation. The latter were especially amplified in the presence of sulphide, suggesting chemolithotrophic denitrification took place. Despite these high rates, N_2O reduction could outpace its formation, suggesting a balance within the suboxic zone being responsible for the lack of N_2O accumulation. Phylogenetic analysis of the *amoA*, the marker gene for ammonia oxidation, revealed that the *Nitrososphaerales* were dominant. Analysis of denitrification genes revealed a diverse community which included denitrifiers of the *Gammaproteobacteria* and potential N_2O reducing specialists of the *Marinisomatales*. All of these denitrifiers belonged to groups previously associated with sulphur cycling. Therefore, we could demonstrate that despite the lack of N_2O accumulation in the water column, there is an active but well-balanced microbial N_2O cycle.

Finally, in **chapter IV** we investigated N_2O cycling in the Peruvian oxygen minimum zone (OMZ), the single largest marine source of N_2O to the atmosphere. We investigated the shallow (< 100 metres water depth) OMZ using ^{15}N-based stable isotope incubation experiments to identify the main microbial processes of N_2O cycling. The water column seemed to be highly dynamic with oxygen measurements suggesting oxygen intrusions into the OMZ. Rate measurements

showed that aerobic ammonia oxidation was a minor but persistent source of N_2O, with denitrification from both nitrite and nitrate dominating. However, N_2O reduction rates exceeded the combined formation rates from all sources. Therefore, these results suggest that there is the capacity for a microbial N_2O filter to prevent N_2O accumulation. However, this is likely mitigated by the dynamic nature of the environment, thereby making the coastal OMZ an important source of N_2O.

Combined these chapters give new insights into methane and N_2O cycling in understudied marine environments and pose new and exciting questions for future research.

Zusammenfassung

Die Folgen der globalen Erwärmung sind allgegenwärtig, vor allem durch die derzeitigen Rekordhitzewellen in Europa, Nordamerika und Asien. Der natürliche Treibhauseffekt ist für das menschliche Leben auf der Erde unverzichtbar, die anthropogenen Aktivitäten erhöhen jedoch die Treibhausgasemissionen und verstärken den Erwärmungseffekt. Die globale Erwärmung hat auch erhebliche Auswirkungen auf die Meeresumwelt, da sie stärker stratifiziert, saurer und sauerstoffärmer wird, was den natürlichen Kreislauf der Treibhausgase stört.

Methan und Lachgas (N_2O) sind wichtige Treibhausgase mit Schlüsselfunktionen in der Biogeochemie des Meeres und können durch mikrobielle Aktivität sowohl gebildet als auch verbraucht werden. Neue Entdeckungen in Bezug auf Methan und N_2O machen jedoch deutlich, dass die zugrundeliegenden mikrobiellen Umwandlungen weiter erforscht werden müssen, da unser Verständnis noch unvollständig ist. So wurde beispielsweise angenommen, dass die Methanbildung auf die anaerobe Methanogenese beschränkt ist. Es wurde aber gezeigt, dass Methan auch in vollständig sauerstoffhaltigen Umgebungen stattfinden kann, möglicherweise durch eine Vielzahl von mikrobiellen Stoffwechselwegen. Die Bildung und der Verbrauch von N_2O sind gut dokumentiert, insbesondere in sauerstoffarmen Umgebungen, aber sowohl Küstengebiete als auch sauerstoffarme Umgebungen ohne signifikante N_2O-Anreicherung sind noch nicht ausreichend erforscht. Das Verständnis der physikalisch-chemischen Antriebsfaktoren dieser Treibhausgaskreisläufe und der zugrundeliegenden mikrobiellen Aktivitäten und Gemeinschaften ist daher von entscheidender Bedeutung für die Vorhersage der Auswirkungen anhaltender Klimastörungen und der daraus resultierenden Folgen für die Flüsse dieser Treibhausgase in die Atmosphäre.

Um einige dieser Wissenslücken zu schließen, wurde in dieser Dissertation der mikrobielle Methan- und N_2O-Kreislauf in verschiedenen ozeanischen Regionen untersucht. Dazu wurden umfangreiche Feldmessungen mit Hilfe von Inkubationsexperimenten mit stabilen Isotopen und molekularen Analysen kombiniert, um die zugrundeliegenden mikrobiellen Prozesse und Kontrollfaktoren aufzuklären.

Aktuelle Forschungsergebnisse deuten darauf hin, dass die Nutzung von Methylphosphonat (MPn) in sauerstoffreichen Gewässern zur Methanbildung führen kann, insbesondere in phosphatarmen Regionen, in denen die mikrobielle Gemeinschaft es als alternative Phosphorquelle nutzen kann.

In **Kapitel II** untersuchten wir mit Hilfe von ^{13}C-MPn das Ausmaß der MPn-bedingten Methanbildung in den oberen 200 Metern des westlichen tropischen Nordatlantiks vor Barbados sowie die mikrobielle Gemeinschaft und die Kontrollfaktoren für ihre Aktivität. Wir zeigen, dass MPn ein wichtiger Methanvorläufer war, wobei die höchste Methanbildung oberhalb des tiefen Chlorophyllmaximums stattgefunden hat. Interessanterweise wurde die Methanbildung sogar in Gegenwart von Phosphat, einer energiereicheren Phosphorquelle, nachgewiesen, was darauf hindeutet, dass die MPn-getriebene Methanbildung auch in phosphatreicheren Regionen stattfinden kann. Die phylogenetische Analyse von *phnJ*, dem Markergen für die MPn-getriebene Methanbildung, zeigte eine vielfältige mikrobielle Gemeinschaft. *Alphaproteobakterien* dominierten im Allgemeinen die mikrobielle Gemeinschaft, die das *phnJ*-Gen besaß, während das Cyanobakterium *Trichodesmium* in den Oberflächengewässern reichlich vorkam. Unsere Ergebnisse deuten darauf hin, dass ein Zusammenhang zwischen Primärproduktivität und Methanbildung besteht, und wir schließen daraus, dass Phosphonate, einschließlich MPn, 11 % des Phosphorbedarfs der Primärproduzenten in den Oberflächengewässern decken könnten.

In **Kapitel III** untersuchten wir den N_2O-Kreislauf in der suboxischen Zone des Schwarzen Meeres. Obwohl das Schwarze Meer eine riesige, sauerstoffarme Wassersäule beherbergt, wird es nur als eine geringe Quelle von N_2O für die Atmosphäre angesehen. Es wurde bereits früher vermutet, dass es in der suboxischen Zone einen aktiven N_2O-Kreislauf gibt, aber die Wege und die mikrobielle Gemeinschaft, die dafür verantwortlich sind, sind noch nicht ausreichend erforscht. Wir verwendeten ^{15}N-basierte Inkubationsexperimente mit stabilen Isotopen, um die Hauptwege der N_2O-Bildung (aerobe Ammoniakoxidation und Denitrifikation) zu identifizieren und die Raten des N_2O-Verbrauchs zu quantifizieren. Wir konnten zeigen, dass die aerobe Ammoniakoxidation zu geringen, aber anhaltenden Raten der N_2O-Bildung führte. Im Gegensatz dazu führte die Nitritreduktion zu sporadischen, aber explosionsartigen Raten der N_2O-Bildung. Letztere waren in Gegenwart von Sulfid besonders hoch, was auf eine chemolithotrophe Denitrifikation schließen lässt. Trotz dieser hohen Raten konnten die N_2O-Reduktionsraten die N_2O-Bildung übertreffen, was darauf schließen lässt, dass ein Gleichgewicht innerhalb der suboxischen Zone für die fehlende N_2O-Akkumulation verantwortlich ist. Die phylogenetische Analyse von *amoA*, dem Markergen für die Ammoniakoxidation, ergab, dass die *Nitrososphaerales* dominieren. Die Analyse der Denitrifikationsgene zeigte eine vielfältige Gemeinschaft, zu der Denitrifizierer der *Gammaproteobakterien* und potenzielle N_2O-reduzierende Spezialisten der *Marinisomatales* gehörten. Alle diese Denitrifikanten waren Teil

von Gruppen, die zuvor mit dem Schwefelkreislauf in Verbindung gebracht wurden. So konnten wir nachweisen, dass es trotz der fehlenden N_2O-Akkumulation in der Wassersäule einen aktiven, aber ausgewogenen mikrobiellen N_2O-Kreislauf gibt.

In **Kapitel IV** schließlich untersuchten wir den N_2O-Kreislauf in der peruanischen Sauerstoffminimumzone (OMZ), der größten marinen N_2O-Quelle für die Atmosphäre. Wir untersuchten die flache (< 100 Meter Wassertiefe) OMZ mit Hilfe von ^{15}N-basierten Inkubationsexperimenten mit stabilen Isotopen, um die wichtigsten mikrobiellen Prozesse des N_2O-Kreislaufs zu identifizieren. Die Wassersäule schien sehr dynamisch zu sein, wobei Sauerstoffmessungen auf ein Eindringen von Sauerstoff in die OMZ hindeuteten. Ratenmessungen zeigten, dass die aerobe Ammoniakoxidation eine geringe, aber beständige N_2O-Quelle war, während die Denitrifikation aus Nitrit und Nitrat dominierte. Die N_2O-Reduktionsraten überstiegen jedoch die kombinierten Bildungsraten aus allen Quellen. Daher deuten diese Ergebnisse darauf hin, dass ein mikrobieller N_2O-Filter die N_2O-Anreicherung verhindern kann. Dies wird jedoch wahrscheinlich durch den dynamischen Charakter der Umwelt abgeschwächt, wodurch die küstennahe OMZ zu einer wichtigen Quelle von N_2O wird.

Zusammengefasst geben diese Kapitel neue Einblicke in den Methan- und N_2O-Kreislauf in wenig untersuchten Meeresumgebungen und werfen neue und spannende Fragen für die zukünftige Forschung auf.

Chapter I – Introduction

1) Greenhouse gas effect

The greenhouse gas effect makes life on Earth, as we know it, possible (Denny 2012). Light emitted from the sun passes through the Earth's atmosphere and is absorbed as it hits land or water. As light is emitted back into the atmosphere in the infrared spectrum, various greenhouse gases absorb and deflect parts of it back onto Earth's surface. This ensures that the surface is not in equilibrium with space, otherwise it would resemble the upper atmosphere, which has an average temperature of -18°C. The four main gases responsible for the greenhouse gas effect are water vapour, carbon dioxide, methane and nitrous oxide (N_2O). All of these are naturally occurring and have their own biogeochemical cycles, which have rapidly been affected by anthropogenic activity. As such, the anthropogenic impact on the greenhouse gas effect is twofold. Firstly, there are direct anthropogenic emissions of greenhouse gases to the atmosphere from sources, such as industry and fossil fuel emissions among many more. A second way is through the disturbance of natural microbial greenhouse gas cycles, such as through increased nutrient loading from fertiliser usage. Combined, this has already resulted in a global surface temperature increase of 0.95 - 1.2°C compared to 1850 – 1900 (Intergovernmental Panel on Climate Change 2023a), with continuous projected increases of up to 1.5 - 4.8°C, compared to the 19th century by 2100 (Intergovernmental Panel on Climate Change 2023b).

The ocean makes up 71% of the Earth's surface and is therefore vital for regulating the climate. It takes up around 25% of the total anthropogenic carbon dioxide emissions (Gruber et al. 2023) and absorbs around 90% of the heat (Intergovernmental Panel on Climate Change 2023c). However, the continuous increase in temperature means the ocean is becoming more thermally stratified (Intergovernmental Panel on Climate Change 2023c; Li et al. 2020) and acidic (Doney et al. 2009). Furthermore, the nutrient runoff from inland waters due to anthropogenic activity has led to increased deoxygenation, through stimulated productivity followed by heterotrophic oxygen-consuming processes (Breitburg et al. 2018; Diaz & Rosenberg 2008; Schmidtko et al. 2017). In combination with the reduced solubility of oxygen in warmer waters, oxygen-limited environments are increasing and expanding. All of these changes affect the natural cycles of the greenhouse gases, including methane and N_2O with potential significant, but at times still poorly constrained, consequences. Understanding the microbially mediated processes leading to the

formation and consumption of both methane and N_2O is therefore vital to assess their continued impact in a changing ocean. In this thesis, I investigated these processes in understudied marine environments, from the coast to the open ocean.

2) Methane

Methane Budget

Methane (CH_4) is a naturally occurring but anthropogenically affected greenhouse gas with an atmospheric concentration of ~1921.7 parts per billion (NOA, 2023). This is around two-and-a-half times higher than pre-industrial levels (Intergovernmental Panel on Climate Change 2023d). Although its concentration is two orders of magnitude below that of carbon dioxide (423.3 parts per million) it is more effective at trapping heat. Additionally, it has a short atmospheric residence time of 9.1 ± 0.9 years (Intergovernmental Panel on Climate Change 2023d). This makes its global warming potential approximately 27 ± 11 times higher than that of carbon dioxide within a span of 100 years (Intergovernmental Panel on Climate Change 2023e). The predominant atmospheric sink is through the reaction of methane with hydroxyl radicals (Cicerone & Oremland 1988). Its overall contribution to the greenhouse effect is thus estimated at around 20% of the radiative climate forcing (Etminan et al. 2016).

When considering the global methane budget (Figure 1), the anthropogenic emissions are well constrained and estimated at 356 (335 - 383) Tg CH_4 yr^{-1} (Intergovernmental Panel on Climate Change 2023d). However, emissions from natural sources have a discrepancy of up to 156 Tg CH_4 yr^{-1} between top down (215 (183 - 248 Tg CH_4 yr^{-1}) and bottom up (371 (245 - 488) Tg CH_4 yr^{-1}) estimates, reflecting a dearth in both measurements and knowledge (Saunois et al. 2020). Contributing to these uncertainties are emission estimates from aquatic environments (median 269.4 (202.3 - 424.6) Tg CH_4 yr^{-1}), which make up around half to the total methane emissions (Rosentreter et al. 2021). These are dominated by both freshwater ecosystems and wetlands, with ocean estimates of 6 - 12 Tg CH_4 yr^{-1} (Weber et al. 2019), although recent median contribution estimates were higher 8.4 (4.8 - 28.4) Tg CH_4 yr^{-1} (Rosentreter et al. 2021). However, due to the methane stored in hydrates, the ocean remains the largest methane reservoir (Intergovernmental Panel on Climate Change 2023d) and shallow coastal environments are considered hotspots for marine methane emissions (Weber et al. 2019). In these environments, methane is formed primarily by anaerobic methanogenesis in the sediments (Barnes & Goldberg 1976). Due to the

shallow dynamic water column, methane has a short residence time, escaping into the atmosphere before being removed through microbial methane oxidation in sediments and the water coulmn (Mao et al. 2022; Reeburgh 2007; Thamdrup et al. 2019). Comparatively, in the open ocean, due to the deep water column, methane oxidation is more efficient in removing sedimentary methane formation (Pack et al. 2015). Nevertheless, the open ocean (> 2000 metre water depth), which covers around 60% of the Earth's surface, is still considered to be a source of methane to the atmosphere, contributing 5 - 23% of the total methane emissions from the marine environment (Weber et al. 2019). These emissions are driven by a historical anomaly that has been coined the "Marine Methane Paradox" (Kiene 1991).

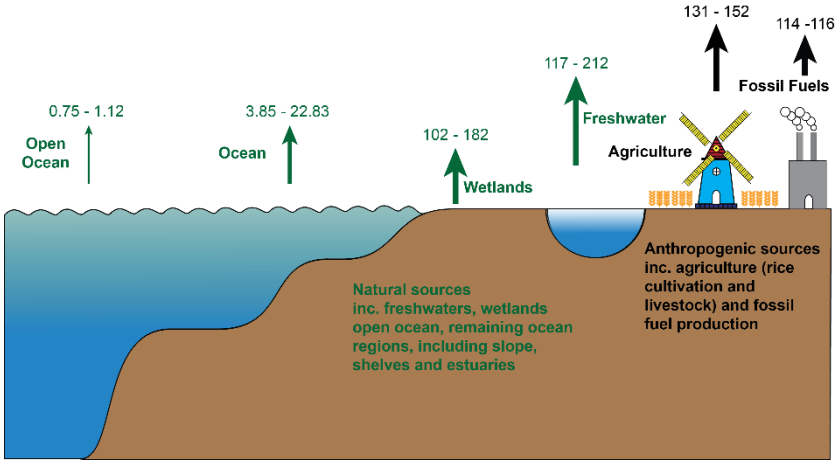

Figure 1. **Sketch of major contributors to methane emissions from both natural and anthropogenic sources.** Estimates were taken from Rosentreter et al. (2021) and the Intergovernmental Panel on Climate Change (2023d). All values are in Tg methane yr^{-1}.

"Marine Methane Paradox"

The "Marine Methane Paradox" describes a methane concentration maximum located in the fully oxic marine surface water column that is sustained through *in-situ* methane formation (Kiene 1991). The paradoxical nature is due to archaeal methanogenesis being strictly anaerobic (e.g. Balch et al. 1979). Reports of this "Paradox" go back to the 1970s with observations in both the

Pacific (Lamontagne et al. 1971, 1973) and Atlantic (Scranton & Brewer 1977). Initial studies investigated methanogenesis in anoxic microniches, such as guts of small-sized zooplankton or fish (Oremland 1979; Traganza et al. 1979) and sinking particles (Bianchi et al. 1992), to help explain the "Paradox". Furthermore, heterocysts, specialised cells of nitrogen-fixing cyanobacteria that protect the oxygen sensitive nitrogenase, have also been proposed as anoxic microniches (Berg et al. 2014; Lupton & Marshall 1981). Nevertheless, most of these anoxic microniches are often ephemeral environments (e.g. Smayada 1969) and thus insufficient in explaining the "Marine Methane Paradox" in its entirety (Simon et al. 2002). More recently, several alternative pathways of methane formation have been proposed for the oxic water column. These can be broadly categorised as originating from either methylated compounds, such as methylphosphonate (MPn; Karl et al. 2008), dimethylsulfoniopropionate (Damm et al. 2010), methylamine (Wang et al. 2021) or methyl radicals (Ernst et al. 2022) or from dissolved inorganic carbon through nitrogen fixation (Zheng et al. 2018), or as a by-product of carbon fixation (Bižić et al. 2020; Lenhart et al. 2016; Perez-Coronel & Michael Beman 2022) and may include many more. Out of all of these pathways, MPn driven methane formation has so far shown the most promise of significant contribution to methane formation (Repeta et al. 2016), as it can be used as an alternative phosphorus source in phosphate (Pi)-limited environments (Karl et al. 2008).

Methylphosphonate-driven methane formation

Phosphorus is an essential element required by all forms of life which can be found, for example, in DNA and RNA, ATP and the cellular membrane. While inorganic Pi is considered to be the preferred phosphorus source (Karl & Yanagi 1997), its concentration can vary by orders of magnitude, ranging from < 1 nmol L^{-1} in the oligotrophic North Atlantic (Cavender-Bares et al. 2001) to > 1 µmol L^{-1} in the Southern Ocean (Sosa et al. 2019a; Figure 2). As such, many marine regions, especially in the tropics and subtropics are considered Pi-limited (Bristow et al. 2017; Karl 2014; Sosa et al. 2019a; Wu et al. 2000). However, under such Pi-limited conditions up to half of the phosphorus demand can be met through phosphorus containing dissolved organic matter (Karl & Björkman 2015), which includes MPn.

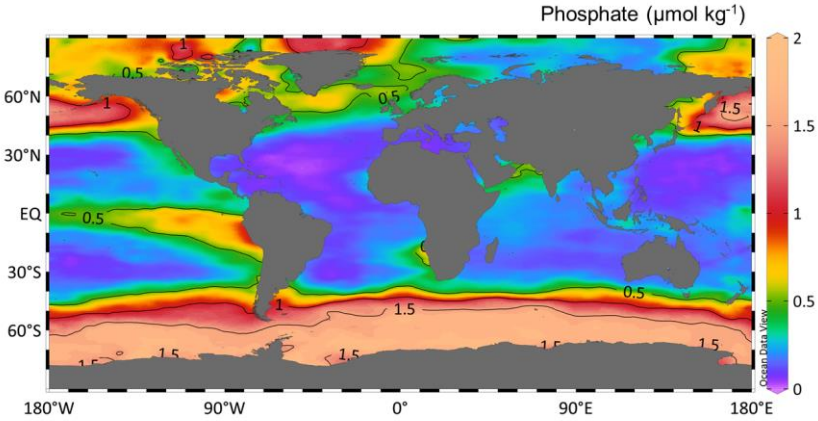

Figure 2. **Annual mean surface phosphate concentrations.** Data was taken from the World Ocean Atlas 2018 at a 1° resolution, 0 m depth.

MPn is the simplest phosphonate, a group of organic phosphorus compounds that are classified by their direct C-P bond. Phosphonates were first discovered in the 1950s by a ninhydrin-positive spot on a chromatogram from the acid hydrolysate of the protozoan *Tetrahymena pyriformis* found in a sheep rumen (Horiguchi & Kandatstu 1959). The compound was later characterised as 2-aminoethane phosphonic acid also known as cillatine and incidentally the most common phosphonate in the marine environment (White & Metcalf 2007). Soon after, the viability of MPn as a sole phosphorus source was demonstrated in cultured *E. coli* (Zeleznick et al. 1963) and the transformation of MPn to methane was first demonstrated in *Pseudomonas testosteroni* (Daughton et al. 1979).

In the marine environment, phosphonates usually make up 10 - 25% of the high molecular weight dissolved organic matter (Clark et al. 1999; Kolowith et al. 2001), making them the largest fraction behind organic phosphorus esters. While there are no reported concentration measurements specifically for MPn, it has been estimated that MPn and 2-Hydroxyethylphosphonate can account for 20% of the phosphorus associated with high molecular weight dissolved organic matter (Repeta et al. 2016), with MPn often bound to polysaccharides through ester bonds. The direct C-P bond makes phosphonates highly resistant towards chemical and enzymatic hydrolysis, as well as

photolysis (Daughton et al. 1979; Ternan et al. 1998). Due to the structural similarity to phosphate-esters, phosphonates may inhibit metabolic pathways (Horsman & Zechel 2017) or confer additional stability, especially in membrane associated phosphonolipids or phosphonoglycans (Kennedy & Thompson 1970; White & Metcalf 2007) and could thus protect from grazing or lysis (Acker et al. 2022). Interestingly, while the natural phosphonate cycle is well documented (see following sections), early interest in environmental phosphonate research increased due to their extensive use as pesticides in agricultural practices, where they are incredibly effective (Stosiek et al. 2020). This became especially prevalent with the introduction of glyphosate containing *Roundup* products introduced by Monsanto in the early 1970s. The longevity and adverse health effects to both flora and fauna and subsequent runoff into the aquatic environments, rapidly increased interest in microbial degradation processes.

Synthesis of methylphosphonate

While there is an abiotic pathway of MPn formation, requiring UV photolysis of acetone in the presence of phosphite (Horsman & Zechel 2017), the main source is likely biological. The formation of MPn, like most other phosphonates, commences from the cellular intermediate phosphoenolpyruvate (Metcalf & Van Der Donk 2009; Metcalf et al. 2012; Taenzer et al. 2020). Through four subsequent enzymatic reactions phosphoenolpyruvate can be transformed to MPn (Figure 3) but it remains unknown how MPn is attached to lipids or polysaccharides (Horsman & Zechel 2017).

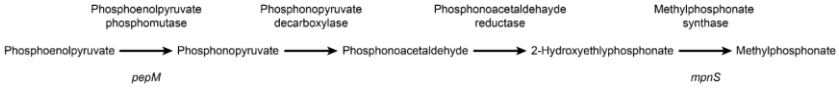

Figure 3. **Methylphosphonate biosynthesis from the precursor phosphoenolpyruvate**. The *pepM* gene encodes for the phosphoenolpyruvate phosphomutase and is used as the marker gene for general phosphonate synthesis as it facilitates the formation of the carbon-phosphorus bond (Acker et al. 2022). The *mpnS* gene encodes for the methylphosphonate synthase and is the marker gene for the specific synthesis of methylphosphonate (Metcalf et al. 2012).

Analysis using global marine metagenomic datasets have revealed the widespread potential of phosphonate synthesis by the microbial community (Acker et al. 2022; Born et al. 2017;

Lockwood et al. 2022; Villarreal-Chiu et al. 2012) with a broad taxonomic diversity but especially prevalent in *Alpha*- and *Gammaproteobacteria*, *Cyanobacteria* and *Thaumarchaeota*, (Lockwood et al. 2022). *Thaumarchaeota* and their newly proposed GTDB taxonomy *Nitrososphaeria* (Parks et al. 2018) were used interchangeably in this thesis. Interestingly, the capacity for both the synthesis and consumption seems to be mostly separated, rarely occurring within the same organism (Acker et al. 2022). However, there are notable exceptions, especially in cosmopolitan species such as *Trichodesmium* and *SAR11* (Born et al. 2017; Carini et al. 2014; Dyhrman et al. 2006, 2009; Lockwood et al. 2022). Estimates based on metagenomic analysis suggest that up to 6 -12% of the surface microbial community can synthesise phosphonates (Metcalf et al. 2012; Villarreal-Chiu et al. 2012; Yu et al. 2013). However, the frequency of phosphonate synthesis genes increases with depth below 100 metres (Acker et al. 2022). At 200 metres up to 40% of the community was capable of synthesising phosphonates, coinciding with higher concentrations of Pi and DOP concentrations, likely reflecting higher energetic requirements for the synthesis of these compounds.

Unlike the general phosphonate synthesis, MPn formation, determined by presence of the *mpnS*, seems to be more conserved. So far, only the *Thaumarchaeum Nitrosopumilus maritimus* (Metcalf et al. 2012) has been shown experimentally to produce MPn. However, Born et al. (2017) were able to show that the *mpnS* was also present in *Pelagibacter ubique*, a member of the *SAR11* clade of the *Alphaproteobacteria*. Additionally, more *mpnS*-like genes were identified in other pro- and eukaryotes, including the dinoflagellate genus *Symbiodinium*, *Cyanobacteria*, *Gammaproteobacteria* and *Crenarchaeota classes* (Born et al. 2017; Lockwood et al. 2022). As such, it cannot only be found in a broad range of organisms but both *SAR11* and *Thaumarchaota* are two of the most abundant groups of microorganisms in the marine environment (Karner et al. 2001; Morris et al. 2002). *MpnS* also has a clear depth distribution, with an abundance of 0.6 - 1.5% in the surface and deep chlorophyll maximum communities (Lockwood et al. 2022; Metcalf et al. 2012) opposed to the 7.7% in the mesopelagic (Lockwood et al. 2022). Interestingly, there was also an inverse relationship between the *mpnS* and Pi concentrations, which was not found for phosphonate synthesis in general (Lockwood et al. 2022).

Methylphosphonate consumption

Due to the stability conferred by the C-P bond, phosphonate degradation requires specific mechanisms. While it has been demonstrated that persistent UV irradiation can lead to the abiotic degradation of MPn into Pi and methane (Yu et al. 2018), this requires UV intensities of over 1200 W to be efficient (Zhang & Ji 2019). Thus, the primary degradation pathway of MPn is likely biological. There are two known pathways of MPn utilisation, MPn oxidation and MPn degradation by the C-P lyase pathway (Figure 4). Of these two, the oxidative pathway has only recently been demonstrated to convert MPn to Pi and formic acid by two enzymatic steps (Gama et al. 2019). MPn is converted to hydroxymethylphosphonic acid by a methylphosphonate hydroxylase (*phnY*) which is oxidised to formic acid and Pi by a (hydroxymethyl)phosphonate dioxygenase (*phnZ*). While initially identified in the *Planctomycete Gimesia maris*, this pathway is also found in *Prochlorococcus* and likely has a cosmopolitan distribution (Gama et al. 2019; Sosa et al. 2019b). However, little is known about this pathway but due to the formation of formate over methane, it is important to constrain this in future work. The more widespread pathway of MPn utilisation is through the C-P lyase which in the case of MPn leads to the formation of Pi and methane (Kamat et al. 2011, 2013).

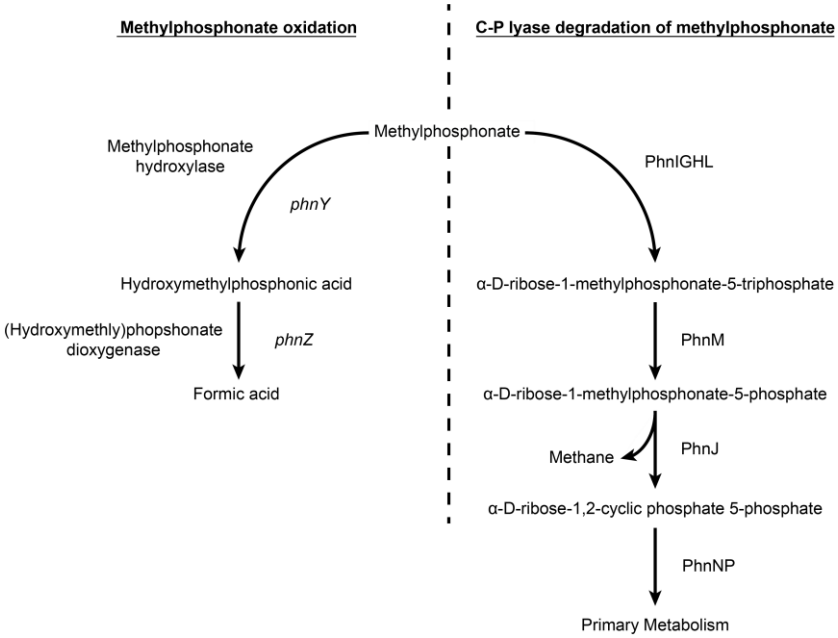

Figure 4. **Schematic of oxidative and carbon-phosphorus lyase pathways of methylphosphonate degradation.** Oxidative pathway is adapted from Gama et al. (2019), C-P lyase from Lockwood et al. (2022), Martinez et al. (2013) and Stosiek et al. (2020).

Carbon-phosphorus lyase pathway

In both *E. coli* and *P. stutzeri* the C-P lyase pathway is encoded by a 14 gene operon (*phnCDEFGHIJKLMNOP*) that includes transporters, the C-P lyase complex as well as accessory proteins. However, not all genes are required for the cleavage of the C-P bond, with the minimal catalytic unit encoded by *phnG-M* (Huang et al. 2005). Additionally, as the absence of the *phnCDE* did not inhibit growth in *E.coli*, it has been suggested that the entire degradation can occur outside the cell (Yakovleva et al. 1998). The C-P lyase complex is a multi-substrate (Wackett et al. 1987), multi-enzyme complex that cleaves phosphonates into Pi and their respective hydrocarbons. The acquisition of MPn into the cell and the cleavage by the C-P lyase complex can be described as follows (Figure 4):

1. MPn can either diffuse freely into the periplasmic space when in dissolved form, or it is released through extracellular degradation of the larger compounds it is bound to (Karl 2014).
2. MPn can be transported into the cell via a specific ABC transporter, which is expressed by the *phnCDE* genes. This transporter can bind phosphonates as well as phosphite and Pi (Feingersch et al. 2012; Stasi et al. 2019).
3. In the cytoplasm PhnI in the presence of PhnGHL catalyses the conversion of MPn to α-D-ribose-1-methylphosphonate-5-triphosphate (RPnTP).
4. PhnM then hydrolyses RPnTP to α-D-ribose-1-methylphosphonate-5-phosphate (PRPn) which is the substrate for breaking the C-P bond.
5. The C-P bond is then cleaved by the PhnJ which produces methane and α-D-ribose-1,2-cyclic phosphate 5-phosphate (PRcP). The *phnJ* is used as the general marker gene for the C-P lyase pathway (Murphy et al. 2021). PRcP is then further transformed by PhnP and PhnN before being funnelled into the primary metabolism.

The known expression of the C-P lyase is regulated by the pho regulon. This is a two component regulatory system that is autophosphorylated in the absence of phosphate (in culture under concentrations of 4 µmol L^{-1}) and also activates high affinity phosphate transporters in addition to the C-P lyase pathway (Santos-Beneit 2015; Stosiek et al. 2020; Wanner 1996). However, the environmental regulation is likely different, as almost all marine environments have Pi concentrations below 4 µmol L^{-1} (Karl 2014). Additionally, in experiments with MPn and Pi in equimolar additions, methane formation was still observed in culture (Beversdorf et al. 2010; Del Valle & Karl 2014), freshwater (Yao et al. 2016) and marine environments (Del Valle & Karl 2014; Karl et al. 2008). Teikari et al. (2018) also only observed an upregulation of the C-P lyase pathway in the presence of phosphonates not solely in the absence of Pi. Thus, the exact regulation remains to be determined and may be species specific.

Metagenomic analysis has revealed that the C-P lyase pathway is more widespread than the phosphonate synthesis pathway (Acker et al. 2022; Coleman & Chisholm 2010; Lockwood et al. 2022; Martinez et al. 2010; Martínez et al. 2013; Sosa et al. 2019a; Villarreal-Chiu et al. 2012). Around 38% of all microorganisms have the capacity to degrade phosphonates (Villarreal-Chiu et al. 2012). The pathway has an inverse correlation with *in-situ* Pi concentrations, especially in the epipelagic (Sosa et al. 2019a), strongly suggesting that the primary use is the acquisition of

phosphorus. As such, it is especially enriched in the surface waters of the North Atlantic and Mediterranean (Sosa et al. 2019a). The primary organisms responsible are *Cyanobacteria* (Dyhrman et al. 2006; Martinez et al. 2010; Teikari et al. 2018) and *SAR11* (Carini et al. 2014) but the C-P lyase pathway is also found in eukaryotes such as *Emiliania huxleyi (CCMP 2090)* and *Micromonas commoda (CCMP 2709*; Whitney & Lomas 2019).

3) Nitrous oxide

Nitrous oxide budget

Nitrous oxide (N_2O) is a naturally occurring greenhouse gas with an atmospheric concentration of ~336.33 parts per billion (NOA, 2022), which is an estimated 25% higher than its pre-industrial levels of 270 ± 6 parts per billion (Intergovernmental Panel on Climate Change 2023d). While its concentration is an order of magnitude below that of methane, its potency arises from a long atmospheric residence time of 116 ± 9 years (Prather et al. 2015) and its ozone depleting capabilities (Portmann et al. 2012; Ravishankara et al. 2009). As such, the global warming potential for N_2O is 273 ± 130 times higher than that of carbon dioxide over a 100-year time period (Intergovernmental Panel on Climate Change 2023e) and its effective radiative forcing is considered ~ 6% (Intergovernmental Panel on Climate Change 2023d). This is likely to increase, as its atmospheric growth in the last decade was 0.95 ± 0.04 parts per billion $year^{-1}$ (Intergovernmental Panel on Climate Change 2023d), accelerating from previous decades. Simultaneously, through the decrease of the anthropogenic halogenated chlorofluorocarbons, it has become the most prevalent ozone depleting substance in the atmosphere (Portmann et al. 2012). Its atmospheric sink occurs through photolysis and the reaction with excited oxygen atoms (McElroy et al. 1976).

The increase in atmospheric N_2O is mainly driven by the ongoing anthropogenic perturbations with combined emissions of 7.3 (4.2 - 11.4) Tg N yr^{-1} (Tian et al. 2020; Figure 5). Of these, the bulk stem from extensive fertiliser usage in agricultural practices, which has led to an estimated increase of 31 ± 0.5 parts per billion between 1980 – 2019 (Tian et al. 2020). The natural flux exceeds the anthropogenic one with 9.7 (8 - 12) Tg N yr^{-1}, with soils dominating. However, unlike methane, the marine contributions are also substantial, estimated as 3.7 (2.8 - 4.7) Tg N yr^{-1}, including rivers and the coastal zones, or around 33% of the total natural emissions (Intergovernmental Panel on Climate Change 2023d; Tian et al. 2020). Marine emissions are not

homogeneously distributed, with oxygen minimum zones, especially in coastal upwelling systems contributing around 20 - 35% of these emissions, despite only making up 1 - 3% of the ocean area (Arévalo-Martínez et al. 2015; Lam & Kuypers 2011; Yang et al. 2020). Oxygen minimum zones can be characterised by low oxygen concentrations (< 20 umol L^{-1}; Lam & Kuypers 2011) which can either be transient or permanent and result from a combination of sluggish local circulation (Wyrtki 1962) and enhanced remineralisation rates that deplete oxygen. In these environments, especially at the oxic-anoxic interface, also referred to as the oxycline, the conditions enable the two main biotic pathways related to N_2O formation, aerobic ammonia oxidation and denitrification to contribute to the N_2O cycling (Babbin et al. 2015).

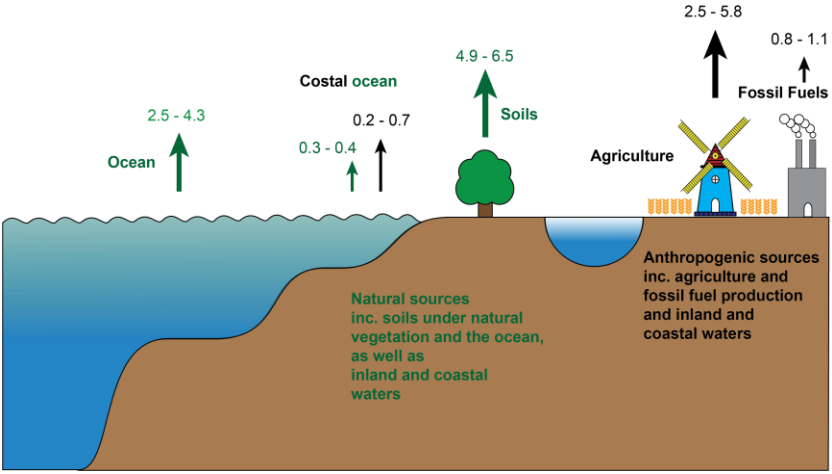

Figure 5. **Sketch of major contributors to nitrous oxide emissions from both natural and anthropogenic sources.** Estimates were taken from Tian et al. (2020) and the Intergovernmental Panel on Climate Change (2023d). All values are in Tg N yr^{-1}.

Ammonia oxidation

One of the two primary biotic pathways that leads to the formation of N_2O is aerobic ammonia oxidation (Santoro et al. 2011; Yoshida & Alexander 1970). Ammonia oxidation was first documented by Schloesing & Muntz (1877) and characterises the stepwise oxidation of ammonia to nitrite (Winogradsky, 1890). While ammonia is always the substrate, it has been shown that

many ammonia oxidisers can also use simple organic nitrogen compounds such as urea or cyanate for ammonia oxidation (e.g. Kitzinger et al. 2019). The nitrite formation is the first step of nitrification, which includes the subsequent oxidation of nitrite to nitrate by separate nitrite oxidisers (Costa et al. 2006). More recently, the two processes were shown to occur within the same organism (Daims et al. 2015; Van Kessel et al. 2015), with the capacity to form N_2O (Kits et al. 2019). However, so far, complete ammonia oxidisers appear to be largely absent from the ocean (Daims et al. 2015). Nitrification is vital for generating nitrite and nitrate that are required for "new production" (Yool et al. 2007), as well as nitrogen reducing reactions (Kuypers et al. 2018). In the marine environment, ammonia oxidation is conducted by two separate chemolithoautotrophic groups of organisms, the ammonia oxidising bacteria (AOB) and the ammonia oxidising archaea (AOA), of which the latter are considered to be the dominant organisms in most marine environments (Francis et al. 2005; Wuchter et al. 2006). While the substrate and the product are the same for the two groups, there are notable differences in the biochemistry of ammonia oxidation, especially regarding the formation of N_2O (Figure 6).

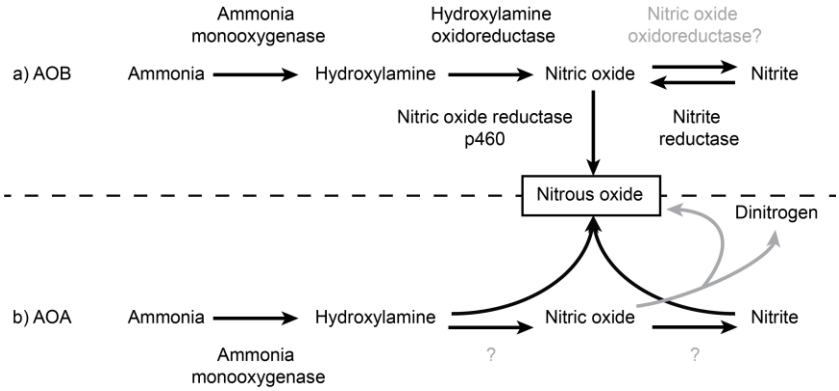

Figure 6. **Aerobic ammonia oxidation and nitrous oxide formation pathways. a,** Ammonia oxidising bacteria. The ammonia oxidation pathway is almost completely resolved (Lancaster et al. 2018) and N_2O can be formed from nitrifier-denitrifcation (Wrage-Mönnig et al. 2018) as well as from hydroxylamine oxidation over nitric oxide (Caranto et al. 2016; Kozlowski et al. 2014). **b**, Ammonia oxidising archaea do not have an enzymatically resolved ammonia oxidation pathway (Prosser et al. 2020) but can form N_2O through a hybrid formation pathway (Kozlowski et al. 2016;

Stein et al. 2021) and possibly through nitric oxide dismutation (Kraft et al. 2022). Grey colours indicate enzymatically unresolved.

Biochemistry of ammonia oxidation and nitrous oxide formation

In both AOB and AOA, the first step of ammonia oxidation is the aerobic oxidation of ammonia to hydroxylamine by the ammonia monooxygenase (AMO; Hooper et al. 1997; Vajrala et al. 2013). The AMO is a copper-based membrane bound oxygenase closely related to the methane monooxygenase (Hakemian & Rosenzweig 2007; Prosser et al. 2020). As such, both enzymes can oxidise each other's substrates, ammonia to hydroxylamine or methane to methanol, however inefficiently (Arp & Stein 2003; Stein & Klotz 2011). The AMO is encoded by a gene complex, of which the *amoA* encoding for the alpha subunit is used as the marker gene for the process (Rotthauwe et al. 1997). Despite the similar reaction, the amino acid identity between the bacterial and archaeal AMO is only 40% (Stahl & de la Torre 2012), thus AMO analysis in conjunction with 16S rRNA can help distinguish between AOB and AOA (Tourna et al. 2008).

In AOB, hydroxylamine is oxidised to nitric oxide by the hydroxylamine oxidoreductase (HAO; Caranto & Lancaster 2017) and subsequently nitric oxide is converted to nitrite. To date, the enzyme responsible for the oxidation of nitric oxide to nitrite, a nitric oxide oxidoreductase (NOO) remains to be clearly identified (Lancaster et al. 2018; Prosser et al. 2020). AOA lack any known homologue of the HAO or a NOO (Lancaster et al. 2018; Prosser et al. 2020), thus the process remains to be elucidated enzymatically. Nevertheless, isotope analysis has revealed that ammonia oxidation in AOA functions similarly to AOB (Santoro et al. 2011), including with nitric oxide as an intermediate (Kozlowski et al. 2016; Lancaster et al. 2018).

The predominant pathway of N_2O formation by AOB is through nitrifier-denitrification (Goreau et al. 1980; Prosser et al. 2020; Wrage-Mönnig et al. 2018). This process characterises the subsequent reduction of the formed nitrite to N_2O over nitric oxide. This reaction uses the same enzymes as denitrification (see below) but to date there has been no evidence for a nitrous oxide reductase in AOB (Prosser et al. 2020). Therefore, N_2O is always the final product. Nitrifier-denitrification occurs primarily under low oxygen concentrations (Goreau et al. 1980; Kozlowski et al. 2014, 2016) but not under anoxia. Unlike in denitrifiers, this process generates little energy (Wrage-Mönnig et al. 2018) and is primarily thought to be used to get rid of excess electrons at high ammonia concentrations (Hink et al. 2017) or used to detoxify nitrite (Arp & Stein 2003).

However, not all N_2O from AOB is formed via nitrifier-denitrification. N_2O can also be produced from hydroxylamine oxidation to nitrite and subsequent reduction to N_2O. This can occur enzymatically either through the cytochrome p460 under anaerobic conditions (Caranto et al. 2016) or by a nitric oxide reductase (Hooper & Terry 1979; Kozlowski et al. 2014).

The primary mechanism of N_2O formation in AOA is different to that of AOB (Figure 6). Firstly, despite many AOAs having a nitrite reductase that may be directly involved in the ammonia oxidation process (Kozlowski et al. 2016), AOAs lack a nitric oxide reductase (Prosser et al. 2020). Therefore, AOA are unable to conduct nitrifier-denitrification or form N_2O enzymatically from nitric oxide reduction during ammonia oxidation. Nevertheless, culture work has demonstrated that AOAs have the capacity to form N_2O during ammonia oxidation under both fully oxic and low oxygen concentrations (Löscher et al. 2012; Santoro et al. 2011; Stieglmeier et al. 2014; Qin et al. 2017). For the N_2O formation, a hybrid pathway has been proposed, where one nitrogen originates from hydroxylamine and is combined with the another originating from nitrite, possibly in the form of nitric oxide (Kozlowski et al. 2016). This reaction is thought to be abiotic but relies on the sufficient supply of the intermediates to take place and is further facilitated by redox-active transition metals (Stein et al. 2021). However, recently it has been shown that viable cells are required for the hybrid formation of N_2O when using hydroxylamine and nitrite, possibly to form nitric oxide enzymatically (Wan et al. 2023). Another pathway of N_2O formation is under low pH conditions catalysed by the cytochrome p450 but this has only been observed in soils so far (Jung et al. 2019). Recently, nitric oxide dismutation to oxygen and N_2 over the intermediate of N_2O has been proposed for the AOA *Nitrosopumilus maritimus* (Kraft et al. 2022). However, this process is not resolved enzymatically and the environmental relevance remains to be assessed. A complication in resolving the N_2O forming mechanisms from ammonia oxidation is that hydroxylamine, nitric oxide and nitrite all have the capacity to abiotically lead to the formation of N_2O (Wan et al. 2023; Zhu-Barker et al. 2015).

Ammonia oxidation in the ocean

Within the marine environment, the AOA are considered as the dominant organisms, making up to 30% of all cells below the thermocline (Karner et al. 2001). Taxonomically, they all belong to the *Thaumarchaeota* (Brochier-Armanet et al. 2008; Spang et al. 2010). Their dominance over the AOB has been attributed to a higher affinity for ammonia (Hink et al. 2018; Martens-Habbena et

al. 2009) as well as a high affinity for oxygen (Bristow et al. 2016). The former enables them to thrive in vast oligotrophic areas with trace amounts of ammonium and the latter aids them in inhabiting and thriving in oxygen-limited environments, especially along the oxycline (Lam et al. 2009; Stewart et al. 2012). Their genes have also been found within the anoxic core (Stewart et al. 2012). The AOB which belong to the *Beta*- and *Gammaproteobacteria* can also be found in the marine environment (Purkhold et al. 2000) but are usually located in areas of high ammonia concentrations (Jia & Conrad 2009) such as coastal waters and estuaries. Ammonia oxidisers are therefore not only cosmopolitan but also highly abundant. Therefore, despite forming N_2O primarily as a by-product, they contribute as much as 80% of the N_2O formation within the marine environment (Freing et al. 2012; Ji et al. 2018).

Denitrification

The second significant biological source of N_2O is denitrification, which is also simultaneously the only biologically significant sink of N_2O. Similar to ammonia oxidation, denitrification was first documented in the 19th century (Gayon & Dupetit 1886; Payne 1986). Conventional denitrification describes the stepwise reduction of nitrate to N_2 over the intermediates of nitrite, nitric oxide and nitrous oxide (e.g. Zumft 1997; Hutchins and Capone 2022; Figure 7). This is a process of anaerobic respiration, with nitrate being the second most energetic electron acceptor behind oxygen (Froelich et al. 1979). While most denitrification is considered to be heterotrophic (Zumft 1997), the process can be methanotrophic (Oswald et al. 2017) and lithotrophic (e.g. Canfield et al. 2010). Lithotrophic denitrification can use electron donors such as sulphide and elemental sulphur, among others and can be either autotrophic or heterotrophic (Callbeck et al. 2021). This can be advantageous, as the electron donor is generally considered the limiting substrate for water column denitrification (Ward et al. 2008). While initial research focused on conventional denitrification, it has become apparent that many organisms have the genetic potential to conduct individual steps of denitrification, so that the process can be divided among different organisms (Garrido-Amador et al. 2021; Lycus et al. 2017; Marchant et al. 2018). This can lead to the accumulation of the intermediates in the environment, such as N_2O. Interestingly, denitrification can be conducted by all three domains of life, including bacteria (Zumft 1997), archaea (Cabello et al. 2004) and eukaryotes such as foraminifera (Risgaard-Petersen et al. 2006) and fungi (Shoun et al. 1992). Of these, fungal denitrification is especially interesting as it combines a nitrogen from an organic source with either nitrate or nitrite (Tanimoto et al. 1992),

which gives the formed N_2O a distinct signal when investigating with stable isotope incubations. Furthermore, fungi lack the nitrous oxide reductase (Richards et al. 2012) making them potential net producers of N_2O in the environment, although their overall contribution remains to be elucidated (Peng & Valentine 2021; Wankel et al. 2017).

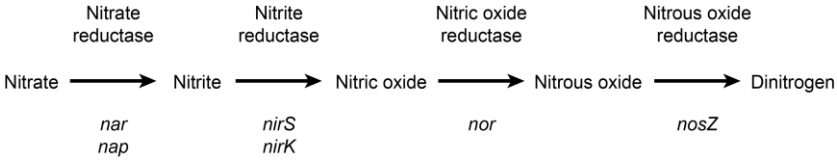

Figure 7. **Denitrification pathway.** Adapted from Kuypers et al. (2018).

Biochemistry of denitrification

Dissimilatory nitrate reduction to nitrite is facilitated by either a periplasmic nitrate reductase or a membrane bound nitrate reductase which are encoded by the *nap* and *nar* gene complex respectively (Moreno-Vivián et al. 1999). Respiratory nitrite reduction to nitric oxide is facilitated by one of two nitrite reductases which are both located in the periplasmic space. These are either the cytochrome-containing one, encoded by the *nirS*, or the copper-containing one, encoded by the *nirK* (Maia & Moura 2014; Zumft 1997). These enzymes are not restricted to denitrifiers. For example, the *nirK* can be found in ammonia oxidisers (Bartossek et al. 2010; Kozlowski et al. 2014; Lund et al. 2012) and the *nirS* in anaerobic ammonia oxidisers (anammox bacteria; Li et al. 2011). Respiratory nitric oxide reduction to N_2O is conducted by nitric oxide reductases of the heme-copper oxidoreductases superfamily that include the cNOR and qNOR (Zumft 2005). However, recently several more nitric oxide reductases have been proposed, including bNOR, eNOR, gNOR, nNOR and sNOR (Murali et al. 2021) of which the eNOR has been shown *in-vivo* and *in-vitro* to conduct nitric oxide reduction. Furthermore, due to the toxic nature of nitric oxide, there are several additional enzyme mediated detoxification processes that lead to the formation of N_2O, such as by a flavorubredoxin nitric oxide reductase (Saraiva et al. 2004).

The final step of denitrification, the reduction of nitrous oxide to di-nitrogen gas is conducted by the copper containing nitrous oxide reductase which is encoded by the *nos* gene complex (Zumft 1997) for which the *nosZ* is the marker gene (Horn et al. 2006). Additionally, there are two clades

of *nosZ*. Clade I is most often associated with conventional denitrifiers while clade II is found mainly in organisms that lack other denitrification genes (Jones et al. 2013; Sanford et al. 2012). Thus the clade II is thought to suggest N_2O reducing specialists, which is supported by the higher affinity for N_2O (Yoon et al. 2016) although this may not be universal (Conthe et al. 2018). Out of all the denitrification genes, the *nosZ* is often thought to be the most sensitive to oxygen concentrations and thus the first to be inhibited (Morley et al. 2008).

Denitrification in the ocean

In the marine environment denitrification is primarily restricted to anaerobic environments such as sediments (Devol 2015) as well as oxygen minimum zones (Lam & Kuypers 2011) and anoxic microniches, for example in organic particles (Ganesh et al. 2015; Karthäuser et al. 2021). Due to the oxygen sensitivity of the individual enzymes, individual steps of denitrification can be repressed. For example, Dalsgaard et al. (2014) found that oxygen concentrations of 300 nmol L^{-1} were enough to suppress both N_2O and N_2 formation by 50% as well as reduce nitrite reduction rates to nitric oxide. Comparatively, nitrate reduction rates to nitrite could still be observed at 25 µmol L^{-1} of oxygen (Kalvelage et al. 2013). Therefore, the overall consensus is that the anoxic core of the oxygen minimum zone is considered to be a N_2O sink (Kock et al. 2016), opposed to the more dynamic conditions along the oxycline which are a net N_2O source through denitrification (Babbin et al. 2015).

4) Study sites

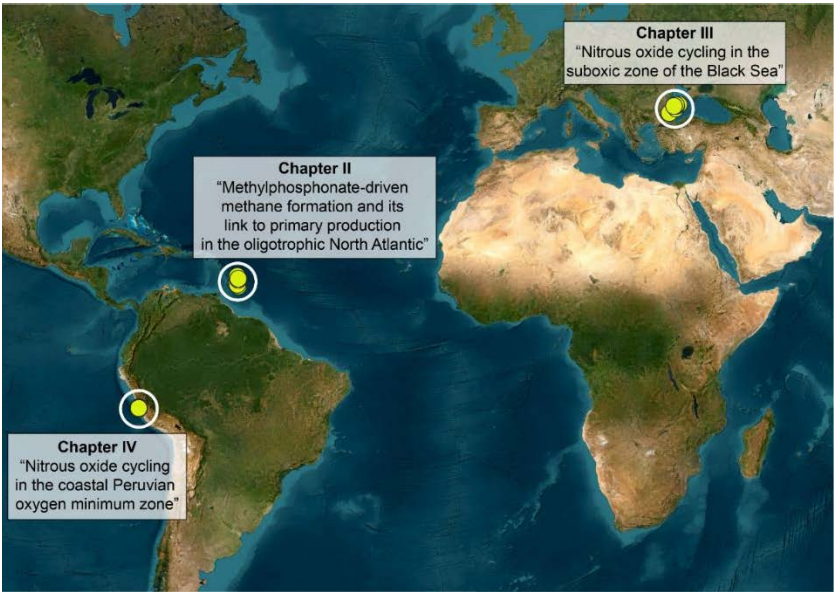

Figure 8. **Sampling sites and titles of chapters II - IV of this thesis.**

Western Tropical North Atlantic

The surface waters of the western tropical North Atlantic are some of the most chronically phosphate (Pi)-limited regions on Earth (Cavender-Bares et al. 2001; Sosa et al. 2019a; Wu et al. 2000). This Pi-limitation is likely due to the increased iron-containing dust depositions in the region which enhances N_2-fixation, further depleting Pi (Wu et al. 2000). However, dissolved organic phosphorus concentrations can reach up to several hundred nanomole per litre in the Pi-limited surface waters (Liang et al. 2022). Therefore, the microbial community is well adapted to use alternative phosphorus sources such as, phosphate-esters (Mather et al. 2008) and phosphonates (Dyhrman et al. 2006; Sosa et al. 2020), as well as inorganic phosphite (Van Mooy et al. 2015). In conjunction with the phosphate limitation, the surface waters of the region are also slightly supersaturated with methane (Holmes et al. 2000; Kolomijeca et al. 2022; Scranton & Brewer 1977). While extensive metagenomic analysis has shown the prevalence of the C-P lyase

pathway in the region (Lockwood et al. 2022; Martínez et al. 2013; Sosa et al. 2019a; Villarreal-Chiu et al. 2012), only a single study has measured rates of MPn-driven methane formation around the area North of Bermuda (Sosa et al. 2020). The western tropical North Atlantic therefore provides the perfect environment to confirm the presence of MPn-driven methane formation as well as to test controlling physico-chemical factors that have so far remained underexplored.

Black Sea

The Black Sea is the largest meromictic basin in the world with a deep sulphidic, methane and ammonium rich anoxic core which is separated from the oxic water column by a 20 - 50 m thick suboxic zone (Murray 1989; Murray et al. 1995). This feature of permanent stratification is a result of the limited water exchange with the Mediterranean Sea over the Bosporus straits in conjunction with the high riverine freshwater inflow. The suboxic zone, which was discovered in the 1980s (Murray 1989; Murray et al. 1989), is characterised by oxygen concentrations below 10 µmol L^{-1} and low concentrations of sulphide (Murray et al. 1995). The permanent stratification ensures that certain nutrient species, such as nitrite and nitrate can be found on lines of equal density within the suboxic zone (Murray et al. 1995), where nitrogen transformation processes occur (Fuchsman et al. 2019; Jensen et al. 2008; Kuypers et al. 2003; Lam et al. 2007; Ward & Kilpatrick 1991; Westley et al. 2006). However, unlike other oxygen-limited environments, the Black Sea is only a minor source of N_2O emissions (Amouroux et al. 2002; Bange et al. 2019; Westley et al. 2006), despite limited evidence of an active N_2O cycle within the suboxic zone (Westley et al. 2006). Furthermore, the Black Sea is considered to have a low microbial species richness compared to other anoxic environments (Francis et al. 2005; Oakley et al. 2007). This makes the Black Sea an interesting model system to investigate the lack of N_2O accumulation in a permanently stratified oxygen-limited environment.

Coastal Peruvian oxygen minimum zone

The Peruvian oxygen minimum zone is located in the eastern tropical South Pacific upwelling system (ETSP). Here, oxygen poor but nutrient rich water is upwelled to the surface through wind induced Ekman transport (Chavez & Messié 2009). These nutrients stimulate primary productivity, making the ETSP one of the most productive regions on Earth (Messié et al. 2009; Pauly & Christensen 1995). High respiration rates combined with local sluggish ventilation lead to the formation of one of the largest oxygen minimum zones, extending 1000 km from the

Peruvian shelf into the Pacific Ocean (Fuenzalida et al. 2009). The Peruvian oxygen minimum zone is considered the single largest source of N_2O from the marine environment, contributing up to 0.9 Tg N yr^{-1} (Arévalo-Martínez et al. 2015; Yang et al. 2020). Both ammonia oxidation and denitrification have been shown to contribute significantly to this flux (Dalsgaard et al. 2014; Frey et al. 2020; Ji et al. 2015; Lam et al. 2009). However, to date, most of the research has focused on the offshore oxygen minimum zone and not the extremely shallow coastal area, which may be even more important for N_2O emissions (Arévalo-Martínez et al. 2015; Frey et al. 2020; Kock et al. 2016).

5) Aims and Outline

The aim of this thesis was to explore both aerobic methane formation and nitrous oxide cycling in understudied environments, in addition to gaining insights into the microorganisms responsible and the controlling environmental parameters. To study these topics, my research focused on conducting experiments in the field (Figure 8). I used stable isotope incubation experiments to determine rates of the individual processes at close to *in-situ* conditions. Those measurements were complemented by investigations of physico-chemical parameters to determine the potential controlling factors. Finally, metagenomic and metatranscriptomic analyses were conducted to look at the microbial community, specifically at key genes involved in the investigated processes.

In **chapter II**, we investigated **"Methylphosphonate (MPn)-driven methane formation and its link to primary production in the oligotrophic North Atlantic"**. This study aimed to confirm, for the first time with rate measurements, MPn-driven methane formation in the Tropical North Atlantic Ocean and investigate the depth distribution of this process in the upper 200 metres of the water column. We conducted stable isotope incubation experiments over 48 hours with ^{13}C-MPn to determine rates of ^{13}C-methane formation. Additional experiments looked at the effect of either phosphate or nitrate on MPn-driven methane formation. Incubations were also conducted with ^{13}C-DIC to test the viability of the compound as a precursor for aerobic methane formation as was previously proposed (Bižić et al. 2020; Lenhart et al. 2016; Perez-Coronel & Michael Beman 2022). Analysis of the *phnJ* gene in different size fractions enabled us to characterise the microbial community responsible for the conversion of MPn to methane. Finally, to assess the potential of this pathway for liberating phosphate for the autotrophic community, we quantified the phosphorus requirements based on the rates of carbon fixation.

Chapters III and IV are dedicated to the investigation of nitrous oxide (N_2O) cycling in two contrasting oxygen-limited environments. **Chapter III** investigated **"Nitrous oxide cycling in the suboxic zone of the Black Sea"**, a system that only emits small amounts of N_2O despite indications of an active cycle (Westley et al. 2006). We conducted stable isotope incubation experiments close to *in-situ* conditions to quantify rates of N_2O formation from denitrification (^{15}N-nitrite) and ammonia oxidation (^{15}N-ammonium) as well as N_2O consumption rates (^{15}N-N_2O). Additionally, we quantified the associated processes of ammonia oxidation to nitrite and complete denitrification to N_2 from nitrite, as well as physico-chemical parameters to contextualise

the N_2O formation rates. Finally, we investigated the microbial community responsible for the measured rates by looking at the functional genes of denitrification and the *amoA* for ammonia oxidation.

In **Chapter IV,** we investigated N_2O cycling in the coastal Peruvian oxygen minimum zone. While there has been extensive work conducted on N_2O cycling in this environment, it has mostly focused on the offshore oxygen minimum zone. There has been evidence that both N_2O concentrations and N_2O cycling may be more intense closer to the coastline (Arévalo-Martínez et al. 2015; Frey et al. 2020; Kock et al. 2016). Therefore, we used a smaller vessel to sample the water column close to the shore (water depths between 45 - 92m). We conducted extensive stable isotope incubation experiments looking at N_2O formation from denitrification (^{15}N-nitrate and ^{15}N-nitrite) and ammonia oxidation (^{15}N-ammonium), as well as N_2O reduction (^{15}N-N_2O), including the associated processes. Furthermore, we quantified N_2O concentrations within the water column and looked at physico-chemical parameters, including particle abundances to investigate controlling factors of the observed rates.

Bibliography

Acker M, Hogle SL, Berube PM, Hackl T, Coe A, et al. 2022. Phosphonate production by marine microbes: Exploring new sources and potential function. *Proc. Natl. Acad. Sci. U. S. A.* 119(11):

Amouroux D, Roberts G, Rapsomanikis S, Andreae MO. 2002. Biogenic gas (CH4, N2O, DMS) emission to the atmosphere from near-shore and shelf waters of the north-western Black Sea. *Estuar. Coast. Shelf Sci.* 54(3):575–87

Arévalo-Martínez DL, Kock A, Löscher CR, Schmitz RA, Bange HW. 2015. Massive nitrous oxide emissions from the tropical South Pacific Ocean. *Nat. Geosci.* 8(7):530–33

Arp DJ, Stein LY. 2003. Metabolism of Inorganic N Compounds by Ammonia-Oxidizing Bacteria. *Crit. Rev. Biochem. Mol. Biol*. 38(6):471–95

Babbin AR, Bianchi D, Jayakumar A, Ward BB. 2015. Rapid nitrous oxide cycling in the suboxic ocean. *Science (80-.).* 348(6239):1127–29

Balch WE, Fox GE, Magrum LJ, Woese CR, Wolfe RS. 1979. Methanogens: reevaluation of a unique biological group. *Microbiol. Rev.* 43(2):260–96

Bange HW, Arévalo-Martínez DL, Paz M de la, Farías L, Kaiser J, et al. 2019. A harmonized nitrous oxide (N2O) ocean observation network for the 21st century. *Front. Mar. Sci.* 6(APR):1–10

Barnes RO, Goldberg ED. 1976. Methane production and consumption in anoxic marine sediments. *Geology*. 4(5):297–300

Bartossek R, Nicol GW, Lanzen A, Klenk HP, Schleper C. 2010. Homologues of nitrite reductases in ammonia-oxidizing archaea: Diversity and genomic context. *Environ. Microbiol.* 12(4):1075–88

Berg A, Lindblad P, Svensson BH. 2014. Cyanobacteria as a source of hydrogen for methane formation. *World J. Microbiol. Biotechnol.* 30(2):539–45

Beversdorf LJ, White AE, Björkman KM, Letelier RM, Karl DM. 2010. Phosphonate metabolism by Trichodesmium IMS101 and the production of greenhouse gases. *Limnol. Oceanogr.* 55(4):1768–78

Bianchi M, Marty D, Teyssie JL, Fowler SW. 1992. Strictly aerobic and anaerobic bacteria associated with sinking particulate matter and zooplankton fecal pellets. *Mar. Ecol. Prog. Ser.* 88(1):55–60

Bižić M, Klintzsch T, Ionescu D, Hindiyeh MY, Günthel M, et al. 2020. Aquatic and terrestrial cyanobacteria produce methane. *Sci. Adv.* 6(3):1–10

Born DA, Ulrich EC, Ju KS, Peck SC, Van Der Donk WA, Drennan CL. 2017. Structural basis for methylphosphonate biosynthesis. *Science (80-.).* 358(6368):1336–39

Breitburg D, Levin LA, Oschlies A, Grégoire M, Chavez FP, et al. 2018. Declining oxygen in the global ocean and coastal waters. *Science (80-.).* 359(6371):

Bristow LA, Dalsgaard T, Tiano L, Mills DB, Bertagnolli AD, et al. 2016. Ammonium and nitrite oxidation at nanomolar oxygen concentrations in oxygen minimum zone waters. *Proc. Natl. Acad. Sci. U. S. A.* 113(38):10601–6

Bristow LA, Mohr W, Ahmerkamp S, Kuypers MMM. 2017. Nutrients that limit growth in the ocean. *Curr. Biol.* 27(11):R474–78

Brochier-Armanet C, Boussau B, Gribaldo S, Forterre P. 2008. Mesophilic crenarchaeota: Proposal for a third archaeal phylum, the Thaumarchaeota. *Nat. Rev. Microbiol.* 6(3):245–52

Cabello P, Roldán MD, Moreno-Vivián C. 2004. Nitrate reduction and the nitrogen cycle in archaea. *Microbiology*. 150(11):3527–46

Callbeck CM, Canfield DE, Kuypers MMM, Yilmaz P, Lavik G, et al. 2021. Sulfur cycling in oceanic oxygen minimum zones. *Limnol. Oceanogr.* 66(6):2360–92

Canfield DE, Stewart FJ, Thamdrup B, De Brabandere L, Dalsgaard T, et al. 2010. A cryptic sulfur cycle in oxygen-minimum-zone waters off the Chilean coast. *Science (80-.).* 330(6009):1375–78

Caranto JD, Lancaster KM. 2017. Nitric oxide is an obligate bacterial nitrification intermediate produced by hydroxylamine oxidoreductase. *Proc. Natl. Acad. Sci. U. S. A.* 114(31):8217–22

Caranto JD, Vilbert AC, Lancaster KM. 2016. Nitrosomonas europaea cytochrome P460 is a direct link between nitrification and nitrous oxide emission . *Proc. Natl. Acad. Sci.* 113(51):14704–9

Carini P, White AE, Campbell EO, Giovannoni SJ. 2014. Methane production by phosphate-starved SAR11 chemoheterotrophic marine bacteria. *Nat. Commun.* 5:1–7

Cavender-Bares KK, Karl DM, Chisholm SW. 2001. Nutrient gradients in the western North Atlantic Ocean: Relationship to microbial community structure and comparison to patterns in the Pacific Ocean. *Deep. Res. Part I Oceanogr. Res. Pap.* 48(11):2373–95

Chavez FP, Messié M. 2009. A comparison of Eastern Boundary Upwelling Ecosystems. *Prog. Oceanogr.* 83(1–4):80–96

Cicerone RJ, Oremland RS. 1988. Biogeochemical aspects of atmospheric methane. *Global Biogeochem. Cycles*. 2(4):299–327

Clark LL, Ingall ED, Benner R. 1999. Marine organic phosphorus cycling: Novel insights from nuclear magnetic resonance. *Am. J. Sci.* 299(7–9):724–37

Coleman ML, Chisholm SW. 2010. Ecosystem-specific selection pressures revealed through comparative population genomics. *Proc. Natl. Acad. Sci. U. S. A.* 107(43):18634–39

Conthe M, Wittorf L, Kuenen JG, Kleerebezem R, Van Loosdrecht MCM, Hallin S. 2018. Life on N2O: Deciphering the ecophysiology of N2O respiring bacterial communities in a continuous culture. *ISME J.* 12(4):1142–53

Costa E, Pérez J, Kreft JU. 2006. Why is metabolic labour divided in nitrification? *Trends Microbiol.* 14(5):213–19

Daims H, Lebedeva E V., Pjevac P, Han P, Herbold C, et al. 2015. Complete nitrification by Nitrospira bacteria. *Nature*. 528(7583):504–9

Dalsgaard T, Stewart FJ, Thamdrup B, De Brabandere L, Revsbech NP, et al. 2014. Oxygen at nanomolar levels reversibly suppresses process rates and gene expression in anammox and denitrification in the oxygen minimum zone off Northern Chile. *MBio*. 5(6):1–14

Damm E, Helmke E, Thoms S, Schauer U, Nöthig E, et al. 2010. Methane production in aerobic oligotrophic surface water in the central Arctic Ocean. *Biogeosciences*. 7(3):1099–1108

Daughton CG, Cook AM, Alexander M. 1979. Biodegradation of phosphonate toxicants yields methane or ethane on cleavage of the C-P bond. *FEMS Microbiol. Lett.* 5(2):91–93

Del Valle DA, Karl DM. 2014. Aerobic production of methane from dissolved water-column methylphosphonate and sinking particles in the North Pacific Subtropical Gyre. *Aquat. Microb. Ecol.* 73(2):93–105

Denny M. 2012. *How the Ocean Works*. Princeton University Press

Devol AH. 2015. Denitrification, anammox, and N2 production in marine sediments. *Ann. Rev. Mar. Sci.* 7:403–23

Diaz RJ, Rosenberg R. 2008. Spreading dead zones and consequences for marine ecosystems. *Science (80-.).* 321(5891):926–29

Doney SC, Fabry VJ, Feely RA, Kleypas JA. 2009. Ocean acidification: The other CO2 problem. *Ann. Rev. Mar. Sci.* 1:169–92

Dyhrman ST, Benitez-Nelson CR, Orchard ED, Haley ST, Pellechia PJ. 2009. A microbial source of phosphonates in oligotrophic marine systems. *Nat. Geosci.* 2(10):696–99

Dyhrman ST, Chappell PD, Haley ST, Moffett JW, Orchard ED, et al. 2006. Phosphonate utilization by the globally important marine diazotroph Trichodesmium. *Nature*. 439(7072):68–71

Ernst L, Steinfeld B, Barayeu U, Klintzsch T, Kurth M, et al. 2022. Methane formation driven by reactive oxygen species across all living organisms. *Nature*. 603(7901):482–87

Etminan M, Myhre G, Highwood EJ, Shine KP. 2016. Radiative forcing of carbon dioxide, methane, and nitrous oxide: A significant revision of the methane radiative forcing. *Geophys. Res. Lett.* 43(24):12,614-12,623

Feingersch R, Philosof A, Mejuch T, Glaser F, Alalouf O, et al. 2012. Potential for phosphite and phosphonate utilization by Prochlorococcus. *ISME J.* 6(4):827–34

Francis CA, Roberts KJ, Beman JM, Santoro AE, Oakley BB. 2005. Ubiquity and diversity of ammonia-oxidizing archaea in water columns and sediments of the ocean. *Proc. Natl. Acad. Sci.* 102(41):14683–88

Freing A, Wallace DWR, Bange HW. 2012. Global oceanic production of nitrous oxide. *Philos. Trans. R. Soc. B Biol. Sci.* 367(1593):1245–55

Frey C, Bange HW, Achterberg EP, Jayakumar A, Löscher CR, et al. 2020. Regulation of nitrous oxide production in low-oxygen waters off the coast of Peru. *Biogeosciences*. 17(8):2263–87

Froelich PN, Klinkhammer GP, Bender ML, Luedtke NA, Heath GR, et al. 1979. Early oxidation of organic matter in pelagic sediments of the eastern equatorial Atlantic: suboxic diagenesis. *Geochim. Cosmochim. Acta*. 43(7):1075–90

Fuchsman CA, Paul B, Staley JT, Yakushev E V., Murray JW. 2019. Detection of Transient Denitrification During a High Organic Matter Event in the Black Sea. *Global Biogeochem. Cycles*. 33(2):143–62

Fuenzalida R, Schneider W, Garcés-Vargas J, Bravo L, Lange C. 2009. Vertical and horizontal extension of the oxygen minimum zone in the eastern South Pacific Ocean. *Deep. Res. Part II Top. Stud. Oceanogr.* 56(16):992–1003

Gama SR, Vogt M, Kalina T, Hupp K, Hammerschmidt F, et al. 2019. An Oxidative Pathway for Microbial Utilization of Methylphosphonic Acid as a Phosphate Source. *ACS Chem. Biol.* 14(4):735–41

Ganesh S, Bristow LA, Larsen M, Sarode N, Thamdrup B, Stewart FJ. 2015. Size-fraction partitioning of community gene transcription and nitrogen metabolism in a marine oxygen minimum zone. *ISME J.* 9(12):2682–96

Garrido-Amador P, Kniaziuk M, Vekeman B, Kartal B. 2021. Learning from microorganisms: using new insights in microbial physiology for sustainable nitrogen management. *Curr. Opin. Biotechnol.* 67:42–48

Gayon U. and Dupetit G. 1886. Recherches sur la reduction des nitrates par les infiniment petits. *Mem. Sot. Sci. Phys. Nat. Bordeaux Ser.* 3. 2:201-307.

Goreau TJ, Kaplan WA, Wofsy SC, McElroy MB, Valois FW, Watson SW. 1980. Production of NO 2 - and N2O by Nitrifying Bacteria at Reduced Concentrations of Oxygen. *Appl. Environ. Microbiol.* 40(3):526–32

Gruber N, Bakker DCE, DeVries T, Gregor L, Hauck J, et al. 2023. Trends and variability in the ocean carbon sink. *Nat. Rev. Earth Environ.* 4(2):119–34

Hakemian AS, Rosenzweig AC. 2007. The biochemistry of methane oxidation. *Annu. Rev. Biochem.* 76:223–41

Hink L, Gubry-Rangin C, Nicol GW, Prosser JI. 2018. The consequences of niche and physiological differentiation of archaeal and bacterial ammonia oxidisers for nitrous oxide emissions. *ISME J.* 12(4):1084–93

Hink L, Lycus P, Gubry-Rangin C, Frostegård Å, Nicol GW, et al. 2017. Kinetics of NH3-oxidation, NO-turnover, N2O-production and electron flow during oxygen depletion in model bacterial and archaeal ammonia oxidisers. *Environ. Microbiol.* 19(12):4882–96

Holmes ME, Sansone FJ, Rust TM, Popp BN. 2000. Methane production, consumption, and air-sea exchange in the open ocean: An Evaluation based on carbon isotopic ratios. *Global Biogeochem. Cycles*. 14(1):1–10

Hooper AB, Terry KR. 1979. Hydroxylamine oxidoreductase of Nitrosomonas. Production of nitric oxide from hydroxylamine. *BBA - Enzymol.* 571(1):12–20

Hooper AB, Vannelli T, Bergmann DJ, Arciero DM. 1997. Enzymology of the oxidationof ammonia to nitrate by bacteriaHooper, A. B., Vannelli, T., Bergmann, D. J., & Arciero, D. M. (1997). Enzymology of the oxidationof ammonia to nitrate by bacteria. Antonie van Leeuwenhoek, 71, 59–67. *Antonie Van Leeuwenhoek*. 71:59–67

Horiguchi M, Kandatstu M. 1959. Isolation of 2-Aminoethane Phosphonic Acid from Rumen Protozoa. *Nature*. 184(4690):901–2

Horn MA, Drake HL, Schramm A. 2006. Nitrous oxide reductase genes (nosZ) of denitrifying microbial populations in soil and the earthworm gut are phylogenetically similar. *Appl. Environ. Microbiol.* 72(2):1019–26

Horsman GP, Zechel DL. 2017. Phosphonate Biochemistry. *Chem. Rev.* 117(8):5704–83

Huang J, Su Z, Xu Y. 2005. The evolution of microbial phosphonate degradative pathways. *J. Mol. Evol.* 61(5):682–90

Hutchins DA, Capone DG. 2022. The marine nitrogen cycle: new developments and global change. *Nat. Rev. Microbiol.* 20(7):401–14

Intergovernmental Panel on Climate Change. 2023a. *Framing, Context, and Methods*

Intergovernmental Panel on Climate Change. 2023b. *Future Global Climate: Scenario-Based Projections and Near-Term Information*

Intergovernmental Panel on Climate Change. 2023c. *Ocean, Cryosphere and Sea Level Change*

Intergovernmental Panel on Climate Change. 2023d. *Global Carbon and Other Biogeochemical Cycles and Feedbacks*

Intergovernmental Panel on Climate Change. 2023e. *The Earth's Energy Budget, Climate Feedbacks and Climate Sensitivity*

Jensen MM, Kuypers MMM, Lavik G, Thamdrup B. 2008. Rates and regulation of anaerobic ammonium oxidation and denitrification in the Black Sea. *Limnol. Oceanogr.* 53(1):23–36

Ji Q, Buitenhuis E, Suntharalingam P, Sarmiento JL, Ward BB. 2018. Global Nitrous Oxide Production Determined by Oxygen Sensitivity of Nitrification and Denitrification. *Global Biogeochem. Cycles*. 32(12):1790–1802

Jia Z, Conrad R. 2009. Bacteria rather than Archaea dominate microbial ammonia oxidation in an agricultural soil. *Environ. Microbiol.* 11(7):1658–71

Jones CM, Graf DRH, Bru D, Philippot L, Hallin S. 2013. The unaccounted yet abundant nitrous oxide-reducing microbial community: A potential nitrous oxide sink. *ISME J.* 7(2):417–26

Jung MY, Gwak JH, Rohe L, Giesemann A, Kim JG, et al. 2019. Indications for enzymatic denitrification to N2O at low pH in an ammonia-oxidizing archaeon. *ISME J.* 13(10):2633–38

Kalvelage T, Lavik G, Lam P, Contreras S, Arteaga L, et al. 2013. Nitrogen cycling driven by organic matter export in the South Pacific oxygen minimum zone. *Nat. Geosci.* 6(3):228–34

Kamat SS, Williams HJ, Dangott LJ, Chakrabarti M, Raushel FM. 2013. The catalytic mechanism for aerobic formation of methane by bacteria. *Nature*. 497(7447):132–36

Kamat SS, Williams HJ, Raushel FM. 2011. Intermediates in the transformation of phosphonates to phosphate by bacteria. *Nature*. 480(7378):570–73

Karl DM. 2014. Microbially mediated transformations of phosphorus in the sea: New views of an old cycle. *Ann. Rev. Mar. Sci.* 6:279–337

Karl DM, Beversdorf L, Björkman KM, Church MJ, Martinez A, Delong EF. 2008. Aerobic production of methane in the sea. *Nat. Geosci.* 1(7):473–78

Karl DM, Björkman KM. 2015. Dynamics of Dissolved Organic Phosphorus. In *Biogeochemistry of Marine Dissolved Organic Matter*, pp. 233–334. Elsevier

Karl DM, Yanagi K. 1997. Partial characterization of the dissolved organic phosphorus pool in the oligotrophic North Pacific Ocean. *Limnol. Oceanogr.* 42(6):1398–1405

Karner MB, DeLong EF, Karl DM. 2001. Archaeal dominance in the mesopelagic zone of the Pacific Ocean. *Nature*. 409(6819):507–10

Karthäuser C, Ahmerkamp S, Marchant HK, Bristow LA, Hauss H, et al. 2021. Small sinking particles control anammox rates in the Peruvian oxygen minimum zone. *Nat. Commun.* 12(1):1–12

Kennedy KE, Thompson GA. 1970. Phosphonolipids: Localization in Surface Membranes of Tetrahymena. *Science (80-.).* 168(3934):989–91

Kiene RP. 1991. Production and consumption of methane in aquatic systems. In J. E. Rogers, & W. B. Whitman (Eds.), Microbial Production and Consumption of Greenhouse Gases: Methane, Nitrogen Oxides and Halomethanes (pp. 111–146). Washington, DC: American Society for Microbiology

Kits KD, Jung MY, Vierheilig J, Pjevac P, Sedlacek CJ, et al. 2019. Low yield and abiotic origin of N2O formed by the complete nitrifier Nitrospira inopinata. *Nat. Commun.* 10(1):1–12

Kitzinger K, Padilla CC, Marchant HK, Hach PF, Herbold CW, et al. 2019. Cyanate and urea are substrates for nitrification by Thaumarchaeota in the marine environment. *Nat. Microbiol.* 4(2):234–43

Kock A, Arevalo-Martinez DL, Loscher CR, Bange HW. 2016. Extreme N2O accumulation in the coastal oxygen minimum zone off Peru. *Biogeosciences*. 13(3):827–40

Kolomijeca A, Marx L, Reynolds S, Cariou T, Mawji E, Boulart C. 2022. An update on dissolved methane distribution in the subtropical North Atlantic Ocean. *Ocean Sci.* 18(5):1377–88

Kolowith LC, Ingall ED, Benner R. 2001. Composition and cycling of marine organic phosphorus. *Limnol. Oceanogr.* 46(2):309–20

Kozlowski JA, Price J, Stein LY. 2014. Revision of N2O-producing pathways in the ammonia-oxidizing bacterium Nitrosomonas europaea ATCC 19718. *Appl. Environ. Microbiol.* 80(16):4930–35

Kozlowski JA, Stieglmeier M, Schleper C, Klotz MG, Stein LY. 2016. Pathways and key intermediates required for obligate aerobic ammonia-dependent chemolithotrophy in bacteria and Thaumarchaeota. *ISME J.* 10(8):1836–45

Kraft B, Jehmlich N, Larsen M, Bristow LA, Könneke M, et al. 2022. Oxygen and nitrogen production by an ammonia-oxidizing archaeon. *Science (80-.).* 375(6576):97–100

Kuypers MMM, Marchant HK, Kartal B. 2018. The microbial nitrogen-cycling network. *Nat. Rev. Microbiol.* 16(5):263–76

Kuypers MMM, Silekers AO, Lavik G, Schmid M, Jøorgensen BB, et al. 2003. Anaerobic ammonium oxidation by anammox bacteria in the Black Sea. *Nature*. 422(6932):608–11

Lam P, Jensen MM, Lavik G, McGinnis DF, Müller B, et al. 2007. Linking crenarchaeal and bacterial nitrification to anammox in the Black Sea. *Proc. Natl. Acad. Sci. U. S. A.* 104(17):7104–9

Lam P, Kuypers MMM. 2011. Microbial nitrogen cycling processes in oxygen minimum zones. *Ann. Rev. Mar. Sci.* 3:317–45

Lam P, Lavik G, Jensen MM, van de Vossenberg J, Schmid M, et al. 2009. Revising the nitrogen cycle in the Peruvian oxygen minimum zone. *Proc. Natl. Acad. Sci.* 106(12):4752–57

Lamontagne R a, Swinnerton JW, Linnenbom VJ, Smith WD. 1973. Methane concentrations in various marine environments. *J. Geophys. Res.* 78(24):5317–24

Lamontagne RA, Swinnerton JW, Linnenbom VJ. 1971. Nonequilibrium of carbon monoxide and methane at the air-sea interface. *J. Geophys. Res.* 76(21):5117–21

Lancaster KM, Caranto JD, Majer SH, Smith MA. 2018. Alternative Bioenergy: Updates to and Challenges in Nitrification Metalloenzymology. *Joule*. 2(3):421–41

Lenhart K, Klintzsch T, Langer G, Nehrke G, Bunge M, et al. 2016. Evidence for methane production by the marine algae Emiliania huxleyi. *Biogeosciences*. 13(10):3163–74

Li G, Cheng L, Zhu J, Trenberth KE, Mann ME, Abraham JP. 2020. Increasing ocean stratification over the past half-century. *Nat. Clim. Chang.* 10(12):1116–23

Li M, Ford T, Li X, Gu JD. 2011. Cytochrome cd1 -containing nitrite reductase encoding gene nirS as a new functional biomarker for detection of anaerobic ammonium oxidizing (anammox) bacteria. *Environ. Sci. Technol.* 45(8):3547–53

Liang Z, Letscher RT, Knapp AN. 2022. Dissolved organic phosphorus concentrations in the surface ocean controlled by both phosphate and iron stress. *Nat. Geosci.* 15(8):651–57

Lockwood S, Greening C, Baltar F, Morales SE. 2022. Global and seasonal variation of marine phosphonate metabolism. *ISME J.* 16(9):2198–2212

Löscher CR, Kock A, Könneke M, Laroche J, Bange HW, Schmitz RA. 2012. Production of oceanic nitrous oxide by ammonia-oxidizing archaea. *Biogeosciences*. 9(7):2419–29

Lund MB, Smith JM, Francis CA. 2012. Diversity, abundance and expression of nitrite reductase (nirK)-like genes in marine thaumarchaea. *ISME J.* 6(10):1966–77

Lupton FS, Marshall KC. 1981. Specific Adhesion of Bacteria to Heterocysts of Anabaena spp. and Its Ecological Significance . *Appl. Environ. Microbiol.* 42(6):1085–92

Lycus P, Bøthun KL, Bergaust L, Shapleigh JP, Bakken LR, Frostegård Å. 2017. Phenotypic and genotypic richness of denitrifiers revealed by a novel isolation strategy. *ISME J.* 11(10):2219–32

Maia LB, Moura JJG. 2014. How biology handles nitrite. *Chem. Rev.* 114(10):5273–5357

Mao SH, Zhang HH, Zhuang GC, Li XJ, Liu Q, et al. 2022. Aerobic oxidation of methane significantly reduces global diffusive methane emissions from shallow marine waters. *Nat. Commun.* 13(1):1–10

Marchant HK, Tegetmeyer HE, Ahmerkamp S, Holtappels M, Lavik G, et al. 2018. Metabolic specialization of denitrifiers in permeable sediments controls N2O emissions. *Environ. Microbiol.* 20(12):4486–4502

Martens-Habbena W, Berube PM, Urakawa H, De La Torre JR, Stahl DA. 2009. Ammonia oxidation kinetics determine niche separation of nitrifying Archaea and Bacteria. *Nature*. 461(7266):976–79

Martinez A, Tyson GW, Delong EF. 2010. Widespread known and novel phosphonate utilization pathways in marine bacteria revealed by functional screening and metagenomic analyses. *Environ. Microbiol.* 12(1):222–38

Martínez A, Ventouras LA, Wilson ST, Karl DM, DeLong EF. 2013. Metatranscriptomic and functional metagenomic analysis of methylphosphonate utilization by marine bacteria. *Front. Microbiol.* 4(NOV):1–18

Mather RL, Reynolds SE, Wolff GA, Williams RG, Torres-Valdes S, et al. 2008. Phosphorus cycling in the North and South Atlantic Ocean subtropical gyres. *Nat. Geosci.* 1(7):439–43

McElroy MB, Elkins JW, Wofsy SC, Yung YL. 1976. Sources and sinks for atmospheric N2O. *Rev. Geophys.* 14(2):143–50

Messié M, Ledesma J, Kolber DD, Michisaki RP, Foley DG, Chavez FP. 2009. Potential new production estimates in four eastern boundary upwelling ecosystems. *Prog. Oceanogr.* 83(1–4):151–58

Metcalf WW, Griffin BM, Cicchillo RM, Gao J, Janga C, et al. 2012. Supplementary Materials for Methane in the Aerobic Ocean. . 1104(August):1104–7

Metcalf WW, Van Der Donk WA. 2009. Biosynthesis of phosphonic and phosphinic acid natural products. *Annu. Rev. Biochem.* 78:65–94

Moreno-Vivián C, Cabello P, Martínez-Luque M, Blasco R, Castillo F. 1999. Prokaryotic nitrate reduction: Molecular properties and functional distinction among bacterial nitrate reductases. *J. Bacteriol.* 181(21):6573–84

Morley N, Baggs EM, Dörsch P, Bakken L. 2008. Production of NO, N2O and N2 by extracted soil bacteria, regulation by NO2- and O2 concentrations. *FEMS Microbiol. Ecol.* 65(1):102–12

Morris RM, Rappé MS, Connon SA, Vergin KL, Siebold WA, et al. 2002. SAR11 clade dominates ocean surface bacterioplankton communities. *Nature*. 420(6917):806–10

Murali R, Pace LA, Sanford RA, Hatzenpichler R, Ward LM, et al. 2021. Diversity and evolution of nitric oxide reduction. *bioRxiv*. 2021.10.15.464467

Murphy ARJ, Scanlan DJ, Chen Y, Adams NBP, Cadman WA, et al. 2021. Transporter characterisation reveals aminoethylphosphonate mineralisation as a key step in the marine phosphorus redox cycle. *Nat. Commun.* 12(1):1–12

Murray J. 1989. The 1988 Black Sea Oceanographic Expedition: Overview and New Discoveries. *Oceanography*. 2(1):15–21

Murray JW, Codispoti LA, Friederich GE. 1995. Oxidation-Reduction Environments. In *Aquatic Chemistry: Interfacial and Interspecies Processes.*, pp. 157–76

Murray JW, Jannasch HW, Honjo S, Anderson RF, Reeburgh WS, et al. 1989. Unexpected changes in the oxic/anoxic interface in the Black Sea. *Nature*. 338(6214):411–13

Oakley BB, Francis CA, Roberts KJ, Fuchsman CA, Srinivasan S, Staley JT. 2007. Analysis of nitrite reductase (nirK and nirS) genes and cultivation reveal depauperate community of denitrifying bacteria in the Black Sea suboxic zone. *Environ. Microbiol.* 9(1):118–30

Oremland RS. 1979. Methanogenic activity in plankton samples and fish intestines A mechanism for in situ methanogenesis in oceanic surface waters. *Limnol. Oceanogr.* 24(6):1136–41

Oswald K, Graf JS, Littmann S, Tienken D, Brand A, et al. 2017. Crenothrix are major methane consumers in stratified lakes. *ISME J.* 11(9):2124–40

Pack M, Heintz MB, Reeburgh WS, Trumbore SE, Valentine DL, et al. 2015. Methane oxidation in the eastern tropical North Pacific Ocean water column. *J. Geophys. Res. Biogeosciences*. 120(6):1078–92

Parks DH, Chuvochina M, Waite DW, Rinke C, Skarshewski A, et al. 2018. A standardized bacterial taxonomy based on genome phylogeny substantially revises the tree of life. *Nat. Biotechnol.* 36(10):996–1004

Pauly D, Christensen V. 1995. Primary production required to sustain global fisheries. *Nature*. 374(6519):255–57

Payne WJ. 1986. Centenary of the isolation of denitrifying bacteria. ASM News. 1986;52(12):627-9.

Peng X, Valentine DL. 2021. Diversity and n2o production potential of fungi in an oceanic oxygen minimum zone. *J. Fungi*. 7(3):

Perez-Coronel E, Michael Beman J. 2022. Multiple sources of aerobic methane production in aquatic ecosystems include bacterial photosynthesis. *Nat. Commun.* 13(1):

Portmann RW, Daniel JS, Ravishankara AR. 2012. Stratospheric ozone depletion due to nitrous oxide: Influences of other gases. *Philos. Trans. R. Soc. B Biol. Sci.* 367(1593):1256–64

Prather MJ, Hsu J, DeLuca NM, Jackman CH, Oman LD, et al. 2015. Measuring and modeling the lifetime of nitrous oxide including its variability. *J. Geophys. Res. Atmos.* 120(11):5693–5705

Prosser JI, Hink L, Gubry-Rangin C, Nicol GW. 2020. Nitrous oxide production by ammonia oxidizers: Physiological diversity, niche differentiation and potential mitigation strategies. *Glob. Chang. Biol.* 26(1):103–18

Purkhold U, Pommerening-Röser A, Juretschko S, Schmid MC, Koops H-P, Wagner M. 2000. Phylogeny of All Recognized Species of Ammonia Oxidizers Based on Comparative 16S rRNA and amoA Sequence Analysis: Implications for Molecular Diversity Surveys. *Appl. Environ. Microbiol.* 66(12):5368–82

Qin W, Meinhardt KA, Moffett JW, Devol AH, Virginia Armbrust E, et al. 2017. Influence of oxygen availability on the activities of ammonia-oxidizing archaea. *Environ. Microbiol. Rep.* 9(3):250–56

Ravishankara AR, Daniel JS, Portmann RW. 2009. Nitrous oxide (N2O): The dominant ozone-depleting substance emitted in the 21st century. *Science (80-.).* 326(5949):123–25

Reeburgh WS. 2007. Oceanic methane biogeochemistry. *Chem. Rev.* 107(2):486–513

Repeta DJ, Ferrón S, Sosa OA, Johnson CG, Repeta LD, et al. 2016. Marine methane paradox explained by bacterial degradation of dissolved organic matter. *Nat. Geosci.* 9(12):884–87

Richards TA, Jones MDM, Leonard G, Bass D. 2012. Marine fungi: Their ecology and molecular diversity. *Ann. Rev. Mar. Sci.* 4:495–522

Risgaard-Petersen N, Langezaal AM, Ingvardsen S, Schmid MC, Jetten MSM, et al. 2006. Evidence for complete denitrification in a benthic foraminifer. *Nature*. 443(7107):93–96

Rosentreter JA, Borges A V., Deemer BR, Holgerson MA, Liu S, et al. 2021. Half of global methane emissions come from highly variable aquatic ecosystem sources. *Nat. Geosci.* 14(4):225–30

Rotthauwe JH, Witzel KP, Liesack W. 1997. The ammonia monooxygenase structural gene amoA as a functional marker: molecular fine-scale analysis of natural ammonia-oxidizing populations. *Appl. Environ. Microbiol.* 63(12):4704–12

Sanford RA, Wagner DD, Wu Q, Chee-Sanford JC, Thomas SH, et al. 2012. Unexpected nondenitrifier nitrous oxide reductase gene diversity and abundance in soils. *Proc. Natl. Acad. Sci. U. S. A.* 109(48):19709–14

Santoro AE, Buchwald C, McIlvin MR, Casciotti KL. 2011. Isotopic Signature of N2O Produced by Marine Ammonia-Oxidizing Archaea. *Science (80-.).* 333(6047):1282–85

Santos-Beneit F. 2015. The Pho regulon: A huge regulatory network in bacteria. *Front. Microbiol.* 6(APR):1–13

Saraiva LM, Vicente JB, Teixeira M. 2004. The Role of the Flavodiiron Proteins in Microbial Nitric Oxide Detoxification. , pp. 77–129

Saunois M, Stavert AR, Poulter B, Bousquet P, Canadell JG, et al. 2020. The Global Methane Budget 2000–2017. *Earth Syst. Sci. Data*. 12(3):1561–1623

Schloesing T, Muntz A. 1877. Sur la nitrification par les ferments organises. *Comptes rendus de l'Académie des sciences.*84:301-3.

Schmidtko S, Stramma L, Visbeck M. 2017. Decline in global oceanic oxygen content during the past five decades. *Nature*. 542(7641):335–39

Scranton MI, Brewer PG. 1977. Occurrence of methane in the near-surface waters of the western subtropical North-Atlantic. *Deep. Res.* 24(2):127–38

Shoun H, Kim DH, Uchiyama H, Sugiyama J. 1992. Denitrification by fungi. *FEMS Microbiol. Lett.* 94(3):277–81

Simon M, Grossart HP, Schweitzer B, Ploug H. 2002. Microbial ecology of organic aggregates in aquatic ecosystems. *Aquat. Microb. Ecol.* 28(2):175–211

Smayada TJ. 1969. Some Measurements of the Sinking Rate of Fecal Pellets. *Limnol. Oceanogr.* 14(4):621–25

Sosa OA, Burrell TJ, Wilson ST, Foreman RK, Karl DM, Repeta DJ. 2020. Phosphonate cycling supports methane and ethylene supersaturation in the phosphate-depleted western North Atlantic Ocean. *Limnol. Oceanogr.* 65(10):2443–59

Sosa OA, Repeta DJ, DeLong EF, Ashkezari MD, Karl DM. 2019a. Phosphate-limited ocean regions select for bacterial populations enriched in the carbon–phosphorus lyase pathway for phosphonate degradation. *Environ. Microbiol.* 21(7):2402–14

Sosa OA, Casey JR, Karl DM. 2019b. Methylphosphonate Oxidation in Prochlorococcus Strain MIT9301 Supports Phosphate Acquisition, Formate Excretion, and Carbon Assimilation into Purines. *Appl. Environ. Microbiol.* 85(13):1–12

Spang A, Hatzenpichler R, Brochier-Armanet C, Rattei T, Tischler P, et al. 2010. Distinct gene set in two different lineages of ammonia-oxidizing archaea supports the phylum Thaumarchaeota. *Trends Microbiol.* 18(8):331–40

Spang A, Poehlein A, Offre P, Zumbrägel S, Haider S, et al. 2012. The genome of the ammonia-oxidizing candidatus nitrososphaera gargensis: Insights into metabolic versatility and environmental adaptations. *Environ. Microbiol.* 14(12):3122–45

Stahl DA, de la Torre JR. 2012. Physiology and Diversity of Ammonia-Oxidizing Archaea. *Annu. Rev. Microbiol.* 66(1):83–101

Stasi R, Neves HI, Spira B. 2019. Phosphate uptake by the phosphonate transport system PhnCDE. *BMC Microbiol.* 19(1):1–8

Stein LY, Klotz MG. 2011. Nitrifying and denitrifying pathways of methanotrophic bacteria. *Biochem. Soc. Trans.* 39(6):1826–31

Stein LY, Klotz MG, Lancaster KM, Nicol GW, Qin W, et al. 2021. Comment on"A Critical Review on Nitrous Oxide Production by Ammonia-Oxidizing Archaea" by Lan Wu, Xueming Chen, Wei Wei, Yiwen Liu, Dongbo Wang, and Bing-Jie Ni. *Environ. Sci. Technol.* 55(1):797–98

Stewart FJ, Ulloa O, Delong EF. 2012. Microbial metatranscriptomics in a permanent marine oxygen minimum zone. *Environ. Microbiol.* 14(1):23–40

Stieglmeier M, Mooshammer M, Kitzler B, Wanek W, Zechmeister-Boltenstern S, et al. 2014. Aerobic nitrous oxide production through N-nitrosating hybrid formation in ammonia-oxidizing archaea. *ISME J.* 8(5):1135–46

Stosiek N, Talma M, Klimek-Ochab M. 2020. Carbon-Phosphorus Lyase—the State of the Art. *Appl. Biochem. Biotechnol.* 190(4):1525–52

Taenzer L, Carini PC, Masterson AM, Bourque B, Gaube JH, Leavitt WD. 2020. Microbial Methane From Methylphosphonate Isotopically Records Source. *Geophys. Res. Lett.* 47(1):1–9

Tanimoto T, Hatano K, Kim D, Uchiyama H, Shoun H. 1992. Co-denitrification by the denitrifying system of the fungus Fusarium oxysporum. *FEMS Microbiol. Lett.* 93(2):177–80

Teikari JE, Fewer DP, Shrestha R, Hou S, Leikoski N, et al. 2018. Strains of the toxic and bloom-forming Nodularia spumigena (cyanobacteria) can degrade methylphosphonate and release methane. *ISME J.* 12(6):1619–30

Ternan NG, Mc Grath JW, Mc Mullan G, Quinn JP. 1998. Review: Organophosphonates: Occurrence, synthesis and biodegradation by microorganisms. *World J. Microbiol. Biotechnol.* 14(5):635–47

Thamdrup B, Steinsdóttir HGR, Bertagnolli AD, Padilla CC, Patin N V., et al. 2019. Anaerobic methane oxidation is an important sink for methane in the ocean's largest oxygen minimum zone. *Limnol. Oceanogr.* 64(6):2569–85

Tian H, Xu R, Canadell JG, Thompson RL, Winiwarter W, et al. 2020. A comprehensive quantification of global nitrous oxide sources and sinks. *Nature*. 586(7828):248–56

Tourna M, Freitag TE, Nicol GW, Prosser JI. 2008. Growth, activity and temperature responses of ammonia-oxidizing archaea and bacteria in soil microcosms. *Environ. Microbiol.* 10(5):1357–64

Traganza ED, Swinnerton JW, Cheek CH. 1979. Methane supersaturation and ATP-zooplankton blooms in near-surface waters of the Western Mediterranean and the subtropical North Atlantic Ocean. *Deep Sea Res. Part A. Oceanogr. Res. Pap.* 26(11):1237–45

Vajrala N, Martens-Habbena W, Sayavedra-Soto LA, Schauer A, Bottomley PJ, et al. 2013. Hydroxylamine as an intermediate in ammonia oxidation by globally abundant marine archaea. *Proc. Natl. Acad. Sci.* 110(3):1006–11

Van Kessel MAHJ, Speth DR, Albertsen M, Nielsen PH, Op Den Camp HJM, et al. 2015. Complete nitrification by a single microorganism. *Nature*. 528(7583):555–59

Van Mooy BAS, Krupke A, Dyhrman ST, Fredricks HF, Frischkorn KR, et al. 2015. Major role of planktonic phosphate reduction in the marine phosphorus redox cycle. *Science (80-.).* 348(6236):783–85

Villarreal-Chiu JF, Quinn JP, McGrath JW. 2012. The genes and enzymes of phosphonate metabolism by bacteria, and their distribution in the marine environment. *Front. Microbiol.* 3(JAN):1–13

Wackett LP, Shames SL, Venditti CP, Walsh CT. 1987. Bacterial carbon-phosphorus lyase: Products, rates, and regulation of phosphonic and phosphinic acid metabolism. *J. Bacteriol.* 169(2):710–17

Wan XS, Hou L, Kao S-J, Zhang Y, Sheng H-X, et al. 2023. Pathways of N2O production by marine ammonia-oxidizing archaea determined from dual-isotope labeling. *Proc. Natl. Acad. Sci.* 120(11):2017

Wang Q, Alowaifeer A, Kerner P, Balasubramanian N, Patterson A, et al. 2021. Aerobic bacterial methane synthesis. *Proc. Natl. Acad. Sci. U. S. A.* 118(27):

Wankel SD, Ziebis W, Buchwald C, Charoenpong C, De Beer Di, et al. 2017. Evidence for fungal and chemodenitrification based N2O flux from nitrogen impacted coastal sediments. *Nat. Commun.* 8:1–11

Wanner BL. 1996. Signal transduction in the control of phosphate-regulated genes of Escherichia coli. *Kidney Int.* 49(4):964–67

Ward BB, Kilpatrick KA. 1991. Nitrogen Transformations in the Oxic Layer of Permanent Anoxic Basins: The Black Sea and the Cariaco Trench. In *Black Sea Oceanography*, pp. 111–24. Dordrecht: Springer Netherlands

Ward BB, Tuit CB, Jayakumar A, Rich JJ, Moffett J, Naqvi SWA. 2008. Organic carbon, and not copper, controls denitrification in oxygen minimum zones of the ocean. *Deep. Res. Part I Oceanogr. Res. Pap.* 55(12):1672–83

Weber T, Wiseman NA, Kock A. 2019. Global ocean methane emissions dominated by shallow coastal waters. *Nat. Commun.* 10(1):1–10

Westley MB, Yamagishi H, Popp BN, Yoshida N. 2006. Nitrous oxide cycling in the Black Sea inferred from stable isotope and isotopomer distributions. *Deep. Res. Part II Top. Stud. Oceanogr.* 53(17–19):1802–16

White AK, Metcalf WW. 2007. Microbial metabolism of reduced phosphorus compounds. *Annu. Rev. Microbiol.* 61:379–400

Whitney LAP, Lomas MW. 2019. Phosphonate utilization by eukaryotic phytoplankton. *Limnol. Oceanogr. Lett.* 4(1):18–24

Winogradsky S. 1890. Recherches sur les organisms de la nitrification. *Ann. Inst. Pasteur.* 4:213-31.

Wrage-Mönnig N, Horn MA, Well R, Müller C, Velthof G, Oenema O. 2018. The role of nitrifier denitrification in the production of nitrous oxide revisited. *Soil Biol. Biochem.* 123(April):A3–16

Wu J, Sunda W, Boyle EA, Karl DM. 2000. Phosphate depletion in the Western North Atlantic Ocean. *Science (80-.).* 289(5480):759–62

Wuchter C, Abbas B, Coolen MJL, Herfort L, Van Bleijswijk J, et al. 2006. Archaeal nitrification in the ocean. *Proc. Natl. Acad. Sci. U. S. A.* 103(33):12317–22

Wyrtki K. 1962. The oxygen minima in relation to ocean circulation. *Deep. Res. Oceanogr. Abstr.* 9(1–2):11–23

Yakovleva GM, Kim SK, Wanner BL. 1998. Phosphate-independent expression of the carbon-phosphorus lyase activity of Escherichia coli. *Appl. Microbiol. Biotechnol.* 49(5):573–78

Yang S, Chang BX, Warner MJ, Weber TS, Bourbonnais AM, et al. 2020. Global reconstruction reduces the uncertainty of oceanic nitrous oxide emissions and reveals a vigorous seasonal cycle. *Proc. Natl. Acad. Sci. U. S. A.* 117(22):

Yao M, Henny C, Maresca JA. 2016. Freshwater bacteria release methane as a by-product of phosphorus acquisition. *Appl. Environ. Microbiol.* 82(23):6994–7003

Yool A, Martin AP, Fernández C, Clark DR. 2007. The significance of nitrification for oceanic new production. *Nature*. 447(7147):999–1002

Yoon S, Nissen S, Park D, Sanford RA, Löffler E. 2016. Clade I NosZ from Those Harboring Clade II NosZ. *Appl. Envioronmental Microbiol.* 82(13):3793–3800

Yoshida T, Alexander M. 1970. Nitrous Oxide Formation by Nitrosomonas Europaea and Heterotrophie Microorganisms. *Soil Sci. Soc. Am. J.* 34(6):880–82

Yu C, Wang F, Chang SJ, Yao J, Blake RE. 2018. Phosphate oxygen isotope evidence for methylphosphonate sources of methane and dissolved inorganic phosphate. *Sci. Total Environ.* 644:747–53

Yu X, Doroghazi JR, Janga SC, Zhang JK, Circello B, et al. 2013. Diversity and abundance of phosphonate biosynthetic genes in nature. *Proc. Natl. Acad. Sci. U. S. A.* 110(51):20759–64

Zeleznick LD, Myers TC, Titchener EB. 1963. Growth of Escherichia coli on methyl- and ethylphosphonic acids. *BBA - Biochim. Biophys. Acta*. 78(3):546–47

Zhang C, Ji HB. 2019. Effects of environmental parameters on the ultraviolet degradation of methylphosphonate. *Appl. Ecol. Environ. Res.* 17(4):9473–82

Zheng Y, Harris DF, Yu Z, Fu Y, Poudel S, et al. 2018. A pathway for biological methane production using bacterial iron-only nitrogenase. *Nat. Microbiol.* 3(3):281–86

Zhu-Barker X, Cavazos AR, Ostrom NE, Horwath WR, Glass JB. 2015. The importance of abiotic reactions for nitrous oxide production. *Biogeochemistry*. 126(3):251–67

Zumft WG. 1997. Cell biology and molecular basis of denitrification. *Microbiol. Mol. Biol. Rev.* 61(4):533–616

Zumft WG. 2005. Nitric oxide reductases of prokaryotes with emphasis on the respiratory, heme-copper oxidase type. *J. Inorg. Biochem.* 99(1):194–215

Chapter II

Methylphosphonate-driven methane formation and its link to primary production in the oligotrophic North Atlantic

Jan N. von Arx[1], Abiel T. Kidane[1], Miriam Philippi[1,2], Wiebke Mohr[1], Gaute Lavik[1], Sina Schorn[1], Marcel M. M. Kuypers[1] and Jana Milucka[1]

Author affiliations

[1]Max Planck Institute for Marine Microbiology, Bremen, Germany

[2]Alfred Wegener Institute Helmholtz Centre for Polar and Marine Research, Bremen, Germany

Manuscript accepted for publication in Nature Communications
https://doi.org/10.1038/s41467-023-42304-4

Author contributions

W.M., A.T.K. and I (J.v.A) conducted the field sampling. I performed the incubation experiments for methane formation and measured the samples. I carried out the rate analysis and calculations with guidance from G.L. Carbon fixation experiments were conducted by A.T.K. and W.M. I was responsible for the DNA and RNA extraction and metagenomic and metatranscriptomic analyses were performed by M.P. The study was designed by me, M.M.M.K., S.S., and J.M. I discussed and interpreted the data with M.M.M.K. and J.M. I visualised the presented dataset. J.M. and I wrote the manuscript with contributions from all other authors.

Abstract

Methylphosphonate (MPn) is an organic phosphorus compound used by microorganisms when phosphate, a key nutrient that is limiting growth in most contemporary ocean surface waters, becomes unavailable. Microbial MPn use has been shown to result in the formation of methane, a potent greenhouse gas, in oxic waters where methane production was previously not expected. The extent and controlling factors of such aerobic methane formation remain underexplored. Here, we show high potential net rates of MPn-driven methane formation (median 0.4 nmol methane L^{-1} d^{-1}) in the upper water column of the western Tropical North Atlantic. The rates were repressed but still quantifiable in the presence of *in-situ* or added phosphate, suggesting that some MPn-driven methane formation persists in phosphate-replete waters. The genetic potential for MPn utilisation was present in and transcribed by key photo- and heterotrophic microbial taxa, such as *Pelagibacterales*, *SAR116*, and *Trichodesmium*. While the large cyanobacterial N_2 fixers dominated in the surface layer, phosphonate utilisation by *Alphaproteobacteria* appeared to become more important in deeper depths. We estimated that at our study site, a substantial part (median 11%) of the measured surface carbon fixation could be sustained by phosphorus liberated from phosphonate utilisation, highlighting the ecological importance of phosphonates in the carbon cycle of the oligotrophic ocean.

Introduction

The open ocean (>2000 m water depth) emits up to an estimated 0.5 mmol m^{-2} yr^{-1} of the biogenic greenhouse gas methane (CH_4) to the atmosphere (Weber et al. 2019), which amounts to ca. 5 - 23% of the total estimated emissions from the marine environment (Weber et al. 2019). Intriguingly, the underlying cause of these emissions is to a large extent methane supersaturation in oxic surface waters (Lamontagne et al. 1971, 1973; Scranton & Brewer 1977), which has been dubbed the so-called 'Marine Methane Paradox' (Kiene 1991). The paradoxical nature of this phenomenon stems from the fact that biological methane production by methanogenic archaea is a strictly anaerobic process (Balch et al. 1979). While some methanogenesis can occur in discrete anoxic microniches such as fish and zooplankton guts and/or particles (Bianchi et al. 1992; Oremland 1979; Traganza et al. 1979), the prevailing mechanisms behind the marine methane paradox are likely truly aerobic methane formation processes. In recent years, diverse aerobic bacteria have been shown to possess the capacity to form methane both from methylated organic compounds (e.g. methylphosphonate (MPn); Karl et al. 2008, methylamine (Wang et al. 2021), dimethylsulfoniopropionate (Damm et al. 2010) or methyl radicals (Ernst et al. 2022)) or dissolved inorganic carbon (DIC; Bižić et al. 2020; Lenhart et al. 2016; Zheng et al. 2018).

MPn utilisation has been identified as the underlying cause of methane supersaturation in the oligotrophic gyres of the North Pacific and Atlantic, where organic phosphorus compounds are used as a source of phosphorus due to the unavailability of inorganic phosphate (Pi; Karl et al. 2008; Repeta et al. 2016; Sosa et al. 2019a). Phosphonates are characterised by a stable carbon-phosphorus bond that can be cleaved by the multisubstrate enzyme carbon-phosphorus lyase (C-P lyase; Wackett et al. 1987). The *phnJ* gene, encoding for the catalytic subunit (Kamat et al. 2011), is therefore used as a marker gene for phosphonate-utilising microorganisms (Murphy et al. 2021).

Despite the important role of MPn utilisation in the marine carbon and phosphorus cycles, the process has so far been experimentally confirmed only in a handful of oceanic regions, mainly around station ALOHA in the eastern tropical North Pacific (Del Valle & Karl 2014; Karl et al. 2008; Repeta et al. 2016) and in the Sargasso Sea (Sosa et al. 2020). To date, little is known about the depth distribution of the process in the water column and the physico-chemical factors that control it. The process is thought to be induced under Pi-limitation, which is prevalent in the

subtropical gyres but can be found in most of the surface open ocean (Martiny et al. 2019). One of the most chronically Pi-limited marine regions is the western North Atlantic (Cavender-Bares et al. 2001; Sosa et al. 2019a; Wu et al. 2000), a region with low productivity (Chien et al. 2016; Mills et al. 2008) that is reliant on recycled nutrients. As such, the usage of organic phosphorus compounds by the microbial community is widespread (Dyhrman et al. 2002; Sosa et al. 2020; Van Mooy et al. 2015). While subsurface methane concentration maxima were observed in the North Atlantic (Kolomijeca et al. 2022; Scranton & Brewer 1977), their sources are not well constrained, particularly for the tropical region. Additionally, the potential of MPn for sustaining primary productivity in oligotrophic ocean waters is so far unknown.

During the cruise M161, we investigated aerobic methane formation in the upper 200 metres of the water column east of Barbados (Figure 1) using a range of experimental and molecular methods. Our data strongly support the primary role of MPn as a source of methane in this region with detectable potential net rates across the whole investigated water column, including the Pi-rich waters below the deep chlorophyll maximum. We identify the abundant marine bacterial photo- as well as heterotrophic organisms, including *Trichodesmium*, *SAR11*, *SAR116* and *Rhodobacteraceae* as potential candidates behind aerobic methane formation in the western Tropical North Atlantic.

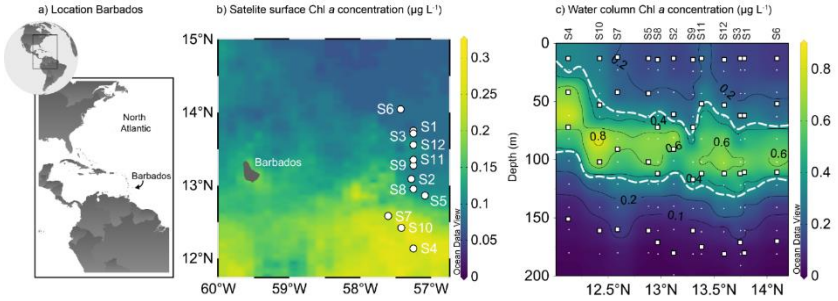

Figure 1. **Chlorophyll *a* (Chl *a*) concentrations of the sampling area in the western Tropical North Atlantic east of Barbados. a,** Sampling site location. **b,** Satellite surface Chl *a* concentrations averaged for the duration of the sampling campaign revealed a clear north-south divide, with higher Chl *a* concentrations in the southern stations 4, 7 and 10 compared to the northern ones. **c,** Water column Chl *a* concentrations for the upper 200 m. The dashed white line outlines the deep chlorophyll maximum (area between 0.35 µg L^{-1} Chl *a*). White squares represent the incubation depths and white points the sampling depths from the profiling CTD cast.

Results and Discussion

Rates of methylphosphonate-driven methane formation decrease with depth

The western North Atlantic is one of the most phosphate (Pi) limited oceanic regions worldwide, with Pi concentrations of 0.2 – 1 nmol L^{-1} in the surface waters (Sosa et al. 2019a; Wu et al. 2000). Correspondingly, the surface waters of our study area east of Barbados (Figure 1a) were depleted in both nitrogen (NOx below detection) and Pi (below detection; Figure 2).

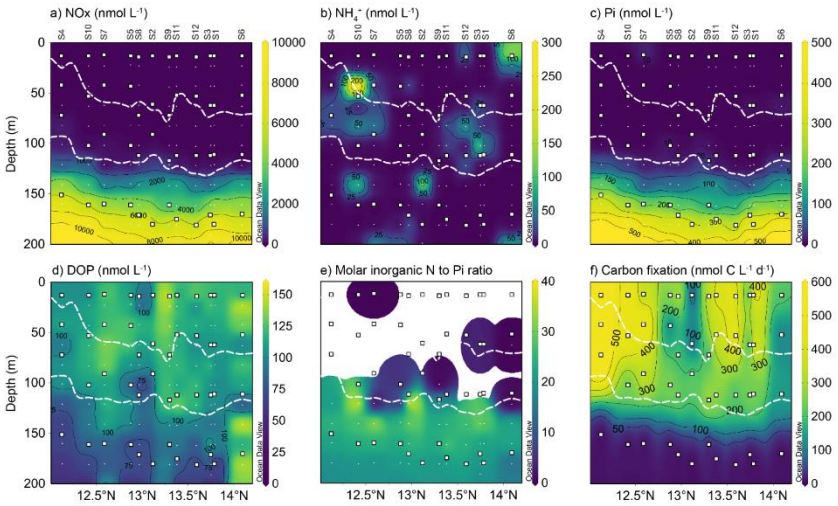

Figure 2. **Water column chemistry of nitrogen- and phosphorus-species (a-e) and carbon fixation rates (f) of the upper 200 m of the western Tropical North Atlantic east of Barbados.** **a,** Nitrate + nitrite (NOx). **b**, Ammonium (NH_4^+). **c**, Phosphate (Pi). **d**, Dissolved organic carbon (DOP). **e**, Molar inorganic nitrogen (NOx + ammonium) to phosphate ratios (N to Pi). **f**, Carbon fixation rates. White squares represent depths of the incubation experiments and white circles indicate sampling depths for concentration measurements. The white dotted line represents the outline of the deep chlorophyll maximum. Lack of values in the N to Pi ratio panel is a consequence of largely non-detectable nitrogen and Pi, as seen on (a-c).

Dissolved organic phosphorus (DOP) was present throughout the water column at concentrations comparable to e.g. the Sargasso Sea (Liang et al. 2022; Sosa et al. 2020; up to 167 nmol L^{-1}; Figure 2d). Satellite measurements of the region revealed elevated chlorophyll *a* (Chl *a*) concentrations in the three southernmost stations (stations 4, 7 and 10; Figure 1b). This distinction was reflected by a shallower deep chlorophyll maximum (DCM; defined here as the Gaussian area encompassing Chl *a* concentration above 0.35 µg L^{-1}) located below the mixed layer in these stations (Figure 1c; Supplementary Figure S1). Inorganic N (nitrogen oxides + ammonium) to P (Pi) ratios were not quantifiable for most of the water column above and within the DCM, as concentrations of Pi were consistently below the detection limit (10 nmol L^{-1}; Figure 2e). Below the DCM, inorganic N to Pi ratios increased to excesses of 20, as observed previously in the Sargasso Sea (Wu et al. 2000), suggesting, based on the Redfield ratio (Redfield 1958), that even the deeper waters remained Pi-limited. This pattern was also observed within the particulate organic fraction in the POC:PON:POP ratios (Supplementary Figure S2, S3). Carbon fixation rates, measured as the incorporation of dissolved inorganic carbon (^{13}C-DIC) into biomass, were comparable among the upper three incubation depths and usually in the range of 200 and 600 nmol C L^{-1} d^{-1} (Figure 2f). Rates were still measurable below the DCM, but reduced ca. 100-fold, likely due to light limitation and a lower abundance of primary producers with increasing depth (Behrenfeld & Falkowski 1997; Cullen 2015). Carbon fixation rates were consistently higher in the southern "high chlorophyll" stations (Figure 2f).

Methylphosphonate (MPn) driven methane (CH_4) formation (MPn-addition experiment) was quantifiable in all stations and at all investigated depths (10-metre surface depth, an intermediate depth above the DCM, at the DCM and below the DCM). The variability of the methane formation rate between duplicate incubations (from the same station and depth) was comparable to the variability observed across the twelve stations; therefore, rates from all stations were combined for further analyses (Figure 3). The onset of methane formation in MPn incubations was mostly immediate and linear over the course of 24 hours of incubation but often followed by exponential increases after 24 hours (Supplementary text; Supplementary Figure S4). The rates did not appear to vary substantially in response to the day and night cycle (see Supplementary text for discussion on abiotic photodegradation of MPn). The highest rates of methane formation were consistently measured in the surface and intermediate depths located above the DCM (Figure 3), with median rates of 0.40 (0.21 - 1.31 interquartile range (IQR)) and 0.30 (0.17 - 1.36

IQR) nmol CH_4 L^{-1} d^{-1} respectively. The maximal rate of 9.57 nmol CH_4 L^{-1} d^{-1} was measured in the intermediate depth of station 4.

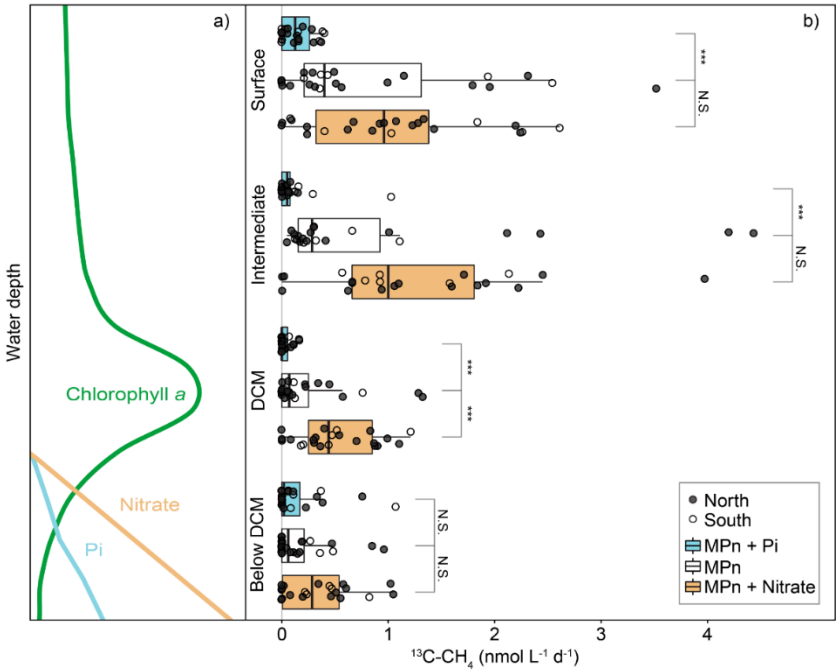

Figure 3. **Significant methane formation rates from ^{13}C-methylphosphonate incubation experiments. a,** Schematic drawing of a typical water column profile at the study site, depicting the chlorophyll *a* (Chl *a*) distribution and nutrient regimes. **b,** Rate measurements of methane (^{13}C-CH_4) from the four incubation depths: 10-metre surface depth, intermediate depth, deep chlorophyll maximum (DCM) and below the DCM and the three incubation experiments: methylphosphonate-addition (MPn), methylphosphonate + phosphate-addition (MPn + Pi) and methylphosphonate + nitrate-addition (MPn + nitrate) from both duplicates and all twelve stations. Each data point represents a statistically significant (Student's t test (2), $p < 0.05$, $R^2 > 0.81$) rate calculated from the linear regression of the first four time points (24h), with both insignificant and exponential rates reported as zero. Filled points represent the northern stations in the low surface

Chl *a* waters and open points the southern stations in the high surface Chl *a* waters. Statistical difference (Pairwise Wilcoxon test, $p < 0.05$) between the MPn-addition and the others is highlighted (*** = $p < 0.01$, N.S. = not significant). From the intermediate depths, the two highest rates of methane formation are not shown in the plot, namely 4.8 and 9.6 nmol CH_4 L^{-1} d^{-1} from S3 and S4 of the MPn-addition experiment respectively, as well as the 9.4 nmol CH_4 L^{-1} d^{-1} from the MPn + nitrate-addition experiment from S12.

The measured rates were comparable to the surface waters of both subtropical gyres and the western North Atlantic (Martínez et al. 2013; Sosa et al. 2020; 0.08 - 4 nmol CH_4 L^{-1} d^{-1}) even though direct comparisons are difficult due to different experimental designs. With increasing water depth, methane formation was still quantifiable but median rates decreased to 0.07 (0 - 0.25 IQR) and 0.06 (0 - 0.21 IQR) nmol CH_4 L^{-1} d^{-1} in the DCM and below respectively. Kruskal-Wallis statistical analysis revealed that methane formation was significantly different ($H(3) = 21$, $p < 0.01$) between the depths, except for the surface and intermediate depths (Pairwise Wilcoxon test, $p = 0.99$) and the DCM and below DCM depths (Pairwise Wilcoxon test, $p = 0.67$), separating the upper water column into an area of high methane formation above the DCM and an area of low formation at the DCM and below it. As our rates were mostly linear over 24 hours of incubation and often without a lag phase (Supplementary Figure S4), the microbial community appears to be well adapted to the utilisation of MPn or other phosphonates.

Our data do not indicate that this process is turned on and off by a certain threshold Pi concentration, even though the highest rates from the MPn-supplemented experiment were consistently recorded in incubations with *in-situ* Pi concentrations below 25 nmol L^{-1} (Supplementary Figure S5). We also did not observe any clear correlation between the methane formation rates and the potential substrate availability (i.e. OP concentration; Supplementary Figure S5). This may be explained by the fact that phosphonates only comprise a small part of DOP (5-10%; Van Mooy et al. 2015). However, cycling of only 0.25% of the phosphonate inventory at station ALOHA was suggested to be sufficient to explain the entire atmospheric flux of methane to the atmosphere there (Repeta et al. 2016).

We should note that our measured rates should be treated as potential net rates, as the methylphosphonate additions (1 µmol L^{-1}) were in excess of the *in-situ* concentrations and potential methane consumption by methane oxidation could not be accurately quantified.

Measurements of aerobic methane oxidation from open ocean surface waters are scarce and often in the range of tens of picomolar, even though occasionally rates of up to 4 nmol L^{-1} d^{-1} were measured (Pack et al. 2015). Furthermore, anaerobic methane oxidation could be occurring in anoxic microniches, although all experiments were set up aerobically with ongoing photosynthesis. However, any methane oxidation occurring in our incubations would have ultimately led to an underestimation of our methane formation rates.

Very little is known about the microbial utilisation of MPn and the resulting methane formation in waters below the mixed layer. There are reports of increased carbon-phosphorus (C-P) lyase activity within the DCM in the subtropical North Pacific (Granzow et al. 2021) and the highest methane concentrations in the subtropical North Atlantic were measured in the DCM (Kolomijeca et al. 2022) indicating aerobic methane formation below the mixed layer. This is peculiar because Pi is usually present below the DCM, and should be the preferred phosphorus source for microorganisms there (Del Valle & Karl 2014). Additionally, the C-P lyase is regulated by the pho-regulon, and its expression is turned off in the presence of Pi (Wanner 1996). In our incubations, methane formation remained low but quantifiable below the DCM (Figure 3) despite the *in-situ* Pi concentrations of up to 380 nmol L^{-1} (Figure 2c).

Effect of inorganic nutrients on methane formation

This pervasive utilisation of MPn in the presence of Pi was confirmed by our MPn + Pi-addition experiment (Figure 3) where methane formation rates were significantly (Pairwise Wilcoxon test, $p < 0.05$) repressed – but not completely inhibited – in the upper three incubation depths, compared to the MPn-addition incubations. It therefore seems that while elevated Pi concentrations tend to repress aerobic methane formation in general, some MPn utilisation persists even in the presence of Pi (Supplementary text). It should be kept in mind that in our experiments, MPn and Pi were added in equimolar amounts, as previous observations from cultures (Beversdorf et al. 2010; Carini et al. 2014) and field experiments (Yao et al. 2016) suggest that the MPn:Pi ratio might affect the degree to which MPn utilisation is inhibited. However, even under equimolar additions the degree of repression varies strongly between organisms (e.g. 98 % in cultured *SAR11 str HTCC7211* vs. 70% repression in *Trichodesmium* (Beversdorf et al. 2010; Carini et al. 2014)). Interestingly, in the below DCM depth, additions of Pi did not significantly repress methane formation from MPn (Figure 3). As both carbon fixation

and POC concentrations were lowest in this depth (Supplementary Figure S5), it is feasible that availability of labile DOM is an additional controlling factor that affects the rate of MPn utilisation in depths, where dominant MPn utilisers are predominantly mixo- or hetero-trophic. The important implication of these observations is that the utilisation of MPn may extend into environments that are less chronically Pi-limited, thus expanding the potential range for aerobic methane formation.

In contrast to Pi, additions of nitrate were expected to increase the rates of MPn-dependent methane formation, especially as inorganic nitrogen was also limiting in the upper water column (Figure 2). Addition of nitrogen have been shown to enhance both primary productivity (Moore et al. 2008) as well as heterotrophic productivity (Mills et al. 2008) in the Atlantic; moreover, nitrogen supplementation was expected to exacerbate phosphorus stress and thus create even more favourable conditions for the utilisation of MPn. Nitrogen addition experiments have been shown previously to lead to increased methane production rates in the subtropical North Pacific (Del Valle & Karl 2014; Karl et al. 2008). Correspondingly, the median rates of methane formation in the MPn + nitrate-addition incubations increased substantially across all four depths, even though the difference to the MPn-addition experiment was not statistically significant for three out of four depths (Pairwise Wilcoxon test, $p > 0.05$), the exception being the DCM (Pairwise Wilcoxon test, $p = 0.01$). This may be due to the high heterogeneity of the rates observed in the upper two incubation depths. The median rate increase of methane formation (by 2.4 – 6.3) in our MPn + nitrate-addition experiment (Figure 3) was comparable to the previous observed increase of 1.7 – 2.8 (Del Valle & Karl 2014). We should note that nitrate additions could have simultaneously enhanced methane oxidation rates, as many methanotrophic bacteria and archaea can use nitrate as an electron acceptor. Increased rates of methane oxidation would have obscured the true impact of nitrate on methane production.

C-P lyase enzyme mainly encoded by Trichodesmium *and* Alphaproteobacteria

The observed decline of MPn-driven methane formation rates with depth was accompanied by a decrease in the relative abundance of *phnJ*-containing microorganisms in each size fraction [large (>10 μm), medium (3 - 10 μm) and small (0.22 - 3 μm); Table 1].

Table 1. Relative abundance of the *phnJ* gene from the different size fractions of station S5 normalised to the *recA* gene, assuming a single copy per bacterium.

Depth	Small (0.22 - 3 µm)	Medium (3 - 10 µm)	Large (>10 µm)
Surface	2.47%	1.33%	14.71%
Intermediate	2.24%	1%	4.18%
Deep chlorophyll maximum	0.8%	0.16%	0.56%
Below deep chlorophyll maximum	0.04%	0.04%	4.66%

In the surface and intermediate depths, 14.7 and 4.2% of all microorganisms in the large size fraction contained the *phnJ* gene respectively, compared to 2.5 and 2.2% in the small one. In the medium size fraction, only around 1% of all microorganisms from the upper two depths contained the *phnJ* gene, indicating that comparatively this size fraction is least important. At the DCM, less than 1% and below the DCM, less than 0.1% of all microorganisms in each size fraction encoded for the *phnJ* gene. The only exception to this was the large fraction in the below DCM depth, where the relative abundance was still 4.7%. A similar pattern has been observed at the Bermuda Atlantic Time Series station, with the *phnJ* containing community decreasing ca. 2-3-fold between 20 and 100 m depth (Martinez et al. 2010).

Within the large size fraction the *phnJ* genes were taxonomically affiliated almost exclusively with the filamentous cyanobacterial genus *Trichodesmium*, (Figure 4).

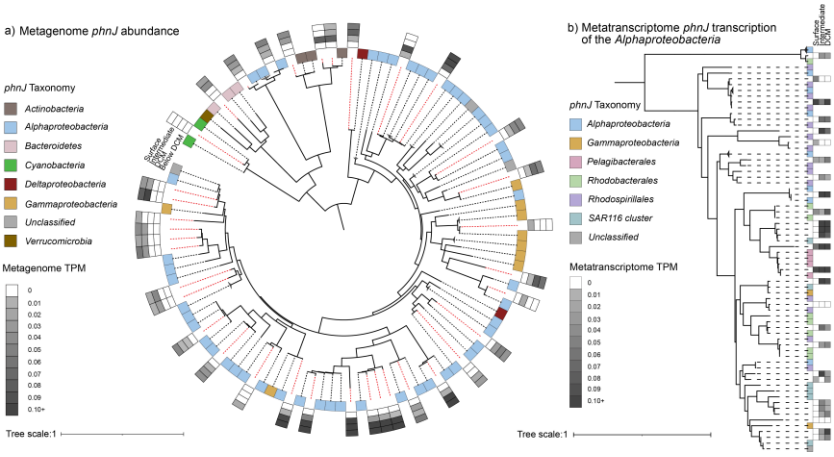

Figure 4. ***PhnJ* diversity, relative abundance and transcription. a,** Phylogenetic tree of all assembled *phnJ* sequences from all depths (10-metre surface depth, intermediate depth, deep chlorophyll maximum (DCM) and below the DCM) of the smallest size fractions and the respective reference sequences. The NCBI taxonomy of the reference sequences is indicated by the colour code of the inner boxes, the new sequences are indicated by the dashed red line. Relative abundance (TPM values) of the *phnJ* sequences in the metagenomic samples from the small (0.22 - 3 µm) size fraction in the four different depths are shown in the outer four boxes. In the metagenomes of the large (>10 µm) size fraction, only the sequence clustering with *Cyanobacteria* showed high TPM values in the surface, intermediate and DCM depths (0.77, 0.18 and 0.13 respectively; data not shown in the figure). **b,** Pruned phylogenetic tree including only *phnJ* sequences clustering with *Alphaproteobacteria*. NCBI taxonomy of the reference sequences is represented by the colour code in the first column. Transcription levels (TPM values) in the metatranscriptome samples of the small (0.22 - 3 µm) size fraction of the upper three depths is depicted in the following three columns. For more information, refer to supplementary Figure S6.

Their distribution matched the percentage of microorganisms from this size fraction containing the *phnJ* (Table 1), suggesting that *Trichodesmium* was the dominant *phnJ* containing organism in the large size fraction. Additionally, some of the *phnJ* containing bacteria identified in the larger size fraction may constitute part of the *Trichodesmium* microbiome *in-situ*, as previously

shown (Frischkorn et al. 2017). While most abundant above the DCM, the *Trichodesmium phnJ* was still detected in ca. 4% of the genomes in the large size fraction below the DCM (Table 1), possibly due to migrating or sinking cells (Villareal & Carpenter 2003). *Trichodesmium* is a key primary producer, as well as a N_2-fixing organism in the western North Atlantic (Capone et al. 1997) and has the capacity to utilise MPn and release methane even in the presence of Pi (Beversdorf et al. 2010; Dyhrman et al. 2006; Karl et al. 2008). Moreover, some *Trichodesmium* species also have the capacity to synthesise phosphonates (Dyhrman et al. 2009), albeit not MPn specifically (Frischkorn et al. 2018), and may thus contribute to phosphonate cycling at this site (see also Supplementary Text).

Our combined results indicate that *Trichodesmium* may contribute to MPn utilisation in the surface and intermediate depths during both Pi-deplete and replete conditions. Due to their large size and patchy distribution, *Trichodesmium* may also contribute to the high heterogeneity of the measured methane formation rates (a difference of up to 8.5 nmol CH_4 L^{-1} d^{-1} between duplicates in the intermediate depth of S4). This heterogeneity was often more pronounced above the DCM, supporting the presumed key role of larger phytoplankton and/or particle-associated bacterioplankton in MPn-driven methane formation (Del Valle & Karl 2014; Dyhrman et al. 2006).

Within the small size fraction, the *Alphaproteobacteria* were the most numerous, matching the observed depth distribution of the *phnJ*-encoding microorganisms of this fraction in the upper three incubation depths (Figure 4). The *phnJ*-containing *Alphaproteobacteria* were very diverse, with sequences clustering with representatives of *SAR116*, *Pelagibacterales*, *Rhodobacteraceae* and *Rhodospirillaceae* (Supplementary Figure S6), similar to previously observed C-P lyase containing microbial communities in e.g. the Sargasso Sea (Dyhrman et al. 2006; Sosa et al. 2019a). *Pelagibacterales* have been shown to produce methane from MPn under Pi-limitation in culture experiments (Carini et al. 2014). Due to their high abundance, particularly in regions like the Sargasso Sea where they can make up 52% of the C-P lyase-containing community (Martinez et al. 2010), they are expected to be important global contributors to MPn-driven methane formation. *SAR116* is also known to utilise phosphonates under Pi-limitation (Roda-Garcia et al. 2021) and has been shown to be a dominant group in both the Sargasso- and the Mediterranean Sea (Sosa et al. 2019a). The *Rhodobacterales* are a bacterial taxon that includes competitive opportunists with the capacity to form blooms (Bolaños et al. 2021), that were

shown to increase in abundance after MPn addition (Martínez et al. 2013). As such, they too may have contributed to the observed exponential nature of some of the methane formation rates.

Transcriptomic analysis of the small fraction revealed *in-situ* transcription of the C-P lyase pathway (Figure 4b), with most *phnJ* transcripts assigned to *Alphaproteobacteria* followed by *Gammaproteobacteria* (Supplementary Figure S6). Interestingly, relative transcript abundances did not follow the vertical rate distribution, with higher C-P lyase transcription in the intermediate and DCM depths compared to the surface. This suggests that comparatively, *alphaproteobacterial* phosphonate utilisation becomes more important deeper in the water column, whereas the large size organisms like the N_2-fixing cyanobacterium *Trichodesmium* appear to dominate above the DCM. The widespread distribution and expression of the *phnJ* gene across many microbial taxa *in-situ* (Figure 4) combined with the immediate onset and linear trend of the methane formation rates strongly implies that the microbial community was well adapted to metabolise MPn in particular and phosphonates in general through the C-P lyase pathway. As the *phnJ*-containing taxa include some of the most abundant marine auto- and heterotrophic microorganisms, MPn or more general phosphonate utilisation might be a key metabolic feature for microorganisms living in Pi-limited oligotrophic oceanic regions where primary productivity relies on recycled nutrients.

Aerobic methane formation and phytoplankton activity

Aerobic methane formation in aquatic environments (both marine and freshwater) is linked to the activity of primary producers (Perez-Coronel & Michael Beman 2022; Weber et al. 2019), either through direct methane formation from DIC during carbon fixation (Bižić et al. 2020; Lenhart et al. 2016) or through the metabolism of methylated compounds such as MPn (Del Valle & Karl 2014; Karl et al. 2008). At our study site, the processes of aerobic methane formation and primary production can be linked through MPn-utilisation by the primary producer *Trichodesmium*. Despite this potential direct link, neither the surface Chl *a* concentrations, the parameter used to estimate primary productivity, nor our directly measured carbon fixation rates, showed a significant correlation with methane formation rates (Supplementary Figure S5, S7). Hence, our results suggest that surface Chl *a* and carbon fixation rates may not be universally suitable as predictors of aerobic methane formation. We also investigated the possibility that DIC can be converted to methane in the investigated study site,

for which we set up parallel experiments in duplicate using only ^{13}C-DIC. However, out of 96 incubations we were only able to detect one substantial rate (0.58 nmol CH_4 L^{-1} d^{-1}), in the DCM of station S12. Moreover, due to the long incubation time (48 hours) we cannot say with confidence whether methane was produced directly from DIC, or from any of the many carbon intermediates that are formed during autotrophic cell metabolism. We conclude that DIC likely was not a major contributor to the methane formation in the western Tropical North Atlantic at this time, with any rates being either hugely sporadic or much lower than the ones from MPn. Instead, demethylation of MPn by phytoplankton and bacterioplankton was likely the main source of aerobic methane formed in this region.

Role of MPn in carbon drawdown

In Pi-limited regions, organic phosphorus compounds represent a key phosphorus source to sustain productivity (Karl 2014). For example, DOP degradation by alkaline phosphatases could explain 12- 30% of the phosphorus requirements in the North Atlantic subtropical gyre (Mather et al. 2008) but similar estimates are lacking for phosphonate degradation through C-P lyases. As, methane and Pi are stoichiometrically formed during MPn demethylation (Wackett et al. 1987), our measured rates of potential net methane formation can be used to determine the maximum of Pi liberated during this process to potentially fuel e.g. primary production. Based on the median net carbon fixation rate in the surface depth (370 nmol C L^{-1} d^{-1}), we estimate a redfieldian Pi requirement of 3.5 nmol L^{-1} d^{-1}. Considering the range of our measured methane formation rates, (methyl)phosphonates could support 0 - 100.7% (median 11%) of the Pi needed to sustain the measured rates of primary production, thus making them an important but so far poorly understood contributor of the contemporary oceanic carbon drawdown.

Gross primary productivity in the modern open ocean is sustained to 90% by recycled phosphorus (Karl 2014). Under future climate projections, warmer surface waters and the resulting enhanced stratification will reduce mixing of the nutrient rich deeper waters into the surface, likely decreasing primary productivity in the long run (Fu et al. 2016; Hutchins & Fu 2017). Under these conditions, utilisation of organic phosphorus (as well as nitrogen) may become comparably more widespread, as indicated e.g. by the prevalence of the C-P lyase pathway in extremely Pi-limited environments (Lockwood et al. 2022; Sosa et al. 2019a). Phosphonates are ubiquitous in surface marine waters and they have been shown to be rapidly

turned over (on the time scale of a few days) due to an intense redox cycling between +5 and +3 oxidation states (Van Mooy et al. 2015). If the recycling of phosphorus in the surface waters of the nutrient limited regions intensifies, each phosphorus atom may undergo more cycles of methylation (or alkylation, in general) before being removed from the mixed layer. Combined with the projected expansion of Pi-limited oceanic regions, MPn-driven aerobic methane formation is likely to increase in the long run. However, increasing stratification is also predicted to favour smaller picocyanobacteria (van de Waal & Litchman 2020) like *Prochlorococcus*, which has been shown to encode an alternative MPn degradation pathway that leads to the formation of formate instead of methane (Sosa et al. 2019b). To realistically assess the interplay of those two scenarios and its impact on open-ocean methane emissions, it is imperative to better constrain microbial formation and utilisation of MPn above and below the mixed layer.

Materials and Methods

Sample collection

During the R/V Meteor cruise M161, samples were collected between 19 January and 20 February 2020 from twelve stations in the western Tropical North Atlantic off Barbados (Figure 1). At each station, hydrographical data was recorded by a Sea-Bird conductivity temperature depth (CTD) system equipped with sensors for temperature and salinity (Sea-Bird), dissolved oxygen (Sea-Bird 43), fluorescence (WETLabs) and turbidity (WETLabs), mounted on a 24-way stainless steel frame system equipped with 10 litre Niskin bottles. Water samples were collected from two subsequent CTD casts at each station between 12:30 am and 4:00 am local time to start incubations at sunrise. The first cast profiled the upper 800 m, with discrete water samples taken at regular intervals in the upper 200 m and a reference sample from around 250 m. From each depth, samples were collected for nutrients (nitrate (NO_3^-), nitrite (NO_2^-), ammonium, phosphate (Pi) and total phosphorus (TP)), methane, DNA and RNA, chlorophyll *a* (Chl *a*), particulate organic -carbon (POC), -nitrogen (PON) and -phosphorus (POP). On the second cast, four discrete depths in the upper 200 m were selected based on chlorophyll concentrations: below the deep chlorophyll maximum (DCM), at the DCM, an intermediate depth above the DCM and a 10-metre surface depth. The 10-metre surface depth was chosen due to technical restrictions of sampling with a CTD rosette and to ensure a comparable depth within the surface mixed layer (Supplementary Figure S1). From these depths, samples were taken for nutrients, methane, POC, PON, DNA and RNA, as well as water samples for stable isotope incubation experiments to quantify rates of aerobic methane formation and carbon fixation.

Determination of water column chemistry

Dissolved nutrients

Ammonium concentrations were determined fluorometrically (orthophthaldialdehyde (OPA) method (Holmes et al. 1999)) using unfiltered water samples immediately after sample retrieval. The limit of detection (LOD), calculated as the mean of the blanks plus three times the standard deviation, was 24 nmol L^{-1}. Samples for NO_3^- and NO_2^- were frozen unfiltered at -20°C until simultaneous spectrophotometric measurement using a QuAAtro39 autoanalyser (Seal

Analytical) using standard methods (Strickland & Parsons 1972). It should be noted that freeze thawing may break open cells and release intracellular nutrients (Chapman & Mostert 1990). NO_3^- was determined as the difference between NO_3^- and NO_2^- combined (NOx) and NO_2^-. LODs were 583 nmol L^{-1} (NOx) and 33 nmol L^{-1} (NO_2^-). From the same sample inorganic phosphate (Pi) and total phosphorus (TP) were also determined. These were measured simultaneously using a Liquid Waveguide Capillary Cell (Seal Analytical). Briefly, for TP measurements, TP was irradiated in a UV digester after persulfate addition; this is followed by acid hydrolysis at 90°C before colorimetric measurement at 880 nm after reacting with molybdate, antimony and ascorbic acid (Seal Analytical). LOD for Pi and TP were 10 nmol L^{-1} and 30 - 50 nmol L^{-1}, respectively. The organic phosphorus (OP) fraction was calculated by subtracting Pi from TP.

Particulate carbon, nitrogen and phosphorus

Samples for POP were collected by filtering 3.5 L of seawater onto pre-combusted (4 hours at 450°C) glass fibre (GF/F, Whatman) filters. POP was measured using a modified version of the persulfate oxidation method (Suzumura 2008). Briefly, instead of autoclaving, the samples were heated in a microwave "Mars 1" (CEM) for 20 minutes to reach 150°C and were then incubated for 15 minutes, followed by 20 minutes of cooling. Subtracting the POP from the calculated OP (see previous section), yielded the dissolved organic phosphorus (DOP) concentrations. POC and PON were determined from an additional 3.5 L of seawater filtered onto pre-combusted GF/F filters (Whatman) and dried at 50°C overnight. Samples were decalcified by hydrochloric acid (37%, Merck) fumes in a desiccator overnight, dried and pelleted in tin cups and subsequently measured by an element analyser (Thermo Flash EA, 1112 Series) coupled to a continuous-flow isotope ratio mass spectrometer (Delta Plus XP IRMS, Thermo Finnigan).

Dissolved in-situ *methane concentration measurements*

Duplicate samples for methane concentrations were filled headspace free with a triple overflow into 60 ml serum bottles using gas-tight Viton tubing. Microbial activity was inhibited by adding a scoop of copper(I)chloride (Merck) and the bottles were stoppered (Glasgerätebau Ochs) and crimped. Before analysis, a 20 ml headspace was set with synthetic air (80% nitrogen, 20% oxygen; Air Liquide) before methane measurements on a gas concentration analyser (Picarro

G2308). Samples were calibrated against three standards: degassed MiliQ water, air-saturated MiliQ water and air-saturated saline solution (10% sodium chloride). However, an interference from the stoppers (Butyl-Septen für Hals N20, Glasgerätebau Ochs Laborfachhandel) through apparent methane leakage invalidated the measurements, making them void. This was confirmed by observing increases in methane concentration over time in a MiliQ experiment that was initially air saturated.

Chlorophyll a

For discrete water column Chl *a* samples, 600 ml of water was filtered onto a 25 mm pre-combusted GF/F filter (Whatman). Chl *a* was extracted in 90% acetone from filters and measured fluorometrically (Turner Designs (Arar & Collins 1997). Results were calibrated against a Chl *a* standard (Sigma Aldrich). The concentration measurements from all depths and stations were then used to calibrate the fluorescence sensor of the CTD, by linear regression, converting relative fluorescence units into µg L^{-1} Chl *a* (Supplementary Figure S8) for stations 3 and 7, where Chl *a* samples were not taken. Satellite surface Chl *a* concentrations were obtained from Earth Data and downloaded through the Giovanni online data system, which is developed and maintained by the NASA GES DISC, for the timeframe between 01 January and 29 February, creating a composite snapshot using the MODIS-Aqua, monthly, 4 km resolution for the region between 56.75 - 60° W and 11.75 - 15° N.

Stable isotope incubations and rate calculations

Methane formation

Rates of methane formation were quantified at each station from four depths from ^{13}C stable isotope incubation experiments with either dissolved methylphosphonate (MPn; $^{13}CH_5O_3P$, 99 atom % ^{13}C, dissolved in MilliQ water, Sigma-Aldrich) or dissolved inorganic carbon (DIC; $NaH^{13}CO_3$, 98 atom % ^{13}C, dissolved in MilliQ water; Sigma-Aldrich) set up in biological duplicates. Briefly, acid-washed 250 mL serum bottles were filled headspace-free, stoppered (Geo-Microbial Technologies) and crimped. A 50 mL headspace was set with synthetic air (80% nitrogen, 20% oxygen; Air Liquide) before tracers were added. All bottles were swirled for mixing after the additions. Four experiments were set up in separate incubation bottles: MPn-

addition (1 µmol L^{-1} ^{13}C-MPn), MPn + Pi-addition (1 µmol L^{-1} ^{13}C-MPn + 1 µmol L^{-1} Pi), MPn + nitrate addition (1 µmol L^{-1} ^{13}C-MPn + 16 µmol L^{-1} NO_3^-) and the DIC incubation (200 µmol L^{-1} ^{13}C-DIC). In one replicate of both the MPn-addition and DIC incubation experiments 10% of the water was replaced by deuterium oxide (D_2O, 99.9 atom %, Sigma Aldrich). The incubation bottles were incubated in two *on-deck* incubators at surface water temperatures and close to *in-situ* light conditions. To achieve this, the incubators were covered with two different blue filters (Ocean Blue #724 and Tokyo blue #071, Lee Filters, https://www.leefilters.com/lighting/colour-list.html; Supplementary Figure S9), with the below DCM and DCM as well as the intermediate and surface depths incubated together. At five time points, after 0, 6, 12, 24 and 48 hours of incubation, the headspace was subsampled. At each time point, 5 mL of the headspace was sampled with a gas-tight syringe whilst replacing the removed volume with synthetic air. The headspace sample was injected into a 12 mL Exetainer (Labco UK) pre-filled with MilliQ-water, setting a 5 mL headspace for later analysis. Gas samples were preserved through the addition of 100 µL mercuric chloride solution ($HgCl_2$, 0.7 g/100ml) to inhibit microbial activity and stored overhead. Samples were measured on a cavity-ring down spectrometer (G2201-i coupled to Liaison A0301, Picarro Inc., connected to an AutoMate Prep device, Bushnell).

Methane formation rates were calculated from incubations that showed a statistically significant linear increase of excess ^{13}C-methane over the first four time points (24 hours; Supplementary Figure S4). Significance was determined by a one sided student's t-test ($p < 0.05$) applied to the linear regression ($R^2 > 0.81$) of the excess ^{13}C-methane formation. Clearly exponential rates (formation only in the 24 hour time point) were set to zero to ensure comparable analysis, this only affected a single incubation. All rates were corrected for the dilution factor and labelling percentage. For MPn-amended incubations, the labelling was assumed to be 100%, as the *in-situ* concentrations cannot be determined. For the DIC-amended incubations, labelling was ~10%. To compare the methane formation rates across depth and incubation type, Kruskal-Wallis statistical analysis was conducted after a Shapiro-Wilk normality test followed by a pairwise Wilcoxon test with a Benjamini-Hochberg adjusted p-value, all one-sided and performed in RStudio. To investigate correlating parameters with methane formation rates, Spearman Ranked correlation analysis was performed in RStudio using all available parameters.

Carbon fixation rates

Carbon fixation experiments were set up in parallel bottles to the aerobic methane formation experiments. Briefly, biological triplicate water samples in 4.6 L polycarbonate bottles were amended with ^{13}C-DIC ($NaHCO_3$, >98% at% ^{13}C, Sigma Aldrich) to achieve a labelling percentage of ~ 5 at% and gently agitated to mix for 15 minutes. Bottles were then incubated, headspace-free, for 24 hours under dawn to dawn conditions in the two *on-deck* incubators (see above). One additional unamended sample per depth was also incubated as a natural abundance control incubation. After 24 hours, 3.5 L were filtered onto a pre-combusted (4 hours at 450°C) 25 mm GF/F filter (Whatman) and dried at ~ 55°C overnight. Filters were processed as described above (POC/PON) and samples were measured with an element analyser (Thermo Flash EA, 1112 Series) coupled to a continuous-flow isotope ratio mass spectrometer (Delta Plus XP IRMS, Thermo Finnigan). Rates of primary productivity were determined from the uptake of ^{13}C-DIC into biomass (Marra 2009) with carbon fixation rates calculated according to Großkopf (Großkopf et al. 2012).

DNA and RNA isolation and metagenome and metatranscriptome sequencing

At each incubation depth, twice ten litres of seawater were sequentially filtered through a 10 µm pore size polycarbonate filter and a 3 µm pore size polycarbonate filter before being split into two Sterivex filters (each received 5 L of water). All filters were immediately frozen in liquid nitrogen and stored at -80°C until DNA or RNA extraction. Station 5 was chosen as a representative station for DNA and RNA extraction. DNA was isolated by the chloroform/isoamyl alcohol (24:1) method (Zhou et al. 1996). RNA was extracted by standard protocol of the RNeasy PowerWater kit (Qiagen), with an additional heating step at 65°C for 10 minutes prior to bead beating. Samples were sequenced with 2 * 150 bp paired-end Illumina technology. RNA samples were sequenced after rRNA depletion, which was only possible for the small (0.22 - 3 µm) size fraction of the upper three incubation depths due to limited RNA quantities. For metagenomes a total of >10 Gb and for metatranscriptomes a total of >20 Gb were sequenced per sample.

Metagenomic and metatranscriptomic analysis

Metagenomic and metatranscriptomic reads were adapter and quality trimmed using Trimmomatics version 0.39 (Bolger et al. 2014). Metagenomic samples were used for distance estimation and clustering using mash version 2.3 (Supplementary Figure S10; Ondov et al. 2016), revealing that the surface and intermediate depths as well as the DCM and below DCM samples and the different size fractions, clustered together. Based on these clusters, the samples were co-assembled using megahit version 1.2.9 (Li et al. 2015) for a total of six co-assemblies. All co-assemblies were then put into the SqueezeMeta pipeline version 1.3 (Tamames & Puente-Sánchez 2019). From all open reading frames, 135 genes annotated as *phnJ* were extracted. The amino acid sequences were clustered with CD-HIT version 4.6 (Fu et al. 2012; Li & Godzik 2006; Li et al. 2001, 2002), using a 95% sequence identity cut-off over 90% of the length of all sequences, resulting in 78 unique sequences. The sequences were used in blastp search (Camacho et al. 2009) to the NCBI nr database (2nd December 2021). The best two hits per query were used as references, resulting in 104 unique reference sequences. A multiple sequence alignment was conducted with MAFFT v7.475 (Katoh & Standley 2013), manually filtered and trimmed with trimAL v1.4.rev15 (Capella-Gutiérrez et al. 2009). This left 128 sequences, 36 from the original samples, to construct a phylogenetic tree with IQ tree including the Modelfinder (Hoang et al. 2018; Kalyaanamoorthy et al. 2017; Minh et al. 2020). To map both the metagenomic and metatranscriptomic reads to the tree sequences, bowtie2 version 2.3.4.1 (Langmead & Salzberg 2012) was used. Read counts with a sequence identity >80% were extracted using coverM version 0.6.1. TPM values for both metagenomic and metatranscriptomic samples were calculated in accordance with Wagner (Wagner et al. 2012).

To constrain the relative *phnJ* abundance within the different size fractions, *phnJ* read counts were corrected for read counts to the single copy marker gene *recA*, as described previously (Martinez et al. 2010). Sequences annotated as *recA* were clustered and used for mapping of the metagenomic reads as described above. Read counts of both *phnJ* and *recA* genes were normalised by ORF length and set in relation.

Figure generation

Maps and nutrient figures were generated using the quantum geographic information system (QGIS; version 3.18.3) or Ocean Data View (version 5.1.7; Schlitzer 2019). Rate analysis was conducted in Microsoft Excel (2016) and figures were generated in RStudio 2023.3.0.386 (Team 2023) versions 4.1.3 and 4.2.2 (R Core Team) using the ggplot2 (Wickham 2016) package. The phylogenetic tree was visualised in iTOL (Letunic & Bork 2021).

Data deposition

All new *phnJ* sequences have been deposited to NCBI under accession numbers OQ435733-68. The reference sequences for the phylogenetic tree are included in Supplementary Figure S6 with their accession numbers.

Code availability

All statistical analysis was performed in RStudio 2023.3.0.386 (Team 2023) versions 4.1.3 and 4.2.2 (R Core Team) which is publically available.

Acknowledgments

We would like to thank the captain and crew of the FS Meteor during the M161 cruise for all their assistance during the expedition; D. Baranowski and his CTD team for helping with the sampling, providing the CTD data and calculating the mixed layer depths; B. Stevens and S. Bony for coordinating the EUREC^{4}A project; M. Knutzen, G. Klockgether, S. Lilienthal, K. Imhoff, S. Piosek, N. Rujanski and D. Tienken for the technical support; S. Ahmerkamp, C. Frey, F. M. Jalaluddin, K. Kitzinger, H. Marchant, A. S. McDermott and D. Speth for the helpful discussions and comments on the manuscript; the Leitstelle Deutsche Forschungsschiffe for their support; the funding for the cruise by the Deutsche Forschungsgemeinschaft (Fördernummer: GPF18-1-69, EUREC^{4}A^{++}), Bundesministerium für Bildung und Forschung; the funding of this study by the Max Planck Society.

Bibliography

Arar EJ. Collins GB. 1997. Method 445.0: In vitro determination of chlorophyll a and pheophytin a in marine and freshwater algae by fluorescence. U.S. EnvironmentalProtection Agency, Washington, DC

Balch WE, Fox GE, Magrum LJ, Woese CR, Wolfe RS. 1979. Methanogens: reevaluation of a unique biological group. *Microbiol. Rev.* 43(2):260–96

Behrenfeld MJ, Falkowski PG. 1997. Photosynthetic rates derived from satellite-based chlorophyll concentration. *Limnol. Oceanogr.* 42(1):1–20

Beversdorf LJ, White AE, Björkman KM, Letelier RM, Karl DM. 2010. Phosphonate metabolism by Trichodesmium IMS101 and the production of greenhouse gases. *Limnol. Oceanogr.* 55(4):1768–78

Bianchi M, Marty D, Teyssie JL, Fowler SW. 1992. Strictly aerobic and anaerobic bacteria associated with sinking particulate matter and zooplankton fecal pellets. *Mar. Ecol. Prog. Ser.* 88(1):55–60

Bižić M, Klintzsch T, Ionescu D, Hindiyeh MY, Günthel M, et al. 2020. Aquatic and terrestrial cyanobacteria produce methane. *Sci. Adv.* 6(3):1–10

Bolaños LM, Choi CJ, Worden AZ, Baetge N, Carlson CA, Giovannoni S. 2021. Seasonality of the Microbial Community Composition in the North Atlantic. *Front. Mar. Sci.* 8(February):1–16

Bolger AM, Lohse M, Usadel B. 2014. Trimmomatic: A flexible trimmer for Illumina sequence data. *Bioinformatics*. 30(15):2114–20

Camacho C, Coulouris G, Avagyan V, Ma N, Papadopoulos J, et al. 2009. BLAST+: Architecture and applications. *BMC Bioinformatics*. 10:1–9

Capella-Gutiérrez S, Silla-Martínez JM, Gabaldón T. 2009. trimAl: A tool for automated alignment trimming in large-scale phylogenetic analyses. *Bioinformatics*. 25(15):1972–73

Capone DG, Zehr JP, Paerl HW, Bergman B, Carpenter EJ. 1997. Trichodesmium, a globally significant marine cyanobacterium. *Science (80-.).* 276(5316):1221–29

Carini P, White AE, Campbell EO, Giovannoni SJ. 2014. Methane production by phosphate-starved SAR11 chemoheterotrophic marine bacteria. *Nat. Commun.* 5:1–7

Cavender-Bares KK, Karl DM, Chisholm SW. 2001. Nutrient gradients in the western North Atlantic Ocean: Relationship to microbial community structure and comparison to patterns in the Pacific Ocean. *Deep. Res. Part I Oceanogr. Res. Pap.* 48(11):2373–95

Chapman P, Mostert SA. 1990. Does freezing of nutrient samples cause analytical errors? *South African J. Mar. Sci.* 9(1):239–47

Chien C-T, Mackey KRM, Dutkiewicz S, Mahowald NM, Prospero JM, Paytan A. 2016. Effects of African dust deposition on phytoplankton in the western tropical Atlantic Ocean off Barbados. *Global Biogeochem. Cycles*. 30(5):716–34

Cullen JJ. 2015. Subsurface chlorophyll maximum layers: Enduring enigma or mystery solved? *Ann. Rev. Mar. Sci.* 7:207–39

Damm E, Helmke E, Thoms S, Schauer U, Nöthig E, et al. 2010. Methane production in aerobic oligotrophic surface water in the central Arctic Ocean. *Biogeosciences*. 7(3):1099–1108

Del Valle DA, Karl DM. 2014. Aerobic production of methane from dissolved water-column methylphosphonate and sinking particles in the North Pacific Subtropical Gyre. *Aquat. Microb. Ecol.* 73(2):93–105

Dyhrman ST, Benitez-Nelson CR, Orchard ED, Haley ST, Pellechia PJ. 2009. A microbial source of phosphonates in oligotrophic marine systems. *Nat. Geosci.* 2(10):696–99

Dyhrman ST, Chappell PD, Haley ST, Moffett JW, Orchard ED, et al. 2006. Phosphonate utilization by the globally important marine diazotroph Trichodesmium. *Nature*. 439(7072):68–71

Dyhrman ST, Webb EA, Anderson DM, Moffett JW, Waterbury JB. 2002. Cell-specific detection of phosphorus stress in Trichodesmium from the Western North Atlantic. *Limnol. Oceanogr.* 47(6):1832–36

Ernst L, Steinfeld B, Barayeu U, Klintzsch T, Kurth M, et al. 2022. Methane formation driven by reactive oxygen species across all living organisms. *Nature*. 603(7901):482–87

Frischkorn KR, Krupke A, Guieu C, Louis J, Rouco M, et al. 2018. Trichodesmium physiological ecology and phosphate reduction in the western tropical South Pacific. *Biogeosciences*. 15(19):5761–78

Frischkorn KR, Rouco M, Van Mooy BAS, Dyhrman ST. 2017. Epibionts dominate metabolic functional potential of Trichodesmium colonies from the oligotrophic ocean. *ISME J.* 11(9):2090–2101

Fu L, Niu B, Zhu Z, Wu S, Li W. 2012. CD-HIT: Accelerated for clustering the next-generation sequencing data. *Bioinformatics*. 28(23):3150–52

Fu W, Randerson JT, Keith Moore J. 2016. Climate change impacts on net primary production (NPP) and export production (EP) regulated by increasing stratification and phytoplankton community structure in the CMIP5 models. *Biogeosciences*. 13(18):5151–70

Granzow BN, Sosa OA, Gonnelli M, Santinelli C, Karl DM, Repeta DJ. 2021. A sensitive fluorescent assay for measuring carbon-phosphorus lyase activity in aquatic systems. *Limnol. Oceanogr. Methods*. 19(4):235–44

Großkopf T, Mohr W, Baustian T, Schunck H, Gill D, et al. 2012. Doubling of marine dinitrogen-fixation rates based on direct measurements. *Nature*. 488(7411):361–64

Hoang DT, Chernomor O, Von Haeseler A, Minh BQ, Vinh LS. 2018. UFBoot2: Improving the ultrafast bootstrap approximation. *Mol. Biol. Evol.* 35(2):518–22

Holmes RM, Aminot A, Kérouel R, Hooker BA, Peterson BJ. 1999. A simple and precise method for measuring ammonium in marine and freshwater ecosystems. *Can. J. Fish. Aquat. Sci.* 56(10):1801–8

Hutchins DA, Fu F. 2017. Microorganisms and ocean global change. *Nat. Microbiol.* 2(May):

Kalyaanamoorthy S, Minh BQ, Wong TKF, Von Haeseler A, Jermiin LS. 2017. ModelFinder: Fast model selection for accurate phylogenetic estimates. *Nat. Methods*. 14(6):587–89

Kamat SS, Williams HJ, Raushel FM. 2011. Intermediates in the transformation of phosphonates to phosphate by bacteria. *Nature*. 480(7378):570–73

Karl DM. 2014. Microbially mediated transformations of phosphorus in the sea: New views of an old cycle. *Ann. Rev. Mar. Sci.* 6:279–337

Karl DM, Beversdorf L, Björkman KM, Church MJ, Martinez A, Delong EF. 2008. Aerobic production of methane in the sea. *Nat. Geosci.* 1(7):473–78

Katoh K, Standley DM. 2013. MAFFT multiple sequence alignment software version 7: Improvements in performance and usability. *Mol. Biol. Evol.* 30(4):772–80

Kiene RP. 1991. Production and consumption of methane in aquatic systems. In J. E. Rogers, & W. B. Whitman (Eds.), Microbial Production and Consumption of Greenhouse Gases: Methane, Nitrogen Oxides and Halomethanes (pp. 111–146). Washington, DC: American Society for Microbiology.

Kolomijeca A, Marx L, Reynolds S, Cariou T, Mawji E, Boulart C. 2022. An update on dissolved methane distribution in the subtropical North Atlantic Ocean. *Ocean Sci.* 18(5):1377–88

Lamontagne R a, Swinnerton JW, Linnenbom VJ, Smith WD. 1973. Methane concentrations in various marine environments. *J. Geophys. Res.* 78(24):5317–24

Lamontagne RA, Swinnerton JW, Linnenbom VJ. 1971. Nonequilibrium of carbon monoxide and methane at the air-sea interface. *J. Geophys. Res.* 76(21):5117–21

Langmead B, Salzberg SL. 2012. Fast gapped-read alignment with Bowtie 2. *Nat. Methods*. 9(4):357–59

Lenhart K, Klintzsch T, Langer G, Nehrke G, Bunge M, et al. 2016. Evidence for methane production by the marine algae Emiliania huxleyi. *Biogeosciences*. 13(10):3163–74

Letunic I, Bork P. 2021. Interactive tree of life (iTOL) v5: An online tool for phylogenetic tree display and annotation. *Nucleic Acids Res.* 49(W1):W293–96

Li D, Liu CM, Luo R, Sadakane K, Lam TW. 2015. MEGAHIT: An ultra-fast single-node solution for large and complex metagenomics assembly via succinct de Bruijn graph. *Bioinformatics*. 31(10):1674–76

Li W, Godzik A. 2006. Cd-hit: A fast program for clustering and comparing large sets of protein or nucleotide sequences. *Bioinformatics*. 22(13):1658–59

Li W, Jaroszewski L, Godzik A. 2001. Clustering of highly homologous sequences to reduce the size of large protein databases. *Bioinformatics*. 17(3):282–83

Li W, Jaroszewski L, Godzik A. 2002. Tolerating some redundancy significantly speeds up clustering of large protein databases. *Bioinformatics*. 18(1):77–82

Liang Z, Letscher RT, Knapp AN. 2022. Dissolved organic phosphorus concentrations in the surface ocean controlled by both phosphate and iron stress. *Nat. Geosci.* 15(8):651–57

Lockwood S, Greening C, Baltar F, Morales SE. 2022. Global and seasonal variation of marine phosphonate metabolism. *ISME J.* 16(9):2198–2212

Marra J. 2009. Net and gross productivity: Weighing in with 14C. *Aquat. Microb. Ecol.* 56(2–3):123–31

Martinez A, Tyson GW, Delong EF. 2010. Widespread known and novel phosphonate utilization pathways in marine bacteria revealed by functional screening and metagenomic analyses. *Environ. Microbiol.* 12(1):222–38

Martínez A, Ventouras LA, Wilson ST, Karl DM, DeLong EF. 2013. Metatranscriptomic and functional metagenomic analysis of methylphosphonate utilization by marine bacteria. *Front. Microbiol.* 4(NOV):1–18

Martiny AC, Lomas MW, Fu W, Boyd PW, Chen Y ling L, et al. 2019. Biogeochemical controls of surface ocean phosphate. *Sci. Adv.* 5(8):1–10

Mather RL, Reynolds SE, Wolff GA, Williams RG, Torres-Valdes S, et al. 2008. Phosphorus cycling in the North and South Atlantic Ocean subtropical gyres. *Nat. Geosci.* 1(7):439–43

Mills MM, Moore CM, Langlois R, Milne A, Achterberg E, et al. 2008. Nitrogen and phosphorus co-limitation of bacterial productivity and growth in the oligotrophic subtropical North Atlantic. *Limnol. Oceanogr.* 53(2):824–34

Minh BQ, Schmidt HA, Chernomor O, Schrempf D, Woodhams MD, et al. 2020. IQ-TREE 2: New Models and Efficient Methods for Phylogenetic Inference in the Genomic Era. *Mol. Biol. Evol.* 37(5):1530–34

Moore CM, Mills MM, Langlois R, Milne A, Achterberg EP, et al. 2008. Relative influence of nitrogen and phosphorus availability on phytoplankton physiology and productivity in the oligotrophic sub-tropical North Atlantic Ocean. *Limnol. Oceanogr.* 53(1):291–305

Murphy ARJ, Scanlan DJ, Chen Y, Adams NBP, Cadman WA, et al. 2021. Transporter characterisation reveals aminoethylphosphonate mineralisation as a key step in the marine phosphorus redox cycle. *Nat. Commun.* 12(1):1–12

Ondov BD, Treangen TJ, Melsted P, Mallonee AB, Bergman NH, et al. 2016. Mash: Fast genome and metagenome distance estimation using MinHash. *Genome Biol.* 17(1):1–14

Oremland RS. 1979. Methanogenic activity in plankton samples and fish intestines A mechanism for in situ methanogenesis in oceanic surface waters. *Limnol. Oceanogr.* 24(6):1136–41

Pack M, Heintz MB, Reeburgh WS, Trumbore SE, Valentine DL, et al. 2015. Methane oxidation in the eastern tropical North Pacific Ocean water column. *J. Geophys. Res. Biogeosciences*. 120(6):1078–92

Perez-Coronel E, Michael Beman J. 2022. Multiple sources of aerobic methane production in aquatic ecosystems include bacterial photosynthesis. *Nat. Commun.* 13(1):

Redfield AC. 1958. The Biological Control of Chemical Factors in the Environment. *Am. Sci.* 46(3):205–21

Repeta DJ, Ferrón S, Sosa OA, Johnson CG, Repeta LD, et al. 2016. Marine methane paradox explained by bacterial degradation of dissolved organic matter. *Nat. Geosci.* 9(12):884–87

Roda-Garcia JJ, Haro-Moreno JM, Huschet LA, Rodriguez-Valera F, López-Pérez M. 2021. Phylogenomics of SAR116 Clade Reveals Two Subclades with Different Evolutionary Trajectories and an Important Role in the Ocean Sulfur Cycle. *mSystems*. 6(5):

Schlitzer R. 2019. Ocean Data View

Scranton MI, Brewer PG. 1977. Occurrence of methane in the near-surface waters of the western subtropical North-Atlantic. *Deep. Res.* 24(2):127–38

Sosa OA, Burrell TJ, Wilson ST, Foreman RK, Karl DM, Repeta DJ. 2020. Phosphonate cycling supports methane and ethylene supersaturation in the phosphate-depleted western North Atlantic Ocean. *Limnol. Oceanogr.* 65(10):2443–59

Sosa OA, Repeta DJ, DeLong EF, Ashkezari MD, Karl DM. 2019a. Phosphate-limited ocean regions select for bacterial populations enriched in the carbon–phosphorus lyase pathway for phosphonate degradation. *Environ. Microbiol.* 21(7):2402–14

Sosa OA, Casey JR, Karl DM. 2019b. Methylphosphonate Oxidation in Prochlorococcus Strain MIT9301 Supports Phosphate Acquisition, Formate Excretion, and Carbon Assimilation into Purines. *Appl. Environ. Microbiol.* 85(13):1–12

Strickland JDH & Parsons TR. 1972. *A Practical Handbook of Seawater Analysis*. Bulletin no. 167

Suzumura M. 2008. Persulfate chemical wet oxidation method for the determination of particulate phosphorus in comparison with a high-temperature dry combustion method. *Limnol. Oceanogr. Methods*. 6(11):619–29

Tamames J, Puente-Sánchez F. 2019. SqueezeMeta, a highly portable, fully automatic metagenomic analysis pipeline. *Front. Microbiol.* 10(JAN):1–10

Team P. 2023. RStudio: Integrated Development Environment for R

Traganza ED, Swinnerton JW, Cheek CH. 1979. Methane supersaturation and ATP-zooplankton blooms in near-surface waters of the Western Mediterranean and the subtropical North Atlantic Ocean. *Deep Sea Res. Part A. Oceanogr. Res. Pap.* 26(11):1237–45

van de Waal DB, Litchman E. 2020. Multiple global change stressor effects on phytoplankton nutrient acquisition in a future ocean. *Philos. Trans. R. Soc. B Biol. Sci.* 375(1798):1–8

Van Mooy BAS, Krupke A, Dyhrman ST, Fredricks HF, Frischkorn KR, et al. 2015. Major role of planktonic phosphate reduction in the marine phosphorus redox cycle. *Science (80-.).* 348(6236):783–85

Villareal TA, Carpenter EJ. 2003. Buoyancy regulation and the potential for vertical migration in the oceanic cyanobacterium Trichodesmium. *Microb. Ecol.* 45(1):1–10

Wackett LP, Shames SL, Venditti CP, Walsh CT. 1987. Bacterial carbon-phosphorus lyase: Products, rates, and regulation of phosphonic and phosphinic acid metabolism. *J. Bacteriol.* 169(2):710–17

Wagner GP, Kin K, Lynch VJ. 2012. Measurement of mRNA abundance using RNA-seq data: RPKM measure is inconsistent among samples. *Theory Biosci.* 131(4):281–85

Wang Q, Alowaifeer A, Kerner P, Balasubramanian N, Patterson A, et al. 2021. Aerobic bacterial methane synthesis. *Proc. Natl. Acad. Sci. U. S. A.* 118(27):

Wanner BL. 1996. Signal transduction in the control of phosphate-regulated genes of Escherichia coli. *Kidney Int.* 49(4):964–67

Weber T, Wiseman NA, Kock A. 2019. Global ocean methane emissions dominated by shallow coastal waters. *Nat. Commun.* 10(1):1–10

Wickham H. 2016. *Ggplot2: Elegant Graphics for Data Analysis*. Springer-Verlag New York

Wu J, Sunda W, Boyle EA, Karl DM. 2000. Phosphate depletion in the Western North Atlantic Ocean. *Science (80-.).* 289(5480):759–62

Yao M, Henny C, Maresca JA. 2016. Freshwater bacteria release methane as a by-product of phosphorus acquisition. *Appl. Environ. Microbiol.* 82(23):6994–7003

Zheng Y, Harris DF, Yu Z, Fu Y, Poudel S, et al. 2018. A pathway for biological methane production using bacterial iron-only nitrogenase. *Nat. Microbiol.* 3(3):281–86

Zhou J, Bruns MA, Tiedje JM. 1996. DNA recovery from soils of diverse composition. *Appl. Environ. Microbiol.* 62(2):316–22

Supplement

Supplementary Text

Abiotic photodegradation of methylphosphonate

It has been shown that methylphosphonate (MPn) can decompose into methane and phosphate (Pi) under prolonged UV irradiation (Yu et al. 2018; Zhang & Ji 2019). While we did not specifically test for photochemical degradation of MPn, we argue that the contribution of any such process is likely marginal at best and will not affect the rates measured in our study.

First of all, the conditions under which photochemical MPn degradation was shown to occur are not comparable to the conditions in our incubations or *in-situ*. Our incubation times were (much) shorter than the tested incubation times of 2100 hours (Yu et al. 2018) and 58 hours (Zhang & Ji 2019). Furthermore, most efficient MPn degradation was observed under both highly alkaline and acidic conditions, unlike seawater which was expected to have a pH of around 8. Highest rates of abiotic MPn degradation were observed using a UV lamp with an intensity of 1200W (Zhang & Ji 2019), while our samples were incubated in natural light with Lee filter papers (Supplementary Figure S9).

Most importantly, our incubations (48 hours) covered two day and night cycles (with up to 12 h 15 minutes of darkness), whereas methane production proceeded linearly over time, without any clear relation to light availability (Supplementary Figure S4). Additionally, abiotic methane formation would be expected to produce similar amounts of methane in incubations exposed to the same light conditions and containing the same amount of ^{13}C-MPn tracer. This was not the case. Methane production in the surface and intermediate depths (which were incubated in the same incubator) varied by one to two orders of magnitude, as did even duplicate samples from the same depths. Additionally, water samples, to which Pi was added had significantly lower methane production rates than the MPn incubations only, even though they were set up from the same water, with the same amount of MPn tracer and incubated under the same light conditions. We therefore conclude that the ^{13}C-methane produced in our incubations is a result of biological turnover of MPn and not photochemical degradation.

In-situ, the UV penetration depth Z10% for both UV-A and UV-B likely does not exceed 35 m (Tedetti & Sempéré 2006 and references therein) and thus would not significantly affect most incubation depths. Nonetheless, it would surely be worthwhile to test for photochemical MPn degradation under a range of environmentally-relevant settings (pH, irradiation intensity, temperature, time).

Methylphosphonate-driven methane formation rate measurements

While only the data from the first 24 hours was used to quantify MPn-driven methane formation rates, our incubations lasted 48 hours, with one additional time point. Within this timeframe many incubations started to show exponential behaviour, a phenomenon we attribute to opportunistic growth under prolonged incubation times. This is especially expected due to the high ^{13}C-MPn supplementations as well as nutrient additions. Based on these observations, we caution against deriving rates of aerobic methane formation from incubations lasting over 24 hours, in which case multiple time points should be taken within the incubation time frame that allow for monitoring any potential onset of exponential rates.

In the MPn-supplemented incubations 22 out of 96 incubations did not show significant linear methane formation within the first 24 hours of incubation. However, all except one displayed substantial (28 - 4972 pmol L^{-1}) methane formation in the last time point, indicating that the capacity to metabolise MPn was there in most of the samples taken. Furthermore, 17 out of the 21 incubations were from the deep chlorophyll maximum (DCM) or the below DCM depths, suggesting that the MPn use is more variable in these depths. The single incubation without any formation was from the below DCM depth. In the experiment with equimolar amounts of phosphate (Pi) and MPn, 40 out of 90 incubations did not show significant linear methane formation within 24 hours of incubation, a clear increase from the MPn-supplemented experiment. However, methane formation was observed in 33 out of these incubations within 48 hours, suggesting that the capacity was still there, albeit at a reduced rate compared to the MPn-supplemented ones. The majority (25 out of 40) of incubations without linear rates were from the DCM and below DCM depths. In the MPn + nitrate-addition experiment 13 out of 91 incubations had no significant linear methane formation within 24 hours. Of these, only two had no quantifiable methane formation after 48 hours, originating from the DCM and below DCM

depths. Overall, over prolonged incubation times methane formation can be quantified from most experiments but at a higher variability from the DCM and below DCM depths.

Methylphosphonate utilisation in the presence of phosphate

Methane production in the presence of Pi might be an indication for a persistent expression of the C-P lyase pathway. It is conceivable that competition for MPn or phosphonates in general is less fierce than for inorganic phosphate, hence their utilisation might offer an ecological advantage, particularly if carbon is limiting. Alternatively, some organisms may be able to afford to express pathways that allow them to co-metabolise organic phosphorus compounds (such as MPn) and inorganic phosphate, as shown for *Trichodesmium* (Beversdorf et al. 2010). Additionally, the enzyme might be expressed to e.g. deal with the degradation of phosphonates, which might have cytotoxic or protective effects, rather than for the purpose of obtaining phosphorus (Acker et al. 2022; Horsman & Zechel 2017). It would be of great interest to explore whether there is a universal threshold inhibitory Pi concentration that turns MPn utilisation on and off or whether this value responds to the respective biogeochemical parameters (e.g. availability of carbon, nutrients and dominant MPn utilising taxa) of a given environment.

Trichodesmium *as a phosphonate producer and consumer*

Trichodesmium - together with *SAR11* (Born et al. 2017; Carini et al. 2014) - belongs to the small group of organisms that have the capacity to be both phosphonate producers and consumers (Acker et al. 2022). The capacity to degrade phosphonates with the C-P lyase pathway seems to be widespread in the *Trichodesmium* genus and includes *T. erythraeum*, *T. thiebautii*, *T. tenue*, and *T. spiralis* (Dyhrman et al. 2006) as well as members of its microbiome (Frischkorn et al. 2017). On the other hand, the synthesis of phosphonates has only been confirmed for *T. erythraeum* (Dyhrman et al. 2009) as well as the microbiome (Frischkorn et al. 2017). It has been proposed that phosphonate formation and consumption may additionally be strain specific (Acker et al. 2022; Schowanek & Verstraete 1990).

Phosphonate synthesis may be temporally or spatially separated from phosphonate utilisation, for example during the vertical migration in the water column (Villareal & Carpenter 2003) between Pi rich bottom waters and Pi deplete surface waters, which may promote phosphonate synthesis

(the former) or utilisation (the latter). Additionally, an organism like *Trichodesmium*, which has a huge genome (7.75 Mbp; Bergman et al. 2013)) and lives under energy surplus may afford to encode and express 'luxury' metabolic pathways that are not key for its survival. It has also been proposed that *Trichodesmium* may produce phosphonates to restrict access to this critical nutrient to microbes other than its own epibionts (Frischkorn et al. 2018). Phosphonate synthesis and degradation might also serve other purposes than phosphorus acquisition, such as defence, as many phosphonates are potent antibiotics (Acker et al. 2022). In any case, the capacity to both produce and utilise organic phosphorus compounds may decisively contribute to the ecological success of *Trichodesmium* in low phosphate, oligotrophic systems (Dyhrman et al. 2006).

Origin of methylphosphonate in surface waters remains elusive

While the carbon phosphorus (C-P) lyase pathway is widespread in the surface waters, the origin of MPn (and phosphonates in general) in these waters is still largely unresolved. The genetic potential for MPn synthesis is inferred based on the presence of the *mpnS* gene encoding for MPn synthase (Metcalf et al. 2012). In our samples, we found only a few fragmented *mpnS* gene-related sequences (data not shown), predominantly from below the DCM and associated with the ammonia oxidising *Thaumarchaeota*. Indeed, the ammonia-oxidising *Nitrosopumilus maritimus* (Metcalf et al. 2012) is - together with *Pelagibacter ubique SAR11* (Born et al. 2017) - the only organism with a confirmed capacity to synthesise MPn. However, there are indications that other pro- and eukaryotes may have the capability to form MPn as well (Born et al. 2017). For example, abundant cyanobacteria like *Proclorococcus* and *Trichodesmium* have the capacity to synthesise phosphonates (Acker et al. 2022; Dyhrman et al. 2009). However, so far neither *Prochlorococcus*, *Trichodesmium* or its associated microbiome has been shown to have the capacity to synthesise MPn specifically (Frischkorn et al. 2018). Both *N. maritimus* and *P. ubique SAR11* are some of the most abundant microorganisms in the marine environment (Giovannoni 2017; Karner et al. 2001). While *SAR11* can be abundant in the euphotic surface ocean, *N. maritimus* is usually found below the photic layer. This conforms to the observation that phosphonate synthesis generally increases below 100 m depth (Acker et al. 2022), presumably due to the increased availability of Pi required for phosphonate synthesis. This is further supported by a global bioinformatic analysis that looked the *mpnS* more specifically in conjunction with other phosphonate genes (Lockwood et al. 2022). They found that the *mpnS* was present in 7.7% of the community inhabiting the mesopelagic ocean and in less than 1.5% of

those inhabiting the surface and DCM but their transcripts remained below 0.25 per 100000 reads. The supply of phosphonates to the surface waters must then be achieved by means of physical mixing across the thermocline (Cavender-Bares et al. 2001). However, this transport, like that of Pi, is probably restricted and it thus remains an open question whether there are additional biological sources of MPn in marine surface waters.

Supplementary Figures

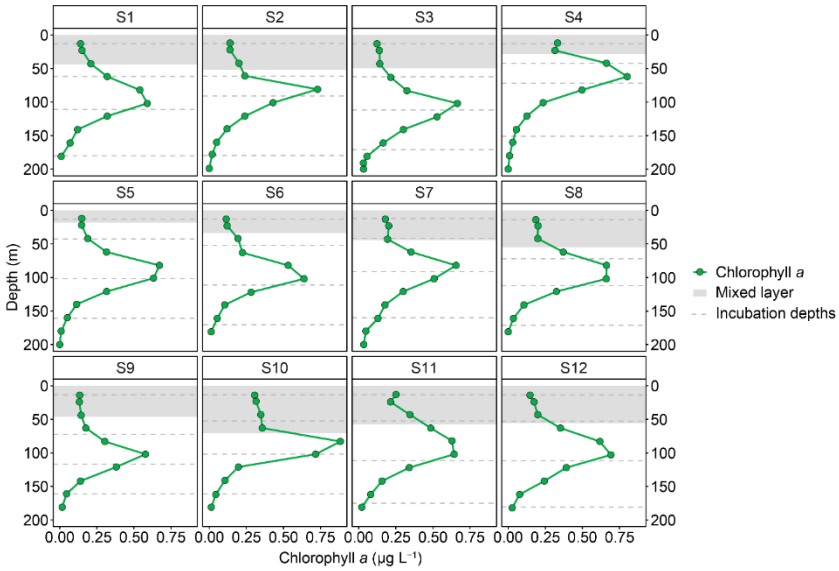

Figure S1. **Surface mixed layer in each station in relation to the deep chlorophyll maximum.** Mixed layer was defined as depth at which potential density is by 0.3 kg m^{-3} larger than at reference depth at 10 m. The surface depth was always located within the mixed layer, but the intermediate depth was only in the mixed layer for stations S7, S10, S11 and S12. The deep chlorophyll maximum was consistently below the mixed layer.

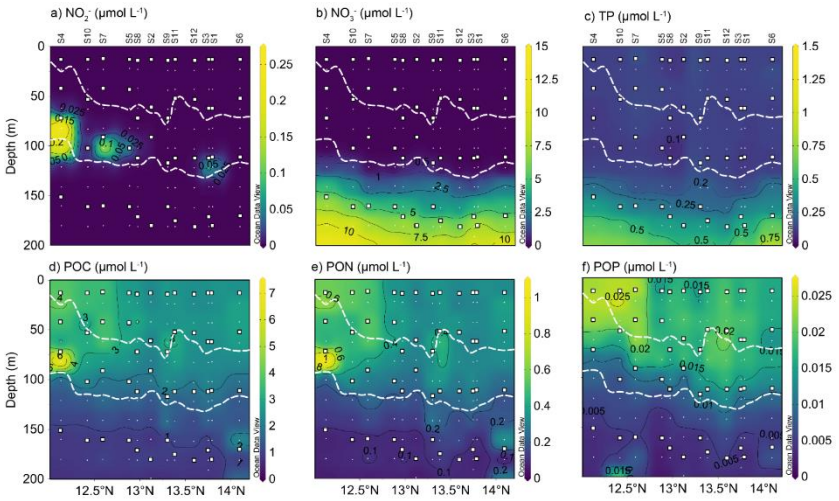

Figure S2. **Additional chemical parameters of the upper 200 m of the water column in the western Tropical North Atlantic east of Barbados. a,** Nitrite (NO_2^-). **b,** Nitrate (NO_3^-). **c,** Total phosphorus (TP). **d,** Particulate organic carbon (POC). **e,** Particulate organic nitrogen (PON). **f,** Particulate organic phosphorus (POP). White squares represent depths of the incubation experiments and white circles indicate additional sampling depths for concentration measurements. The white dotted line represents the outline of the deep chlorophyll maximum, defined as the area between 0.35 µg L^{-1} chlorophyll *a*.

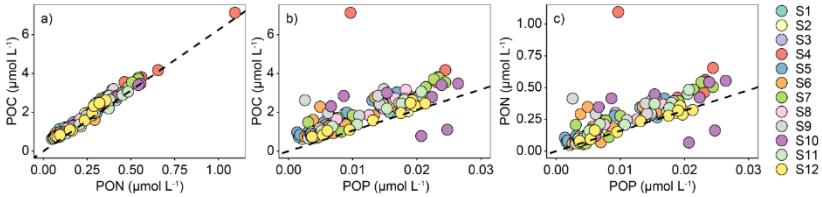

Figure S3. **Carbon, nitrogen and phosphorus ratios in the particulate organic fractions. a,** POC:PON. **b,** POC:POP. **c,** PON:POP. The lines represent the Redfield ratio of 106:16:1 (C:N:P).

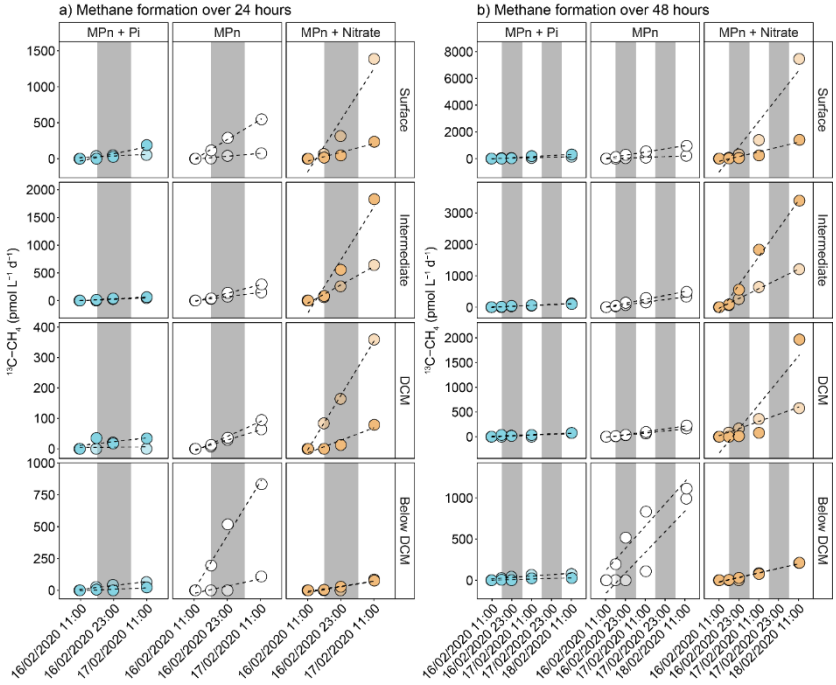

Figure S4. **Methane formation over time in representative incubations from station 11. a,** Methane formation over 24 hours of incubation. Rates were tested for linearity and significance prior to rate calculation. **b,** Methane formation over the complete 48 hour incubation period. While some rates remained linear over this time period, often exponential rates could be observed. Replicate incubations are shown. Dark bars represent the time between sunset and sunrise.

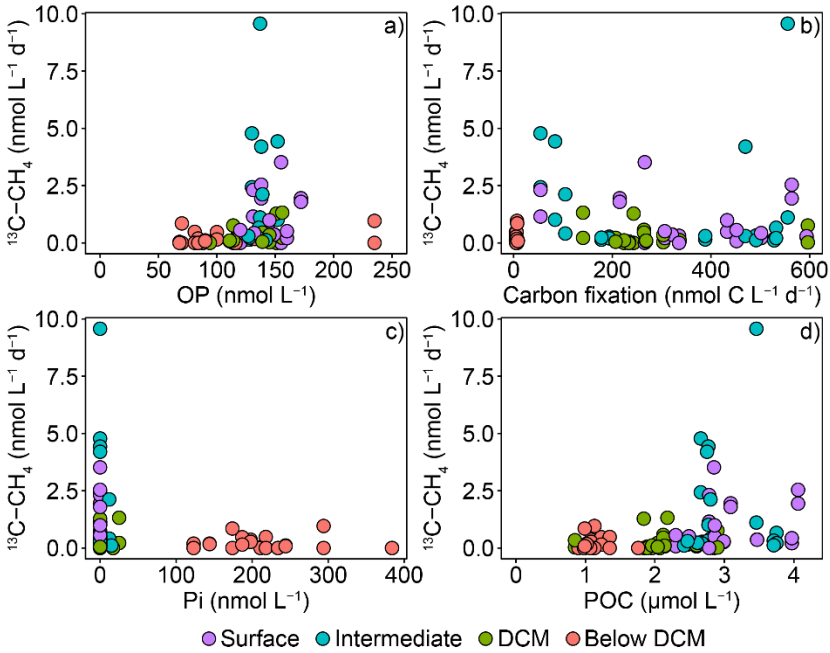

Figure S5. **Methane formation from the methylphosphonate-addition experiment as a function of organic phosphorus (OP) concentrations (a), carbon fixation rates (b), phosphate (Pi) concentrations and particulate organic carbon concentrations (d).** The depths from all twelve stations were used: a 10-metre surface depth, intermediate depth, deep chlorophyll maximum (DCM) and below the DCM, except for S2 where nutrient data was unavailable. The mean rate of the triplicate carbon fixation incubations is presented in the graph, whereas the duplicates of the MPn incubation are shown separately.

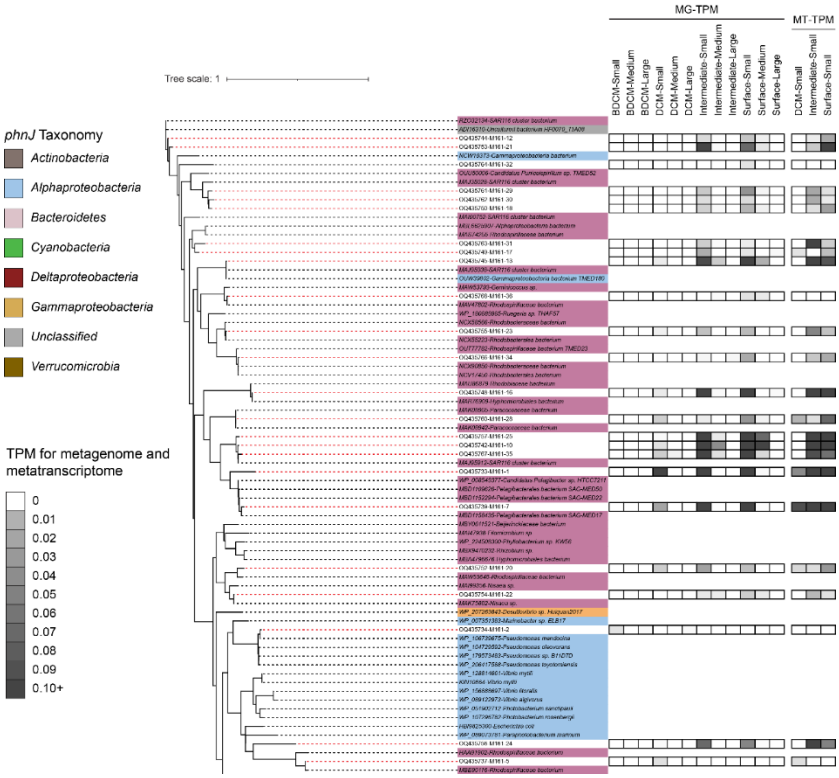

Figure S6. Continued

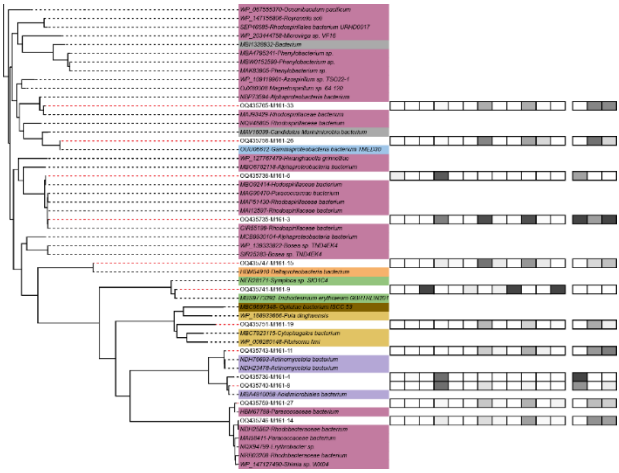

Figure S6. **Phylogenetic tree of the *phnJ* gene from Figure 4 with the reference sequences including accession numbers and TPM values.** All three size fractions: small (0.22 - 3 µm), medium (3 - 10 µm) and large (>10 µm) are included. The new sequences are indicated by the dashed red lines.

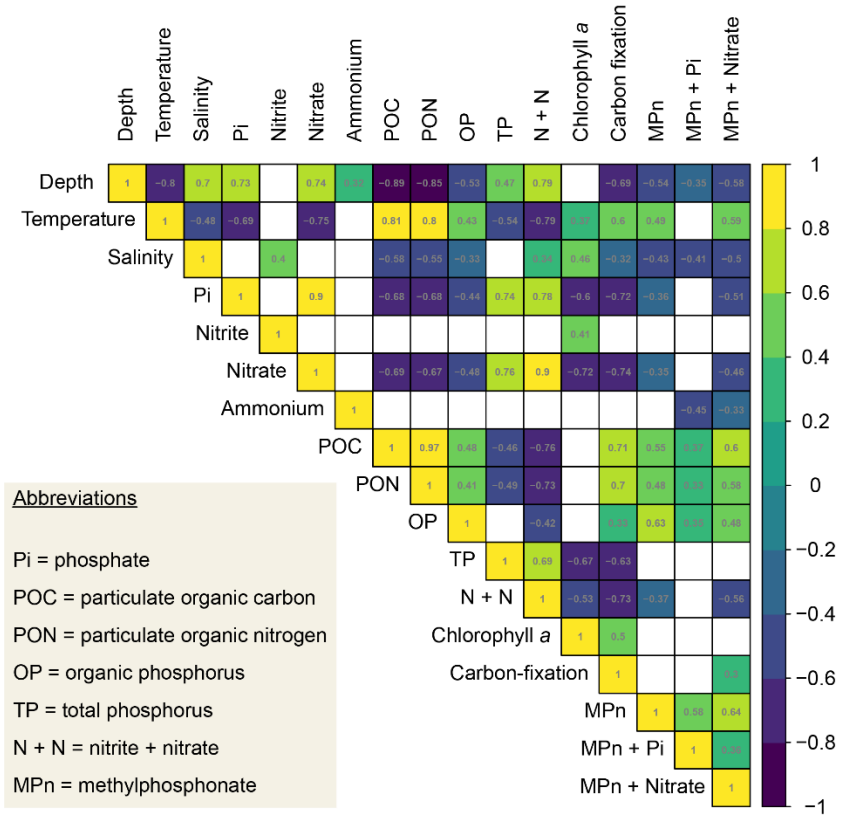

Figure S7. **Spearman ranked correlation analysis on all measured parameters.** All stations were used, except S2 where the nutrient data was unavailable. Insignificant correlations are left blank. Both mean carbon fixation and methylphosphonate-driven methane formation rates were used. Numbers in the squares indicate degree of correlation.

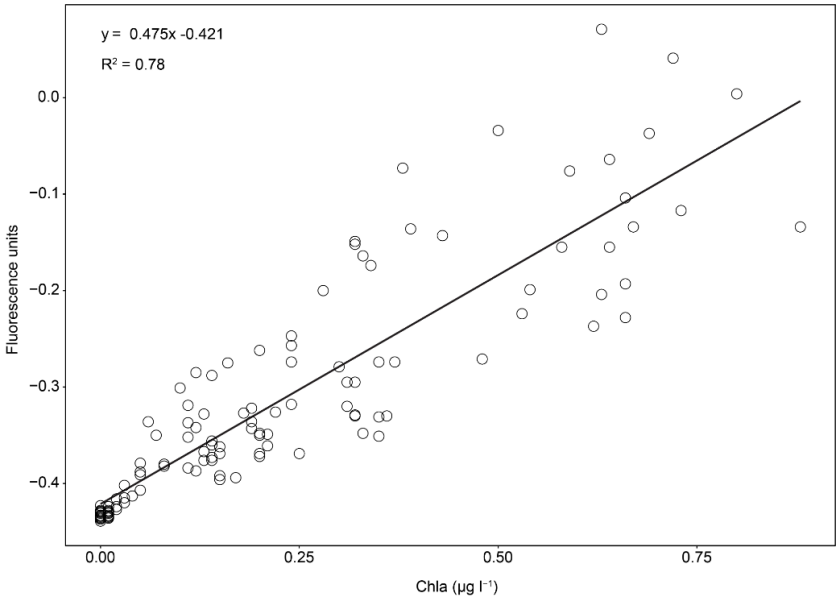

Figure S8. **Calibration of the fluorescence sensor with measured chlorophyll *a* (Chl *a*) values.** The limit of detection (calculated as the mean of the blanks plus three times the standard deviation) for the sensor (0.013 µg L^{-1}) was worse than for the measured Chl *a* values (0.008 µg L^{-1}). Therefore only the missing values (S3, S7, S1 201m, S8 201m and second CTD cast) were calibrated for plotting in Figure 1.

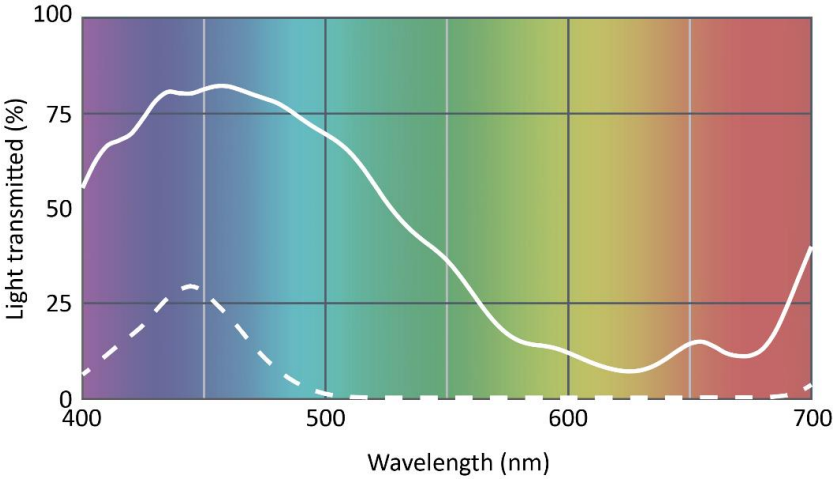

Figure S9. **Light profiles of the Lee filter papers: Ocean Blue #724 (solid line) and Tokyo Blue #071 (dashed line) used for the two incubators.** Ocean Blue #724 was used for the surface and intermediate depth, Tokyo Blue #071 for the deep chlorophyll maximum and below deep chlorophyll maximum incubation depths to simulate *in-situ* light profiles. Light spectra were also directly measured previously (Duerschlag et al. 2022).

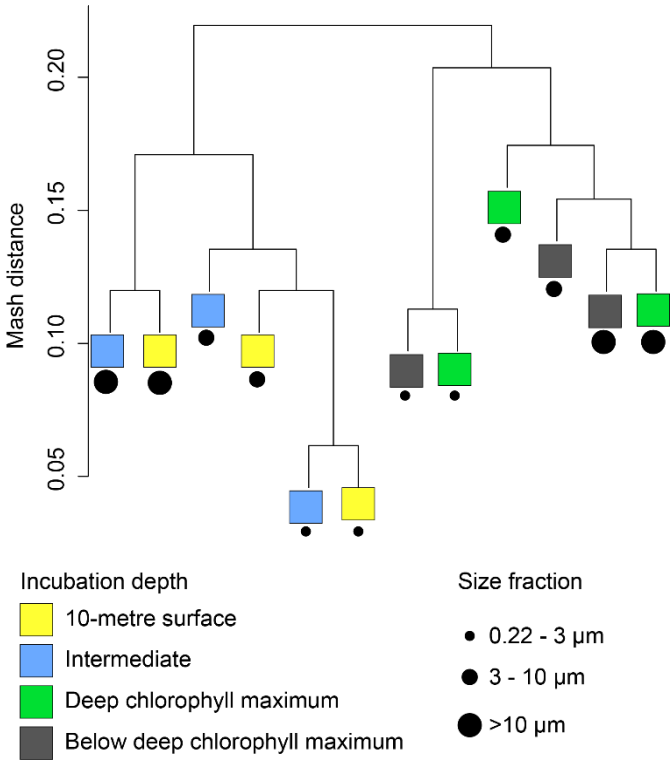

Figure S10. **Distance between the sequenced trimmed reads retrieved from station 5 as calculated by mash.** Two clear clusters formed between the two upper and two lower incubation depths. These are followed by subsequent clustering of the different size fractions. The 3 - 10 µm size fraction was clustering closer to the 0.22 - 3 µm one than the >10 µm fraction. As a result, samples were co-assembled in six co-assemblies based on size fraction and depth.

Bibliography

Acker M, Hogle SL, Berube PM, Hackl T, Coe A, et al. 2022. Phosphonate production by marine microbes: Exploring new sources and potential function. *Proc. Natl. Acad. Sci. U. S. A.* 119(11):

Bergman B, Sandh G, Lin S, Larsson J, Carpenter EJ. 2013. Trichodesmium - a widespread marine cyanobacterium with unusual nitrogen fixation properties. *FEMS Microbiol. Rev.* 37(3):286–302

Beversdorf LJ, White AE, Björkman KM, Letelier RM, Karl DM. 2010. Phosphonate metabolism by Trichodesmium IMS101 and the production of greenhouse gases. *Limnol. Oceanogr.* 55(4):1768–78

Born DA, Ulrich EC, Ju KS, Peck SC, Van Der Donk WA, Drennan CL. 2017. Structural basis for methylphosphonate biosynthesis. *Science (80-.).* 358(6368):1336–39

Carini P, White AE, Campbell EO, Giovannoni SJ. 2014. Methane production by phosphate-starved SAR11 chemoheterotrophic marine bacteria. *Nat. Commun.* 5:1–7

Cavender-Bares KK, Karl DM, Chisholm SW. 2001. Nutrient gradients in the western North Atlantic Ocean: Relationship to microbial community structure and comparison to patterns in the Pacific Ocean. *Deep. Res. Part I Oceanogr. Res. Pap.* 48(11):2373–95

Duerschlag J, Mohr W, Ferdelman TG, LaRoche J, Desai D, et al. 2022. Niche partitioning by photosynthetic plankton as a driver of CO2-fixation across the oligotrophic South Pacific Subtropical Ocean. *ISME J.* 16(2):465–76

Dyhrman ST, Benitez-Nelson CR, Orchard ED, Haley ST, Pellechia PJ. 2009. A microbial source of phosphonates in oligotrophic marine systems. *Nat. Geosci.* 2(10):696–99

Dyhrman ST, Chappell PD, Haley ST, Moffett JW, Orchard ED, et al. 2006. Phosphonate utilization by the globally important marine diazotroph Trichodesmium. *Nature*. 439(7072):68–71

Frischkorn KR, Krupke A, Guieu C, Louis J, Rouco M, et al. 2018. Trichodesmium physiological ecology and phosphate reduction in the western tropical South Pacific. *Biogeosciences*. 15(19):5761–78

Frischkorn KR, Rouco M, Van Mooy BAS, Dyhrman ST. 2017. Epibionts dominate metabolic functional potential of Trichodesmium colonies from the oligotrophic ocean. *ISME J.* 11(9):2090–2101

Giovannoni SJ. 2017. SAR11 Bacteria: The Most Abundant Plankton in the Oceans. *Ann. Rev. Mar. Sci.* 9(1):231–55

Horsman GP, Zechel DL. 2017. Phosphonate Biochemistry. *Chem. Rev.* 117(8):5704–83

Karner MB, Delong EF, Karl DM. 2001. Archaeal dominance in the mesopelagic zone of the Pacific Ocean. *Nature*. 409(6819):507–10

Lockwood S, Greening C, Baltar F, Morales SE. 2022. Global and seasonal variation of marine phosphonate metabolism. *ISME J.* 16(9):2198–2212

Metcalf WW, Griffin BM, Cicchillo RM, Gao J, Janga SC, et al. 2012. Synthesis of Methylphosphonic Acid by Marine Microbes: A Source for Methane in the Aerobic Ocean. *Science (80-.).* 337(6098):1104–7

Schowanek D, Verstraete W. 1990. Phosphonate utilization by bacterial cultures and enrichments from environmental samples. *Appl. Environ. Microbiol.* 56(4):895–903

Tedetti M, Sempéré R. 2006. Penetration of Ultraviolet Radiation in the Marine Environment. A Review. *Photochem. Photobiol.* 82(2):389

Villareal TA, Carpenter EJ. 2003. Buoyancy regulation and the potential for vertical migration in the oceanic cyanobacterium Trichodesmium. *Microb. Ecol.* 45(1):1–10

Yu C, Wang F, Chang SJ, Yao J, Blake RE. 2018. Phosphate oxygen isotope evidence for methylphosphonate sources of methane and dissolved inorganic phosphate. *Sci. Total Environ.* 644:747–53

Zhang C, Ji HB. 2019. Effects of environmental parameters on the ultraviolet degradation of methylphosphonate. *Appl. Ecol. Environ. Res.* 17(4):9473–82

Chapter III

Nitrous oxide cycling in the suboxic zone of the Black Sea

Jan N. von Arx[1], Katharina Kitzinger[1], Hannah Marchant[1], Gaute Lavik[1], Jördis Stührenberg[1], Jon Graf[1], Daan Speth[1], Marcel M. M. Kuypers[1] and Jana Milucka[1]

Author affiliations

[1]Max Planck Institute for Marine Microbiology, Bremen, Germany

In preparation

Author contributions

I (J.v.A) designed the study together with M.M.M.K., and J.M. Fieldwork was conducted by me, K.K., H.M., J.G., and J.M. Stable isotope incubation experiments were set up by K.K., H.M., and I, with K.K. and I measuring the samples. Rate analysis and calculations were carried out by G.L. and I. DNA and RNA were extracted by K.K. and metagenomic and metatranscriptomic analyses were performed by J.S. and D.S. I discussed and interpreted the data with J.M. I visualised the presented dataset. The manuscript was written by J.M. and I.

Abstract

The Black Sea is the largest meromictic marine basin characterised by a well-oxygenated surface layer and a deep sulfidic anoxic core, separated by a suboxic zone. In other oxygen-depleted marine environments, nitrogen cycling at oxic-anoxic boundaries has been identified as a major source of nitrous oxide (N_2O). Yet, there appears to be negligible net production of N_2O within the suboxic zone of the Black Sea, and the region is considered only a minor source of N_2O. So far, the sources and sinks of this powerful greenhouse gas in the Black Sea are poorly constrained, as are the microorganisms which mediate N_2O cycling. We combined stable isotope rate measurements with metagenomic and metatranscriptomic analyses to investigate N_2O cycling in the suboxic zone of the western Black Sea. We show persistent N_2O formation from ammonia oxidation (up to 0.2 nmol L^{-1} d^{-1}) and sporadic rates of high N_2O production from denitrification (up to 20 nmol L^{-1} d^{-1}). Interestingly, the measured N_2O reduction rates (up to 24 nmol N L^{-1} d^{-1}) could exceed N_2O formation, thus explaining the lack of N_2O accumulation in the water column. Molecular analysis of the *amoA* gene revealed that the *Nitrososphaerales* were the dominant ammonia oxidisers, while the genetic potential to form N_2O from nitrite was mainly encoded by *Alpha*- and *Gammaproteobacteria*. N_2O reducers were diverse but were dominated by *Gammaproteobacteria* and *Marinisomatia*. Our results suggest that, despite the diverse pathways of N_2O production in the Black Sea, emissions are low due to tight balancing of N_2O production and consumption, which is facilitated by the presence and activity of specialised N_2O reducers.

Introduction

With an atmospheric mixing ratio of ~336.33 parts per billion (NOA, 2022), nitrous oxide (N_2O) is the third most abundant anthropogenically impacted greenhouse gas (Intergovernmental Panel on Climate Change 2023) and the most prevalent ozone depleting substance in the atmosphere (Portmann et al. 2012; Ravishankara et al. 2009). Its concentration continues to increase by an estimated 0.95 ± 0.04 parts per billion year^{-1} (Intergovernmental Panel on Climate Change 2023) and marine environments contribute an estimated one third of all natural N_2O emissions (Tian et al. 2020). Oxygen depleted marine environments are hotspots of N_2O emissions (Babbin et al. 2015; Naqvi et al. 2010; Yang et al. 2020) despite only comprising around 1% of the ocean's volume (Lam & Kuypers 2011). These environments are characterised by low (< 20 µmol L^{-1}) oxygen concentrations (Lam & Kuypers 2011) due to oxygen depletion by organic matter remineralisation combined with sluggish ventilation (Wyrtki 1962).

The Black Sea is the largest permanently stratified basin in the world, with a 20 - 50 m thick suboxic zone separating the oxygenated surface waters from the deep anoxic sulphidic and methane rich core (Murray 1989). The suboxic zone is characterised by oxygen concentrations below 10 µmol L^{-1} and low concentrations of sulphide (Murray et al. 1995) with active microbial nitrogen transformations taking place (Jensen et al. 2008; Kuypers et al. 2003; Lam et al. 2007; Ward & Kilpatrick 1991; Westley et al. 2006). Despite indications of an active N_2O cycle within the suboxic zone (Westley et al. 2006), the Black Sea is considered only a minor source of N_2O to the atmosphere (Amouroux et al. 2002; Bange et al. 2019), with little N_2O accumulation in the water column.

The two major microbial processes that are responsible for most of the biological N_2O formation are aerobic ammonia oxidation and denitrification, both of which can be found along the peripheries of oxygen-limited environments (Babbin et al. 2015; Codispoti 2010). Aerobic ammonia oxidation is a process of stepwise oxidation of ammonia to nitrite over the obligate intermediate hydroxylamine (Lees 1952; Prosser et al. 2020; Vajrala et al. 2013). This process is conducted by aerobic ammonia oxidising bacteria (AOB) and aerobic ammonia oxidising archaea (AOA). The latter are the dominant marine ammonia oxidisers (Francis et al. 2005; Wuchter et al. 2006), including in oxygen-depleted environments, and are taxonomically constrained to the *Nitrososphaerales* (Brochier-Armanet et al. 2008; Spang et al. 2010). The less abundant AOBs

(Wuchter et al. 2006) belong to the *Proteobacteria* (Purkhold et al. 2000). The two groups of ammonia oxidisers can be identified by their marker gene *amoA*, which encodes the alpha subunit of the ammonia monooxygenase that converts ammonia to hydroxylamine (Francis et al. 2005; Rotthauwe et al. 1997). Both AOBs and AOAs have the capacity to produce N_2O (Santoro et al. 2011; Yoshida & Alexander 1970) but the underlying mechanisms appear to differ. In AOAs, the primary mechanism is thought to be a hybrid formation pathway that combines a nitrogen molecule from hydroxylamine and another from nitrite or nitric oxide (Kozlowski et al. 2016; Stieglmeier et al. 2014; Wan et al. 2023). N_2O can also be formed under low pH conditions by the putative cytochrome p450 but the specific conditions required likely make this a niche reaction in marine environments (Jung et al. 2019). Recently AOA have been shown to form N_2O through a putatively novel process of nitric oxide dismutation to oxygen and N_2; however, so far the mechanisms and the environmental relevance are yet to be explored (Kraft et al. 2022). In AOBs, N_2O can be formed through the oxidation of hydroxylamine with nitric oxide as an intermediate (Caranto et al. 2016; Kozlowski et al. 2014). However, the primary N_2O formation pathway in AOBs is thought to be nitrifier-denitrification, where the formed nitrite is reduced to N_2O through the intermediate of nitric oxide. This process becomes prevalent under low oxygen concentrations (Goreau et al. 1980; Wrage-Mönnig et al. 2018) and utilises the same enzymes as denitrification. Additionally, hydroxylamine, nitric oxide and nitrite can all degrade abiotically to N_2O, complicating the process of N_2O formation from ammonia oxidation (Wan et al. 2023; Zhu-Barker et al. 2015).

Conventional denitrification refers to the anaerobic process of stepwise reduction of nitrate to N_2, over the intermediates nitrite, nitric oxide and N_2O (e.g. Zumft 1997). This process can be performed by a broad range of microbial taxa across all three domains of life (Kuypers et al. 2018). Denitrification is predominantly heterotrophic using organic carbon as the electron donor but both methanotrophic (Oswald et al. 2017) and chemolithotrophic denitrification, especially linked to the oxidation of sulphide, has been observed in oxygen depleted environments (Callbeck et al. 2021; Canfield et al. 2010; Dalsgaard et al. 2014; Lavik et al. 2009). The final step of denitrification, the reduction of N_2O to N_2, is also the only biologically relevant N_2O sink (Thomson et al. 2012). While the individual steps of conventional denitrification can be found within a single organism, they are more often separated (Garrido-Amador et al. 2021; Graf et al. 2014; Kuypers et al. 2018; Lycus et al. 2017). This can decouple the process of N_2O formation and consumption, directly affecting N_2O emissions.

Ongoing climate perturbations and eutrophication have led to the expansion of oxygen depleted environments over the last century, and they are predicted to increase in the future (Diaz & Rosenberg 2008; Schmidtko et al. 2017). As this effect may be reinforced by the increasing N_2O emissions, it is vital to constrain the underlying mechanisms that control the cycling of N_2O in these environments and parameters that control them. To investigate the sources and sinks of N_2O in the suboxic zone, we sampled six stations in the western Black Sea during the POS539 cruise in November 2019 (Figure 1a). We combined stable isotope incubation experiments (^{15}N-ammonium, ^{15}N-nitrite and ^{15}N-N_2O) with metagenomic and metatranscriptomic analysis of the key genes involved in ammonia oxidation (*amoA*) and denitrification (*nirK*, *nirS*, eNOR, cNOR and *nosZ*). Our data revealed an active cycle of N_2O in the suboxic zone of the Black Sea, with N_2O reduction outpacing N_2O formation at most depths. While the ammonia oxidisers were dominated by ammonia oxidising archaea, the denitrifiers were diverse and dominated by *Gammaproteobacteria* as well as likely N_2O reducing specialists of the *Marinisomatales*. Our results suggest that the N_2O emissions from the hypoxic zone of the Black Sea are controlled by the efficient coupling of N_2O producing and consuming processes, facilitated by the stable stratification of the water column.

Results and Discussion

Water column characteristics

During cruise POS539 in November 2019, the suboxic zone of six stations in the western Black Sea (Figure 1a) was investigated for the cycling of the greenhouse gas nitrous oxide (N_2O). Due to the riverine freshwater inflow into the Black Sea as well as the high salinity water from the Mediterranean Sea, the Black Sea water column is permanently density stratified (Murray et al. 1995). This phenomenon results in discrete profiles of nutrients such as nitrogen oxides, ammonium and sulphide found at similar densities (σT) within the suboxic zone (Murray et al. 1995; Figure 1b). In the six investigated stations, oxygen concentrations reached ~10 µmol L^{-1} (the upper boundary of the suboxic zone) between σT = 15.55 - 15.70 kg m^{-3}. However, the upper boundary can be dynamic as it is controlled by oxygen intrusions from the overlaying water column (Murray & Yakushev 2006). The suboxic zone for the sampled stations extended to σT = 16.24 - 16.35 kg m^{-3}, where sulphide concentrations increased above 1 µmol L^{-1}, this spanning 30 - 56 metres. This is in accordance with previous studies (Kirkpatrick et al. 2012; Lam et al. 2007).

At station P1, the lower boundary of the suboxic zone was never reached and all incubation depths had *in-situ* oxygen concentrations above 6 µmol L^{-1}. A nitrate concentration maximum of 5.6 - 6.0 µmol L^{-1} was observed at each station, located between σT = 15.21 - 16.02 kg m^{-3}. At stations W1 and W2 the nitrate maximum was located just above the suboxic zone, whilst in the other stations it was within. In general the nitrate peak was broader than previously observed but equal in magnitude and found along a similar density surface (Kirkpatrick et al. 2012; Lam et al. 2007; Murray & Yakushev 2006). Nitrite usually formed a primary nitrite maximum just above the nitrate maximum (Supplementary Figure S1) reaching concentrations of 0.2 µmol L^{-1}. Only station W2 had a clear secondary nitrite maximum at σT = 16.27 kg m^{-3}, with nitrite concentrations of up to 0.2 µmol L^{-1}. While the secondary nitrite maximum is an established feature of the suboxic zone (Murray et al. 1995) it has not always been observed (Jensen et al. 2008). Ammonium concentrations were below the limit of detection (ca. 40 nmol L^{-1}) within the suboxic zone, with the exception of stations W3 and P1 where concentrations reached 124 nmol L^{-1}. In the lower section of the suboxic zone (σT = 15.93 - 16.19 kg m^{-3}) and below the nitrate peak, ammonium concentrations started to increase linearly at each station to several µmol L^{-1}. Sulphide concentrations started to increase linearly from σT = 16.13 - 16.33 kg m^{-3} to several µmol L^{-1}. As such, the deepest incubation depth of station W1 was within the sulphidic waters and the deepest incubation depth of station S3 had 7.83 µmol L^{-1} of sulphide. Both the ammonium and sulphide concentration increases agree with previous observations (Murray & Yakushev 2006; Murray et al. 1995).

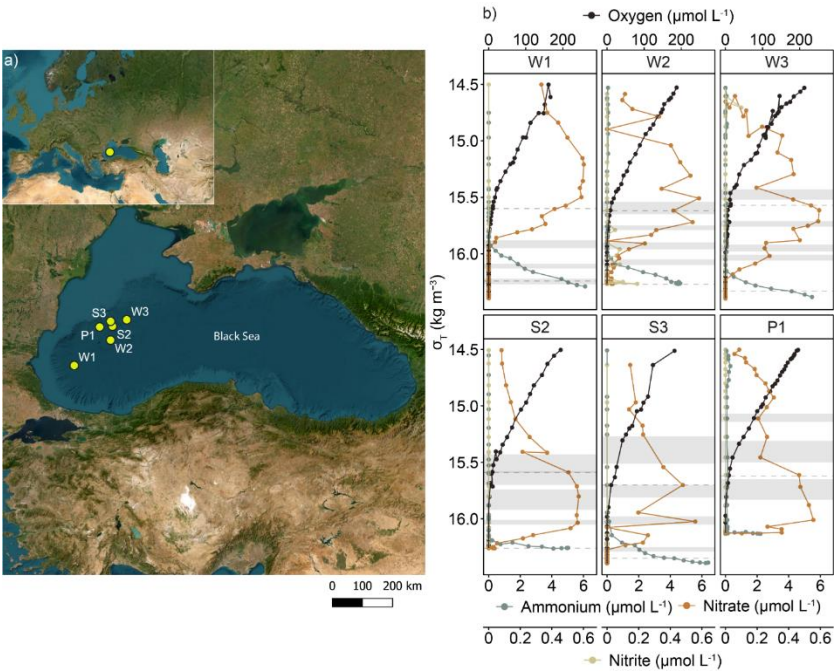

Figure 1. **Water column chemistry of the investigated stations in the western Black Sea. a,** Map of the sampled stations during the POS539 cruise to the Black Sea. **b,** Nutrient profiles from the investigated stations. All samples originate from the downcast of the pump CTD system. Dashed grey lines outline the suboxic zone with the upper boundary set to 10 µmol L^{-1} oxygen and the lower boundary where sulphide concentrations increased (sulphide > 1 µmol L^{-1}). Grey boxes indicate the incubation depths sampled during the upcast and include the movement in the water column during sampling.

Nitrous oxide cycling

Stable isotope incubation experiments with either ^{15}N-ammonium, ^{15}N-nitrite or ^{15}N-N_2O were set up in parallel from up to four different incubation depths (Figure 1b) that included: (I) a deep depth (above the sulphide where ammonium starts to increase), (II) the secondary nitrite maximum, (III)

the nitrate maximum and (IV) at the oxycline. The aim was to quantify rates of N_2O formation and consumption as well as the associated processes of ammonia oxidation and denitrification to N_2.

Ammonia oxidation resulted in systematic nitrous oxide formation

Rates of N_2O formation from ammonia oxidation were quantified from all stations and depths from two separate experiments: an oxygen-supplemented experiment (10 µmol L^{-1} final concentration of oxygen) and an anoxic experiment (Figure 2; Supplementary Figure S2).

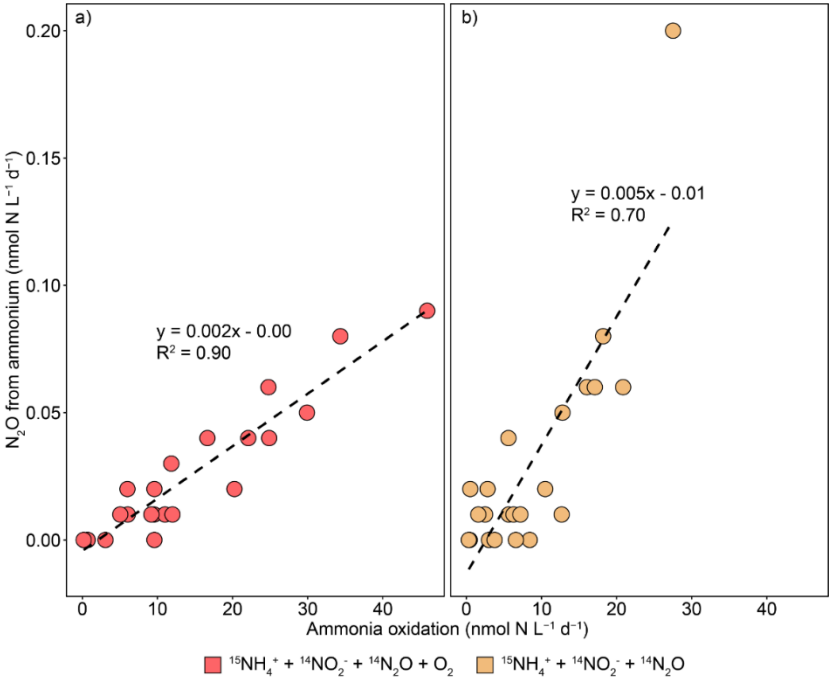

Figure 2. **Nitrous oxide formation as a factor of the ammonia oxidation rates to nitrite. a,** oxygen-supplemented experiment. **b,** anoxic experiment. Each point represents two individual statistically significant (One-sided student's t-test, $p < 0.05$) rates, calculated from the slope of all time points, plotted against each other. Data is from all stations and incubation depths.

Under oxygen-supplemented conditions, N_2O formation rates from ^{15}N-ammonium were quantifiable from 18 out of 22 incubations. The four incubations without significant N_2O formation coincided with the incubation depths with the lowest measured rates of ammonia oxidation to nitrite (below 3.1 nmol N L^{-1} d^{-1}; Figure 2; Supplementary Figure S3). The significant linear N_2O formation rates were between 3 - 92 pmol N L^{-1} d^{-1} and showed no distinct trends between stations or depths, suggesting the potential for ammonium-derived N_2O throughout the suboxic zone. The measured rates were lower but comparable to the previously determined rates from the central gyre (110 - 370 pmol N L^{-1} d^{-1} at $\sigma T = 15.3$; Westley et al. 2006), suggesting a persistent contribution of aerobic ammonia oxidation to the formation of N_2O in the water column of the Black Sea.

Most of the measured N_2O from the oxygen-supplemented ^{15}N-ammonium experiment was retrieved as $^{45}N_2O$ which is consistent with the hybrid formation pathway described for the ammonia oxidising archaea (AOA), combining one nitrogen from nitrite and another from ammonia (Kozlowski et al. 2016; Stieglmeier et al. 2014). While stable isotope incubations cannot distinguish N_2O formation from AOA and ammonia oxidising bacteria (AOB; Prosser et al. 2020), the metagenomic analyses of the *amoA* gene at stations W3 and S3 confirmed the abundance of AOA at all depths (Supplementary Figure S4), as previously observed (Francis et al. 2005; Lam et al. 2007). The hybrid formation pathway is considered to be abiotic but it depends on the supply of intermediates from the ammonia oxidation process (Stein et al. 2021) and recent culture work has shown that viable cells are required (Wan et al. 2023). This is reflected by the observed strong linear relationship ($n = 22$, $R^2 = 0.9$) between the ammonia oxidation rate and the N_2O formation (Figure 2).

In the anoxic ^{15}N-ammonium experiment, N_2O formation was quantifiable from 17 out of 22 incubations and there was no clear depth distribution (Figure 2; Supplementary Figure S2). N_2O formation rates ranged between 4.9 - 198 pmol N L^{-1} d^{-1} and were thus similar to the rates from the oxygen supplemented experiment, with no statistically significant difference between the rates of N_2O formation from the two experiments (Wilcoxon test, $W = 237$, $p = 0.9$). Like in the oxygen-supplemented experiment, most N_2O was produced as $^{45}N_2O$ suggesting a similar mechanism of formation. However, unlike the oxygen-supplemented experiment, the N_2O formation was less well correlated with the ammonia oxidation rates ($n = 22$; $R^2 = 0.7$; (Figure 2), which were overall reduced by ~40% in each depth in the anoxic incubations (Supplementary Figure S3). A decrease in the ammonia oxidation rates from low oxygen conditions to anoxia was observed previously

(Lam et al. 2007; Lipschultz et al. 1990). It should be noted that while no oxygen was added to the anoxic incubation, AOA have been shown to be able to scavenge oxygen at extremely low concentrations (5 - 30 nmol L^{-1} oxygen; Bristow et al. 2016), and these amounts could have been introduced into the incubations during sample collection and manipulation (Holtappels et al. 2011). Due to the different ammonia oxidation rates but comparable N_2O formation rates, the yields of N_2O from ammonia oxidation differed between the two experiments. The mean yield for the oxygen-supplemented experiment was 0.14 ± 0.09% and the one from the anoxic experiment was three times higher at 0.42 ± 0.81%. Both of these exceeded the ones observed from AOA cultures, even under varying oxygen concentrations, by an order of magnitude (Löscher et al. 2012; Qin et al. 2017; Santoro et al. 2011; Stieglmeier et al. 2014) but were within the range of those found in the environment (Frey et al. 2020; Ji et al. 2018). Combined these results suggest that under oxygen limitation (anoxic experiment) N_2O is not formed proportionally to the ammonia oxidation rate, like in the oxygen supplemented experiment but possibly has additional sources. Such as stronger contribution from AOB (Goreau et al. 1980) or from pathway intermediates through abiotic breakdown (Zhu-Barker et al. 2015). This has previously been suggested from culture experiments with AOAs (Qin et al. 2017; Wan et al. 2023).

Nitrous oxide reduction outpaced the formation from nitrite

To investigate the contribution of denitrification to the N_2O formation, an experiment was set up with ^{15}N-nitrite and a ^{14}N-N_2O pool to "trap" the newly formed N_2O. Significant linear N_2O formation rates (between 12 - 19910 pmol N L^{-1} d^{-1}) with a clear depth distribution were measured from eleven out of 22 incubations (Figure 3). Above σT = 16.0 kg m^{-3} N_2O formation rates of up to 1127 pmol N L^{-1} d^{-1} were only sporadically measured but extended into depths that had *in-situ* oxygen concentrations of up to 27.6 µmol L^{-1} (59 pmol N L^{-1} d^{-1}, W3). Below σT = 16.0 kg m^{-3} all stations had significant rates of N_2O formation, extending into the sulphidic waters of stations W1 and S3. In the sulphidic waters of S3 an exceptionally high rate of N_2O production (19910 pmol N L^{-1} d^{-1}) was measured.

It is likely that sulphide present in the deepest incubation depth stimulated the nitrite reduction by acting as an electron donor (Moraes et al. 2012), as has been observed previously in other oxygen depleted environments (Callbeck et al. 2018; Canfield et al. 2010; Dalsgaard et al. 2014; Lavik et al. 2009). This is further supported by the observation that in the sulphidic depth of W1 the nitrite

reduction rate to N_2O was also elevated (413 pmol N L^{-1} d^{-1}) albeit an order of magnitude less than in S3. Previous measurements, using stable isotope incubation experiments, of N_2 and N_2O formation from nitrite through denitrification in the Black Sea are scarce and mostly yielded little to no rates (Jensen et al. 2008; Westley et al. 2006). On the contrary, our results show that N_2O formation in the Black Sea can proceed at rates comparable to those measured in the Peruvian oxygen minimum zone, which is considered to be the largest marine source of N_2O to the atmosphere (Arévalo-Martínez et al. 2015; Frey et al. 2020). It should also be noted that denitrification rates were only measured from the precursor of nitrite in this study. However, there have been suggestions that direct N_2O formation from nitrate can exceed formation from nitrite (Frey et al. 2020; Ji et al. 2015, 2018), possibly due to the higher *in-situ* nitrate concentrations. Nitrate concentrations also exceeded those of nitrite substantially in our study area and additionally the molecular data suggests that nitrate reductase genes were both present and expressed in all depths of stations W3 and S3 (Supplementary Figure S5). Therefore, our reported rates may be underestimated, with denitrification from nitrate as an additional source of N_2O and ultimately N_2.

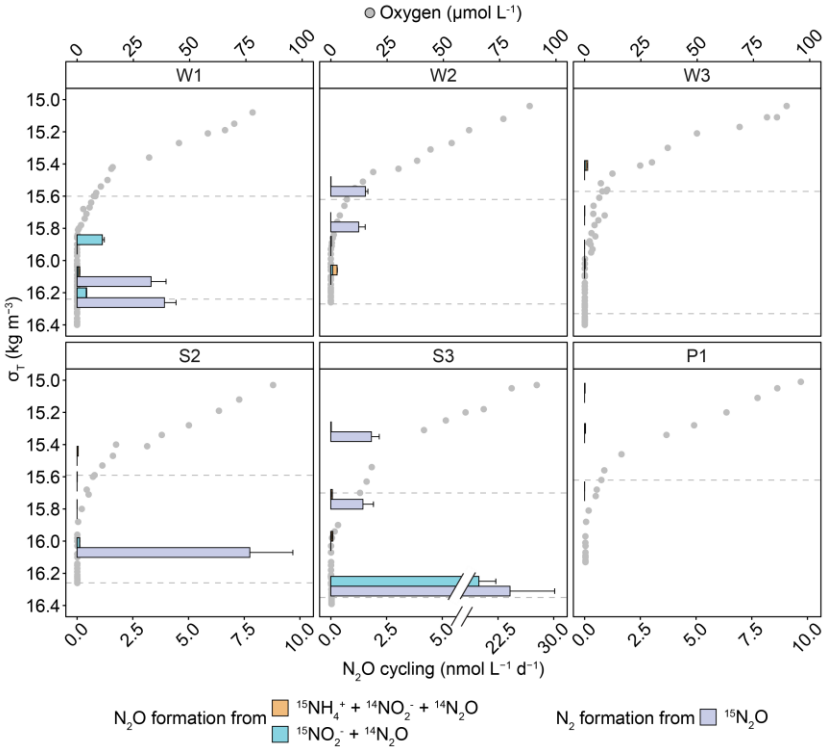

Figure 3. **Nitrous oxide (N_2O) cycling in the suboxic zone of the western Black Sea.** Each bar represents a statistically significant (One-sided student's t-test, $p < 0.05$) rate, calculated from the slope of all time points. N_2O formation is the sum of the N_2O produced in the anoxic ammonium experiment and from the denitrification experiment. N_2O reduction to N_2 is taken from the ^{15}N-N_2O incubation experiment. The suboxic zone is outlined by the dashed line.

Rates of denitrification from nitrite to N_2 were measured simultaneously from the same sample as the N_2O formation rates and N_2 production could be quantified in six out of 22 incubations, ranging between 0.4 - 5.9 nmol N L^{-1} d^{-1} (Supplementary Figure S6). Unlike the N_2O formation, there was no clear depth distribution, with rates measured as shallow as at σT = 15.32 kg m^{-3} where *in-situ* oxygen concentrations were 53 µmol L^{-1}. This potential conforms to a previously observed N_2 maximum in the upper oxycline which was attributed to particle associated denitrification (Fuchsman et al. 2019). However, it should also be noted that due to sample collection and preparation, the oxygen concentrations in our incubations will have differed from the *in-situ* concentrations at the respective depths. Notably, in the deepest depth of S3, where N_2O formation reached 19.9 nmol N L^{-1} d^{-1}, substantial (10.8 nmol N L^{-1}) N_2 formation was only observed in the last time point (after 24 hours of incubation), suggesting that the N_2O formation and the subsequent reduction may occur sequentially in this depth (see below).

To determine the potential for N_2O reduction, an experiment with ^{15}N-N_2O was set up from all incubation depths. From these, eight significant rates were measured, ranging from 1.3 - 24.1 nmol N L^{-1} d^{-1} (Figure 3). Similar to the nitrite-derived N_2 formation rates, there was no clear depth distribution. However, the highest rate of N_2O reduction (24.1 nmol N L^{-1} d^{-1}) was quantified in the deepest depth of S3 and even exceeded the highest N_2O formation rate from nitrite (19.9 nmol N L^{-1} d^{-1}) quantified from this depth. Thus, N_2O reduction could outpace the combined N_2O formation from all investigated sources (ammonia oxidation and nitrite reduction) in all depths with detectable rates.

Combined the results from the stable isotope incubation experiments revealed that there seems to be an active N_2O cycle in the suboxic zone of the Black Sea. The predominant pathway of N_2O formation, by magnitude, was nitrite reduction. However, these rates were only measured in sporadic depths and, more importantly, often coincided with high rates of N_2O reduction. The two processes thus seem to be tightly balanced within the suboxic zone, preventing substantial accumulation of N_2O in the water column. Nevertheless, the Black Sea is still considered to be a minor source of N_2O to the atmosphere (Amouroux et al. 2002; Bange et al. 2019). We speculate that the N_2O emissions may be largely driven by the low but persistent rates of N_2O formation from ammonia oxidation. While ammonia-derived N_2O could also be balanced by the N_2O reduction rates within the suboxic zone, ammonia oxidation is likely to extend into the overlying oxygenated water column. This is supported by the substantial ammonia oxidation rates and N_2O

formation reported in this study, as well as the presence of ammonia oxidising archaea in the oxygenated water column (Pavlovska et al. 2021). Denitrification will be inhibited in the presence of oxygen in the upper water column (Zumft 1997) and thus likely restricted to anoxic microniches. Therefore, N_2O produced by ammonia oxidation can escape reduction more easily. Taken together, like in most other marine environments (Freing et al. 2012; Martinez-Rey et al. 2015) and despite the comparatively small rates, ammonia oxidation may be the main source of the N_2O emissions of the Black Sea.

Denitrifying organisms were dominated by conventional denitrifiers and nitrous oxide reducers

To identify the microorganisms with the potential for denitrification that could be responsible for N_2O cycling in the Black Sea, taxonomic analysis of key functional genes involved in denitrification was performed. The abundances of genes coding for nitrite reductases (*nirK*, *nirS*), nitric oxide reductases (eNOR, cNOR) and the nitrous oxide reductase (*nosZ*) was assessed using metagenomic and metatranscriptomic reads from all incubation depths of stations W3 and S3 (Figure 4), Supplementary Figure S5).

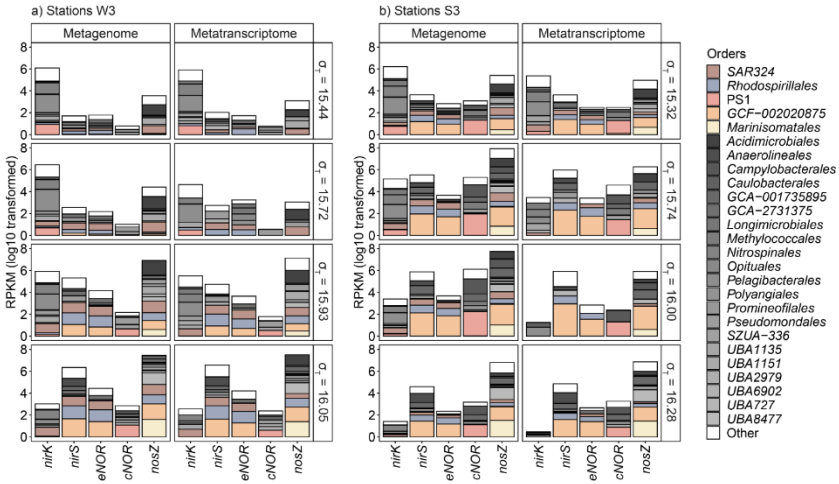

Figure 4. **Taxonomic diversity of denitrifying organisms and key genes. a,** station W3. **b,** station S3. Shown are bacterial orders with the highest abundance and transcription (top 10%) of key denitrifying genes. The dominant orders are coloured. GTDB taxonomy was assigned based on best hit against custom marker gene databases.

The community composition of bacterial denitrifiers was highly diverse but similar to previous molecular investigations from the Black Sea (Cabello-Yeves et al. 2021; Fuchsman et al. 2011; Pavlovska et al. 2021; Suominen et al. 2021; van Vliet et al. 2021). Interestingly, the two stations only shared nine out of 26 orders of denitrifiers between them, which included the most abundant groups containing at least one gene: *GCF-002020875*, *PS1* and *Rhodospirillales, SAR324* and *Marinisomatales*.

The order *GCF-002020875* was the most dominant in terms of gene abundance and transcription, especially throughout all the depths of S3 and the lower two of W3, containing *nirS*, eNOR (predominantly), cNOR and *nosZ*. This order belongs to the *Gammaproteobacteria* and is also referred to as *Gammaproteobacterial BS-GSO2 clade* which contains the *Candidatus Thiopontia* genus (van Vliet et al. 2021). This group was previously identified at the sulphidic interface of the Black Sea (Glaubitz et al. 2010; Kirkpatrick et al. 2012). So far, the only available metagenome assembled genome (MAG) of *Thiopontia autotrophica* is from the Black Sea and encodes all the genes required for conventional denitrification as well as sulphur oxidation genes and the Calvin-Benson-Bassam cycle (van Vliet et al. 2021), possibly making it a chemolithoautotrophic denitrifier. Other dominant orders that contained all the genes for N_2 formation from nitrite included the *Rhodospirillales* and *SAR324*. The *Rhodospirillales* mainly contained *nirS*, eNOR and *nosZ*. These organisms belong to the *Alphaproteobacteria* and were previously identified as potential N_2O reducers due to the presence of the *nosZ* in a MAG from the oxic-anoxic interface of the Black Sea (Cabello-Yeves et al. 2021). This MAG also harboured genes for sulphur cycling. However, not all *Rhodospirillales* in the Black Sea seem to contain the *nosZ* (van Vliet et al. 2021), thus they can be both N_2O formers and reducers. The *SAR324* encoded and transcribed *nirK*, *nirS*, eNOR and *nosZ* and was previously implicated in dissimilatory sulphate reduction (Cao et al. 2016; Sheik et al. 2014).

The order *PS1* also belongs to the *Gammaproteobacteria* and contains the cosmopolitan genus *SUP05* which is often found in oxygen minimum zones (Callbeck et al. 2018; Canfield et al. 2010; Lavik et al. 2009). This group was found to mainly encode and transcribe *nirK* and cNOR throughout all depths of S3 as well as the lower two of W3. Previously, *SUP05* have been identified in the suboxic zone of the Black Sea (Cabello-Yeves et al. 2021; van Vliet et al. 2021), where they can make up to 10% of the total microbial community (Glaubitz et al. 2013). Their metabolism is mainly associated with chemolithotrophic sulphur oxidation coupled to nitrate

reduction (Glaubitz et al. 2010; Shah et al. 2017) including N_2O formation (Walsh et al. 2009). While some members have the capacity to denitrify all the way to N_2 (Callbeck et al. 2018), this does not seem to be the case for the Black Sea as indicated by the absence and lack of *nosZ* expression. Therefore, they may be a net producer of N_2O in the suboxic zone of the Black Sea.

Finally, the presence and transcription exclusively of the *nosZ* by the *Marinisomatales* was a strong indicator of a N_2O reducing specialist. The *Marinisomatales* belong to the *Marinisomatota* and were dominating the *nosZ* abundance and transcription in the deepest incubation depth of both stations, before gradually disappearing in the upper incubation depths (Figure 4). These organisms belong to the microbial dark matter that do not have a cultured representative (Hawley et al. 2017) but are a cosmopolitan group found in oxygen minimum zones (Bertagnolli et al. 2017) and previously in the Black Sea (Fuchsman et al. 2011; Oakley et al. 2007). Their N_2O reduction is typically facilitated by the type II N_2O reductase which is associated with N_2O reducing specialists (Sanford et al. 2012) and has a higher affinity for N_2O (Yoon et al. 2016) than the type I reductase. Additionally, they usually encode for genes involved in dissimilatory nitrate reduction to ammonium and sulphur reduction (Wright et al. 2014). It was previously speculated that they have the potential to act as filters for the N_2O formation of incomplete denitrifiers as well as from ammonia oxidation (Hawley et al. 2017). While the prevalence of the *Marinisomatales* deeper in the water column may restrict their overall "filter" role, they may nevertheless be vital for the lack of N_2O accumulation, in the water column of the Black Sea.

Due to the ongoing climate perturbations, the oceans are experiencing continuous de-oxygenation that has led to and is going to continue to lead to the expansion of oxygen-depleted environments (Diaz & Rosenberg 2008; Schmidtko et al. 2017). As these environments are hotspots for the formation and emission of N_2O (Arévalo-Martínez et al. 2015; Babbin et al. 2015; Yang et al. 2020), it is vital to understand the underlying mechanisms and microbial community that regulate the formation and reduction of this potent greenhouse gas. Additionally, due to climate induced warming, many parts of the oceans are going to become more stratified (Li et al. 2020), which already has disastrous effects in more eutrophied ecosystems like the Baltic Sea (Conley et al. 2009). Albeit stratification in the Black Sea is salinity-driven the basin nonetheless provides an excellent model system for studying N_2O cycling under conditions that are likely dominated by diffusive transport. In this study we were able to show that under these conditions the apparent lack of N_2O accumulation in the water column is due to N_2O reduction outpacing the formation

within the suboxic zone which, in part, is likely facilitated by N_2O reducing specialists of the *Marinisomatales*. The potential contributor to the weak N_2O emissions to the atmosphere is likely ammonia oxidation which can extend into the oxygenated water column. Another distinct feature of the Black Sea is the presence of the sulphide rich deep anoxic core (Konovalov et al. 2005). While sulphide itself was below detection in all incubation depths except two, the denitrifying community everywhere was dominated by organisms that have the capacity to utilise the reduced sulphur compounds. Sulphidic events may also be increasing (Pratihary et al. 2023) and have previously been shown to stimulate N_2O formation in oxygen depleted environments (Dalsgaard et al. 2014). Identifying the controlling factors that prevent N_2O accumulation in the water column of the Black Sea and other similar environments will be vital to determine the potential effect of continuous de-oxygenation on greenhouse gas cycling.

Materials and Methods

Sample collection

During cruise POS539 on R/V Poseidon, between 7th and 19th November 2019, water samples were collected from six stations in the western Black Sea (Figure 1). At each station hydrographical data was recorded and water was collected using a pump cast conductivity temperature depth (pCTD) system equipped with sensors for: temperature and salinity (Seabird SBE49 FastCAT), fluorescence (Turner Designs Cyclops-7F), high- (Pyroscience FSO2-Subport) and low-resolution oxygen concentrations (aanderaa optode 4831). At each station samples for nutrients (nitrogen oxides (NOx), nitrite, phosphate, ammonium and sulphide) were collected in a ~3 m interval on a downcast to profile the upper 150 m of the water column down to the lower edge of the suboxic zone. Subsequently three to four depths were selected based on the density for incubation experiments from within and just above the suboxic zone: a deep reference depth (above the sulphide where ammonium and methane start to increase), the secondary nitrite maximum, the nitrate maximum and at the oxycline. From these depths samples were taken for nutrients, DNA, RNA, as well as water samples for stable isotope experiments to investigate the production and consumption processes of nitrous oxide (N_2O).

Water column chemistry

Dissolved nutrients

Ammonium concentrations were determined on-board on unfiltered samples using the orthophthaldialdehyde (OPA) method (Holmes et al. 1999). The limit of detection (LOD) was 43 nmol L^{-1} d^{-1}, calculated from the mean of all blanks plus three times the standard deviation. Samples for NOx, nitrite and phosphate were sterile filtered through a 0.22 µm filter (Millipore) and frozen at -20°C until simultaneous spectrophotometric analysis using a standard methods (Strickland & Parsons 1972) on a QuAAtro39 autoanalyser (Seal Analytical). Nitrate concentrations were calculated as the difference between NOx and nitrite. LODs were 244 nmol L^{-1} (NOx), 51 nmol L^{-1} (nitrite) and 86 nmol L^{-1} (phosphate). Sulphide samples were fixed with zinc acetate before being measured spectrophotometrically on-board using the diamine method (Cline 1969).

Stable isotope incubations and rate calculations

Set up and rate determination

From each station and depth ^{15}N stable isotope incubation experiments were set up to determine potential rates of N_2O formation and consumption. Briefly, acid washed 250 mL serum bottles were filled headspace-free using gas-tight Viton tubing from the pCTD and overflown three times before being stoppered with pre-degassed (He, Air Liquide), 20 mm butyl rubber stoppers (Supelco) and crimped. Subsequently, all bottles were bubbled with helium (Air Liquide) for 20 minutes to reduce any oxygen introduced during the sampling and both tracers and pools were added (Table 1).

Table 1. **Overview of stable isotope incubation experiments.** Tracer additions were 5 µmol L^{-1} for ^{15}N-ammonium, ^{15}N-nitrite and ^{14}N-nitrite; 200 nmol L^{-1} for ^{15}N-nitrous oxide and ^{14}N-nitrous oxide; 200 µmol L^{-1} for ^{13}C-dissolved inorganic carbon and 10 µmol L^{-1} oxygen.

Experiment	Added tracers
Oxygen-supplemented ammonia oxidation	^{15}N-NH_4^+, ^{14}N-NO_2^-, ^{14}N-N_2O, ^{13}C-DIC, O_2
Anoxic ammonia oxidation	^{15}N-NH_4^+, ^{14}N-NO_2^-, ^{14}N-N_2O, ^{13}C-DIC
Denitrification from nitrite	^{15}N-NO_2^-, ^{14}N-N_2O, ^{13}C-DIC
Nitrous oxide reduction	^{15}N-N_2O, ^{13}C-DIC

After additions, incubation bottles were mixed for five minutes on a magnetic stirrer before being aliquoted into 12 mL gas-tight glass exetainers (Labco UK). Exetainers were incubated close to *in-situ* temperature (ca. 8°C) in the dark for up to 24 hours. At five time points after 0, 3, 6, 12 and 24 hours one exetainer had its biological activity inhibited through the addition of 100 µL of mercury (II) chloride ($HgCl_2$, 7 g/100ml).

In Bremen the isotopic composition of both N_2O and N_2 was determined after exchanging 5.5 mL of sample with a helium headspace before isotope ratio ($^{14}N^{14}N$, $^{14}N^{15}N$ and $^{15}N^{15}N$) measurements using a GC-IRMS (customised TraceGas coupled to a multicollector IsoPrime100, Manchester,

UK). The concentrations of $^{45}N_2O$, $^{46}N_2O$ were calculated from the excess of each relative to a N_2O sample and for $^{29}N_2$ and $^{30}N_2$ from the excess relative to an air sample (Holtappels et al. 2011). Significant rate formation was determined from the statistical analysis (One-sided student's t-test, $p < 0.05$) applied to the linear regression ($R^2 > 0.67$) of all five time points (24 hours of incubation), with the exception of the ^{15}N-N_2O experiment where only the first four time points were used.

N_2O formation from ammonium

N_2O formation from ammonium was investigated in all incubation depths from two separate experiments: an oxygen-supplemented ammonia oxidation experiment, replenished with a final oxygen concentration of 10 µmol L^{-1} and an anoxic ammonia oxidation experiment (Table 1). Both experiments had unlabelled nitrite and N_2O added as pools to "trap" any of the newly formed labelled N_2O and nitrite, to quantify rates of ^{15}N-N_2O and ^{15}N-nitrite formation from ammonia oxidation. Rates of N_2O formation were calculated using a modified version of Ji et al. (2015) (Eq. 1).

N_2O (from ammonium in nmol N L^{-1} d^{-1}) = $^{45}N_2O/f + 2 * {}^{46}N_2O/f$ (Eq. 1)

Where the $^{45}N_2O$ and $^{46}N_2O$ are the significant rates of formation. The f is the fraction of labelled ^{15}N-ammonium at the start of the incubation. This was determined by quantifying the added ^{15}N-ammonium from time point zero, after gas measurements, by hypobromite conversion (Waremburg 1993) and calculating the labelled fraction using the *in-situ* nutrient concentrations. Additionally, the rate of ^{15}N-ammonium oxidation to ^{15}N-nitrite was measured from the same incubation exetainers by converting the nitrite to N_2O using the sodium azide method (McIlvin & Altabet 2005). Ammonia oxidation rates were calculated as in Eq. 2.

Ammonia oxidation to nitrite (nmol N L^{-1} d^{-1}) = $^{29}N_2/f$ (Eq. 2)

Where $^{45}N_2O$ is the significant rate of production and the f is the same as in Eq 1. The percentage yield of N_2O from ammonia oxidation was calculated according to Eq 3.

Yield of N_2O from ammonia oxidation = (N_2O (ammonium) / ammonia oxidation to nitrite) * 100 (Eq. 3)

Rates between the oxygen-supplemented and anoxic incubation experiments were compared using an unpaired two samples Wilcoxon test after determining that the data was not normally distributed by Shapiro-Wilk's test.

N_2O production from denitrification and N_2O reduction

N_2O formation from denitrification was investigated from the precursor ^{15}N-nitrite and amended with a ^{14}N-N_2O "trap" (Table 1). Rates of both N_2O and N_2 formation were determined simultaneously and calculated according to Eq. 4 and Eq. 5, using a slightly modified version of Thamdrup & Dalsgaard (2002).

Rates of N_2O and N_2 formation were determined simultaneously and calculated according to Eq 5 and 6.

N_2O (denitrification in nmol N L^{-1} d^{-1}) = $^{46}N_2O/f^2$ *2 (Eq. 4)

N_2 (denitrification nmol N L^{-1} d^{-1}) = $^{30}N_2/f^2$ * 2 (Eq. 5)

Where $^{46}N_2O$ and $^{30}N_2$ are the significant rates of formation. The f is the fraction of labelled ^{15}N-NO_2^- at the beginning of the incubation. This was quantified by measuring the added ^{15}N-nitirte from time point zero by sulphamic acid conversion (Granger & Sigman 2009) and calculating the labelled fraction using the *in-situ* nutrient concentrations. ^{15}N-N_2O reduction to N_2 was also calculated using Eq. 5, assuming 100% labelling.

DNA and RNA isolation and sequencing of metagenome and metatranscriptome

From each incubation depth, four litres of seawater were filtered onto a 0.22 µm filter (Sterivex, Millipore). For DNA samples the filters were purged with air before being frozen at -20°C until back in Bremen, where they were frozen at -80°C. RNA samples were treated analogously but instead of air were filled up with RNAlater before being frozen at -20°C and subsequently at -80°C. Stations W3 and S3 were chosen for DNA and RNA extraction. DNA was isolated using the DNeasy PowerWater Kit (Qiagen) with an additional heating step at 65°C for 10 minutes before beat beating. RNA was extracted using the RNeasy PowerWater Kit also with the additional heating step. Samples were sequenced on Illumina MiSeq with paired-end run (2*150 bp). For metagenomes a total of 15 Gb and for metatranscriptomes 15 Gb were sequenced per sample.

Analysis of metagenomes and metatranscriptomes

Metagenomic and metatranscriptomic reads were trimmed using trim-galore (version 0.6.7) with Cutadapt (v4.0; Martin 2011). For each investigated gene (*amoA*, *narG*, *napA* (monomeric), *napA* (heterodimeric), *nirS*, *nirK*, bNOR, cNOR, eNOR, gNOR, sNOR and *nosZ*) a custom database was compiled from the protein complement of a de-replicated dataset of the species representatives of the genome taxonomy database (GTDB, version 207; Parks et al. 2022) and the "GEM-OTU" set of the genomic catalog of Earth's microbiomes (GEM; Nayfach et al. 2021), containing 78768 genomes. The general database construction procedure is described in Speth & Orphan (2018) and in detail for each gene on github.com/dspeth. Trimmed reads were compared to the reference databases using DIAMOND blastx (Buchfink et al. 2021) and the BLAST score ratio approach (Rasko et al. 2005) as described previously (Speth & Orphan 2018). Briefly, the BLAST score ratio of the reads were calculated from the alignment scores of the hits to the reference database. The cut-off values were minimum score 100, BLAST score ratio > 0.9 to extract true positive hits. For each sequence in the reference database the true positive reads were counted which is referred to as the read counts. RPKM values were calculated according to Eq 6.

RPKM = (Read Counts / (Total Reads / 1000000)) / ((average protein length * 3) / 1000) (Eq. 6)

Because the reference protein databases only contain sequences originating from (draft) genomes, taxonomic assignment of the parent genome was used as the taxonomic affiliation of the reference sequences. Read counts per taxonomic group were obtained by summing the read counts against all protein sequences assigned to a taxonomic group. All scripts used for the database construction, read searching and taxonomic assignment are available from github.com/dspeth.

Figure generation

Quantum geographic information system (QGIS; version 3.32.0) was used to generate the map. Rate analysis was conducted in Microsoft Excel (2016) and figures were generated in RStudio 2023.3.0.386 version 4.1.3 (R Core Team) using the ggplot package (Wickham 2016). Due to the stratified nature of the Black Sea, distinct water column characteristics are found at similar densities (Murray et al. 1995) and thus the results are presented plotted against σT instead of depths in metres.

Acknowledgments

We would like to thank the captain and crew of the FS Poseidon for all of their kind assistance and help during the expedition; M. Knutzen, G. Klockgether, S. Lilienthal, K. Imhoff, S. Piosek, N. Rujanski and D. Tienken for their exceptional technical support; C. Frey, F.M Jalaluddin, A. S. McDermott, W. Mohr, S. Schorn, B. Tschitschko and S. Wu for their helpful discussions and comments; the logistical support provided by MARUM and the University of Bremen; the funding of this study by the Max Planck Society and the DFG (Fördernummer: GPF19-1_91). This work was supported by the Max Planck Society.

Bibliography

Amouroux D, Roberts G, Rapsomanikis S, Andreae MO. 2002. Biogenic gas (CH4, N2O, DMS) emission to the atmosphere from near-shore and shelf waters of the north-western Black Sea. *Estuar. Coast. Shelf Sci.* 54(3):575–87

Arévalo-Martínez DL, Kock A, Löscher CR, Schmitz RA, Bange HW. 2015. Massive nitrous oxide emissions from the tropical South Pacific Ocean. *Nat. Geosci.* 8(7):530–33

Babbin AR, Bianchi D, Jayakumar A, Ward BB. 2015. Rapid nitrous oxide cycling in the suboxic ocean. *Science (80-.).* 348(6239):1127–29

Bange HW, Arévalo-Martínez DL, Paz M de la, Farías L, Kaiser J, et al. 2019. A harmonized nitrous oxide (N2O) ocean observation network for the 21st century. *Front. Mar. Sci.* 6(APR):1–10

Bertagnolli AD, Padilla CC, Glass JB, Thamdrup B, Stewart FJ. 2017. Metabolic potential and in situ activity of marine Marinimicrobia bacteria in an anoxic water column. *Environ. Microbiol.* 19(11):4392–4416

Bristow LA, Dalsgaard T, Tiano L, Mills DB, Bertagnolli AD, et al. 2016. Ammonium and nitrite oxidation at nanomolar oxygen concentrations in oxygen minimum zone waters. *Proc. Natl. Acad. Sci. U. S. A.* 113(38):10601–6

Brochier-Armanet C, Boussau B, Gribaldo S, Forterre P. 2008. Mesophilic crenarchaeota: Proposal for a third archaeal phylum, the Thaumarchaeota. *Nat. Rev. Microbiol.* 6(3):245–52

Buchfink B, Reuter K, Drost HG. 2021. Sensitive protein alignments at tree-of-life scale using DIAMOND. *Nat. Methods*. 18(4):366–68

Cabello-Yeves PJ, Callieri C, Picazo A, Mehrshad M, Haro-Moreno JM, et al. 2021. The microbiome of the Black Sea water column analyzed by shotgun and genome centric metagenomics. *Environ. Microbiomes*. 16(1):1–15

Callbeck CM, Canfield DE, Kuypers MMM, Yilmaz P, Lavik G, et al. 2021. Sulfur cycling in oceanic oxygen minimum zones. *Limnol. Oceanogr.* 66(6):2360–92

Callbeck CM, Lavik G, Ferdelman TG, Fuchs B, Gruber-Vodicka HR, et al. 2018. Oxygen minimum zone cryptic sulfur cycling sustained by offshore transport of key sulfur oxidizing bacteria. *Nat. Commun.* 9(1):1–11

Canfield DE, Stewart FJ, Thamdrup B, De Brabandere L, Dalsgaard T, et al. 2010. A cryptic sulfur cycle in oxygen-minimum-zone waters off the Chilean coast. *Science (80-.).* 330(6009):1375–78

Cao H, Dong C, Bougouffa S, Li J, Zhang W, et al. 2016. Delta-proteobacterial SAR324 group in hydrothermal plumes on the South Mid-Atlantic Ridge. *Sci. Rep.* 6(March 2015):1–9

Caranto JD, Vilbert AC, Lancaster KM. 2016. Nitrosomonas europaea cytochrome P460 is a direct link between nitrification and nitrous oxide emission . *Proc. Natl. Acad. Sci.* 113(51):14704–9

Cline JD. 1969. Spectrophotometric Determination of Hydrogen Sulfide in Natural Waters. *Limnol. Oceanogr.* 14(3):454–58

Codispoti LA. 2010. Interesting times for marine N2O. *Science (80-.).* 327(5971):1339–40

Conley DJ, Björck S, Bonsdorff E, Carstensen J, Destouni G, et al. 2009. Hypoxia-Related Processes in the Baltic Sea. *Environ. Sci. Technol.* 43(10):3412–20

Dalsgaard T, Stewart FJ, Thamdrup B, De Brabandere L, Revsbech NP, et al. 2014. Oxygen at nanomolar levels reversibly suppresses process rates and gene expression in anammox and denitrification in the oxygen minimum zone off Northern Chile. *MBio*. 5(6):1–14

Diaz RJ, Rosenberg R. 2008. Spreading dead zones and consequences for marine ecosystems. *Science (80-.).* 321(5891):926–29

Francis CA, Roberts KJ, Beman JM, Santoro AE, Oakley BB. 2005. Ubiquity and diversity of ammonia-oxidizing archaea in water columns and sediments of the ocean. *Proc. Natl. Acad. Sci.* 102(41):14683–88

Freing A, Wallace DWR, Bange HW. 2012. Global oceanic production of nitrous oxide. *Philos. Trans. R. Soc. B Biol. Sci.* 367(1593):1245–55

Frey C, Bange HW, Achterberg EP, Jayakumar A, Löscher CR, et al. 2020. Regulation of nitrous oxide production in low-oxygen waters off the coast of Peru. *Biogeosciences*. 17(8):2263–87

Fuchsman CA, Kirkpatrick JB, Brazelton WJ, Murray JW, Staley JT. 2011. Metabolic strategies of free-living and aggregate-associated bacterial communities inferred from biologic and chemical profiles in the Black Sea suboxic zone. *FEMS Microbiol. Ecol.* 78(3):586–603

Fuchsman CA, Paul B, Staley JT, Yakushev E V., Murray JW. 2019. Detection of Transient Denitrification During a High Organic Matter Event in the Black Sea. *Global Biogeochem. Cycles*. 33(2):143–62

Garrido-Amador P, Kniaziuk M, Vekeman B, Kartal B. 2021. Learning from microorganisms: using new insights in microbial physiology for sustainable nitrogen management. *Curr. Opin. Biotechnol.* 67:42–48

Glaubitz S, Kießlich K, Meeske C, Labrenz M, Jürgens K. 2013. SUP05 Dominates the gammaproteobacterial sulfur oxidizer assemblages in pelagic redoxclines of the central baltic and black seas. *Appl. Environ. Microbiol.* 79(8):2767–76

Glaubitz S, Labrenz M, Jost G, Jürgens K. 2010. Diversity of active chemolithoautotrophic prokaryotes in the sulfidic zone of a Black Sea pelagic redoxcline as determined by rRNA-based stable isotope probing. *FEMS Microbiol. Ecol.* 74(1):32–41

Goreau TJ, Kaplan WA, Wofsy SC, McElroy MB, Valois FW, Watson SW. 1980. Production of NO2- and N2O by Nitrifying Bacteria at Reduced Concentrations of Oxygen. *Appl. Environ. Microbiol.* 40(3):526–32

Graf DRH, Jones CM, Hallin S. 2014. Intergenomic comparisons highlight modularity of the denitrification pathway and underpin the importance of community structure for N2O emissions. *PLoS One*. 9(12):1–20

Granger J, Sigman DM. 2009. Removal of nitrite with sulfamic acid for nitrate N and O isotope analysis with the denitrifier method. *Rapid Commun. Mass Spectrom.* 23(23):3753–62

Hawley AK, Nobu MK, Wright JJ, Durno WE, Morgan-Lang C, et al. 2017. Diverse Marinimicrobia bacteria may mediate coupled biogeochemical cycles along eco-thermodynamic gradients. *Nat. Commun.* 8(1):1–9

Holmes RM, Aminot A, Kérouel R, Hooker BA, Peterson BJ. 1999. A simple and precise method for measuring ammonium in marine and freshwater ecosystems. *Can. J. Fish. Aquat. Sci.* 56(10):1801–8

Holtappels M, Lavik G, Jensen MM, Kuypers MMM. 2011. 15N-Labeling Experiments to Dissect the Contributions of Heterotrophic Denitrification and Anammox to Nitrogen Removal in the OMZ Waters of the Ocean. In *Methods in Enzymology*, Vol. 486, pp. 223–51. Elsevier Inc. 1st ed.

Intergovernmental Panel on Climate Change. 2023. Global Carbon and Other Biogeochemical Cycles and Feedbacks. In *Climate Change 2021 – The Physical Science Basis*, pp. 673–816. Cambridge University Press

Jensen MM, Kuypers MMM, Lavik G, Thamdrup B. 2008. Rates and regulation of anaerobic ammonium oxidation and denitrification in the Black Sea. *Limnol. Oceanogr.* 53(1):23–36

Ji Q, Babbin AR, Jayakumar A, Oleynik S, Ward BB. 2015. Nitrous oxide production by nitrification and denitrification in the Eastern Tropical South Pacific oxygen minimum zone. *Geophys. Res. Lett.* 42(24):10,755-10,764

Ji Q, Buitenhuis E, Suntharalingam P, Sarmiento JL, Ward BB. 2018. Global Nitrous Oxide Production Determined by Oxygen Sensitivity of Nitrification and Denitrification. *Global Biogeochem. Cycles*. 32(12):1790–1802

Jung MY, Gwak JH, Rohe L, Giesemann A, Kim JG, et al. 2019. Indications for enzymatic denitrification to N2O at low pH in an ammonia-oxidizing archaeon. *ISME J.* 13(10):2633–38

Kirkpatrick JB, Fuchsman CA, Yakushev E, Staley JT, Murray JW. 2012. Concurrent activity of anammox and denitrifying bacteria in the Black sea. *Front. Microbiol.* 3(JUL):1–12

Konovalov SK, Murray JW, Luther GW. 2005. Basic processes of Black Sea biogeochemistry. *Oceanography*. 18(SPL.ISS.2):24–35

Kozlowski JA, Price J, Stein LY. 2014. Revision of N2O-producing pathways in the ammonia-oxidizing bacterium Nitrosomonas europaea ATCC 19718. *Appl. Environ. Microbiol.* 80(16):4930–35

Kozlowski JA, Stieglmeier M, Schleper C, Klotz MG, Stein LY. 2016. Pathways and key intermediates required for obligate aerobic ammonia-dependent chemolithotrophy in bacteria and Thaumarchaeota. *ISME J.* 10(8):1836–45

Kraft B, Jehmlich N, Larsen M, Bristow LA, Könneke M, et al. 2022. Oxygen and nitrogen production by an ammonia-oxidizing archaeon. *Science (80-.).* 375(6576):97–100

Kuypers MMM, Marchant HK, Kartal B. 2018. The microbial nitrogen-cycling network. *Nat. Rev. Microbiol.* 16(5):263–76

Kuypers MMM, Silekers AO, Lavik G, Schmid M, Jøorgensen BB, et al. 2003. Anaerobic ammonium oxidation by anammox bacteria in the Black Sea. *Nature*. 422(6932):608–11

Lam P, Jensen MM, Lavik G, McGinnis DF, Müller B, et al. 2007. Linking crenarchaeal and bacterial nitrification to anammox in the Black Sea. *Proc. Natl. Acad. Sci. U. S. A.* 104(17):7104–9

Lam P, Kuypers MMM. 2011. Microbial nitrogen cycling processes in oxygen minimum zones. *Ann. Rev. Mar. Sci.* 3:317–45

Lavik G, Stührmann T, Brüchert V, Van Der Plas A, Mohrholz V, et al. 2009. Detoxification of sulphidic African shelf waters by blooming chemolithotrophs. *Nature*. 457(7229):581–84

Lees H. 1952. Hydroxylamine as an intermediate in nitrification. *Nature*. 169(4291):156–57

Li G, Cheng L, Zhu J, Trenberth KE, Mann ME, Abraham JP. 2020. Increasing ocean stratification over the past half-century. *Nat. Clim. Chang.* 10(12):1116–23

Lipschultz F, Wofsy SC, Ward BB, Codispoti LA, Friedrich G, Elkins JW. 1990. Bacterial transformations of inorganic nitrogen in the oxygen-deficient waters of the Eastern Tropical South Pacific Ocean. *Deep Sea Res. Part A, Oceanogr. Res. Pap.* 37(10):1513–41

Löscher CR, Kock A, Könneke M, Laroche J, Bange HW, Schmitz RA. 2012. Production of oceanic nitrous oxide by ammonia-oxidizing archaea. *Biogeosciences*. 9(7):2419–29

Lycus P, Bøthun KL, Bergaust L, Shapleigh JP, Bakken LR, Frostegård Å. 2017. Phenotypic and genotypic richness of denitrifiers revealed by a novel isolation strategy. *ISME J.* 11(10):2219–32

Martin M. 2011. Cutadapt removes adapter sequences from high-throughput sequencing reads. *EMBnet.journal*. 17(1):10

Martinez-Rey J, Bopp L, Gehlen M, Tagliabue A, Gruber N. 2015. Projections of oceanic N2O emissions in the 21st century using the IPSL Earth system model. *Biogeosciences*. 12(13):4133–48

McIlvin MR, Altabet MA. 2005. Chemical conversion of nitrate and nitrite to nitrous oxide for nitrogen and oxygen isotopic analysis in freshwater and seawater. *Anal. Chem.* 77(17):5589–95

Moraes BS, Souza TSO, Foresti E. 2012. Effect of sulfide concentration on autotrophic denitrification from nitrate and nitrite in vertical fixed-bed reactors. *Process Biochem.* 47(9):1395–1401

Murray J. 1989. The 1988 Black Sea Oceanographic Expedition: Overview and New Discoveries. *Oceanography*. 2(1):15–21

Murray JW, Codispoti LA, Friederich GE. 1995. Oxidation-Reduction Environments. In *Aquatic Chemistry: Interfacial and Interspecies Processes.*, pp. 157–76

Murray JW, Yakushev E. 2006. THE SUBOXIC TRANSITION ZONE IN THE BLACK SEA. In *Past and Present Water Column Anoxia*, pp. 105–38. Dordrecht: Kluwer Academic Publishers

Naqvi SWA, Bange HW, FarÃ-As L, Monteiro PMS, Scranton MI, Zhang J. 2010. Marine hypoxia/anoxia as a source of CH4 and N2O. *Biogeosciences*. 7(7):2159–90

Nayfach S, Roux S, Seshadri R, Udwary D, Varghese N, et al. 2021. A genomic catalog of Earth's microbiomes. *Nat. Biotechnol.* 39(4):499–509

Oakley BB, Francis CA, Roberts KJ, Fuchsman CA, Srinivasan S, Staley JT. 2007. Analysis of nitrite reductase (nirK and nirS) genes and cultivation reveal depauperate community of denitrifying bacteria in the Black Sea suboxic zone. *Environ. Microbiol.* 9(1):118–30

Oswald K, Graf JS, Littmann S, Tienken D, Brand A, et al. 2017. Crenothrix are major methane consumers in stratified lakes. *ISME J.* 11(9):2124–40

Parks DH, Chuvochina M, Rinke C, Mussig AJ, Chaumeil PA, Hugenholtz P. 2022. GTDB: An ongoing census of bacterial and archaeal diversity through a phylogenetically consistent, rank normalized and complete genome-based taxonomy. *Nucleic Acids Res.* 50(D1):D785–94

Pavlovska M, Prekrasna I, Dykyi E, Zotov A, Dzhulai A, et al. 2021. Niche partitioning of bacterial communities along the stratified water column in the Black Sea. *Microbiologyopen*. 10(3):1–24

Portmann RW, Daniel JS, Ravishankara AR. 2012. Stratospheric ozone depletion due to nitrous oxide: Influences of other gases. *Philos. Trans. R. Soc. B Biol. Sci.* 367(1593):1256–64

Pratihary A, Lavik G, Naqvi SWA, Shirodkar G, Sarkar A, et al. 2023. Chemolithoautotrophic denitrification intensifies nitrogen loss in the Eastern Arabian Sea Shelf waters during sulphidic events. *Prog. Oceanogr.* 217:103075

Prosser JI, Hink L, Gubry-Rangin C, Nicol GW. 2020. Nitrous oxide production by ammonia oxidizers: Physiological diversity, niche differentiation and potential mitigation strategies. *Glob. Chang. Biol.* 26(1):103–18

Purkhold U, Pommerening-Röser A, Juretschko S, Schmid MC, Koops H-P, Wagner M. 2000. Phylogeny of All Recognized Species of Ammonia Oxidizers Based on Comparative 16S rRNA and amoA Sequence Analysis: Implications for Molecular Diversity Surveys. *Appl. Environ. Microbiol.* 66(12):5368–82

Qin W, Meinhardt KA, Moffett JW, Devol AH, Virginia Armbrust E, et al. 2017. Influence of oxygen availability on the activities of ammonia-oxidizing archaea. *Environ. Microbiol. Rep.* 9(3):250–56

Rasko DA, Myers GSA, Ravel J. 2005. Visualization of comparative genomic analyses by BLAST score ratio. *BMC Bioinformatics*. 6:1–7

Ravishankara AR, Daniel JS, Portmann RW. 2009. Nitrous oxide (N2O): The dominant ozone-depleting substance emitted in the 21st century. *Science (80-.).* 326(5949):123–25

Rotthauwe JH, Witzel KP, Liesack W. 1997. The ammonia monooxygenase structural gene amoA as a functional marker: molecular fine-scale analysis of natural ammonia-oxidizing populations. *Appl. Environ. Microbiol.* 63(12):4704–12

Sanford RA, Wagner DD, Wu Q, Chee-Sanford JC, Thomas SH, et al. 2012. Unexpected nondenitrifier nitrous oxide reductase gene diversity and abundance in soils. *Proc. Natl. Acad. Sci. U. S. A.* 109(48):19709–14

Santoro AE, Buchwald C, McIlvin MR, Casciotti KL. 2011. Isotopic Signature of N2O Produced by Marine Ammonia-Oxidizing Archaea. *Science (80-.).* 333(6047):1282–85

Schmidtko S, Stramma L, Visbeck M. 2017. Decline in global oceanic oxygen content during the past five decades. *Nature*. 542(7641):335–39

Shah V, Chang BX, Morris RM. 2017. Cultivation of a chemoautotroph from the SUP05 clade of marine bacteria that produces nitrite and consumes ammonium. *ISME J.* 11(1):263–71

Sheik CS, Jain S, Dick GJ. 2014. Metabolic flexibility of enigmatic SAR324 revealed through metagenomics and metatranscriptomics. *Environ. Microbiol.* 16(1):304–17

Spang A, Hatzenpichler R, Brochier-Armanet C, Rattei T, Tischler P, et al. 2010. Distinct gene set in two different lineages of ammonia-oxidizing archaea supports the phylum Thaumarchaeota. *Trends Microbiol.* 18(8):331–40

Speth DR, Orphan VJ. 2018. Metabolic marker gene mining provides insight in global mcrA diversity and, coupled with targeted genome reconstruction, sheds further light on metabolic potential of the Methanomassiliicoccales. *PeerJ*. 2018(9):

Stein LY, Klotz MG, Lancaster KM, Nicol GW, Qin W, et al. 2021. Comment on"A Critical Review on Nitrous Oxide Production by Ammonia-Oxidizing Archaea" by Lan Wu, Xueming Chen, Wei Wei, Yiwen Liu, Dongbo Wang, and Bing-Jie Ni. *Environ. Sci. Technol.* 55(1):797–98

Stieglmeier M, Mooshammer M, Kitzler B, Wanek W, Zechmeister-Boltenstern S, et al. 2014. Aerobic nitrous oxide production through N-nitrosating hybrid formation in ammonia-oxidizing archaea. *ISME J.* 8(5):1135–46

Strickland JDH & Parsons TR. 1972. *A Practical Handbook of Seawater Analysis*. Bulletin no. 167

Suominen S, Dombrowski N, Sinninghe Damsté JS, Villanueva L. 2021. A diverse uncultivated microbial community is responsible for organic matter degradation in the Black Sea sulphidic zone. *Environ. Microbiol.* 23(6):2709–28

Thamdrup B, Dalsgaard T. 2002. Production of N2 through anaerobic ammonium oxidation coupled to nitrate reduction in marine sediments. *Appl. Environ. Microbiol.* 68(3):1312–18

Thomson AJ, Giannopoulos G, Pretty J, Baggs EM, Richardson DJ. 2012. Biological sources and sinks of nitrous oxide and strategies to mitigate emissions. *Philos. Trans. R. Soc. B Biol. Sci.* 367(1593):1157–68

Tian H, Xu R, Canadell JG, Thompson RL, Winiwarter W, et al. 2020. A comprehensive quantification of global nitrous oxide sources and sinks. *Nature*. 586(7828):248–56

Vajrala N, Martens-Habbena W, Sayavedra-Soto LA, Schauer A, Bottomley PJ, et al. 2013. Hydroxylamine as an intermediate in ammonia oxidation by globally abundant marine archaea. *Proc. Natl. Acad. Sci.* 110(3):1006–11

van Vliet DM, von Meijenfeldt FAB, Dutilh BE, Villanueva L, Sinninghe Damsté JS, et al. 2021. The bacterial sulfur cycle in expanding dysoxic and euxinic marine waters. *Environ. Microbiol.* 23(6):2834–57

Walsh DA, Zaikova E, Howes CG, Song YC, Wright JJ, et al. 2009. Metagenome of a versatile chemolithoautotroph from expanding oceanic dead zones. *Science (80-.).* 326(5952):578–82

Wan XS, Hou L, Kao S-J, Zhang Y, Sheng H-X, et al. 2023. Pathways of N2O production by marine ammonia-oxidizing archaea determined from dual-isotope labeling. *Proc. Natl. Acad. Sci.* 120(11):2017

Ward BB, Kilpatrick KA. 1991. Nitrogen Transformations in the Oxic Layer of Permanent Anoxic Basins: The Black Sea and the Cariaco Trench. In *Black Sea Oceanography*, pp. 111–24. Dordrecht: Springer Netherlands

Warembourg FR. 1993. Nitrogen fixation in soil and plant system. In: Knowles R, Blackburn TH (eds) Nitrogen isotopes techniques. Academic Press: New York, pp 127–155

Westley MB, Yamagishi H, Popp BN, Yoshida N. 2006. Nitrous oxide cycling in the Black Sea inferred from stable isotope and isotopomer distributions. *Deep. Res. Part II Top. Stud. Oceanogr.* 53(17–19):1802–16

Wickham H. 2016. *Ggplot2: Elegant Graphics for Data Analysis*. Springer-Verlag New York

Wrage-Mönnig N, Horn MA, Well R, Müller C, Velthof G, Oenema O. 2018. The role of nitrifier denitrification in the production of nitrous oxide revisited. *Soil Biol. Biochem.* 123:A3–16

Wright JJ, Mewis K, Hanson NW, Konwar KM, Maas KR, Hallam SJ. 2014. Genomic properties of Marine Group A bacteria indicate a role in the marine sulfur cycle. *ISME J.* 8(2):455–68

Wuchter C, Abbas B, Coolen MJL, Herfort L, Van Bleijswijk J, et al. 2006. Archaeal nitrification in the ocean. *Proc. Natl. Acad. Sci. U. S. A.* 103(33):12317–22

Wyrtki K. 1962. The oxygen minima in relation to ocean circulation. *Deep. Res. Oceanogr. Abstr.* 9(1–2):11–23

Yang S, Chang BX, Warner MJ, Weber TS, Bourbonnais AM, et al. 2020. Global reconstruction reduces the uncertainty of oceanic nitrous oxide emissions and reveals a vigorous seasonal cycle. *Proc. Natl. Acad. Sci. U. S. A.* 117(22):

Yoon S, Nissen S, Park D, Sanford RA, Löffler E. 2016. Clade I NosZ from Those Harboring Clade II NosZ. *Appl. Envioronmental Microbiol.* 82(13):3793–3800

Yoshida T, Alexander M. 1970. Nitrous Oxide Formation by Nitrosomonas Europaea and Heterotrophie Microorganisms. *Soil Sci. Soc. Am. J.* 34(6):880–82

Zhu-Barker X, Cavazos AR, Ostrom NE, Horwath WR, Glass JB. 2015. The importance of abiotic reactions for nitrous oxide production. *Biogeochemistry*. 126(3):251–67

Zumft WG. 1997. Cell biology and molecular basis of denitrification. *Microbiol. Mol. Biol. Rev.* 61(4):533–616

Supplement

Supplementary Figures

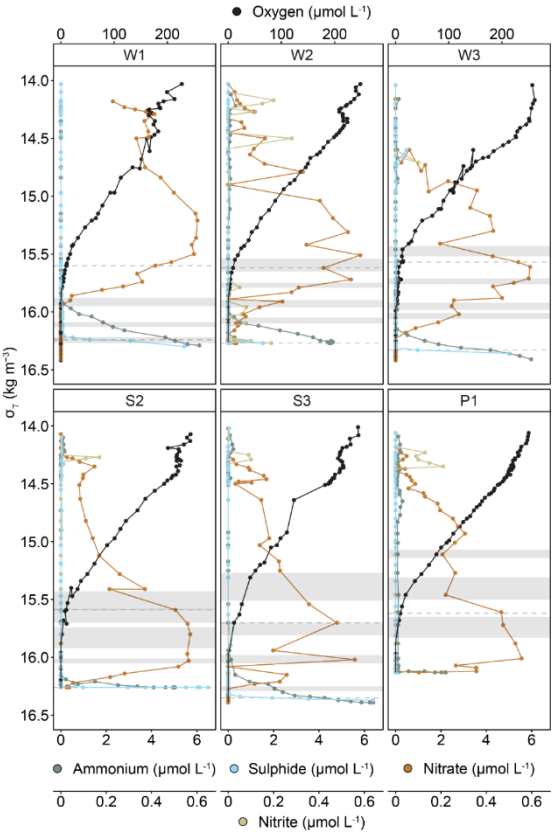

Figure S1. **Extended nutrient profile of Figure 2.** All samples originate from the downcast of the pump CTD system. Dashed grey lines outline the suboxic zone with the upper boundary set to 10 µmol L^{-1} oxygen and the lower boundary where sulphide concentrations increased (Sulphide > 1 µmol L^{-1}). Grey boxes indicate the incubation depths sampled during the upcast and include the movement in the water column during sampling.

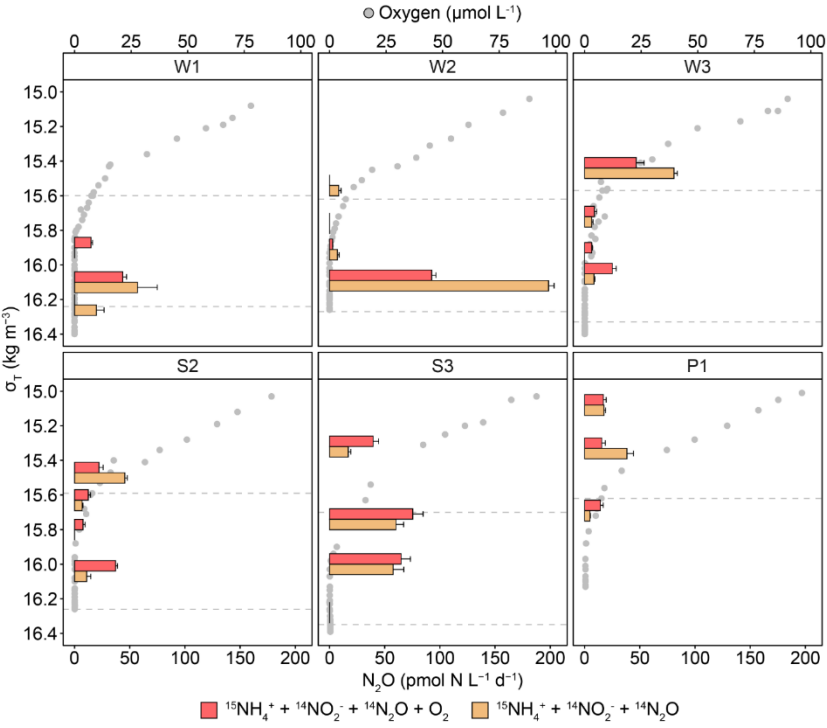

Figure S2. **Nitrous oxide formation from the oxygen-supplemented and anoxic ammonia oxidation experiments**. Each bar represents a statistically significant (One-sided student's t-test, $p < 0.05$) rate calculated from the slope across the incubation time points, with error bars representing the standard error of the slopes. Dashed grey lines outline the suboxic zone with the upper boundary set to 10 µmol L^{-1} oxygen and the lower boundary where sulphide concentrations increased (Sulphide > 1 µmol L^{-1}). Non-linear rates are depicted as zero.

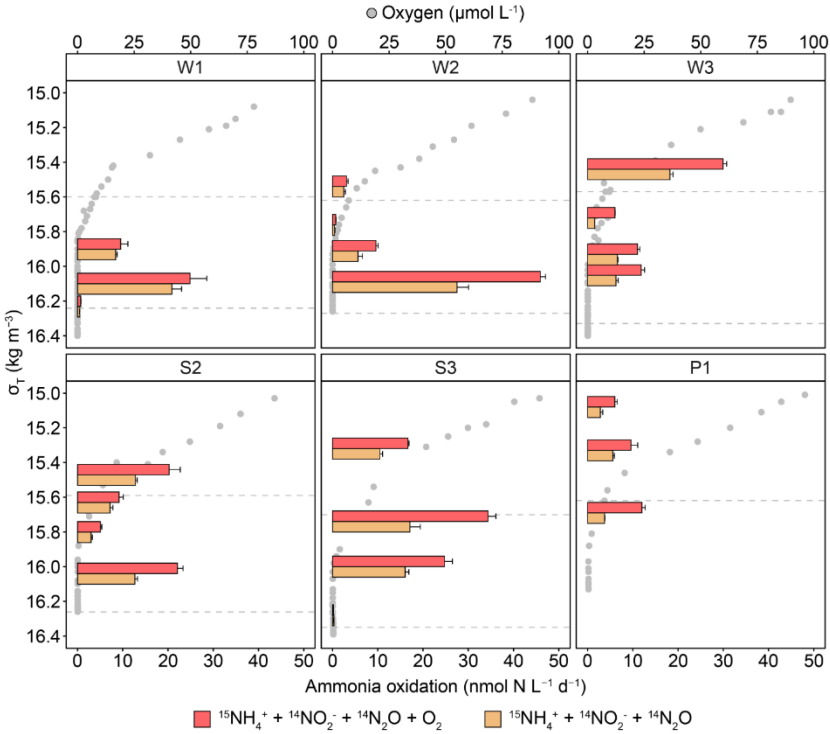

Figure S3. **Comparison of ammonia oxidation rates to nitrite from the oxygen-supplemented ammonia oxidation experiment and anoxic ammonia oxidation experiment**. Each bar represents a statistically significant (One-sided student's t-test, $p < 0.05$) rate calculated from the slope across the incubation time points, with error bars representing the standard error of the slopes. Dashed grey lines outline the suboxic zone with the upper boundary set to 10 µmol L^{-1} oxygen and the lower boundary where sulphide concentrations increased (Sulphide > 1 µmol L^{-1}). Non-linear rates are depicted as zero.

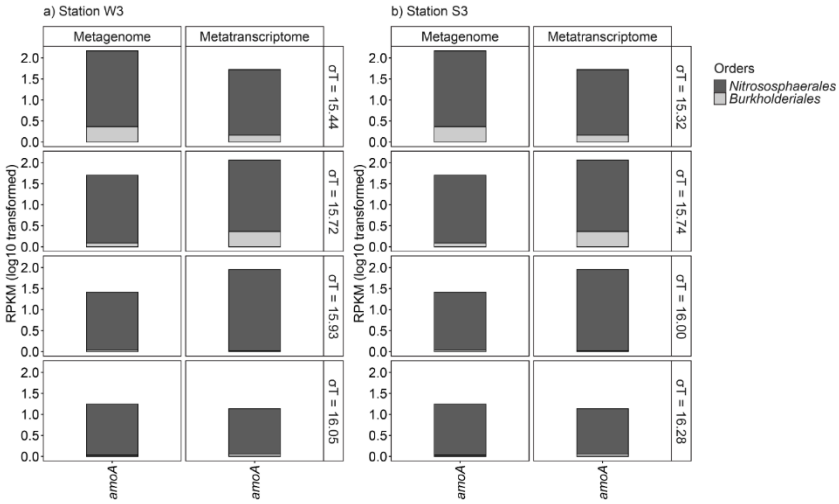

Figure S4. **Taxonomic diversity of *amoA* containing organisms.** Metagenomic and metatransciptomic abundance of key functional gene *amoA* on order-level at **a,** W3 and **b,** S3. GTDB taxonomy was assigned based on best hit against custom marker gene databases.

Figure S5**. Metagenomic and metatranscriptomic abundances of denitrifying key functional genes and *amoA* from read-based analysis. a,** Metagenome. **b,** Metatranscriptome. Samples were taken from all incubation depths of W3 and S3.

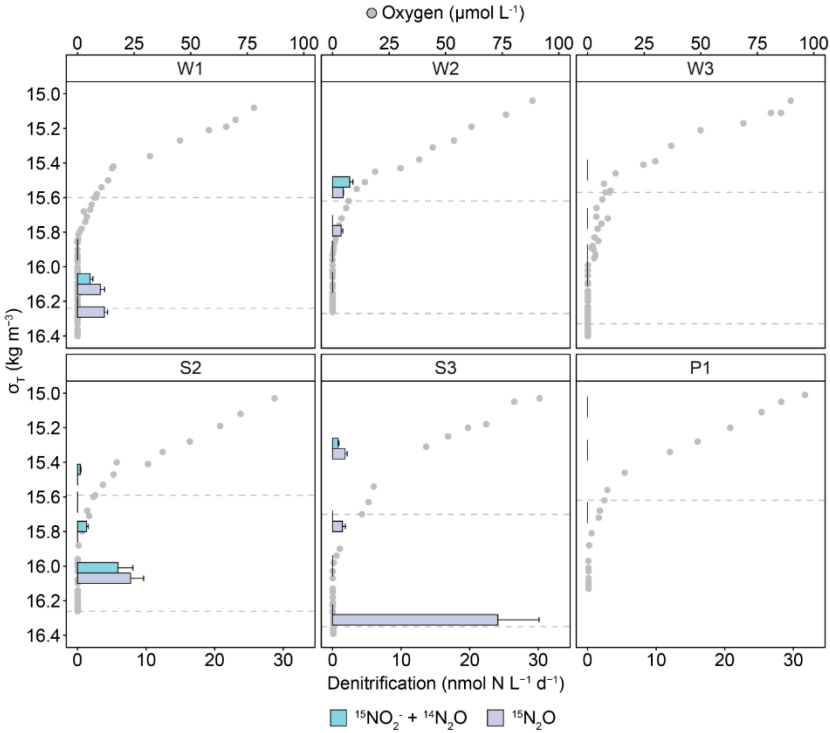

Figure S6. **Comparison of the N_2 formation from nitrite from denitrification with the ^{15}N-nitrous oxide reduction experiment.** Each bar represents a statistically significant (One-sided student's t-test, $p < 0.05$) rate calculated from the slope across the incubation time points, with error bars representing the standard error of the slopes. Dashed grey lines outline the suboxic zone with the upper boundary set to 10 µmol L^{-1} oxygen and the lower boundary where sulphide concentrations increased (Sulphide > 1 µmol L^{-1}). Non-linear rates are depicted as zero.

Chapter IV

Nitrous oxide cycling in the coastal Peruvian oxygen minimum zone

Jan N. von Arx[1], Soeren Ahmerkamp[1], Clarissa Karthäuser[1], Katharina Kitzinger[1], Gaute Lavik[1], Jon Graf[1], Sina Schorn[1], Marcel M. M. Kuypers[1] and Jana Milucka[1]

Potential co-authors who were involved in the presented work: Kevin Diaz[2], Michelle Graco[2], Jesus Ledesma[2]

Author affiliation

[1]Max Planck Institute for Marine Microbiology, Bremen, Germany

[2]Dirección de Investigaciones Oceanográficas y Cambio Climático. Instituto del Mar del Perú, Callao, Perú

In preparation

Author Contributions

The study was designed by M.M.M.K. and J.M. Sampling in the field was conducted by S.A., G.L., J.G. and myself (J.v.A.). Stable isotope incubation experiments were set up by K.K., S.S. and M.M.M.K. Rates measurements from stable isotope incubation experiments were carried out by K.K. and I. Rate analysis and calculations were conducted by G.L. and I. I filtered water for the POC and PON concentrations and measured and analysed them. Particle abundance data was provided by S.A. and C.K. I discussed and interpreted the data with J.M. I visualised the presented dataset. The manuscript was written by J.M. and I.

Abstract

The oxygen minimum zone off the coast of Peru is considered to be the single largest marine source of the greenhouse gas nitrous oxide (N_2O) to the atmosphere. Both microbial N_2O producing processes, ammonia oxidation and denitrification, are thought to contribute to the N_2O fluxes from this region. Studies from the offshore oxygen minimum zone and from coastal stations indicate that N_2O concentrations and associated microbial N_2O cycling intensify with increasing proximity to the coast; yet data from stations shallower than 100 metres remain scarce. We quantified rates of both N_2O formation and consumption from six shallow (maximal 92 metres deep) stations off Callao, Peru, using stable isotope incubation experiments. We measured persistent minor rates of N_2O formation from ammonia oxidation (up to 0.68 nmol N L^{-1} d^{-1}) and sporadic, extremely high rates of denitrification to N_2O (up to 29 nmol N L^{-1} d^{-1}). Interestingly, the measured N_2O reduction rates exceeded the combined N_2O formation from all quantified sources, with maximal rates of up to 106 nmol N L^{-1} d^{-1}. Our data suggest that while the microbial filter has the potential to counteract N_2O production in principle, it fails to do so *in-situ*, where physical mixing and oxygen intrusions decouple N_2O production and consumption processes and likely repress consumption rates. Our results reveal intense N_2O cycling in a shallow near-shore region that underpins the key function of these regions for marine greenhouse gas emissions.

Introduction

Nitrous oxide (N_2O) is the third most abundant greenhouse gas emitted by anthropogenic activity (Intergovernmental Panel on Climate Change 2023) and the most significant ozone depleting substance in the atmosphere (Portmann et al. 2012; Ravishankara et al. 2009). Marine environments are one of the most important sources of N_2O to the atmosphere, contributing around 3.7 (2.8 - 4.7) Tg N yr^{-1}, approximately a third of all natural emissions (Intergovernmental Panel on Climate Change 2023; Tian et al. 2020). Within the marine environment, the Peruvian oxygen minimum zone (OMZ) is the single largest source of N_2O (Arévalo-Martínez et al. 2015; Kock et al. 2016; Yang et al. 2020), accounting for a flux of at least 0.25 Tg N yr^{-1} (Yang et al. 2020) with estimates reaching as high as 0.9 Tg N yr^{-1} based on N_2O supersaturation (Arévalo-Martínez et al. 2015). The Peruvian oxygen minimum zone is located in the eastern tropical South Pacific upwelling system (ETSP), where nutrient rich but oxygen poor deep water is transported to the surface through wind induced Ekman transport (Chavez & Messié 2009). The upwelling stimulates primary productivity, making the ETSP one of the most productive marine areas globally (Messié et al. 2009; Pauly & Christensen 1995). The elevated productivity leads to higher concentrations of organic matter, which is respired, thereby depleting oxygen concentrations. Combined with the local sluggish ventilation (Karstensen et al. 2008), these factors lead to the formation of an OMZ that extends 1000 km from the Peruvian shelf into the Pacific Ocean (Fuenzalida et al. 2009). The OMZ can be operationally defined by waters where oxygen concentrations fall below 20 µmol L^{-1} (Lam & Kuypers 2011). However, the core of the OMZ can be entirely anoxic, with oxygen concentrations below the detection limit of a switchable trace oxygen sensor (Thamdrup et al. 2012). Therefore, conditions within and around the OMZ are highly favourable for both aerobic and anaerobic microbial N_2O cycling processes (Babbin et al. 2015; Codispotti et al. 2010).

N_2O is formed biologically through two main processes, aerobic ammonia oxidation and denitrification. Ammonia oxidation describes the stepwise oxidation of ammonia to nitrite in the presence of oxygen (Lancaster et al. 2018). The process is carried out by taxonomically distinct ammonia oxidising archaea (AOA) and ammonia oxidising bacteria (AOB). The AOA are considered to be the dominant species in the marine environment (Francis et al. 2005; Wuchter et al. 2006) and are taxonomically constrained to the *Thaumarchaeota*, while the AOB are more often associated with coastal areas and belong to the *Beta-* and *Gammaproteobacteria* (Purkhold et al. 2000). Both of these groups can form N_2O during ammonia oxidation, primarily as a by-

product. In AOA, the N_2O formation appears to occur as a result of a hybrid pathway, where a nitrogen atom originating from ammonia is combined with one from nitrite (Kozlowski et al. 2016; Stieglmeier et al. 2014; Wan et al. 2023). However, there is evidence that other pathways exist, including N_2O formation under low pH (Jung et al. 2019) and nitric oxide dismutation (Kraft et al. 2022). The primary mechanism of N_2O formation in AOB appears to be nitrifier-denitrification, where nitrite is reduced to N_2O at low oxygen concentrations using canonical nitrite and nitric oxide reductases (Goreau et al. 1980; Wrage-Mönnig 2018). Alternatively, N_2O formation in AOB has been attributed to enzymatically mediated hydroxylamine oxidation (Caranto et al. 2016; Kozlowski et al. 2014). Finally, in both groups of organisms N_2O can be formed abiotically through interactions of the intermediates hydroxylamine, nitric oxide and nitrite (Wan et al. 2023; Zhu-Barker et al. 2015).

Denitrification is a process of anaerobic respiration in which microorganisms use inorganic N-compounds (nitrate, nitrite, nitric oxide and nitrous oxide) as an electron acceptor. This typically takes place in low oxygen and anoxic waters and results in the production of N_2-gas, thus removing bioavailable N from the environment (Zumft 1997). Notably, denitrification is also the only known significant biological N_2O sink, removing N_2O through its reduction to N_2. The individual steps of denitrification can be performed by a single organism, or by a denitrifying community, in which individual members are metabolically specialised to respire one, or multiple intermediates, which can lead to the accumulation of the intermediates (Garrido-Amador et al. 2021; Graf et al. 2014; Kuypers et al. 2018; Lycus et al. 2017; Marchant et al. 2018). Denitrification can be heterotrophic, where organic carbon sources serve as the electron donor, (Zumft 1997), methanotrophic (Oswald et al. 2017) and lithotrophic, using alternative electron donors such as hydrogen sulphide or elemental sulphur among other compounds (Canfield et al. 2010; Lavik et al. 2009).

The nitrogen transformation processes in the Peruvian OMZ have been intensely studied. The available data suggest that ammonia oxidation is a minor source of N_2O (Bourbonnais et al. 2017; Frey et al. 2020; Ji et al. 2015, 2018), contributing around 11% to the N_2O sources within the entire ETSP (McCoy et al. 2023). Instead, denitrification, especially along the peripheries of the anoxic OMZ core, is considered to be the main source of N_2O *in-situ* (Bourbonnais et al. 2017; Frey et al. 2020; Ji et al. 2015, 2018). However, denitrification to N_2 only occurs sporadically (Dalsgaard et al. 2012, 2014) and N_2-loss is dominated by anaerobic ammonia oxidation (anammox; Hamersley et al. 2007; Kalvelage et al. 2011; Lam et al. 2009; Kalvelage et al. 2013), which does not involve

N_2O as an intermediate. However, these data were largely collected from the open ocean OMZ or deeper (>100 m) coastal areas. The shallow coastal areas remain underexplored, despite being potentially significant sources of N_2O emissions (Arévalo-Martínez et al. 2015; Intergovernmental Panel on Climate Change 2023). In this study, we investigated N_2O cycling and the associated nitrogen transformation processes, including nitrogen removal, in six stations in the coastal Peruvian OMZ ranging between 45 - 92 metres depth. We combined measurements of *in-situ* N_2O concentrations with stable isotope labelling experiments to resolve the processes responsible for the formation and consumption of N_2O.

Results

Water column chemistry

During the austral autumn of 2019, we investigated pelagic nitrous oxide (N_2O) cycling at six stations in the coastal Peruvian oxygen minimum zone (OMZ) off Callao, Peru (Figure 1a).

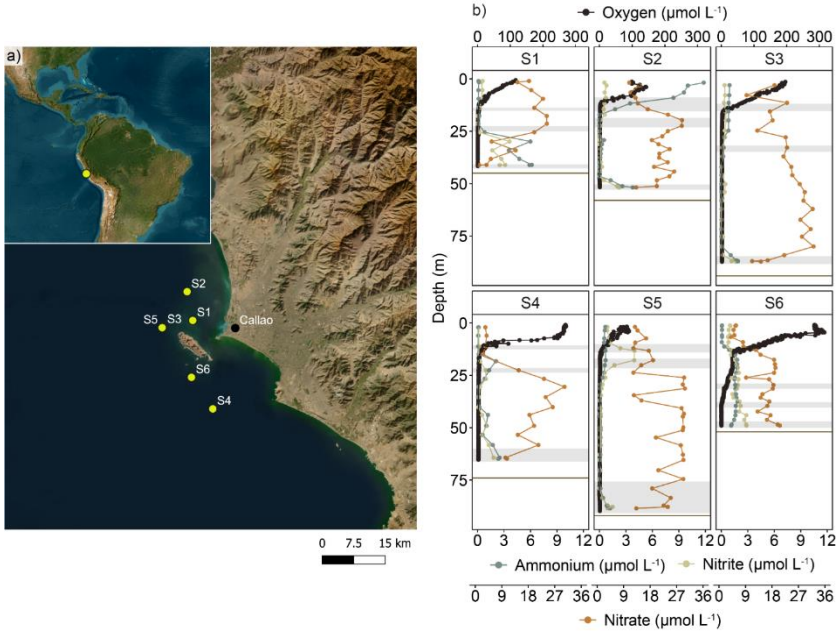

Figure 1. **Water column chemistry of the investigated station in the coastal Peruvian oxygen minimum zone. a,** Map of the sampled stations. **b,** Nutrient profiles from the investigated stations. All samples originate from the downcast of the pump CTD system. Grey boxes outline the incubation depths sampled during the upcast, taking into consideration the movement in the water column during sampling. Brown line indicates the sediment interface.

All stations were shallow (45 - 92m) and characterised by a eutrophied water column (Figure 1b). Density profiles (Supplementary Figure S1) indicated that the water column was stratified, driven

by temperature differences with depth. However, density profiles differed between closely located stations, indicating that the system has high spatial variability. Additionally, there was substantial temporal variability, as indicated by the different density profiles measured at stations S3 and S5, which were at the same location but sampled four days apart. This temporal difference was also reflected in the oxygen profiles at S3 and S5 (Figure 1b) with surface oxygen concentrations differing by up to 110 µmol L^{-1}. Overall, the surface waters were undersaturated with oxygen at all stations except S4 and S6, where undersaturation occurred within the upper 7 metres. Despite overall oxygen undersaturation, at S2 and S6 there was indication of oxygen formation within the upper 10 metres, reflected by a peak in oxygen concentration. With increasing depth, a sharp oxycline was detected at all stations with oxygen concentrations reaching 20 µmol L^{-1} within the upper 10 - 14 metres at stations S1 - S5. At S6, two oxyclines were observed, a sharp shallow one reaching oxygen concentrations of 50 µmol L^{-1} within the first 15 metres before a second gradual decrease with oxygen falling below 20 µmol L^{-1} at 27 metres. The water column below the oxycline, here referred to as the core, exhibited oxygen intrusions (Supplementary Figure 2), suggesting that the bottom waters are not continuously anoxic.

Nitrate concentrations ranged between 0.49 - 31.4 µmol L^{-1} across the water column of each station with highest concentrations measured in the core of the OMZ. Nitrite concentrations reached up to 4 µmol L^{-1} and increased slightly towards the sediment at all stations except S5, where a nitrite maximum of 4 µmol L^{-1} was located between 13 and 18 metres depth. Ammonium concentrations resembled the nitrite distribution and generally increased towards the sediment, except at S2, highest concentrations (above 10 µmol L^{-1}) were found in the surface, before decreasing to below detection limit (30 nmol L^{-1}) within the core. Concentrations of particulate organic carbon (POC) and nitrogen (PON) were reflective of the highly eutrophied water column (Figure 2a). POC and PON concentrations were usually highest (up to 145 µmol L^{-1} and 21 µmol L^{-1} for POC and PON respectively) at 5 metres before declining within the core and increasing slightly above the sediment. However, at S5 the highest concentrations were at, and just below the oxycline. Mean POC to PON ratios were 7.06 ± 0.95 which is slightly above Redfield (Redfield 1958). The particulate organic matter concentrations followed the volumetric distribution of organic particles (Figure 2a). N_2O concentrations were highly variable (Supplementary Figure S3), ranging from undersaturated to 2645 nmol L^{-1} above saturation. ΔN_2O plotted again the apparent oxygen utilisation (Figure 2b) reveals that N_2O was found at both high and low oxygen concentrations.

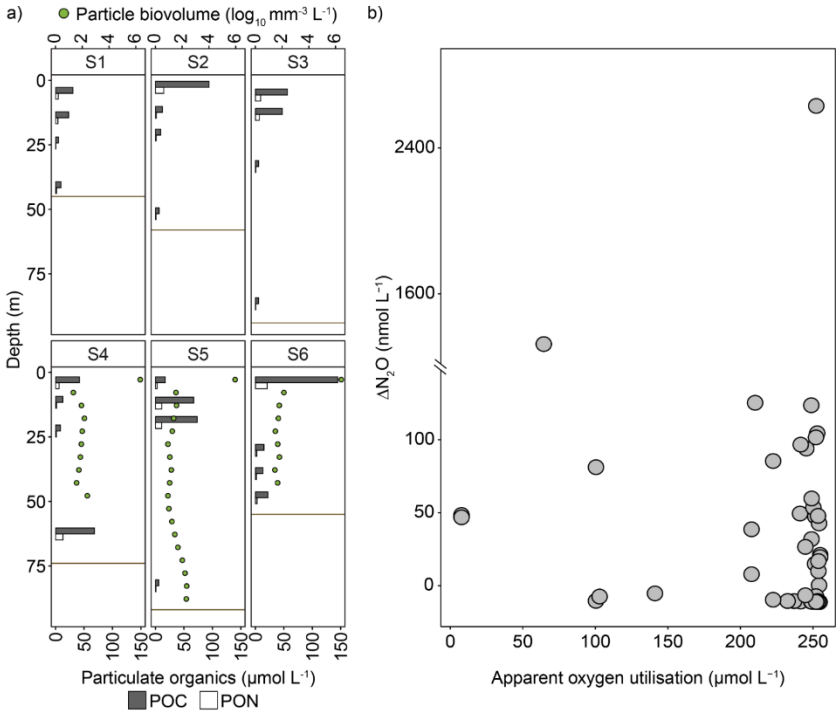

Figure 2. **Organic matter and nitrous oxide concentrations in the coastal Peruvian oxygen minimum zone. a,** Particulate organic -carbon and -nitrogen concentrations from the three incubation depths, as well as an additional surface depth. At stations S4 - S6 particle biovolume is also shown, taken with an underwater vision profiler. Brown line indicates the sediment interface. **b,** ΔN_2O concentrations plotted against the apparent oxygen utilisation from all stations and depths, with duplicates plotted separately. Concentration samples all originated from then pump CTD upcast. For resolved depth profiles see supplementary Figure S3.

Rate measurements from stable isotope incubation experiments

To determine the sources and sinks of N_2O, as well as N_2 formation processes, stable isotope incubation experiments with ^{15}N-labelled substrates were set up from three different depths (Figure

1b): five metres above the sediment, within the core of the OMZ and at the base of the oxycline (~5 µmol L^{-1} oxygen).

Nitrous oxide formation from ammonia oxidation

N_2O formation from aerobic ammonia oxidation was investigated in two parallel experiments: an oxygen-supplemented experiment, with a final oxygen concentration of 5 µmol L^{-1}, and an anoxic experiment (Table 1). In all incubations ^{15}N-ammonium, as well as a ^{14}N-nitrite and a ^{14}N-N_2O pool was added. The oxygen-supplemented experiment was only conducted at the oxycline depth. In this experiment, N_2O formation was measurable at all six stations and depths with rates between 0.08 - 0.37 nmol N L^{-1} d^{-1} (Figure 3a; Supplementary Figure S4).

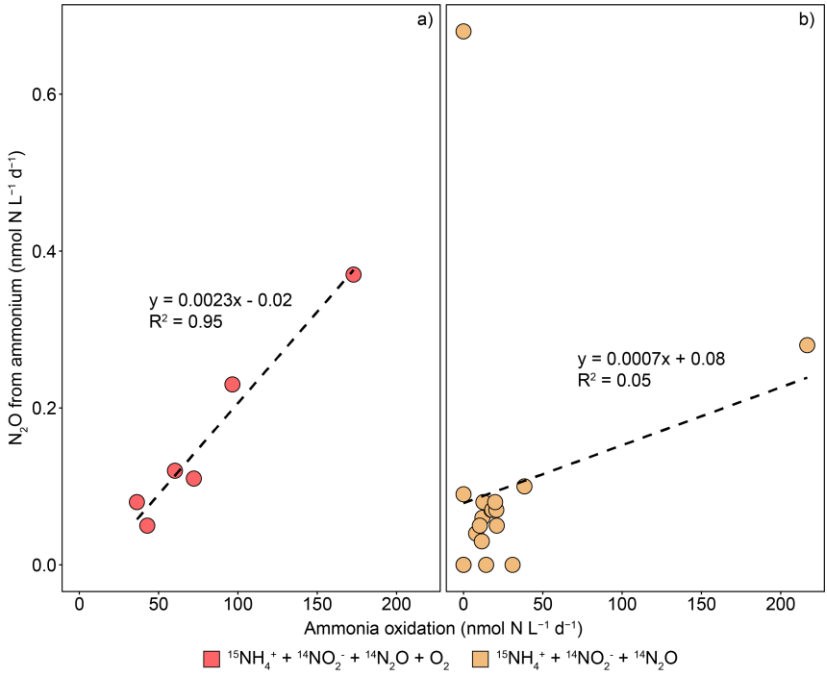

Figure 3. **Nitrous oxide formation as a factor of the ammonia oxidation rates to nitrite. a,** oxygen-supplemented incubation experiment, taken only from the oxycline depth. **b,** anoxic experiment taken from all incubation depths. Each point represents two individual statistically significant (One-sided student's t-test, $p < 0.05$) rates, calculated from the slope of all time points, plotted against each other. Insignificant rates are shown as zeroes.

The N_2O was measured predominantly as $^{45}N_2O$ but significant $^{46}N_2O$ production was observed at four stations. However, there was no clear pattern of $^{46}N_2O$ formation between the depths or stations. Rates of ammonia oxidation to nitrite were quantified from the same incubations and from all stations and depths, with significant rates between 36 - 173 nmol N L^{-1} d^{-1} (Figure 3a; Supplementary Figure S5). Overall, we found a linear correlation between N_2O formation and ammonia oxidation rates ($n = 6$, $R^2 = 0.95$), with the highest rates of both observed at S5 and a mean yield of N_2O from ammonia oxidation of 0.2 ± 0.05%. This suggests that in the oxygen-supplemented incubations the N_2O formation was proportional to the ammonia oxidation rates.

Under anoxic conditions, significant linear N_2O formation from ammonia was quantifiable in 14 out of 18 samples with rates between 0.03 - 0.68 nmol N L^{-1} d^{-1} (Figure 3b; Supplementary Figure S4). N_2O formation was also detected at the oxycline of S2, S3 and S5, as well as the core depth of S6, however we were unable to calculate a rate in these incubations. In all of the oxycline depths an initial N_2O formation was observed (up to 0.7 nmol N L^{-1}) but this N_2O was subsequently consumed in later time points (Supplementary Figure S6). In all but three of the 18 incubations, N_2O formation was observed solely as $^{45}N_2O$. Rates of ammonia oxidation to nitrite were quantifiable from 14 out of 18 incubations with linear rates ranging between 8 - 217 nmol N L^{-1} d^{-1}. At S3 - S6, we observed non-linear rates within the oxycline, wherein there was an initial formation of nitrite followed by a consumption; similar to the N_2O formation (Supplementary Figure S6). The initial formation of both N_2O and nitrite in these incubations indicates that ammonia oxidation was likely occurring coupled to trace amounts of oxygen left over in the incubation bottles after degassing. However, due to the net consumption of both N_2O and nitrite in some incubations, we speculate nitrogen-consuming processes co-occurred, depleting the products of ammonia oxidation. Unlike in the oxygen-supplemented experiment, there was no clear linear correlation between the N_2O formation and the ammonia oxidation rates ($n = 18$, $R^2 = 0.05$; Figure 3b) and the mean yield of 0.32 ± 0.19% was higher.

Nitrous oxide formation from denitrification

To determine N_2O formation rates from denitrification, experiments were set up with either ^{15}N-nitrate or ^{15}N-nitrite (Table 1). The nitrite experiment was additionally amended with a ^{14}N-N_2O pool to trap any formed N_2O. In 13 out of 18 nitrite amended incubations linear N_2O formation rates were observed that ranged from 0.08 - 7.18 nmol N L^{-1} d^{-1} (Figure 4). The highest rates were found at the deepest depth of all stations, with the exception of S6 where they were found at the oxycline. At the base of the oxycline of stations S2 - S5 N_2O formation was observed, however we could not calculate a production rate as the formation was either exponential over time (S2 and S3) or the formed N_2O was reduced in the later time points (S4 and S5, including the core depth of S5; Supplementary Figure S6). However, N_2O formation at the oxycline was exceptionally high, reaching concentrations of up to 47 nmol N L^{-1}, suggesting a high potential for N_2O formation from denitrification at oxic-anoxic interface.

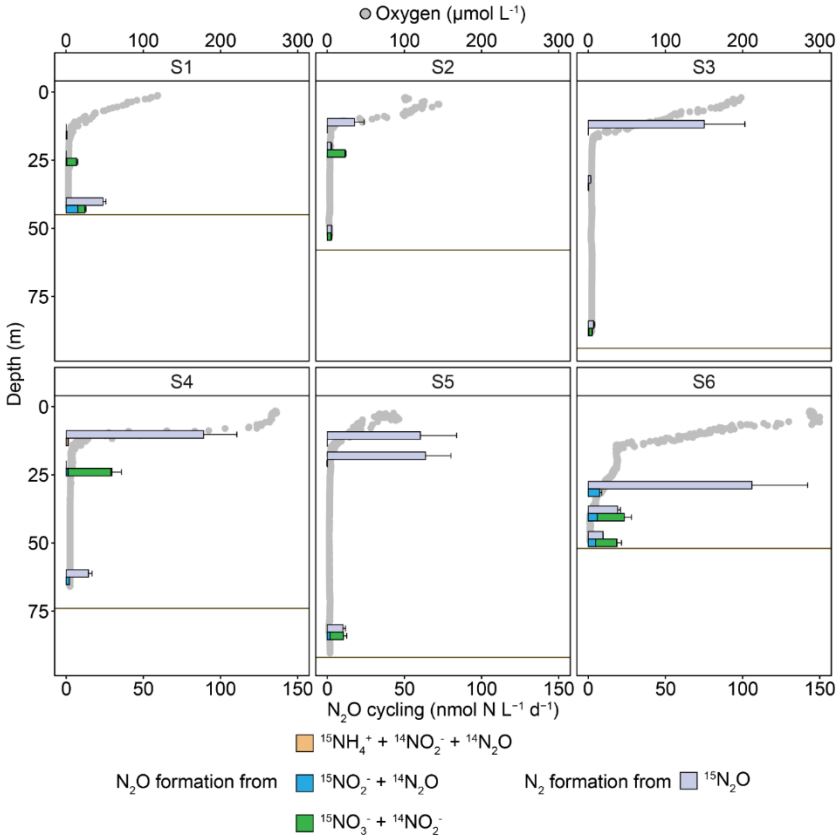

Figure 4. **Nitrous oxide (N_2O) cycling in the coastal Peruvian oxygen minimum zone.** Each bar represents a statistically significant (One-sided student's t-test, $p < 0.05$) rate calculated from the slope across the incubation time points, with error bars representing the standard error of the slopes. Data from all three incubation depths: oxycline, core and five metres above the sediment is shown. N_2O formation is depicted as the sum of the N_2O produced from the anoxic ammonium incubation experiment as well as from the two denitrification experiments with nitrate and nitrite. Specific N_2O consumption to N_2 is quantified from the ^{15}N-N_2O incubation experiment. Brown line indicates the sediment interface. Non-linear rates are depicted as zero and include exponential rates, insignificant rates, as well rates with net N_2O consumption.

Interestingly, in the ^{15}N-nitrite experiment, the production of $^{45}N_2O$ was in excess of what could be expected based on the initial labelled fraction of nitrite and binomial pairing (Song et al. 2016). We assessed possible sources of the excess $^{45}N_2O$, finding that it could not be accounted for by ammonium-derived $^{45}N_2O$, assuming comparable rates to the anoxic ammonia oxidation experiment. We also investigated whether a potential label dilution could account for $^{45}N_2O$ formation by quantifying the ^{15}N-nitrite in each time point. This revealed substantial (up to 1.3 µmol L^{-1}) reduction of the measured label at the oxycline of S4 and S5, coinciding with depths that had net N_2O and nitrite consumption. This suggests high rates of nitrite reduction as well as likely dilution of the labelled fraction, which could underestimate the rates from these depths. However, significant excess $^{45}N_2O$ formation was also observed in incubations where the labelled fraction did not change over time. As we were unable to accurately determine the unlabelled fraction within each time point we cannot completely exclude significant label dilution. Nevertheless, the excess $^{45}N_2O$ could suggest an alternative source of N_2O in these incubations, with substantial linear rates of up to 1.9 nmol N L^{-1} d^{-1} but without a clear depth distribution (Supplementary Figure S7).

In the nitrate experiment, linear rates of N_2O formation were quantifiable from nine out of 18 incubation depths, with rates between 2 - 28 nmol N L^{-1} d^{-1} (Figure 4). N_2O formation was mostly observed within the core and five metres above the sediment, and in two cases at the oxycline. However, this experiment lacked the ^{14}N-N_2O pool and in the remaining nine incubations we observed non-linear rates, due to net N_2O consumption (Supplementary Figure S6). Analysis of any excess $^{45}N_2O$ akin to the nitrite experiment also revealed significant excess $^{45}N_2O$ formation of up to 2.7 nmol N L^{-1} d^{-1} (Supplementary Figure S7). Therefore, excess $^{45}N_2O$ formation may also originate from nitrate in addition to nitrite. Importantly, due to the pool of unlabelled nitrite (5 µmol L^{-1}) that was added to the nitrate experiment, $^{45}N_2O$ likely originated directly from the nitrate and not through nitrate reduction to nitrite and subsequent coupling, unless conducted within the same cell. Although nitrate reduction rates to nitrite were high with rates between 45 - 6090 nmol L^{-1} d^{-1} (Supplementary Figure S8), significant excess formation was observed at low (45 nmol L^{-1} d^{-1}) and high (6041 nmol L^{-1} d^{-1}) rates and nitrate reduction rates to nitrite were not correlated to the excess $^{45}N_2O$ (Supplementary Figure S9).

Nitrous oxide reduction

To investigate the potential for N_2O reduction, an incubation experiment was set up with ^{15}N-N_2O (Table 1). Linear rates ranging between 1.58 - 106 nmol N L^{-1} d^{-1} were quantifiable from all but three depths, where substantial N_2O consumption was still observed but in an exponential manner (Figure 4). Interestingly, the highest rates were quantified from the oxycline and typically exceeded the sum of N_2O formed from denitrification and ammonia oxidation (excluding the excess $^{45}N_2O$). This suggests that under stable incubation conditions there was a higher potential for N_2O reduction than for formation, especially at the oxycline. Deeper in the water column, this relationship was more dynamic with either N_2O formation or consumption outpacing the other.

N_2 loss from denitrification and anammox

To determine rates of nitrogen loss, denitrification rates to N_2 were quantified simultaneously with the N_2O formation rates, from both the nitrite and nitrate addition experiments. Additionally, rates of anaerobic ammonia oxidation (anammox) were quantified from the anoxic ammonia oxidation experiment and the nitrite experiment. Linear rates of N_2 formation via denitrification from nitrite were quantifiable in eight out of 18 incubation depths, and ranged between 1 - 1106 nmol N L^{-1} d^{-1} (Figure 5).

The remaining incubation depths had either exponential rates (oxycline of S2, S3 and S6) or were insignificant. Similarly, linear rates of N_2 formation were quantified from the nitrate experiment in all incubation depths with rates of 4 - 449 nmol N L^{-1} d^{-1} (Figure 5). Overall, there was no distinct depth distribution but the highest rates were quantifiable from the oxycline of S4 and S5 as well as the core depth of S5, which were comparatively one or two orders of magnitude higher than the remaining rates.

Anammox rates from the anoxic ammonia experiment were quantifiable from all stations and depths and ranged from 0.7 - 205 nmol N L^{-1} d^{-1} with no discernible depth distribution (Figure 5). These rates were reproducible when calculating them using the excess $^{29}N_2$ from the nitrite experiment to quantify the anammox rates (Supplementary Figure S10), and there was a strong positive correlation between the two (Supplementary Figure S9). The exceptions to this were the rates from the oxycline of S4 and S5 as well as the core depth of S5, which had much higher calculated anammox rates from nitrite. However, this mismatch is likely driven by the observed

change in labelling percentage. Such comparable rates thus suggest no excess $^{29}N_2$ similar to $^{45}N_2O$. Overall, anammox rates generally outpaced nitrogen loss rates from denitrification, even when taking into account the N_2O formation, making it the dominant nitrogen sink in the coastal Peruvian oxygen minimum zone.

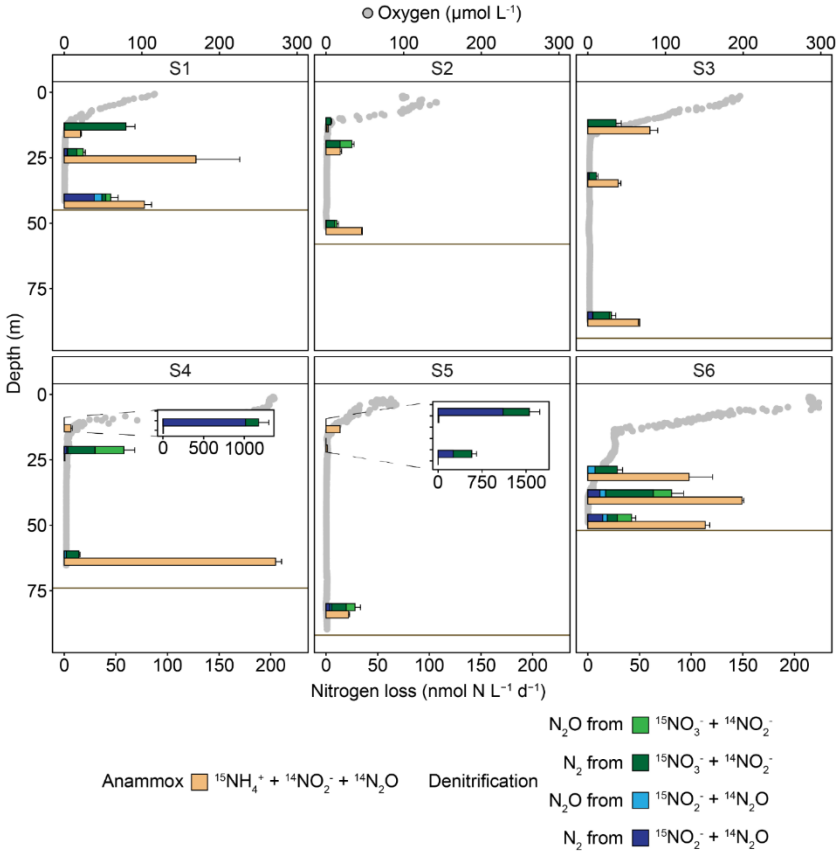

Figure 5. **Nitrogen loss in the coastal Peruvian oxygen minimum zone.** Each bar represents a statistically significant (One-sided student's t-test, $p < 0.05$) rate calculated from the slope across the incubation time points, with error bars representing the standard error of the slopes. Data from all three incubation depths: oxycline, core and five metres above the sediment is shown. Nitrogen loss from denitrification is depicted as the sum of N_2 and N_2O produced from the two denitrification experiments with nitrate and nitrite. Anammox rates were quantified from the anoxic ammonia oxidation experiment. Non-linear rates are depicted as zero and include exponential rates, insignificant rates, as well as rates with net N_2O consumption.

Discussion

The shallow coastal Peruvian oxygen minimum has highly variably N_2O concentrations

N_2O cycling in the shallow, eutrophied coastal waters off the coast of Peru in the Eastern Tropical South Pacific oxygen minimum zone (OMZ) remains understudied. In this study we aimed to understand the processes responsible for N_2O formation and consumption in the shallow (< 100 metres) oxygen-limited water column close to the Peruvian coast. We observed a eutrophied water column with highly variable N_2O concentrations ranging from below saturation up to 2600 nmol L^{-1} (Supplementary Figure S3). This supports the previously observed trend of increasing variability and accumulation of N_2O concentration from the offshore OMZ towards the coastal one (80 nmol L^{-1} - 986 nmol L^{-1}; Arévalo-Martínez et al. 2015; Kock et al. 2016).

Denitrification is the dominant source of N_2O

We could show that both denitrification and ammonia oxidation were potential sources of N_2O in the coastal Peruvian OMZ. However, our incubations revealed that N_2O formation from denitrification was up to two orders of magnitude higher than from aerobic ammonia oxidation (up to 29 nmol N L^{-1} d^{-1} and 0.68 nmol N L^{-1} d^{-1}, respectively). Our N_2O formation rates from denitrification are comparable, albeit on the higher end of those measured previously in deeper waters of the Peruvian OMZ, strongly indicating that denitrification is the dominant N_2O source throughout this region (Dalsgaard et al. 2012, 2014; Frey et al. 2020; Ji et al. 2015). Intriguingly, we found that incubations carried out with either nitrite or nitrate yielded different N_2O production rates. The rates from the nitrate incubation experiment exceeded those from the nitrite experiment (Figure 4), despite the addition of a ^{14}N-N_2O pool in the nitrite treatment which should have "trapped" ^{15}N-N_2O as it formed, allowing it to accumulate (a pool which was absent from the nitrate experiment). Similar results have been observed before (Frey et al. 2020; Ji et al. 2015, 2018). It has been suggested that this may be due to the microbial community being more adapted to the use of nitrate, as it is more prevalent *in-situ* (Ji et al. 2015, 2018). The same could have been the case in our study, as nitrate concentrations were usually an order of magnitude above those of nitrite. Furthermore, we found that N_2O formed in the nitrate incubations did not appear to mix with the *in-situ* nitrite pool, this "nitrite shunting" (De Brabandere et al. 2014) suggests that N_2O was produced by microorganisms adapted to reduce nitrate internally to N_2O.

Ammonia oxidation is a pervasive but minor source of N_2O

Rates of N_2O formation by ammonia oxidation were low in comparison to those from denitrification, but were more consistent, occurring throughout the OMZ at mean rates of 0.16 ± 0.12 and 0.10 ± 0.16 nmol N L^{-1} d^{-1} for the oxygen-supplemented and anoxic experiments respectively. These rates are comparable to previous measurements from the Peruvian OMZ (which ranged from 0.02 - 0.16 nmol N L^{-1} d^{-1}; (Frey et al. 2020; Ji et al. 2015), suggesting that although the contribution of ammonia oxidation to N_2O sources is low, it is consistent and pervasive.

Both ammonia oxidising -archaea (AOA) and -bacteria (AOB) have the capacity to form nitrous oxide (Santoro et al. 2011; Yoshida & Alexander 1970) and respond differently to variable oxygen concentrations. Culture studies with AOB have suggested that N_2O formation from nitrifier-denitrification is enhanced as oxygen concentrations decrease (Goreau et al. 1980; Kozlowski et al. 2014; Löscher et al. 2012), however in AOA the relationship with oxygen is less straightforward. Culture studies with AOA have shown contradictory results, with both increasing as well as decreasing rates of N_2O formation at low oxygen concentrations (Löscher et al. 2012; Qin et al. 2017; Stieglmeier et al. 2014). Previously, both AOA and AOB have been shown to be abundant in the Peruvian OMZ (Lam et al. 2009; Peng et al. 2013), however preliminary 16S rRNA analysis (Wu et al. in prep) has indicated that the ammonia oxidising community was dominated by AOA during the period our study was carried out. Furthermore, we were able to quantify aerobic ammonia oxidation rates in incubations, which were putatively anoxic (see below), supporting the presence of AOA, which have extremely high oxygen affinities (Bristow et al. 2016). Similar to previous observations (Frey et al. 2020), the N_2O formed in both experiments was predominately retrieved as single labelled $^{45}N_2O$, which is consistent with the hybrid formation pathway of the AOA (Kozlowski et al. 2016). This is further supported by the comparable rates of N_2O formation between the oxygen-supplemented and anoxic experiments (Supplementary Figure S4). Therefore, our data suggests that there is no clear relationship between the investigated oxygen concentrations and N_2O formation from ammonia oxidation but that N_2O production via ammonia oxidation has the potential to occur whenever traces of oxygen are present in the OMZ, likely facilitated by AOA.

N_2O formation was proportional to ammonia oxidation under oxygen-supplemented conditions

Aerobic ammonia oxidation rates to nitrite ranged between 36 - 172 nmol N L^{-1} d^{-1}, which is comparable to the previous rate measurements of 5 - 150 nmol N L^{-1} d^{-1} in the ETSP (Frey et al. 2020; Ji et al. 2015; Kalvelage et al. 2011, 2013; Lam et al. 2009; Lipschultz et al. 1990; Ward et al. 1989). Significant rates of 8 - 217 nmol N L^{-1} d^{-1} were also quantifiable from the anoxic ammonia experiment. However, despite the anoxic terminology, traces of oxygen (likely several hundred nmol L^{-1}) will have remained as degassing will likely only have reduced oxygen concentrations by 80% of *in-situ* concentrations (Holtappels et al. 2011) and thus were sufficient to account for the observed rates. While ammonia oxidation rates were broadly comparable to the oxygen-supplemented experiment, there were indications of a slight reduction in the anoxic incubations, as observed previously (Lam et al. 2007; Lipschultz et al. 1990). Interestingly, in the oxygen-supplemented experiment the N_2O formation was directly proportional to the ammonia oxidation rates strongly suggesting when oxygen was plentiful, most of the N_2O formed was directly related to ammonia oxidation. While the hybrid formation pathway of AOA is considered to be abiotic (Kozlowski et al. 2016), it still relies on the supply of the intermediates. Additionally, culture work suggests that the process may still be reliant on enzyme mediated steps, likely for the reduction of nitrite to nitric oxide (Wan et al. 2023). The mean proportion of N_2O formed from ammonia oxidation under oxic conditions was 0.2 ± 0.05% which is comparable to environmental yields previously observed in the Peruvian OMZ (Frey et al. 2020; Ji et al. 2015, 2018). However, in the anoxic experiment there was no clear correlation between the N_2O formation and the ammonia oxidation rates, suggesting that potentially other mechanisms contributed to the formation of N_2O. This could be through additional side reactions, such as the conversion of hydroxylamine to N_2O by cytochrome p460 as observed in AOB (Caranto et al. 2016), or through abiotic breakdown of intermediates (Zhu-Barker et al. 2015).

Excess $^{45}N_2O$ from NOx could potentially be fungal denitrification

In addition to denitrification and ammonia oxidation, we found indications for an additional source of N_2O in the Peruvian OMZ. While in nitrite and nitrate addition experiments N_2O was primarily quantified as $^{46}N_2O$, we also observed formation of $^{45}N_2O$ in excess of what can be expected from isotope pairing during denitrification (Song et al. 2016). Due to the substantial nitrate reduction rates to nitrite (up to 6 µmol N L^{-1} d^{-1}) and the high *in-situ* concentrations of ^{14}N-nitrate, we cannot

completely exclude label dilution or re-combination of the labelled nitrite and newly formed unlabelled nitrite. Nevertheless, the excess $^{45}N_2O$ may represent an additional source of N_2O next to bacterial denitrification and ammonia oxidation. The labelled formation is consistent with fungal denitrification, which can combine one nitrogen atom from nitrite or nitrate with one from organic nitrogen (Shoun et al. 1992; Tanimoto et al. 1992). Fungal denitrification remains understudied in the marine environment but has been shown to contribute substantially to N_2O formation in both coastal sediments (Wankel et al. 2017) and OMZs (Peng & Valentine 2021). It is especially noteworthy as fungi lack the nitrous oxide reductase (Richards et al. 2012) and therefore are a net source of N_2O. While we cannot confirm fungal denitrification with rate measurements alone, they can be a feasible possibility in this system and future work should investigate this further.

Denitrification was also a sink for N_2O

Even though denitrification was the main source of N_2O in the OMZ, it is also the only significant known sink for this potent greenhouse gas. Overall, denitrification rates to N_2, from both the nitrite and nitrate experiments, were up to two orders of magnitude higher than to N_2O. Additionally, at several depths in both experiments, we were unable to quantify linear rates of N_2O formation due to the high rates of N_2 production within the same incubation. This affected the nitrate experiment more strongly, due to the absence of the N_2O pool. Considering the importance of nitrous oxide reduction in controlling N_2O emissions, we conducted experiments with ^{15}N-N_2O to gain further insights into the mechanism of this process.

We found that the potential for N_2O consumption exceeded the N_2O formation rates from all quantified sources, including formation rates measured in the presence of a ^{14}N-N_2O pool. Intriguingly, we found that the highest potential for N_2O consumption occurred at the oxycline, which contrasts with previous results which have suggested that nitrous oxide reduction mainly occurs in the anoxic core of the OMZ (Babbin et al. 2015). This may be because we removed the oxygen in the N_2O consumption incubations carried out at the oxycline and it may be that *in-situ* oxygen concentrations could inhibit N_2O consumption as it has been suggested that N_2O reductase is the most oxygen sensitive enzyme of the denitrification machinery (Morley et al. 2008). Nevertheless, our results show that there is very high potential for N_2O consumption at these depths, and that the enzymatic machinery required to conduct this process is functional

immediately upon oxygen removal. Given this high potential for N_2O reduction, the observed N_2O accumulation in the water column is most likely a result of a decoupling of formation and reduction processes. This could result from the dynamic conditions observed in our study area, with intense mixing and oxygen intrusions into the OMZ core (Supplementary Figure S2). Such conditions have been observed to lead to temporal N_2O accumulation in both the Arabian Sea (Naqvi et al. 2000) and Chile (Farías et al. 2015). The N_2O can then either be reduced once favourable conditions are resumed, or it can "escape" to the atmosphere.

Anammox was the consistent nitrogen loss process, but denitrification can potentially outpace

While denitrification was the dominant source and sink of N_2O in the coastal Peruvian OMZ, anammox seems to be primarily responsible for nitrogen loss to N_2. Median anammox rates of 32 (0.7 - 205) nmol N L^{-1} d^{-1} were comparable to previous rate measurements (Canfield et al. 2010; De Brabandere et al. 2014; Hamersley et al. 2007; Kalvelage et al. 2011, 2013; Karthäuser et al. 2021). The ecological success of anammox has been attributed to a broader tolerance to oxygen (up to 20 µmol L^{-1}; Kalvelage et al. 2011) compared to denitrification to N_2. This would enable the process to continue during potential oxygen intrusions into the core. Additionally, high rates of nitrate reduction to nitrite can sustain the nitrite requirement of the process (Kalvelage et al. 2013; Lam et al. 2009) and ammonium can originate from the sediment, surface water and remineralisation of organic matter, including particles, which were abundant (Karthäuser et al. 2021). However, denitrification rates, calculated as combined N_2 and N_2O formation from nitrite and nitrate, were also substantial with median rates of 28 (5 - 1555) nmol N L^{-1} d^{-1}, although rates above 100 nmol N L^{-1} d^{-1} were restricted to S4 and S5. These rates were up to three orders of magnitude higher than previous observation of denitrification in the region (Canfield et al. 2010; Dalsgaard et al. 2014; Kalvelage et al. 2013; Karthäuser et al. 2021; Thamdrup et al. 2006). However, many of these studies only investigated denitrification rates to N_2 using a single source, i.e. nitrite, and would thus have likely underestimated the overall contribution of denitrification to nitrogen loss. Intriguingly, the high rates of denitrification reported at S4 and S5 were not associated with a noticeable change in the quantified physico-chemical parameters. Previously, rates of this magnitude have been observed in the Peruvian OMZ during sulphidic events, when N_2 formation from denitrification reached rates of up to 2 µmol N L^{-1} d^{-1} (Callbeck et al. 2018; Schunck et al. 2013). Similarly, sulphide has been shown to stimulate not only N_2 formation but also N_2O formation and included observations of initial N_2O formation followed by consumption

(Canfield et al. 2010; Dalsgaard et al. 2014). As these events seem to be episodic they could lead to highly temporal, see difference between S3 and S5 but intense nitrogen loss from denitrification in the form of both N_2O and N_2 from the coastal Peruvian OMZ.

To conclude, we detected high N_2O concentrations in the water column of the shallow (< 100 metres) coastal Peruvian OMZ. Our rate measurements suggest that denitrification is the main source of this N_2O, while ammonia oxidation makes a more minor but consistent contribution. Furthermore, our data indicate that there may be an additional and overlooked source of this potent greenhouse gas in anoxic waters - putatively from fungi. Despite the observed accumulation of N_2O in the water column, the potential for N_2O consumption was higher than the sum of all formation processes, suggesting that the water column could be a net sink of N_2O under steady state conditions. However, this is likely prevented by the underlying dynamic mixing that results in continuous oxygen intrusions into the core of the shallow OMZ. Overall, the processes in the shallow coastal zone are similar to both the offshore and deeper coastal zone but more intense, suggesting that these shallow coastal environments can be critical for N_2O cycling.

Materials and Methods

Sample collection

Water samples were collected during day trips on the IMPARPE V in the Austral spring between 23rd March and 3rd of April 2019 from six stations in the coastal Peruvian oxygen minimum zone (OMZ; Figure 1a). At each station water samples were collected using a pump cast conductivity temperature depth (pCTD) system and hydrographical data was recorded with sensors for temperature and salinity (Seabird SBE49 FastCAT), fluorescence (Turner Designs Cyclops-7F), high- (Pyroscience FSO2-Subport) and low-resolution oxygen concentrations (aanderaa optode 4831). Samples were collected in two separate casts. On the downcast samples were taken at regular intervals throughout the entire water column (maximum water depth of 94m) for nutrient (ammonium, nitrogen oxides (NOx) and nitrite) concentration measurements. During a subsequent upcast three discrete depths were selected based on their physical properties: around 5 m above the sediment, within the core of the OMZ and at the oxycline for stable isotope incubation measurements. Additionally, samples from these and some additional intermediate depths were taken for nutrients, nitrous oxide and particulate organic -carbon (POC) and nitrogen (PON) concentration measurements. All samples were taken back to the laboratories at IMARPE on the same day for processing.

Water column Chemistry

Dissolved nutrients

Ammonium concentrations were determined from unfiltered samples using the orthophtaldialdehyde (OPA) method (Holmes et al. 1999) *in-situ*. The limit of detection (LOD), calculated from the mean of all blanks plus three times the standard deviation, was 30 nmol L^{-1}. Nutrient (NOx and nitrite) samples were sterile filtered *in-situ* through a 0.22 µm filter (Millipore) and frozen at -20°C until simultaneous measurements on a QuAtro39 autoanalyser (Seal Analytical) using standard methods (Strickland & Parsons 1972). LODs were 123 nmol L^{-1} (NOx) and 63 nmol L^{-1} (nitrite). Nitrate concentrations were calculated by subtracting the nitrite concentrations from the NOx.

Particulate organic carbon and nitrogen

Samples for POC and PON were collected by filtering 1 litre of water onto pre-combusted (4 hours at 450°C) glass fibre filters (GF/F, Whatman), dried at room temperature overnight and then frozen at -20°C until analysis. In addition to the incubation depths, samples were also collected from a surface depth, usually around 4 metres. For analysis, thawed samples were dried at 60°C before being decalcified using fuming hydrochloric acid (37% Merck) overnight, dried, then pelleted into tin cups. Samples were subsequently measured on an element analyser (CHNS/CNS analyser vario Micro cube, elementar).

Nitrous oxide concentrations

Duplicate samples for N_2O concentration measurements were filled headspace-free into 120 mL serum bottles using gas tight Viton tubing. Microbial activity was inhibited by adding copper(I)chloride (Merck) and the bottles were stoppered (Geo-Microbial Technologies) and crimped. Samples were analysed in Bremen using a gas concentrations analyser (Picarro G2308). ΔN_2O and apparent oxygen utilisation (AOU) numbers were calculated according to Kock et al. 2016). Briefly ΔN_2O was calculated by subtracting the equilibrium N_2O concentration (Weiss & Price 1980) from the measured N_2O concentrations. The AOU was calculated by subtracting the measured oxygen concentration (low resolution) from the equilibrium concentration (Weiss 1970).

Particle abundance

Particle abundance and biovolume were determined at stations S4 - S6 using an Underwater Vision Profiler (UVP5, Picheral et al. 2010). Images of particles were taken three times per second, resolving particles sized between 128 - 4096 µm.

Stable isotope incubations and rate calculations

Experimental set up and rate determination

For each incubation depth, ^{15}N stable isotope incubation experiments were set up to investigate potential rates of N_2O formation and consumption, as well as associated processes i.e. ammonia oxidation, denitrification, nitrate reduction and anammox (Table 1). Briefly, acid washed 250 mL serum bottles were filled from the pCTD using Viton tubing and overflown three times to reduce

oxygen contamination before being stoppered with degassed (Helium, Air Liquide), 20 mm butyl rubber stoppers (Supelco) and crimped. Samples were then transported back to the laboratory in the dark. In the laboratory, samples were bubbled with helium for 20 minutes to further reduce any oxygen background and subsequently tracers were added (Table 1). After tracer addition, samples were mixed for five minutes with a magnetic stirrer before being aliquoted into 12 mL gas-tight glass vials (exetainers; Labco UK). The exetainers were then incubated in the dark close to *in-situ* temperatures (ca. 14°C) for 24 hours. At five time points within the first 24 hours biological activity was terminated in an exetainer via the addition of 100 µL of mercury (II) chloride ($HgCl_2$, 7 g/100ml).

Table 1. **Overview of stable isotope incubation experiments.** Tracer additions were 5 µmol L^{-1} for ^{15}N-ammonium, ^{15}N-nitrite and ^{14}N-nitrite; 20 µmol L^{-1} for ^{15}N-nitrate; 200 nmol L^{-1} for ^{15}N-nitrous oxide and ^{14}N-nitrous oxide; 240 µmol L^{-1} for ^{13}C-dissolved inorganic carbon and 5 µmol L^{-1} oxygen.

Experiment	Added tracers
Oxygen-supplemented ammonia oxidation	^{15}N-NH_4^+, ^{14}N-NO_2^-, ^{14}N-N_2O, ^{13}C-DIC, O_2
Anoxic ammonia oxidation	^{15}N-NH_4^+, ^{14}N-NO_2^-, ^{14}N-N_2O, ^{13}C-DIC
Denitrification from nitrite	^{15}N-NO_2^-, ^{14}N-N_2O, ^{13}C-DIC
Denitrification from nitrate	^{15}N-NO_3^-, ^{14}N-NO_2^-, ^{13}C-DIC
Nitrous oxide reduction	^{15}N-N_2O, ^{13}C-DIC

Upon return to the laboratory in Bremen, Germany, the isotopic composition of both N_2O and N_2 was determined simultaneously in each exetainer after setting a 5.5 mL helium headspace. Isotope ratio mass spectrometry ($^{14}N^{14}N$, $^{14}N^{15}N$ and $^{15}N^{15}N$) was carried out using a GC-IRMS (customised TraceGas coupled to a multicollector IsoPrime100, Manchester, UK). The concentrations of $^{45}N_2O$, $^{46}N_2O$ were calculated from the excess of each relative to a standard N_2O sample and for $^{29}N_2$ and $^{30}N_2$ from the excess relative to air (Holtappels et al. 2011). Rates were calculated from a significant one-sided student's t-test ($p < 0.05$) applied to a linear regression over all five time points, with exceptions noted below.

Ammonium incubations

To investigate N_2O formation from ammonia oxidation two separate experiments were set up: an oxygen-supplemented ammonia oxidation experiment, which was carried out only on waters from the oxycline depth with *in-situ* oxygen concentrations and an anoxic incubation from all three incubation depths (Table 1). Both unlabelled nitrite and N_2O were added to reduce the subsequent oxidation of the formed nitrite to nitrate or any reduction of either the formed nitrite or N_2O, allowing us to quantify rates of both ^{15}N-nitrite and ^{15}N-N_2O formation. Rates of N_2O formation were calculated using a modified version of Ji et al. (2015) (Eq. 1)

N_2O (from ammonium in nmol N L^{-1} d^{-1}) = $^{45}N_2O/f + 2 * {}^{46}N_2O/f$ (Eq. 1)

Where the $^{45}N_2O$ and $^{46}N_2O$ are the significant rates of single and double labelled N_2O formed in nmol L^{-1} d^{-1}. The f is the fraction of labelled ^{15}N-ammonium at the beginning of the incubation. This was determined by quantifying the added ^{15}N-ammonium from time point zero using the hypobromite conversion method of (Waremburg 1993). The labelled fraction was then calculated using the *in-situ* nutrient concentrations.

Simultaneously with the N_2O measurements, N_2 was also quantified to determine rates of anaerobic ammonia oxidation (anammox) according to Eq 2, which was slightly modified from Thamdrup et al. (2006).

Anammox (from ammonium in nmol N L^{-1} d^{-1}) = $^{29}N_2/f * 2$ (Eq. 2)

Where $^{29}N_2$ is the significant rate of formation and the f is the same as in Eq 1. After the N_2O and N_2 determination, rates of ammonia oxidation to nitrite were quantified from the same exetainer using the sulphamic acid conversion of nitrite to N_2 (Granger & Sigman 2009).

Ammonia oxidation rates were calculated as in Eq 3.

Ammonia oxidation to nitrite (nmol N L^{-1} d^{-1}) = $^{29}N_2/f$ (Eq. 3)

Where $^{29}N_2$ is the significant rate of production and f is the same as Eq 1. The percentage yield of N_2O from ammonia oxidation was calculated according to Eq 4.

Yield of N_2O from ammonia oxidation = (N_2O (ammonium) / ammonia oxidation to nitrite) * 100 (Eq. 4)

For the anoxic ammonia oxidation experiment only the first four time points (12h) were used for all calculations as there was a stagnation observed in the last time point of the ammonia oxidation rate (Supplementary Figure S6). This is likely due to the oxygen completely running out in this incubation exetainer, thus the changing conditions make comparisons difficult.

Nitrate, nitrite and nitrous oxide incubations

N_2O formation from denitrification was determined from both the precursors nitrate and nitrite (Table 1). In both experiments N_2O and N_2 formation were quantified simultaneously and denitrification rates were calculated according to Eqs 5 and 6 which were slightly modified from (Thamdrup & Dalsgaard 2002).

N_2O (denitrification in nmol N L^{-1} d^{-1}) = $^{46}N_2O/f^2$ *2 (Eq. 5)

N_2 (denitrification nmol N L^{-1} d^{-1}) = $^{30}N_2/f^2$ * 2 (Eq. 6)

Where $^{46}N_2O$ and $^{30}N_2$ are the significant linear rates. F is the fraction of ^{15}N-nitrite or ^{15}N-nitrate at the beginning of the incubation. The ^{15}N-nitrite was quantified by sulphamic acid (Granger & Sigman 2009) and calculated using the *in-situ* nutrient concentrations. The nitrate f was calculated from the added ^{15}N-nitrate (20 µmol L^{-1}) and the *in-situ* nutrient concentrations. To investigate whether all the measured N_2O could be accounted for by either denitrification or ammonia oxidation the excess $^{45}N_2O$ was calculated according to Eq 7.

$^{45}N_2O$ (excess nmol N L^{-1} d^{-1}) = $^{45}N_2O$ (measured) - $^{46}N_2O/f^2$ * f* - $^{45}N_2O$ (anoxic ammonia oxidation) (Eq. 7)

Where the f* is -2*(f*f) + 2*f and accounts for the expected single labelled N_2O formed from denitrification based on the isotope pairing at the measured labelling percentage. Additionally, the measured $^{45}N_2O$ from the anoxic ammonium experiment is subtracted as single labelled N_2O formed during ammonia oxidation can be combined from one nitrogen from nitrite and another from the ammonium (Kozlowski et al. 2016; Stieglmeier et al. 2014). Such a reaction could therefore enhance the $^{45}N_2O$ formed during the ^{15}N-nitrite and nitrate experiments.

Anammox rates were also determined from the nitrite incubations by calculating rates using the excess $^{29}N_2$ according to Eq 8.

Anammox from nitrite (nmol N L^{-1} d^{-1}) = (($^{29}N_2$ - ($^{30}N_2/f^2$ * f*))/f)*2 (Eq. 8)

Where $^{30}N_2/f^2$ * f* calculated the expected $^{29}N_2$ formation from denitrification based on isotope pairing and f* is the same as in Eq 7.

Nitrate reduction rates to nitrite were calculated according to Eq 3 after conducting a sulphamic acid conversion on these samples. N_2O reduction rates to N_2 were calculated according to Eq 6, assuming 100% labelling of the N_2O due to the degassing of the water. This likely underestimates the potential N_2O consumption rates. To investigate correlating parameters with N_2O cycling, Spearman Ranked correlation analysis was performed in RStudio using all available parameters.

Figure generation

The map was generated using the quantum geographic information system (QGIS; version 3.32.0). Rate analysis was conducted in Microsoft Excel (2016) and figures were generated in RStudio 2023.3.0.386 version 4.1.3 (R Core Team) using the ggplot package (Wickham 2016).

Acknowledgments

We would like to thank the captain and crew of the IMARPE V for all their assistance during the expedition; M. Knutzen, G. Klockgether, S. Lilienthal, K. Imhoff, S. Piosek, N. Rujanski and D. Tienken for the technical support; H. Marchant, C. Frey, F. M. Jalaluddin, A. S. McDermott, W. Mohr, D. Speth for their helpful discussions and comments; the funding of this study by the Max Planck Society. This work was supported by the Max Planck Society and the Instituto del Mar del Perú.

Bibliography

Arévalo-Martínez DL, Kock A, Löscher CR, Schmitz RA, Bange HW. 2015. Massive nitrous oxide emissions from the tropical South Pacific Ocean. *Nat. Geosci.* 8(7):530–33

Babbin AR, Bianchi D, Jayakumar A, Ward BB. 2015. Rapid nitrous oxide cycling in the suboxic ocean. *Science (80-.).* 348(6239):1127–29

Bourbonnais A, Letscher RT, Bange HW, Échevin V, Larkum J, et al. 2017. N2O production and consumption from stable isotopic and concentration data in the Peruvian coastal upwelling system. *Global Biogeochem. Cycles*. 31(4):678–98

Bristow LA, Dalsgaard T, Tiano L, Mills DB, Bertagnolli AD, et al. 2016. Ammonium and nitrite oxidation at nanomolar oxygen concentrations in oxygen minimum zone waters. *Proc. Natl. Acad. Sci. U. S. A.* 113(38):10601–6

Callbeck CM, Lavik G, Ferdelman TG, Fuchs B, Gruber-Vodicka HR, et al. 2018. Oxygen minimum zone cryptic sulfur cycling sustained by offshore transport of key sulfur oxidizing bacteria. *Nat. Commun.* 9(1):1–11

Canfield DE, Stewart FJ, Thamdrup B, De Brabandere L, Dalsgaard T, et al. 2010. A cryptic sulfur cycle in oxygen-minimum-zone waters off the Chilean coast. *Science (80-.).* 330(6009):1375–78

Caranto JD, Vilbert AC, Lancaster KM. 2016. Nitrosomonas europaea cytochrome P460 is a direct link between nitrification and nitrous oxide emission . *Proc. Natl. Acad. Sci.* 113(51):14704–9

Chavez FP, Messié M. 2009. A comparison of Eastern Boundary Upwelling Ecosystems. *Prog. Oceanogr.* 83(1–4):80–96

Codispoti LA. 2010. Interesting times for marine N2O. *Science (80-.).* 327(5971):1339–40

Dalsgaard T, Stewart FJ, Thamdrup B, De Brabandere L, Revsbech NP, et al. 2014. Oxygen at nanomolar levels reversibly suppresses process rates and gene expression in anammox and denitrification in the oxygen minimum zone off Northern Chile. *MBio*. 5(6):1–14

Dalsgaard T, Thamdrup B, Farías L, Revsbech NP. 2012. Anammox and denitrification in the oxygen minimum zone of the eastern South Pacific. *Limnol. Oceanogr.* 57(5):1331–46

De Brabandere L, Canfield DE, Dalsgaard T, Friederich GE, Revsbech NP, et al. 2014. Vertical partitioning of nitrogen-loss processes across the oxic-anoxic interface of an oceanic oxygen minimum zone. *Environ. Microbiol.* 16(10):3041–54

Farías L, Besoain V, García-Loyola S. 2015. Presence of nitrous oxide hotspots in the coastal upwelling area off central Chile: An analysis of temporal variability based on ten years of a biogeochemical time series. *Environ. Res. Lett.* 10(4):

Francis CA, Roberts KJ, Beman JM, Santoro AE, Oakley BB. 2005. Ubiquity and diversity of ammonia-oxidizing archaea in water columns and sediments of the ocean. *Proc. Natl. Acad. Sci.* 102(41):14683–88

Frey C, Bange HW, Achterberg EP, Jayakumar A, Löscher CR, et al. 2020. Regulation of nitrous oxide production in low-oxygen waters off the coast of Peru. *Biogeosciences*. 17(8):2263–87

Fuenzalida R, Schneider W, Garcés-Vargas J, Bravo L, Lange C. 2009. Vertical and horizontal extension of the oxygen minimum zone in the eastern South Pacific Ocean. *Deep. Res. Part II Top. Stud. Oceanogr.* 56(16):992–1003

Garrido-Amador P, Kniaziuk M, Vekeman B, Kartal B. 2021. Learning from microorganisms: using new insights in microbial physiology for sustainable nitrogen management. *Curr. Opin. Biotechnol.* 67:42–48

Goreau TJ, Kaplan WA, Wofsy SC, McElroy MB, Valois FW, Watson SW. 1980. Production of NO2- and N2O by Nitrifying Bacteria at Reduced Concentrations of Oxygen. *Appl. Environ. Microbiol.* 40(3):526–32

Graf DRH, Jones CM, Hallin S. 2014. Intergenomic comparisons highlight modularity of the denitrification pathway and underpin the importance of community structure for N2O emissions. *PLoS One*. 9(12):1–20

Granger J, Sigman DM. 2009. Removal of nitrite with sulfamic acid for nitrate N and O isotope analysis with the denitrifier method. *Rapid Commun. Mass Spectrom.* 23(23):3753–62

Hamersley MR, Lavik G, Woebken D, Rattray JE, Lam P, et al. 2007. Anaerobic ammonium oxidation in the Peruvian oxygen minimum zone. *Limnol. Oceanogr.* 52(3):923–33

Holmes RM, Aminot A, Kérouel R, Hooker BA, Peterson BJ. 1999. A simple and precise method for measuring ammonium in marine and freshwater ecosystems. *Can. J. Fish. Aquat. Sci.* 56(10):1801–8

Holtappels M, Lavik G, Jensen MM, Kuypers MMM. 2011. 15N-Labeling Experiments to Dissect the Contributions of Heterotrophic Denitrification and Anammox to Nitrogen Removal in the OMZ Waters of the Ocean. In *Methods in Enzymology*, Vol. 486, pp. 223–51. Elsevier Inc. 1st ed.

Intergovernmental Panel on Climate Change. 2023. *Global Carbon and Other Biogeochemical Cycles and Feedbacks*

Ji Q, Babbin AR, Jayakumar A, Oleynik S, Ward BB. 2015. Nitrous oxide production by nitrification and denitrification in the Eastern Tropical South Pacific oxygen minimum zone. *Geophys. Res. Lett.* 42(24):10,755-10,764

Ji Q, Buitenhuis E, Suntharalingam P, Sarmiento JL, Ward BB. 2018. Global Nitrous Oxide Production Determined by Oxygen Sensitivity of Nitrification and Denitrification. *Global Biogeochem. Cycles*. 32(12):1790–1802

Jung MY, Gwak JH, Rohe L, Giesemann A, Kim JG, et al. 2019. Indications for enzymatic denitrification to N2O at low pH in an ammonia-oxidizing archaeon. *ISME J.* 13(10):2633–38

Kalvelage T, Jensen MM, Contreras S, Revsbech NP, Lam P, et al. 2011. Oxygen sensitivity of anammox and coupled N-cycle processes in oxygen minimum zones. *PLoS One*. 6(12):

Kalvelage T, Lavik G, Lam P, Contreras S, Arteaga L, et al. 2013. Nitrogen cycling driven by organic matter export in the South Pacific oxygen minimum zone. *Nat. Geosci.* 6(3):228–34

Karstensen J, Stramma L, Visbeck M. 2008. Oxygen minimum zones in the eastern tropical Atlantic and Pacific oceans. *Prog. Oceanogr.* 77(4):331–50

Karthäuser C, Ahmerkamp S, Marchant HK, Bristow LA, Hauss H, et al. 2021. Small sinking particles control anammox rates in the Peruvian oxygen minimum zone. *Nat. Commun.* 12(1):1–12

Kock A, Arevalo-Martinez DL, Loscher CR, Bange HW. 2016. Extreme N2O accumulation in the coastal oxygen minimum zone off Peru. *Biogeosciences*. 13(3):827–40

Kozlowski JA, Price J, Stein LY. 2014. Revision of N2O-producing pathways in the ammonia-oxidizing bacterium Nitrosomonas europaea ATCC 19718. *Appl. Environ. Microbiol.* 80(16):4930–35

Kozlowski JA, Stieglmeier M, Schleper C, Klotz MG, Stein LY. 2016. Pathways and key intermediates required for obligate aerobic ammonia-dependent chemolithotrophy in bacteria and Thaumarchaeota. *ISME J.* 10(8):1836–45

Kraft B, Jehmlich N, Larsen M, Bristow LA, Könneke M, et al. 2022. Oxygen and nitrogen production by an ammonia-oxidizing archaeon. *Science (80-.).* 375(6576):97–100

Kuypers MMM, Marchant HK, Kartal B. 2018. The microbial nitrogen-cycling network. *Nat. Rev. Microbiol.* 16(5):263–76

Lam P, Jensen MM, Lavik G, McGinnis DF, Müller B, et al. 2007. Linking crenarchaeal and bacterial nitrification to anammox in the Black Sea. *Proc. Natl. Acad. Sci. U. S. A.* 104(17):7104–9

Lam P, Kuypers MMM. 2011. Microbial nitrogen cycling processes in oxygen minimum zones. *Ann. Rev. Mar. Sci.* 3:317–45

Lam P, Lavik G, Jensen MM, van de Vossenberg J, Schmid M, et al. 2009. Revising the nitrogen cycle in the Peruvian oxygen minimum zone. *Proc. Natl. Acad. Sci.* 106(12):4752–57

Lancaster KM, Caranto JD, Majer SH, Smith MA. 2018. Alternative Bioenergy: Updates to and Challenges in Nitrification Metalloenzymology. *Joule*. 2(3):421–41

Lavik G, Stührmann T, Brüchert V, Van Der Plas A, Mohrholz V, et al. 2009. Detoxification of sulphidic African shelf waters by blooming chemolithotrophs. *Nature*. 457(7229):581–84

Lipschultz F, Wofsy SC, Ward BB, Codispoti LA, Friedrich G, Elkins JW. 1990. Bacterial transformations of inorganic nitrogen in the oxygen-deficient waters of the Eastern Tropical South Pacific Ocean. *Deep Sea Res. Part A, Oceanogr. Res. Pap.* 37(10):1513–41

Löscher CR, Kock A, Könneke M, Laroche J, Bange HW, Schmitz RA. 2012. Production of oceanic nitrous oxide by ammonia-oxidizing archaea. *Biogeosciences*. 9(7):2419–29

Lycus P, Bøthun KL, Bergaust L, Shapleigh JP, Bakken LR, Frostegård Å. 2017. Phenotypic and genotypic richness of denitrifiers revealed by a novel isolation strategy. *ISME J.* 11(10):2219–32

Marchant HK, Tegetmeyer HE, Ahmerkamp S, Holtappels M, Lavik G, et al. 2018. Metabolic specialization of denitrifiers in permeable sediments controls N2O emissions. *Environ. Microbiol.* 20(12):4486–4502

McCoy D, Damien P, Clements D, Yang S, Bianchi D. 2023. Pathways of Nitrous Oxide Production in the Eastern Tropical South Pacific Oxygen Minimum Zone. *Global Biogeochem. Cycles*. 37(7):

Messié M, Ledesma J, Kolber DD, Michisaki RP, Foley DG, Chavez FP. 2009. Potential new production estimates in four eastern boundary upwelling ecosystems. *Prog. Oceanogr.* 83(1–4):151–58

Morley N, Baggs EM, Dörsch P, Bakken L. 2008. Production of NO, N2O and N2 by extracted soil bacteria, regulation by NO2- and O2 concentrations. *FEMS Microbiol. Ecol.* 65(1):102–12

Naqvi SWA, Jayakumar DA, Narvekar P V, Naik H, Sarma VVSS, et al. 2000. Increased marine production of N2O due to intensifying anoxia on the Indian continental shelf. *Nature*. 408(6810):346–49

Oswald K, Graf JS, Littmann S, Tienken D, Brand A, et al. 2017. Crenothrix are major methane consumers in stratified lakes. *ISME J.* 11(9):2124–40

Pauly D, Christensen V. 1995. Primary production required to sustain global fisheries. *Nature*. 374(6519):255–57

Peng X, Jayakumar A, Ward BB. 2013. Community composition of ammonia-oxidizing archaea from surface and anoxic depths of oceanic oxygen minimum zones. *Front. Microbiol.* 4(JUL):1–12

Peng X, Valentine DL. 2021. Diversity and n2o production potential of fungi in an oceanic oxygen minimum zone. *J. Fungi*. 7(3):

Picheral M, Guidi L, Stemmann L, Karl DM, Iddaoud G, Gorsky G. 2010. The Underwater Vision Profiler 5: An advanced instrument for high spatial resolution studies of particle size spectra and zooplankton. *Limnol. Oceanogr. Methods*. 8(9):462–73

Portmann RW, Daniel JS, Ravishankara AR. 2012. Stratospheric ozone depletion due to nitrous oxide: Influences of other gases. *Philos. Trans. R. Soc. B Biol. Sci.* 367(1593):1256–64

Purkhold U, Pommerening-Röser A, Juretschko S, Schmid MC, Koops H-P, Wagner M. 2000. Phylogeny of All Recognized Species of Ammonia Oxidizers Based on Comparative 16S rRNA and amoA Sequence Analysis: Implications for Molecular Diversity Surveys. *Appl. Environ. Microbiol.* 66(12):5368–82

Qin W, Meinhardt KA, Moffett JW, Devol AH, Virginia Armbrust E, et al. 2017. Influence of oxygen availability on the activities of ammonia-oxidizing archaea. *Environ. Microbiol. Rep.* 9(3):250–56

Ravishankara AR, Daniel JS, Portmann RW. 2009. Nitrous oxide (N2O): The dominant ozone-depleting substance emitted in the 21st century. *Science (80-.).* 326(5949):123–25

Redfield AC. 1958. The Biological Control of Chemical Factors in the Environment. *Am. Sci.* 46(3):205–21

Richards TA, Jones MDM, Leonard G, Bass D. 2012. Marine fungi: Their ecology and molecular diversity. *Ann. Rev. Mar. Sci.* 4:495–522

Santoro AE, Buchwald C, McIlvin MR, Casciotti KL. 2011. Isotopic Signature of N2O Produced by Marine Ammonia-Oxidizing Archaea. *Science (80-.).* 333(6047):1282–85

Schunck H, Lavik G, Desai DK, Großkopf T, Kalvelage T, et al. 2013. Giant Hydrogen Sulfide Plume in the Oxygen Minimum Zone off Peru Supports Chemolithoautotrophy. *PLoS One*. 8(8):

Shoun H, Kim DH, Uchiyama H, Sugiyama J. 1992. Denitrification by fungi. *FEMS Microbiol. Lett.* 94(3):277–81

Song GD, Liu SM, Kuypers MMM, Lavik G. 2016. Application of the isotope pairing technique in sediments where anammox, denitrification, and dissimilatory nitrate reduction to ammonium coexist. *Limnol. Oceanogr. Methods*. 14(12):801–15

Stieglmeier M, Mooshammer M, Kitzler B, Wanek W, Zechmeister-Boltenstern S, et al. 2014. Aerobic nitrous oxide production through N-nitrosating hybrid formation in ammonia-oxidizing archaea. *ISME J.* 8(5):1135–46

Strickland JDH & Parsons TR. 1972. *A Practical Handbook of Seawater Analysis*. Bulletin no. 167

Tanimoto T, Hatano K, Kim D, Uchiyama H, Shoun H. 1992. Co-denitrification by the denitrifying system of the fungus Fusarium oxysporum. *FEMS Microbiol. Lett.* 93(2):177–80

Thamdrup B, Dalsgaard T. 2002. Production of N2 through anaerobic ammonium oxidation coupled to nitrate reduction in marine sediments. *Appl. Environ. Microbiol.* 68(3):1312–18

Thamdrup B, Dalsgaard T, Jensen MM, Ulloa O, Farías L, Escribano R. 2006. Anaerobic ammonium oxidation in the oxygen-deficient waters off northern Chile. *Limnol. Oceanogr.* 51(5):2145–56

Thamdrup B, Dalsgaard T, Revsbech NP. 2012. Widespread functional anoxia in the oxygen minimum zone of the Eastern South Pacific. *Deep. Res. Part I Oceanogr. Res. Pap.* 65:36–45

Tian H, Xu R, Canadell JG, Thompson RL, Winiwarter W, et al. 2020. A comprehensive quantification of global nitrous oxide sources and sinks. *Nature*. 586(7828):248–56

Wan XS, Hou L, Kao S-J, Zhang Y, Sheng H-X, et al. 2023. Pathways of N2O production by marine ammonia-oxidizing archaea determined from dual-isotope labeling. *Proc. Natl. Acad. Sci.* 120(11):2017

Wankel SD, Ziebis W, Buchwald C, Charoenpong C, De Beer Di, et al. 2017. Evidence for fungal and chemodenitrification based N2O flux from nitrogen impacted coastal sediments. *Nat. Commun.* 8:1–11

Ward BB, Glover HE, Lipschultz F. 1989. Chemoautotrophic activity and nitrification in the oxygen minimum zone off Peru. *Deep Sea Res. Part A, Oceanogr. Res. Pap.* 36(7):1031–51

Weiss RF. 1970. The solubility of nitrogen, oxygen and argon in water and seawater. *Deep. Res. Oceanogr. Abstr.* 17(4):721–35

Weiss RF, Price BA. 1980. Nitrous oxide solubility in water and seawater. *Mar. Chem.* 8(4):347–59

Wickham H. 2016. *Ggplot2: Elegant Graphics for Data Analysis*. Springer-Verlag New York

Wrage-Mönnig N, Horn MA, Well R, Müller C, Velthof G, Oenema O. 2018. The role of nitrifier denitrification in the production of nitrous oxide revisited. *Soil Biol. Biochem.* 123:A3–16

Wuchter C, Abbas B, Coolen MJL, Herfort L, Van Bleijswijk J, et al. 2006. Archaeal nitrification in the ocean. *Proc. Natl. Acad. Sci. U. S. A.* 103(33):12317–22

Yang S, Chang BX, Warner MJ, Weber TS, Bourbonnais AM, et al. 2020. Global reconstruction reduces the uncertainty of oceanic nitrous oxide emissions and reveals a vigorous seasonal cycle. *Proc. Natl. Acad. Sci. U. S. A.* 117(22):

Yoshida T, Alexander M. 1970. Nitrous Oxide Formation by Nitrosomonas Europaea and Heterotrophie Microorganisms. *Soil Sci. Soc. Am. J.* 34(6):880–82

Zhu-Barker X, Cavazos AR, Ostrom NE, Horwath WR, Glass JB. 2015. The importance of abiotic reactions for nitrous oxide production. *Biogeochemistry*. 126(3):251–67

Zumft WG. 1997. Cell biology and molecular basis of denitrification. *Microbiol. Mol. Biol. Rev.* 61(4):533–616

Supplement

Supplementary Figures

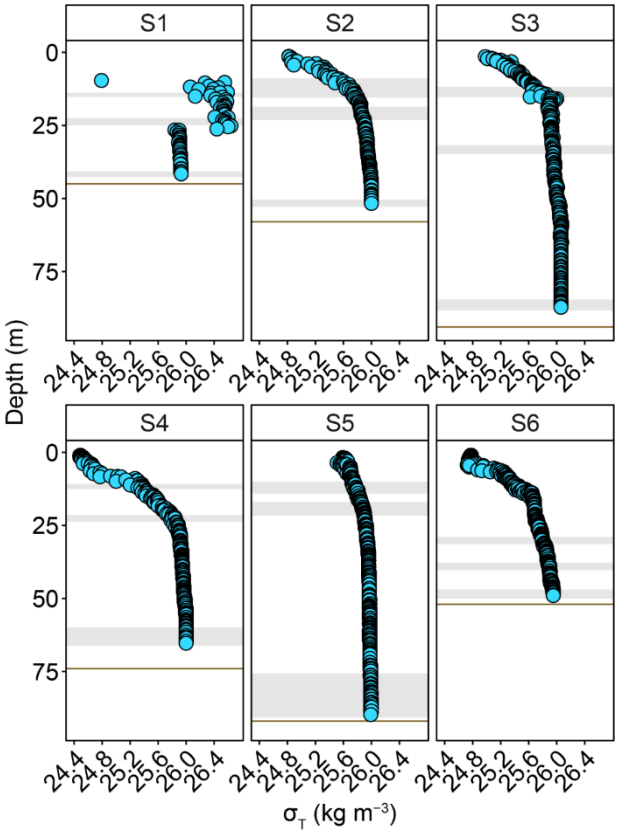

S1. **Water column density profiles from the coastal Peruvian oxygen minimum zone.** Grey boxes represent the incubation depths, including the movement during sampling. Brown bar represents the sediment interface. Station S1 had a freshwater lens that was the driver for the strong change in density in the upper water column. All data points originated from the downcast.

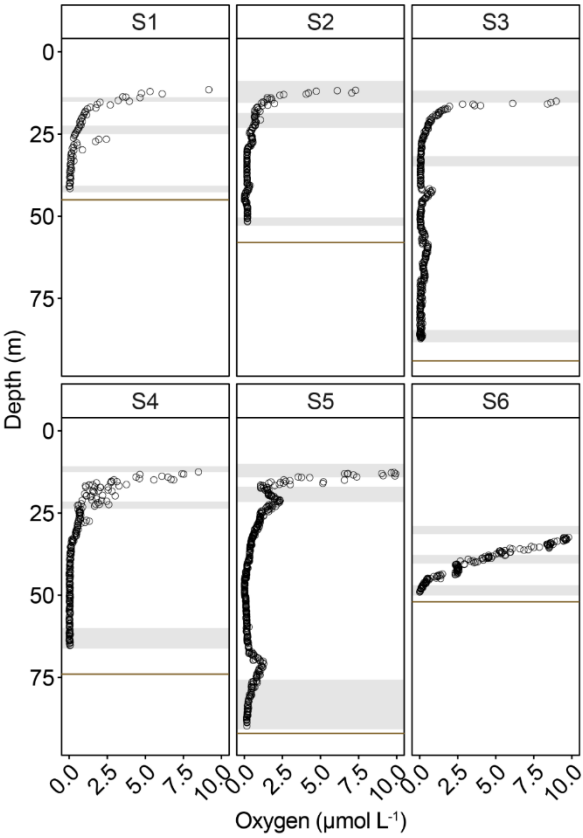

S2. **Oxygen intrusions into the core of the Peruvian oxygen minimum zone.** Grey boxes represent the incubation depths, including the movement during sampling. Brown bar represents the sediment interface. All data points originated from the downcast using the high resolution oxygen sensor.

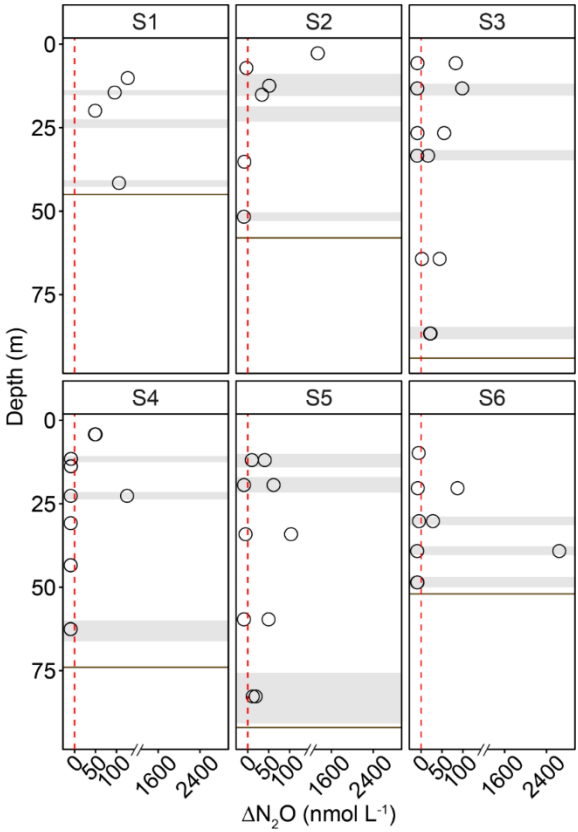

Figure S3. **Water column nitrous oxide (ΔN_2O) concentration profiles.** Each circle represents a discrete sample taken during the upcast with the pump cast CTD system. Duplicate concentration samples are shown where available. Grey lines indicate the incubation depths, including movement in the water column during sampling. Brown line represents the sediment interface**.** Dashed red line indicated equilibrium saturation levels, with samples below indicating water column undersaturation.

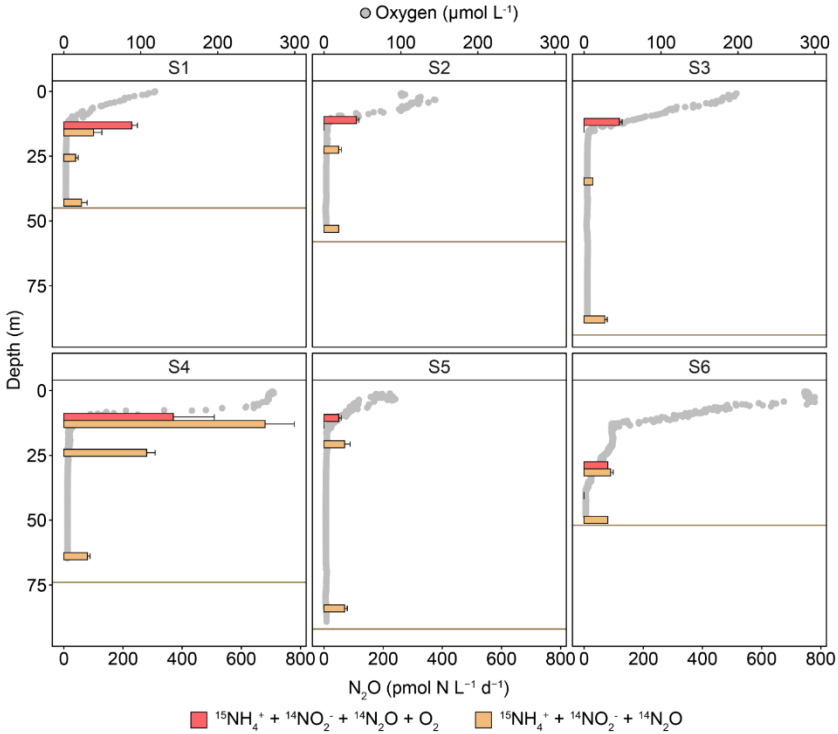

S4. **Nitrous oxide formation from the oxygen-supplemented and anoxic ammonia oxidation experiments**. Each bar represents a statistically significant (One-sided student's t-test, $p < 0.05$) rate calculated from the slope across the incubation time points, with error bars representing the standard error of the slopes. Only the first four time points (12h) were used to calculate the rates from the anoxic ammonium incubation experiment, due to N_2O depletion observed in the last timepoints, likely due to nitrogen reduction processes co-occurring. Data from all three incubation depths: oxycline, core and five metres above the sediment is shown, with the oxygen-supplemented incubation only conducted at the oxycline. Brown line indicates the sediment interface. Non-linear rates are depicted as zero.

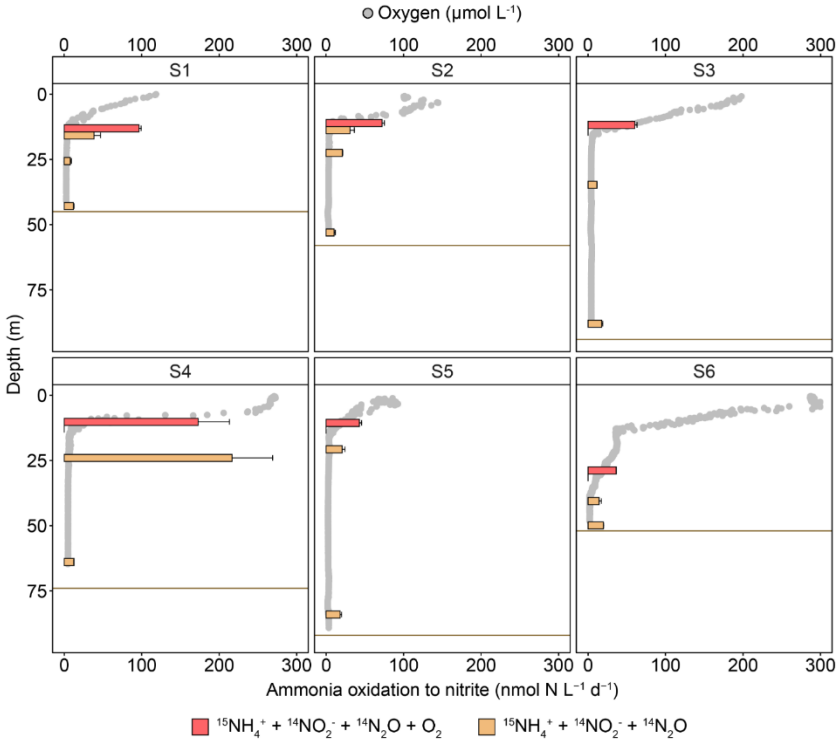

S5. **Ammonia oxidation rates to nitrite from the oxygen-supplemented and anoxic ammonia oxidation experiments**. Each bar represents a statistically significant (One-sided student's t-test, $p < 0.05$) rate calculated from the slope across the incubation time points, with error bars representing the standard error of the slopes. Only the first four time points (12h) were used to calculate the rates from the anoxic ammonium incubation experiment, due to nitrite depletion observed in the last timepoints, likely due to nitrogen reduction processes co-occurring. Data from all three incubation depths: oxycline, core and five metres above the sediment is shown, with the oxygen-supplemented incubation only conducted at the oxycline. Brown line indicates the sediment interface. Non-linear rates are depicted as zero.

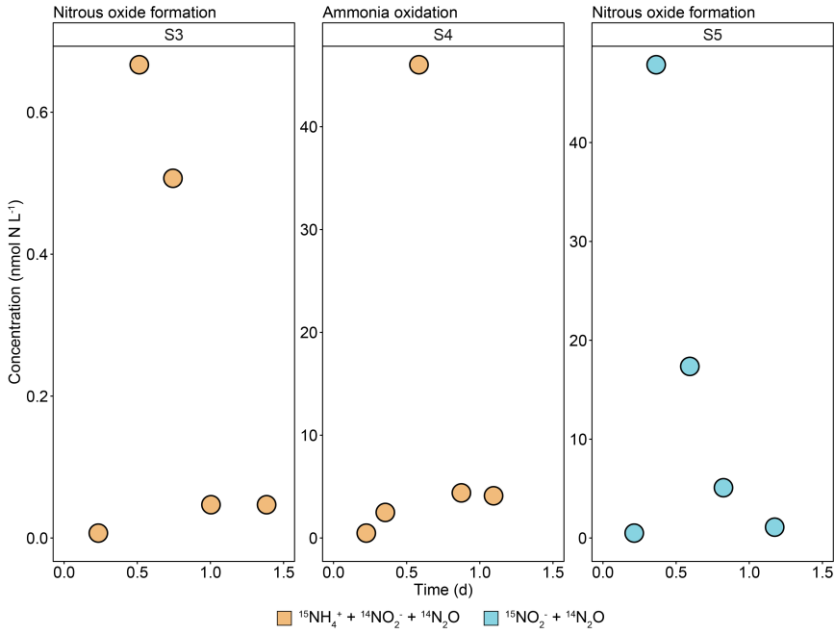

S6. **Selected examples of initial nitrous oxide or nitrite formation followed by consumption within the same time series**. All samples were taken from the oxycline.

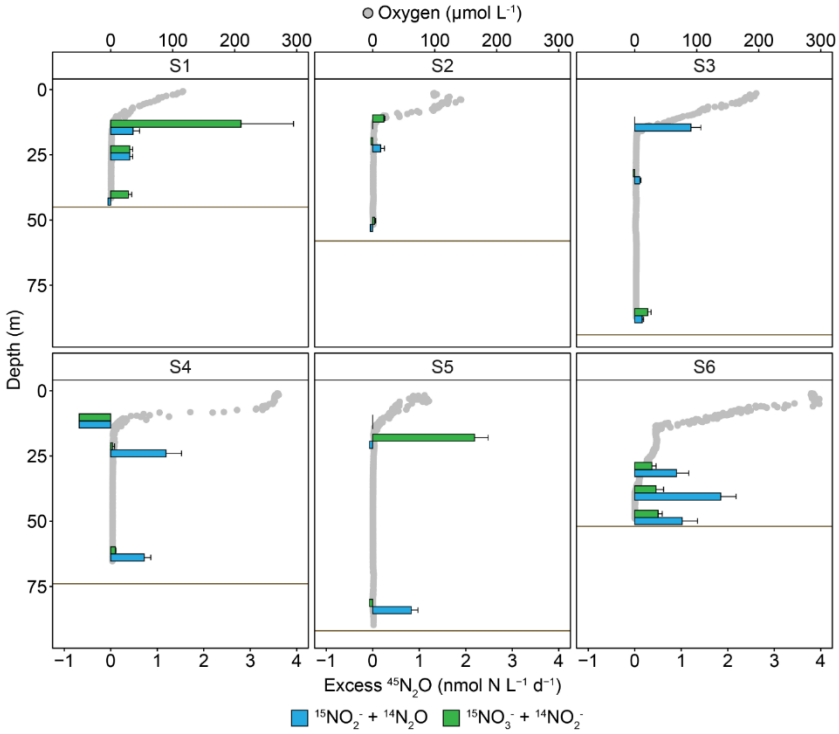

S7. **Significant excess $^{45}N_2O$ formation from nitrite and nitrate beyond the expected $^{45}N_2O$ based on random isotope pairing, as well as from the $^{45}N_2O$ formation from the anoxic ammonia oxidation experiment.** Each bar represents a statistically significant (One-sided student's t-test, $p < 0.05$) rate calculated from the slope across the incubation time points, with error bars representing the standard error of the slopes. Negative rates suggest that no significant excess $^{45}N_2O$ was reported despite significant $^{45}N_2O$ formation from ammonia oxidation. Data from all three incubation depths: oxycline, core and five metres above the sediment is shown. Brown line indicates the sediment interface. Non-linear rates are depicted as zero.

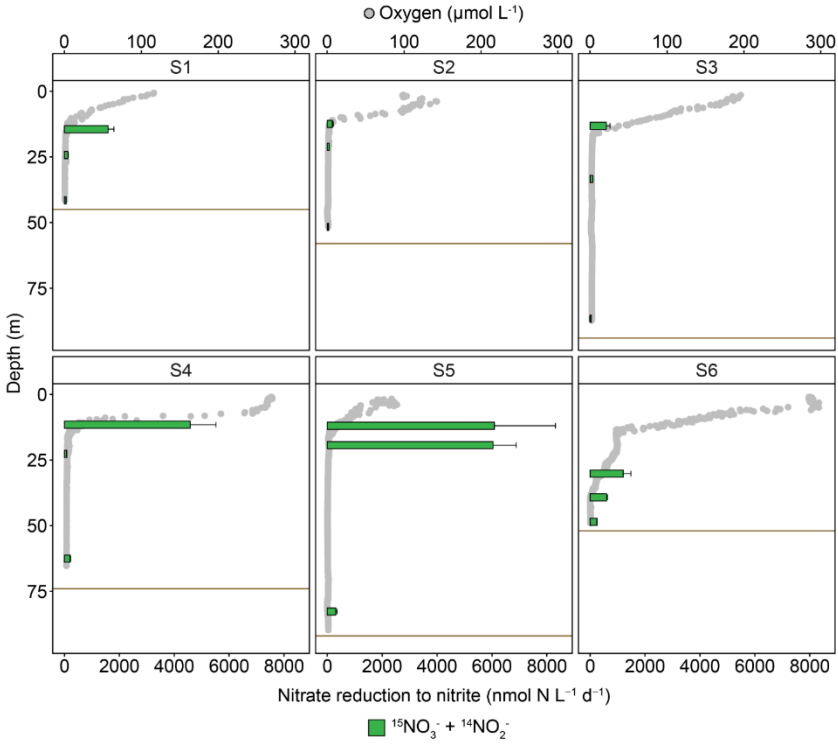

S8. **Nitrate reduction rates to nitrite.** Each bar represents a statistically significant (One-sided student's t-test, $p < 0.05$) rate calculated from the slope across the incubation time points, with error bars representing the standard error of the slopes. Data from all three incubation depths: oxycline, core and five metres above the sediment is shown, with the oxygen-supplemented incubation only conducted in the oxycline depth. Brown line indicates the sediment interface. Non-linear rates are depicted as zero.

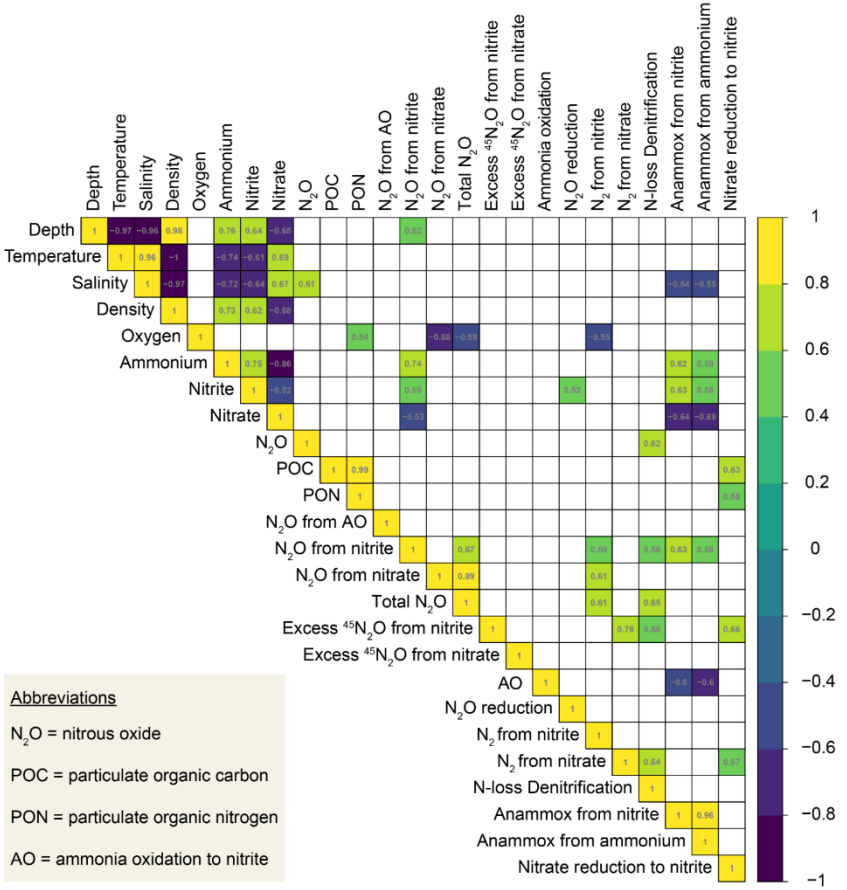

S9. **Spearman ranked correlation analysis on measured parameters.** The upcast data from all stations and incubation depths were used, with the exception of the oxycline depth of S4 and S5 as well as the core depth of S5. Insignificant correlations are left blank and nitrous oxide concentrations were averaged. Numbers in squares indicate degree of correlation.

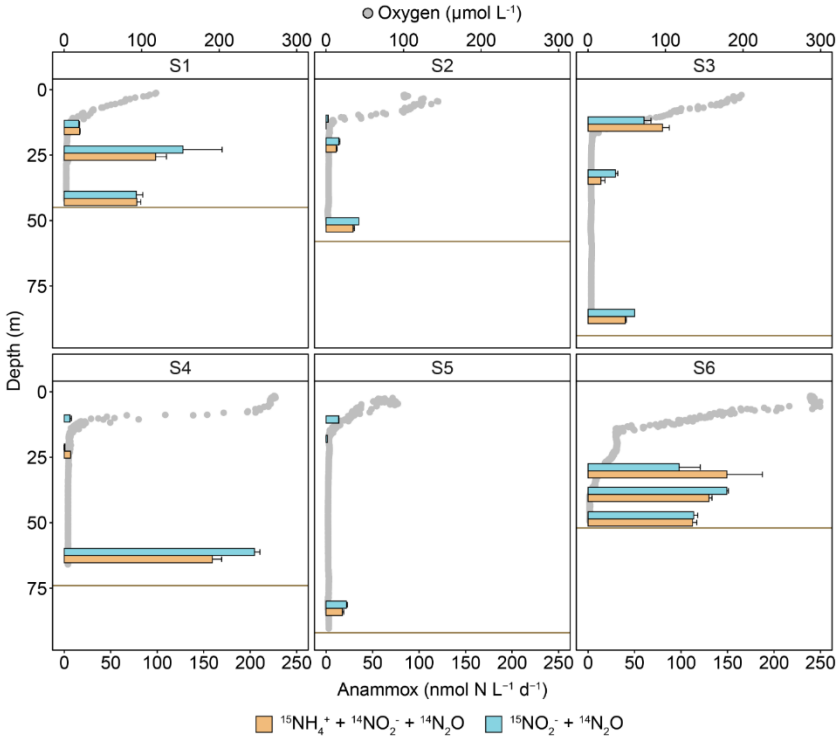

S10. **Comparison of anaerobic ammonia oxidation rates between the ammonium and nitrite experiments.** Each bar represents a statistically significant (One-sided student's t-test, $p < 0.05$) rate calculated from the slope across the incubation time points, with error bars representing the standard error of the slopes. Data from all three incubation depths: oxycline, core and five metres above the sediment is shown. Brown line indicates the sediment interface. Non-linear rates are depicted as zero. Rates from nitrite from the oxycline of S4 and S5 as well as the core depth of S5 are not shown as they were up to 1733 nmol N L^{-1} d^{-1}; however, this was likely due to a label dilution from other nitrogen transformation processes from those depths.

Chapter V

Discussion and Outlook

This thesis aimed to expand our understanding of the microbially driven processes that lead to the formation of the greenhouse gases methane and nitrous oxide (N_2O) in understudied marine environments. It aimed to constrain the formation processes using stable isotope incubation experiments and investigate the driving physico-chemical parameters, as well as to characterise the microbial community responsible. For N_2O, this was complemented by investigating the N_2O consumption, thus characterising both sources and sinks. Overall, the presented results reveal that microbially mediated greenhouse gas cycling is complex and driven by a diverse range of microbes, emphasising how much there is still to explore in order to constrain and understand these processes.

Chapter II investigated aerobic methane formation from the simple organic phosphorus compound methylphosphonate (MPn) in the phosphate-limited western Tropical North Atlantic and for the first time explored rates below the deep chlorophyll maximum (DCM; Figure 1). Using stable isotope incubation experiments, we were able to quantify significant methane formation rates throughout the upper 200 metres of the water column, which has never before been shown in the tropical North Atlantic. While variable, the highest rates were observed above the DCM, before decreasing with increasing depth. Methane is formed from MPn when microorganisms cleave the compound to access phosphate when sources of inorganic phosphate (Pi) are limited. However, even when *in-situ* concentrations of Pi were detectable, methane formation from MPn still occurred. This suggests that MPn-driven methane formation could extend into more Pi-replete environments, or be regulated by mechanisms other than the absence of phosphate. By investigating the marker gene for the carbon-phosphorus lyase pathway, *phnJ*, responsible for the methane formation, we were able to demonstrate that keystone microbial taxa, including *Trichodesmium*, *SAR116* and *Pelagibacter*, all had the capacity to form methane. Finally, we quantified the potential contribution of phosphonates to the phosphorus requirements of primary productivity and found that in the surface waters, this could be substantial, albeit highly variable. In the future, surface waters are set to experience increased phosphate limitation,

therefore the use of organic phosphorus compounds, such as MPn, could become increasingly prevalent.

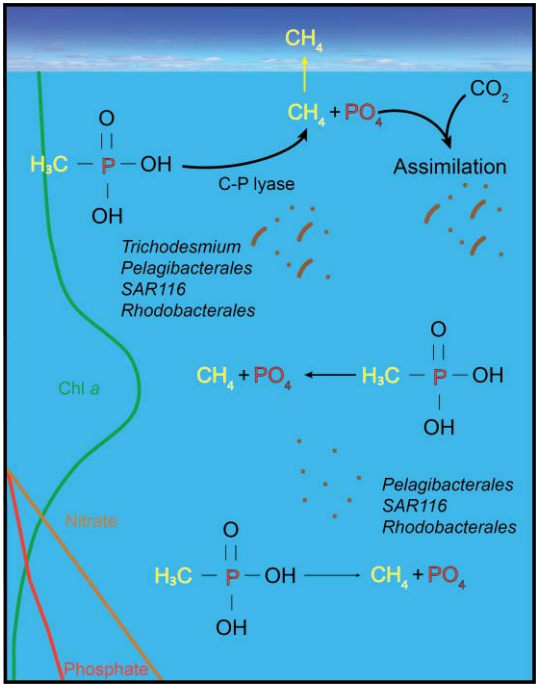

Figure 1. **Sketch depicting the main findings of methylphosphonate-driven methane formation in the western Tropical North Atlantic (chapter II)**. The highest rates of methylphosphonate driven methane formation were observed in the surface waters of the western Tropical North Atlantic, where they appeared to be driven by *Trichodesmium* and *Alphaproteobacteria* based on the presence of the carbon-phosphorus (C-P) lyase pathway. With increasing depth, rates decreased but were still quantifiable in the presence of phosphate. The phosphate liberated from phosphonates could account for a substantial fraction the phosphorus requirement in the surface waters, based on carbon fixation rates.

Chapters III and **IV** investigated the cycling of N_2O in two contrasting oxygen-limited environments (Figure 2). In **chapter III** we studied the suboxic zone of the Black Sea, a permanently stratified system that is only considered a minor source of N_2O to the atmosphere. Using stable isotope incubation experiments, we were able to reveal that despite N_2O not accumulating in the water column, there is an active N_2O cycle in the suboxic zone. Both ammonia oxidation and denitrification from nitrite led to the formation of N_2O, the former consistently but at lower rates than the latter, which was sporadic but explosive. However, incubations with ^{15}N-N_2O revealed that N_2O reduction rates could exceed the sum of both formation processes. Read based analysis of the *amoA*, the marker gene for ammonia oxidation, revealed that the ammonia oxidising archaea, the *Nitrososphaerales*, dominated throughout the investigated water column. Comparatively, read analysis revealed that the denitrifying community was diverse and included several orders capable of sulphur oxidation, suggesting that denitrification in this system could be autotrophic. Additionally, there were indications of specialist N_2O reducers amongst the *Marinisomatales*, which could further explain the balanced of N_2O formation and consumption within this system.

Chapter IV investigated N_2O cycling in a much more dynamic system, the coastal Peruvian oxygen minimum zone, which is located in the highly productive eastern boundary upwelling system and is considered to be the single largest source of marine N_2O. We sampled the shallow (< 100 metres) area of the oxygen minimum zone close to the coast and were able to reveal high but variable N_2O concentrations. Using a suite of stable isotope incubation experiments, we were able to demonstrate that both ammonia oxidation as well as denitrification from both nitrite and nitrate led to the formation of N_2O throughout the entire water column, although denitrification associated N_2O formation was two orders of magnitude higher. In addition to ammonia oxidation and denitrification, we found evidence that suggests a contribution of fungal denitrification to the N_2O formation. Similar to the Black Sea, our stable isotope incubation experiments revealed that the potential for N_2O consumption was higher than the sum of all formation processes, suggesting if the system were stable, it could mitigate N_2O emissions. We speculate that this is prevented due to constant mixing and oxygen intrusions into the core, which could limit N_2O reduction.

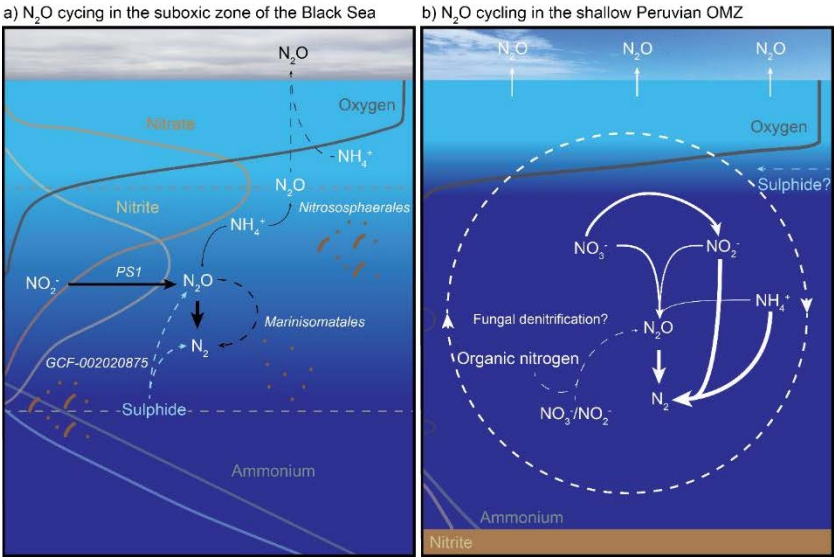

Figure 2. **Main findings pertaining to nitrous oxide (N_2O) cycling in the Black Sea (chapter III) and coastal Peruvian oxygen minimum zone (chapter IV).** In the suboxic zone of the Black Sea N_2O, formation and consumption processes are balanced and facilitated by a diverse microbial community that may include N_2O reducing specialists. In the coastal Peruvian oxygen minimum zone N_2O formation is dominated by denitrification with potential fungal contributions. Rates measurements indicate that formation and consumption could be balanced but mixing and oxygen intrusions likely disrupt the processes.

Extensive discussions for each individual project can be found in respective chapters of this thesis. In the following, I would like to elaborate on some of the findings and explore implications and questions that have been raised while conducting this research.

Methylphosphonate-driven methane - the dominant source of aerobic methane formation in the ocean?

Since the early observations of a subsurface methane concentration maximum in the fully oxygenated surface waters of the ocean, it has been speculated that a pathway for aerobic methane formation likely exists (Lamontagne et al. 1971, 1973; Scranton & Brewer 1977). However, only in the last two decades has this gained more traction due to newly proposed pathways being identified *in-situ*, such as methylphosphonate (MPn)-driven methane formation (Karl et al. 2008) and dimethylsulfoniopropionate-driven methane formation (Damm et al. 2010). Since then, further sources have been proposed, based on observations of dissolved inorganic carbon (DIC)-driven methane formation (Bižić et al. 2020a; Lenhart et al. 2016), methylamine-driven methane formation (Wang et al. 2021) amongst others (e.g. Ernst et al. 2022). Thus, a plethora of potential sources may contribute to methane formation in oxic environments. While some of these have resolved biochemistry (methylamine-driven methane formation; Wang et al. 2021), others do not (DIC-driven, DMSP-driven) and it remains to be seen which pathways are widespread, niche reactions or even occur *in-situ* in the marine environment. In **chapter II** of this thesis we expand upon the handful of environmental studies that have investigated aerobic methane formation in the marine environment *in-situ* and were able to show that MPn and not DIC was the main precursor for aerobic methane formation in the phosphate-limited western Tropical North Atlantic. Our study, together with previous environmental investigations (Del Valle & Karl 2014; Granzow et al. 2021; Karl et al. 2008; Martínez et al. 2013; Repeta et al. 2016; Sosa et al. 2020) and assessments of the global abundance of the carbon-phosphorus lyase pathway (Lockwood et al. 2022; Sosa et al. 2019a), suggests that MPn-driven methane formation may be the dominant pathway of methane formation in the marine environment.

Controlling physico-chemical parameters of methylphosphonate-driven methane formation

As we highlighted in **chapter II**, the controlling physico-chemical parameters of MPn-driven methane formation may be more complex than the simple presence or absence of Pi, as the process extended into the Pi-replete water column. It would be prudent for future work to investigate this further. Recent metagenomic evidence suggests that the gene abundance for phosphonate synthesis and methylphosphonate in general increases with increasing depth, into

the mesopelagic water column, although the C-P lyase remains most abundant in the surface waters (Acker et al. 2022; Lockwood et al. 2022; Sosa et al. 2019a). Nevertheless, it would be interesting to assess the extent of the depth distribution of MPn-driven methane formation. This could be investigated through stable isotope incubation experiments, or to increase the resolution, with radiotracer incubations (Del Valle & Karl 2014). Using radiotracers would also enable the quantification of methane oxidation rates, which we were unable to do in **chapter II**. I speculate that this could reveal a tightly balanced methane cycle, as observed for N_2O in the suboxic zone of the Black Sea (**chapter III)**, as methane does not usually accumulate in the deep ocean. Furthermore, characterising the microorganisms responsible for the MPn-driven methane formation in these depths could give new insights into the controlling mechanisms behind MPn utilisation.

One of the reasons it was difficult to assess factors controlling MPn-driven methane formation in **chapter II** was due to the high variability we observed in the rate measurements between biological replicates. We speculated that this may be due to the contribution of larger organisms, such as the abundant C-P lyase containing *Trichodesmium*, or particles. Therefore, in order to better constrain the driving physico-chemical factors, it would be useful to investigate environments where larger organisms are absent or to conduct size fractionated incubation experiments to assess the contributions of the large and small size fractions. An ideal location for any such experiments would be the Pi-limited Mediterranean Sea. This region has been shown to have the highest abundance of C-P lyase genes in the surface waters (Lockwood et al. 2022; Sosa et al. 2019a), strongly suggesting the possibility of MPn-driven methane formation. Additionally, *Trichodesmium* is generally found to bloom between 30°S and 30°N (Capone et al. 1997), although there have been reports of blooms within the Mediterranean Sea (Spatharis et al. 2012). Therefore, the Mediterranean Sea could be a perfect area to constrain some of the underlying drivers of MPn-driven methane formation, which will be crucial to understand the extent and importance of this pathway to the overall methane emissions, especially in a changing environment.

Methylphosphonate-driven methane formation in other aquatic environments

While **chapter II** addressed MPn-driven methane formation in the marine environment, the findings are also transferable to other aquatic environments. Although the ocean is only

considered a minor source of methane to the atmosphere, aquatic ecosystems can make up half of the total emissions (Rosentreter et al. 2021). Of these, lakes represent an especially variably but important source of methane (Intergovernmental Panel on Climate Change 2023a). Methane formation in lakes is usually dominated by anaerobic methanogenesis in sediments and transport into the surface through ebullition (Bižić et al. 2020b; Tang et al. 2016). However, several studies have demonstrated the potential of MPn-driven methane formation in these environments (Li et al. 2020a; Wang et al. 2017; Yao et al. 2016), especially under phosphate limitation. Therefore, MPn-driven methane formation may be more important for global methane emissions. The continuous activity of the carbon-phosphorus lyase pathway, even in the presence of *in-situ* Pi, as demonstrated in **chapter II**, also suggests that MPn-driven methane formation may not be restricted to oligotrophic Pi-limited lakes but could extend into more eutrophied ones. As we speculated in **chapter II**, regulatory pathways other than Pi-limitation likely exist, as has been suggested by an isolates from *Nodularia spumigena* (Teikari et al. 2018), which only upregulated the C-P lyase pathway in the presence of MPn, not solely the absence of Pi as expected (Stosiek et al. 2020).

One of the limitations when conducting experiments *in-situ* is that the C-P lyase pathway is not substrate specific (Wackett et al. 1987) and can degrade a broad range of phosphonates. This could potentially be problematic as many phosphonates have industrial applications, including in the agricultural sector as pesticides (Horsman & Zechel 2017) and may therefore end up in lakes and more coastal environments. Therefore, care should be taken when assessing rate measurements from these environments using only MPn and complementary methane concentration and flux measurements should be undertaken to help support the validity of the rate measurements. An additional overarching issue is that, to date, there is no protocol in place to accurately assess the concentration of MPn in the environment, where it is usually bound to polysaccharides (Metcalf et al. 2012; Repeta et al. 2016). However, the gene encoding the MPn-synthase, *mpnS*, has been identified (Metcalf et al. 2012) and can help in characterise the microbial members responsible for the MPn synthesis (Born et al. 2017; Lockwood et al. 2022; Metcalf et al. 2012).

Methylphosphonate-driven methane formation in a changing ocean

One of the main consequences of the ongoing climate warming is an increase in the thermal stratification of the water column (Li et al. 2020b). This in turn will reduce the overall exchange with the deeper nutrient rich waters through mixing and result in a reduced Pi delivery into the surface waters (Karl 2014). Therefore, the water column will become more oligotrophic and reduce primary productivity in the long run (Steinacher et al. 2010; Fu et al. 2016). Under such Pi-limitation, organisms are forced to use alternative phosphorus sources and thus may become more dependent on organic phosphorus compounds, which are often directly synthesised from primary producers (Carlson & Hansell 2015) and available at higher concentrations than Pi (Liang et al. 2022). In **chapter II,** we speculated that under these conditions MPn may become more important as a phosphorus source and consequently may offset the carbon drawdown from primary productivity by leading to the continuous formation and emission of methane. However, MPn degradation can also be facilitated by MPn oxidation to formate instead of methane (Gama et al. 2019; Sosa et al. 2019b). This process has been identified in both *Gimesia maris* (Gama et al. 2019) and *Prochlorococcus* (Sosa et al. 2019b). The latter is especially interesting, as *Prochlorococcus* is the dominating cyanobacterium in both the tropical and subtropical ocean (Biller et al. 2015). Additionally, it is expected that a warming ocean will favour picocyanobacteria such as *Prochlorococcus* (van de Waal & Litchman 2020), as a result of this pathway could become disproportionately more important. However, little is known about the extent, organisms and controlling parameters of this process at present, making further research exciting and vital.

Nitrous oxide cycling in oxygen-depleted marine environments

Oxygen depleted environments are considered to be hotspots for the cycling of N_2O. The anoxic waters enable N_2O reduction to N_2 by denitrification, while at the peripheries, low oxygen concentrations favour the formation of N_2O from denitrification while allowing aerobic ammonia oxidation to take place (Babbin et al. 2015; Codispoti et al. 2010; Naqvi et al. 2010). In **chapters III** and **IV** we investigated two contrasting OMZs. The Peruvian OMZ is located in the highly productive Eastern Tropical South Pacific upwelling system, opposed to the Black Sea, which is a permanently stratified sulphidic basin (Ulloa et al. 2012). One of the striking differences between the two systems is that the Black Sea is considered a minor source of N_2O to the atmosphere, compared to Peru which is a major source (Bange et al. 2019). However, we were able to demonstrate that both systems had an active N_2O cycle and in both the potential for N_2O consumption exceeded the combined potential for N_2O formation. We speculated that the reason for the lack of N_2O accumulation in the Black Sea was due to the balancing of the N_2O formation and consumption processes in the suboxic zone, which is facilitated by the permanent stratification of this system. This has also been observed in the analogous sulphidic and stratified Saanich Inlet, where denitrification is a net sink of N_2O and ammonia oxidation is considered the primary source (Ji et al. 2020). Although this system also has a stronger seasonality with deeper mixing of oxygenated waters, stimulating N_2O formation from ammonia oxidation makes the system seasonally supersaturated with N_2O. We speculate that this is also the reason for the high rates of N_2O formation and consumption and the *in-situ* high concentrations of N_2O in the coastal Peruvian OMZ, where the mixing of oxygenated water is not seasonal but potentially diurnal or at least on short timescales, thereby disrupting the N_2O cycling and leading to the accumulation of N_2O. Therefore, the physical nature of the environment could have a significant impact on N_2O cycling and ultimately emissions.

Nitrous oxide and the effect of sulphide

In both **chapters III** and **IV** denitrification was the main source of N_2O throughout the investigated water column, opposed to ammonia oxidation. One of the aspects that was not explored was the potential effect of the electron donor on the denitrification rates. Heterotrophic denitrification in the ocean is considered to be limited by organic carbon (Ward et al. 2008). For example, in the Peruvian OMZ rates of N_2O formation from denitrification could be stimulated

by additions of organic matter (Frey et al. 2020) and it has been speculated that the patchy distribution of denitrification can be due to the episodic inputs of fresh organic material (Dalsgaard et al. 2012). Comparatively, the Black Sea is considered to be more oligotrophic system (Amouroux et al. 2002) and peaks of N_2 have been observed at the oxycline, attributed to organic matter input from blooms and potential particle denitrification (Fuchsman et al. 2019). Therefore, the Black Sea may represent a more organic matter-limited system, opposed to the investigated coastal area of the Peruvian OMZ in **chapter IV**. However, both systems can be affected by sulphide. The suboxic zone of the Black Sea is located on top of the deep anoxic sulphidic core (Murray et al. 1995), whereas the Peruvian OMZ can experience episodic sulphidic events (Callbeck et al. 2018; Canfield et al. 2010; Schunck et al. 2013). The presence of sulphide appears to amplify the rates of both N_2O formation as well as N_2 (Callbeck et al. 2018; Canfield et al. 2010; Lavik et al. 2009; Schunck et al. 2013) likely due to the microorganisms involved being able to bloom (Sievert et al. 2008). We speculate that either sulphide or elemental sulphur contributed to the high rates of N_2O cycling observed in **chapters III** and **IV**. This would be interesting to investigate further. For example in the Black Sea, the order *GCF-002020875* includes the *Candidatus Thiopontia* genus and a metagenome assembled genome of *Thiopontia autotrophica* has been shown to contain all the genes required for denitrification as well as sulphur oxidation and the Calvin-Benson-Bassam cycle (van Vliet et al. 2021). Using the metagenomic data from our study, we could try to obtain bins to reconstruct the genome of a member of the *GCF-002020875* and investigate the metabolic potential. If we were to obtain the 16S rRNA from that bin, we could then design a specific probe for fluorescence *in-situ* hybridisation to identify the organism of the filters that were taken. Combining this with nanoscale secondary ion mass spectrometry, we could then investigate the filters from the ^{15}N experiments that included ^{13}C-bicarbonate, which were taken after 24 hours of incubation and see if the cells are enriched in ^{13}C, thereby linking carbon fixation to denitrification. Furthermore, characterising members of the *Marinisomatales* would also be of great interest due to their potential as ^{15}N-N_2O reducers. It would also be interesting to characterise the microbial community in the coastal Peruvian OMZ as well, as this would enable both the comparison with the open ocean OMZ community, as well as the Black Sea, to grant further insights into the two oxygen-limited environments. Understanding the microorganism responsible for the denitrification and especially sulphide-driven denitrification is of special interest due to the magnitude of the rates as well as the potential increases in sulphidic events (Pratihary et al. 2023).

Greenhouse gas cycling in a changing ocean

The continuing anthropogenic perturbation of the climate has already had a profound effect on the marine environment. The ocean has been steadily de-oxygenating over the last 50 years (Schmidtko et al. 2017) and is projected to continue to do so (Diaz & Rosenberg 2008). Additionally, ocean acidification and thermal stratification continue to increase (Li et al. 2020b). All of these consequences have, and will have, profound effects on the cycling of the two greenhouse gases reported in this thesis. We have already speculated that the increase in stratification may be most impactful as it is likely going to increase both the MPn-driven methane formation and potentially decrease the N_2O emissions by limiting the exchange with the upper water column. However, this may not be straightforward. MPn synthesis is highest in the mesopelagic waters (Acker et al. 2022; Lockwood et al. 2022) and therefore an increase in stratification may restrict the access to MPn for the surface community, resulting in limited MPn-driven methane formation. While we emphasised the potential for N_2O consumption to exceed the formation in **chapters III** and **IV**, this may not be the case under future conditions. A more acidic water column may favour higher formation rates of N_2O from ammonia oxidation (Jung et al. 2019) and it has been shown that the *nosZ* can become inhibited in acidic conditions (Bergaust et al. 2010), consequently reducing the potential N_2O reduction capacity. Furthermore, extreme weather events will increase (Intergovernmental Panel on Climate Change 2023b) thereby potentially disrupting more shallow coastal water columns, breaking down the stratification and increasing the potential flux to the atmosphere. It therefore remains vital to characterise the pathways that lead to N_2O and methane formation in the marine environment and resolve their physico-chemical drivers, in order to ensure that model predictions can become as constrained as possible.

To conclude, the results presented in this thesis have addressed both aerobic methane formation, particularly from MPn, and the cycling of N_2O in two dissimilar oxygen-limited environments. These findings expand on our previous knowledge of the individual processes responsible for the cycling of these greenhouse gases in underexplored marine environments. Using powerful stable isotope incubation experiments, we have quantified rates of microbial transformation processes and supported these with measurements of physico-chemical parameters. Additionally, metagenomic and metatranscriptomic analyses provided insights into the microbial community responsible for the cycling of these significant greenhouse gases. As always, the findings raise

numerous new questions that will be exciting to address in the future and can build on the foundations presented here. Furthermore, they are also transferable to other aquatic environments, broadening the scope of the implications and potentially adding new and exciting environments for future studies. It will be paramount to continue to monitor, quantify, characterise and explore all aspects of marine greenhouse gas cycling in the future, from coast to open ocean.

Bibliography

Acker M, Hogle SL, Berube PM, Hackl T, Coe A, et al. 2022. Phosphonate production by marine microbes: Exploring new sources and potential function. *Proc. Natl. Acad. Sci. U. S. A.* 119(11):

Amouroux D, Roberts G, Rapsomanikis S, Andreae MO. 2002. Biogenic gas (CH4, N2O, DMS) emission to the atmosphere from near-shore and shelf waters of the north-western Black Sea. *Estuar. Coast. Shelf Sci.* 54(3):575–87

Babbin AR, Bianchi D, Jayakumar A, Ward BB. 2015. Rapid nitrous oxide cycling in the suboxic ocean. *Science (80-.).* 348(6239):1127–29

Bange HW, Arévalo-Martínez DL, Paz M de la, Farías L, Kaiser J, et al. 2019. A harmonized nitrous oxide (N2O) ocean observation network for the 21st century. *Front. Mar. Sci.* 6(APR):1–10

Bergaust L, Mao Y, Bakken LR, Frostegård Å. 2010. Denitrification response patterns during the transition to anoxic respiration and posttranscriptional effects of suboptimal ph on nitrogen oxide reductase in paracoccus denitrificans. *Appl. Environ. Microbiol.* 76(19):6387–96

Biller SJ, Berube PM, Lindell D, Chisholm SW. 2015. Prochlorococcus: The structure and function of collective diversity. *Nat. Rev. Microbiol.* 13(1):13–27

Bižić M, Klintzsch T, Ionescu D, Hindiyeh MY, Günthel M, et al. 2020a. Aquatic and terrestrial cyanobacteria produce methane. *Sci. Adv.* 6(3):1–10

Bižić M, Grossart H, Ionescu D. 2020b. Methane Paradox. *eLS*. (February):1–11

Born DA, Ulrich EC, Ju KS, Peck SC, Van Der Donk WA, Drennan CL. 2017. Structural basis for methylphosphonate biosynthesis. *Science (80-.).* 358(6368):1336–39

Callbeck CM, Lavik G, Ferdelman TG, Fuchs B, Gruber-Vodicka HR, et al. 2018. Oxygen minimum zone cryptic sulfur cycling sustained by offshore transport of key sulfur oxidizing bacteria. *Nat. Commun.* 9(1):1–11

Canfield DE, Stewart FJ, Thamdrup B, De Brabandere L, Dalsgaard T, et al. 2010. A cryptic sulfur cycle in oxygen-minimum-zone waters off the Chilean coast. *Science (80-.).* 330(6009):1375–78

Capone DG, Zehr JP, Paerl HW, Bergman B, Carpenter EJ. 1997. Trichodesmium, a globally significant marine cyanobacterium. *Science (80-.).* 276(5316):1221–29

Carlson CA, Hansell DA. 2015. DOM Sources, Sinks, Reactivity, and Budgets. In *Biogeochemistry of Marine Dissolved Organic Matter*, pp. 65–126. Elsevier

Codispoti LA. 2010. Interesting times for marine N2O. *Science (80-.).* 327(5971):1339–40

Dalsgaard T, Thamdrup B, Farías L, Revsbech NP. 2012. Anammox and denitrification in the oxygen minimum zone of the eastern South Pacific. *Limnol. Oceanogr.* 57(5):1331–46

Damm E, Helmke E, Thoms S, Schauer U, Nöthig E, et al. 2010. Methane production in aerobic oligotrophic surface water in the central Arctic Ocean. *Biogeosciences*. 7(3):1099–1108

Del Valle DA, Karl DM. 2014. Aerobic production of methane from dissolved water-column methylphosphonate and sinking particles in the North Pacific Subtropical Gyre. *Aquat. Microb. Ecol.* 73(2):93–105

Diaz RJ, Rosenberg R. 2008. Spreading dead zones and consequences for marine ecosystems. *Science (80-.).* 321(5891):926–29

Ernst L, Steinfeld B, Barayeu U, Klintzsch T, Kurth M, et al. 2022. Methane formation driven by reactive oxygen species across all living organisms. *Nature*. 603(7901):482–87

Frey C, Bange HW, Achterberg EP, Jayakumar A, Löscher CR, et al. 2020. Regulation of nitrous oxide production in low-oxygen waters off the coast of Peru. *Biogeosciences*. 17(8):2263–87

Fu W, Randerson JT, Keith Moore J. 2016. Climate change impacts on net primary production (NPP) and export production (EP) regulated by increasing stratification and phytoplankton community structure in the CMIP5 models. *Biogeosciences*. 13(18):5151–70

Fuchsman CA, Paul B, Staley JT, Yakushev E V., Murray JW. 2019. Detection of Transient Denitrification During a High Organic Matter Event in the Black Sea. *Global Biogeochem. Cycles*. 33(2):143–62

Gama SR, Vogt M, Kalina T, Hupp K, Hammerschmidt F, et al. 2019. An Oxidative Pathway for Microbial Utilization of Methylphosphonic Acid as a Phosphate Source. *ACS Chem. Biol.* 14(4):735–41

Granzow BN, Sosa OA, Gonnelli M, Santinelli C, Karl DM, Repeta DJ. 2021. A sensitive fluorescent assay for measuring carbon-phosphorus lyase activity in aquatic systems. *Limnol. Oceanogr. Methods*. 19(4):235–44

Horsman GP, Zechel DL. 2017. Phosphonate Biochemistry. *Chem. Rev.* 117(8):5704–83

Intergovernmental Panel on Climate Change. 2023a. Global Carbon and Other Biogeochemical Cycles and Feedbacks. In *Climate Change 2021 – The Physical Science Basis*, pp. 673–816. Cambridge University Press

Intergovernmental Panel on Climate Change. 2023b. *Ocean, Cryosphere and Sea Level Change*

Ji Q, Jameson BD, Juniper SK, Grundle DS. 2020. Temporal and Vertical Oxygen Gradients Modulate Nitrous Oxide Production in a Seasonally Anoxic Fjord: Saanich Inlet, British Columbia. *J. Geophys. Res. Biogeosciences*. 125(9):1–14

Jung MY, Gwak JH, Rohe L, Giesemann A, Kim JG, et al. 2019. Indications for enzymatic denitrification to N2O at low pH in an ammonia-oxidizing archaeon. *ISME J.* 13(10):2633–38

Karl DM. 2014. Microbially mediated transformations of phosphorus in the sea: New views of an old cycle. *Ann. Rev. Mar. Sci.* 6:279–337

Karl DM, Beversdorf L, Björkman KM, Church MJ, Martinez A, Delong EF. 2008. Aerobic production of methane in the sea. *Nat. Geosci.* 1(7):473–78

Lamontagne R a, Swinnerton JW, Linnenbom VJ, Smith WD. 1973. Methane concentrations in various marine environments. *J. Geophys. Res.* 78(24):5317–24

Lamontagne RA, Swinnerton JW, Linnenbom VJ. 1971. Nonequilibrium of carbon monoxide and methane at the air-sea interface. *J. Geophys. Res.* 76(21):5117–21

Lavik G, Stührmann T, Brüchert V, Van Der Plas A, Mohrholz V, et al. 2009. Detoxification of sulphidic African shelf waters by blooming chemolithotrophs. *Nature*. 457(7229):581–84

Lenhart K, Klintzsch T, Langer G, Nehrke G, Bunge M, et al. 2016. Evidence for methane production by the marine algae Emiliania huxleyi. *Biogeosciences*. 13(10):3163–74

Li W, Dore JE, Steigmeyer AJ, Cho YJ, Kim OS, et al. 2020a. Methane production in the oxygenated water column of a perennially ice-covered Antarctic lake. *Limnol. Oceanogr.* 65(1):143–56

Li G, Cheng L, Zhu J, Trenberth KE, Mann ME, Abraham JP. 2020b. Increasing ocean stratification over the past half-century. *Nat. Clim. Chang.* 10(12):1116–23

Liang Z, Letscher RT, Knapp AN. 2022. Dissolved organic phosphorus concentrations in the surface ocean controlled by both phosphate and iron stress. *Nat. Geosci.* 15(8):651–57

Lockwood S, Greening C, Baltar F, Morales SE. 2022. Global and seasonal variation of marine phosphonate metabolism. *ISME J.* 16(9):2198–2212

Martínez A, Ventouras LA, Wilson ST, Karl DM, DeLong EF. 2013. Metatranscriptomic and functional metagenomic analysis of methylphosphonate utilization by marine bacteria. *Front. Microbiol.* 4(NOV):1–18

Metcalf WW, Griffin BM, Cicchillo RM, Gao J, Janga C, et al. 2012. Supplementary Materials for Methane in the Aerobic Ocean. . 1104(August):1104–7

Murray JW, Codispoti LA, Friederich GE. 1995. Oxidation-Reduction Environments. In *Aquatic Chemistry: Interfacial and Interspecies Processes.*, pp. 157–76

Naqvi SWA, Bange HW, FarÃ-As L, Monteiro PMS, Scranton MI, Zhang J. 2010. Marine hypoxia/anoxia as a source of CH 4 and N2O. *Biogeosciences*. 7(7):2159–90

Repeta DJ, Ferrón S, Sosa OA, Johnson CG, Repeta LD, et al. 2016. Marine methane paradox explained by bacterial degradation of dissolved organic matter. *Nat. Geosci.* 9(12):884–87

Pratihary A, Lavik G, Naqvi SWA, Shirodkar G, Sarkar A, et al. 2023. Chemolithoautotrophic denitrification intensifies nitrogen loss in the Eastern Arabian Sea Shelf waters during sulphidic events. *Prog. Oceanogr.* 217:103075

Rosentreter JA, Borges A V., Deemer BR, Holgerson MA, Liu S, et al. 2021. Half of global methane emissions come from highly variable aquatic ecosystem sources. *Nat. Geosci.* 14(4):225–30

Schmidtko S, Stramma L, Visbeck M. 2017. Decline in global oceanic oxygen content during the past five decades. *Nature*. 542(7641):335–39

Schunck H, Lavik G, Desai DK, Großkopf T, Kalvelage T, et al. 2013. Giant Hydrogen Sulfide Plume in the Oxygen Minimum Zone off Peru Supports Chemolithoautotrophy. *PLoS One*. 8(8):

Scranton MI, Brewer PG. 1977. Occurrence of methane in the near-surface waters of the western subtropical North-Atlantic. *Deep. Res.* 24(2):127–38

Sievert SM, Scott KM, Klotz MG, Chain PSG, Hauser LJ, et al. 2008. Genome of the Epsilonproteobacterial Chemolithoautotroph. . 74(4):1145–56

Sosa OA, Burrell TJ, Wilson ST, Foreman RK, Karl DM, Repeta DJ. 2020. Phosphonate cycling supports methane and ethylene supersaturation in the phosphate-depleted western North Atlantic Ocean. *Limnol. Oceanogr.* 65(10):2443–59

Sosa OA, Repeta DJ, DeLong EF, Ashkezari MD, Karl DM. 2019a. Phosphate-limited ocean regions select for bacterial populations enriched in the carbon–phosphorus lyase pathway for phosphonate degradation. *Environ. Microbiol.* 21(7):2402–14

Sosa OA, Casey JR, Karl DM. 2019b. Methylphosphonate Oxidation in Prochlorococcus Strain MIT9301 Supports Phosphate Acquisition, Formate Excretion, and Carbon Assimilation into Purines. *Appl. Environ. Microbiol.* 85(13):1–12

Spatharis S, Skliris N, Meziti A, Kormas KA. 2012. First record of a Trichodesmium erythraeum bloom in the Mediterranean Sea. *Can. J. Fish. Aquat. Sci.* 69(8):1444–55

Steinacher M, Joos F, Frölicher TL, Bopp L, Cadule P, et al. 2010. Projected 21st century decrease in marine productivity: A multi-model analysis. *Biogeosciences*. 7(3):979–1005

Stosiek N, Talma M, Klimek-Ochab M. 2020. Carbon-Phosphorus Lyase—the State of the Art. *Appl. Biochem. Biotechnol.* 190(4):1525–52

Tang KW, McGinnis DF, Ionescu D, Grossart HP. 2016. Methane production in oxic lake waters potentially increases aquatic methane flux to air. *Environ. Sci. Technol. Lett.* 3(6):227–33

Teikari JE, Fewer DP, Shrestha R, Hou S, Leikoski N, et al. 2018. Strains of the toxic and bloom-forming Nodularia spumigena (cyanobacteria) can degrade methylphosphonate and release methane. *ISME J.* 12(6):1619–30

Ulloa O, Canfield DE, DeLong EF, Letelier RM, Stewart FJ. 2012. Microbial oceanography of anoxic oxygen minimum zones. *Proc. Natl. Acad. Sci. U. S. A.* 109(40):15996–3

van de Waal DB, Litchman E. 2020. Multiple global change stressor effects on phytoplankton nutrient acquisition in a future ocean. *Philos. Trans. R. Soc. B Biol. Sci.* 375(1798):1–8

van Vliet DM, von Meijenfeldt FAB, Dutilh BE, Villanueva L, Sinninghe Damsté JS, et al. 2021. The bacterial sulfur cycle in expanding dysoxic and euxinic marine waters. *Environ. Microbiol.* 23(6):2834–57

Wackett LP, Shames SL, Venditti CP, Walsh CT. 1987. Bacterial carbon-phosphorus lyase: Products, rates, and regulation of phosphonic and phosphinic acid metabolism. *J. Bacteriol.* 169(2):710–17

Wang Q, Alowaifeer A, Kerner P, Balasubramanian N, Patterson A, et al. 2021. Aerobic bacterial methane synthesis. *Proc. Natl. Acad. Sci. U. S. A.* 118(27):

Wang Q, Dore JE, McDermott TR. 2017. Methylphosphonate metabolism by Pseudomonas sp. populations contributes to the methane oversaturation paradox in an oxic freshwater lake. *Environ. Microbiol.* 19(6):2366–78

Ward BB, Tuit CB, Jayakumar A, Rich JJ, Moffett J, Naqvi SWA. 2008. Organic carbon, and not copper, controls denitrification in oxygen minimum zones of the ocean. *Deep. Res. Part I Oceanogr. Res. Pap.* 55(12):1672–83

Yao M, Henny C, Maresca JA. 2016. Freshwater bacteria release methane as a by-product of phosphorus acquisition. *Appl. Environ. Microbiol.* 82(23):6994–7003

Appendix

Author Contributions

Chapter II: Methylphosphonate-driven methane formation and its link to primary production in the oligotrophic North Atlantic

Jan N. von Arx, Abiel T. Kidane, Miriam Philippi, Wiebke Mohr, Gaute Lavik, Sina Schorn, Marcel M. M. Kuypers and Jana Milucka

W.M., A.T.K. and I (J.v.A) conducted the field sampling. I performed the incubation experiments for methane formation and measured the samples. I carried out the rate analysis and calculations with guidance from G.L. Carbon fixation experiments were conducted by A.T.K. and W.M. I was responsible for the DNA and RNA extraction and metagenomic and metatranscriptomic analyses were performed by M.P. The study was designed by me, M.M.M.K., S.S., and J.M. I discussed and interpreted the data with M.M.M.K. and J.M. I visualised the presented dataset. J.M. and I wrote the manuscript with contributions from all other authors.

Chapter III: Nitrous oxide cycling in the suboxic zone of the Black Sea

Jan N. von Arx, Katharina Kitzinger, Hannah Marchant, Gaute Lavik, Jördis Stührenberg, Jon Graf, Daan Speth, Marcel M. M. Kuypers and Jana Milucka

I (J.v.A) designed the study together with M.M.M.K., and J.M. Fieldwork was conducted by me, K.K., H.M., J.G., and J.M. Stable isotope incubation experiments were set up by K.K., H.M., and I, with K.K. and I measuring the samples. Rate analysis and calculations were carried out by G.L. and I. DNA and RNA were extracted by K.K. and metagenomic and metatranscriptomic analyses were performed by J.S. and D.S. I discussed and interpreted the data with J.M. I visualised the presented dataset. The manuscript was written by J.M. and I.

Chapter IV: Nitrous oxide cycling in the coastal Peruvian oxygen minimum zone

Jan N. von Arx, Soeren Ahmerkamp, Clarissa Karthäuser, Katharina Kitzinger, Gaute Lavik, Jon Graf, Sina Schorn, Marcel M. M. Kuypers and Jana Milucka

The study was designed by M.M.M.K. and J.M. Sampling in the field was conducted by S.A., G.L., J.G. and myself (J.v.A.). Stable isotope incubation experiments were set up by K.K., S.S. and M.M.M.K. Rates measurements from stable isotope incubation experiments were carried out by K.K. and I. Rate analysis and calculations were conducted by G.L. and I. I filtered water for the POC and PON concentrations and measured and analysed them. Particle abundance data was provided by S.A. and C.K. I discussed and interpreted the data with J.M. I visualised the presented dataset. The manuscript was written by J.M. and I.

Versicherung an Eides Statt / *Affirmation in lieu of an oath*

gem. § 5 Abs. 5 der Promotionsordnung vom 18.06.2018 /
according to § 5 (5) of the Doctoral Degree Rules and Regulations of 18 June, 2018

Ich / I, _____
(Vorname / First *Name*, Name / *Name*, Anschrift / *Address*, ggf. Matr.-Nr. / *student ID no., if applicable)*

versichere an Eides Statt durch meine Unterschrift, dass ich die vorliegende Dissertation selbständig und ohne fremde Hilfe angefertigt und alle Stellen, die ich wörtlich dem Sinne nach aus Veröffentlichungen entnommen habe, als solche kenntlich gemacht habe, mich auch keiner anderen als der angegebenen Literatur oder sonstiger Hilfsmittel bedient habe und die zu Prüfungszwecken beigelegte elektronische Version (PDF) der Dissertation mit der abgegebenen gedruckten Version identisch ist. / *With my signature I affirm in lieu of an oath that I prepared the submitted dissertation independently and without illicit assistance from third parties, that I appropriately referenced any text or content from other sources, that I used only literature and resources listed in the dissertation, and that the electronic (PDF) and printed versions of the dissertation are identical.*

Ich versichere an Eides Statt, dass ich die vorgenannten Angaben nach bestem Wissen und Gewissen gemacht habe und dass die Angaben der Wahrheit entsprechen und ich nichts verschwiegen habe. / *I affirm in lieu of an oath that the information provided herein to the best of my knowledge is true and complete.*

Die Strafbarkeit einer falschen eidesstattlichen Versicherung ist mir bekannt, namentlich die Strafandrohung gemäß § 156 StGB bis zu drei Jahren Freiheitsstrafe oder Geldstrafe bei vorsätzlicher Begehung der Tat bzw. gemäß § 161 Abs. 1 StGB bis zu einem Jahr Freiheitsstrafe oder Geldstrafe bei fahrlässiger Begehung. / *I am aware that a false affidavit is a criminal offence which is punishable by law in accordance with § 156 of the German Criminal Code (StGB) with up to three years imprisonment or a fine in case of intention, or in accordance with § 161 (1) of the German Criminal Code with up to one year imprisonment or a fine in case of negligence.*

_____ _____
Ort / *Place*, Datum / *Date* Unterschrift / *Signature*